Co-firing Coal: Feedlot and Litter Biomass (CFB and CLB) Fuels in Pulverized Fuel and Fixed Bed burners

Final Report
6/15/2000 – 05/31/2003

Kalyan Annamalai
John Sweeten
Saqib Mukhtar
Ben Thien
Gengsheng Wei
Soyuz Priyadarsan
Senthil Arumugam
Kevin Heflin

Texas A&M University, College Station, Texas

August 28, 2003

Grant #: DE-FG26-00NT40810

Texas Engineering Experiment Station,
Texas A&M University, College Station, Texas 77843

Submitted to

National Energy Technology Laboratory,
US Department of Energy, Pittsburgh, PA.

Disclaimer

Abstract

Intensive animal feeding operations create large amounts of animal waste that must be safely disposed of in order to avoid environmental degradation. Cattle feedlots and chicken houses are two examples. In feedlots, cattle are confined to small pens and fed a high calorie grain-diet diet in preparation for slaughter. In chicken houses, thousands of chickens are kept in close proximity. In both of these operations, millions of tons of manure are produced every year. The manure could be used as a fuel by mixing it with coal in a 90:10 blend and firing it in an existing coal suspension fired combustion systems. This technique is known as **co-firing**, and the high temperatures produced by the coal will allow the biomass to be completely combusted. Reburn is a process where a small percentage of fuel called reburn fuel is injected above the NO_x producing, conventional coal fired burners in order to reduce NO_x. The manure could also be used as **reburn fuel** for reducing NO_x in coal fired plants. An alternate approach of using animal waste is to adopt the **gasification** process using a fixed bed gasifier and then use the gases for firing in gas turbine combustors. In this report, the cattle manure is referred to as feedlot biomass (FB) and chicken manure as litter biomass (LB). The report generates data on FB and LB fuel characteristics. Co-firing, reburn, and gasification tests of coal, FB, LB, coal: FB blends, and coal: LB blends and modeling on cofiring, reburn systems and economics of use of FB and LB have also been conducted. The biomass fuels are higher in ash, lower in heat content, higher in moisture, and higher in nitrogen and sulfur (which can cause air pollution) compared to coal. Small-scale cofiring experiments revealed that the biomass blends can be successfully fired, and NO_x emissions will be similar to or lower than pollutant emissions when firing coal. Further experiments showed that biomass is twice or more effective than coal when used in a reburning process. Computer simulations for coal: LB blends were performed by modifying an existing computer code to include the drying and phosphorus (P) oxidation models. The gasification studies revealed that there is bed agglomeration in the case of chicken litter biomass due to its higher alkaline oxide content in the ash. Finally, the results of the economic analysis show that considerable fuel cost savings can be achieved with the use of biomass. In the case of higher ash and moisture biomass, the fuel cost savings is reduced.

Table of Contents

List of Figures

List of Tables

1. Introduction

Large concentrated animal feeding operations (CAFO) have expanded all over the country including Texas. Since 1978, the average number of animal units and hence animal waste has increased by 56 % (cattle) and 176 % (poultry litter). Beef cattle are fattened for slaughter in large industrial feeding operations known as feedlots. Cattle are confined to small pens and fed a high calorie ration to induce them to gain weight. In Texas, feedlots are found mainly in the panhandle area near Amarillo. Cattle in a typical feedlot pen, on a feedlot in the Amarillo area are shown in figure 1.1. The average feedlot can have over 10,000 head of cattle, and it is estimated that at any given time there are over 10,000,000 cattle in feedlots in the United States (Eghball *et al.*, 1994). Each calf is typically fed over a period of 4 – 5 months. For example if 3 million heads of feeder cattle are fed over a 5 month period in the Texas Panhandle area, the feedlot has accumulated feedlot compost of 3 million dry tons over 4-5 month period, and they process 6-7 million cattle over 1 year. There are 70 feed yards in the Texas Panhandle area which includes Oklahoma, New Mexico, and the feeding 6-7 million heads (30 % of cattle on feed in USA); the feedlots have capacities greater than 20,000 cattle, with several lots as large as 50,000 to 85,000 head. (http://www.westbioenergy.org/cattle/intro.htm; Texas Cattle Feeders Association, TCFA, http://www.tcfa.org). The cattle waste history from excretion to collection is shown in figure 1.2 and a sample calculation of the total annual manure generation is given in appendix 4. Each of these feeder cattle, feeder steers, or heifers produces about 28.12 kg (62 lb) of wet manure per day containing 88 % moisture and 12 % solids (Sweeten, 1979). The waste production is estimated as dry tons per year: 6 million dry tons per year for Texas Panhandle area and 75 million dry tons for USA. The cattle feeding industry in the Texas Panhandle area is growing at the rate of approximately 100,000 head of feedlot capacity per year. Cattle feeding in the Panhandle area are a $5.5 billion industry with the total economic impact of about $15.5 billion.

Figure 1.1: Cattle in a typical feedlot pen, Amarillo, Texas

Broiler producers under contract from poultry integrators, raise broiler chicken in houses that may contain flocks of 10,000 to 30,000 birds per house. On average, each house produces 5 to 6 flocks per year. Poultry broiler production in the USA has increased dramatically with total broiler meat production increasing from nearly 2.27 billion kg (5 billion lb) in 1961 to more than 18.2 billion kg (40 billion lb) produced by 8.4 billion birds in 2001. Most of the Texas poultry farms are located near the lignite seam belt. For example, one broiler integrator located in Brazos County, Texas processes more than 50 million broilers per year. Most of their broiler houses are located within a 113 km (70-mile) radius of their feed mill in Franklin, Robertson County. Texas ranked sixth in the nation with an estimated total production of 566 million broilers in 2001 (USDA, 2002). Manure

excreted by the birds is mixed with feathers, feed, water, and bedding material, such as saw dust, rice, or peanut hulls. With an average litter production of 1.25 tons per 1000 birds sold (NRAES, 1999) more than 700,000 tons of broiler litter (LB) was produced in Texas in 2001. Although some LB is utilized as supplemental feed for cattle (McCaskey, 1995), a vast majority of the stockpiled or cleaned out litter is land applied as a fertilizer source for crops and pastures. Utilization and disposal of BL is a problem for poultry growing areas where soils exhibit high levels of phosphorus (P). Repeated application of LB at rates above the nutrient intake of plants has the potential for nitrogen (N) and P pollution of surface and ground water (Beauchemin et. al, 1996). Additionally, due to the bulkiness of BL, transportation costs to distant crop and pasturelands may be economically prohibitive. If stockpiled on the farm for longer time periods, excessive odors and ammonia emissions from wetting and drying of LB exposed to precipitation are a concern. Providing extra storage spaces and covers for stockpiling LB on farm are also costly.

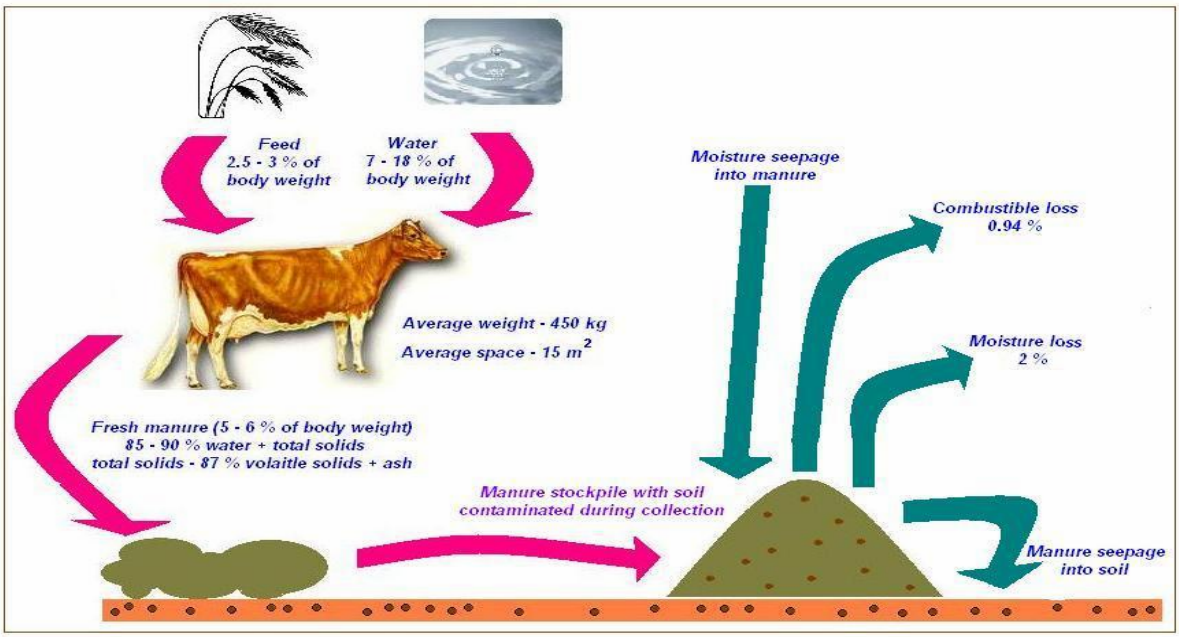

Figure 1.2: A Schematic 450 kg (1000 lb) Cattle Waste Production: Excretion to collection (www.dpi.qld.gov.au/environment/5166.html)

Although land application of manure is the preferred solution, manure is a dilute nutrient and transportation costs increase with handling distance. Beyond a certain radius, manure cannot compete with commercial fertilizer as a nutrient. Some landowners are not willing to accept the use of confinement facility manure as fertilizer due to cost or contaminants such as weed seeds, and finding enough land near the facilities to spread manure each year is a continued management challenge. At high rates of land application, water and air quality problems become more serious.

Manure (FB or LB) releases gases that can cause air pollution. In particular, manure is known to release CH_4 and CO_2, which have been identified as two of the most important gases in global warming. Improperly handled manure is also breeding ground for flies and contains pathogenic bacteria. When the manure gets very wet, the cattle expend more energy moving around in their pens, and gain weight at a slower rate (Hutchinson *et al*., 1995). When the manure gets very dry, the cattle's feet grind the dry manure, creating a dust problem. The total suspended particles (TSP) in feedlot dust can range from 150-260 $\mu g/m^3$ (CA) to 400 $\mu g/m^3$ (TX). Average units have values exceeding 1,000 400 $\mu g/m^3$ (Sweeten et al, 1988) Particulate matter (PM) or dust from feedlot ranges from 8.5 to 12 microns. The PM 10 regulation requires concentration of particles less than 10

μm should be less than 150 μg/m^3. High levels of dust also irritate cattle, resulting in slower weight gain, occasionally pneumonia.

Alternatives to land application of cattle manure may become more attractive as trends continue toward: increased feedlot capacity in the Texas High Plains (1-3 % per year increase), reduced irrigation water availability in the Southern Great Plains, reduced manure nutrient uptake from dry land crops or range grasses vs. irrigated crops, increased feedstuffs importation from the Midwest, and EPA regulatory criteria that limit phosphorus (P) application rates and accumulation in soils.

Figure 1.3: Manure stockpiles in Amarillo, Texas

In many places, the manure is piled into large stockpiles (figure 1.3). A stockpile is the worst method for dealing with the problems of manure disposal. In stockpiles, the insulation provided by the manure allows temperatures to rise, and smoldering or spontaneous combustion can result in stockpile fires. Stockpile fires emit air contaminants and are very hard to put out. Runoff from stockpiles in the event of heavy rains must be collected in holding ponds. Over time, the manure in stockpiles looses its value as a fertilizer, and cannot be easily disposed because it still retains its high phosphorus content with low nitrogen.

A viable solution to the disposal problem is to use the feedlot and litter biomass as fuel for energy conversion. Cattle manure has been considered as a potential energy feedstock for three or more decades through (a) thermal conversion (gasification at stoichiometric oxygen content, pyrolysis at oxygen-starved conditions, or combustion with excess oxygen), or (b) bioconversion (anaerobic digestion of slurry for methane production). Wide variability in feedlot biomass quality (heating value, carbon, etc.), high ash content (including salts, soil, and debris), and moisture has hampered pilot-scale research success and thwarted commercial ventures dealing with both bioconversion and thermal conversion. Sweeten *et al*., (1985) determined the energy or heating values (HV) and found that HV decreases with increase in ash and moisture content of in-situ feedlot biomass. Various technologies, which utilize feedlot biomass as a sole energy source, are summarized in tabular form in Annamalai *et al*. (1987). Prior research with feedlot biomass combustion in the 1980's and 1990's was conducted in circulating and conventional fluidized bed combustors (Sweeten *et al*., 1986, Annamalai *et al*., 1987). Some of these technologies have met with limited technical success. The limitations were primarily due to relying on manure as the sole-source of fuel, despite the highly variable properties (i.e. ash percentage, moisture percentage, salts, etc.) of manure and the associated flame stability problems. Improved manure handling methods (collection, storage, processing, and preparation) are needed to improve homogeneity and optimize energy value while minimizing handling costs and on-site storage requirements. Another technology used for the reduction of feedlot waste is anaerobic digestion. Unfortunately, anaerobic digestion is a slow process that results in the release of emissions over a longer period of time. Anaerobic digestion also requires liquefaction, the

use of precious water, difficulty in transporting digested slurry, and the ash content of the leftover solids poses chronic mechanical problems.

Cofiring

Most of these problems could be eliminated by blending waste/biomass with coal and firing it in existing suspension fired boiler burners since feedlot and litter waste could be readily combusted in the presence of high heat value coal (Annamalai *et al*., 1997, Frazzitta *et al*., 1999). *A blend instead of a solitary fuel may be used due to high variability and high moisture content of animal waste and the possibility of immediate transfer of technology*. Other biomass co-firing experiments include: wood waste (Gold *et al*., 1996), switch-grass in pulverized coal boiler (Aerts *et al.*, 1997), straw (Hansen *et al*., 1998), sewage sludge and tire derived fuels (Abbas *et al*., 1994), and grass (Spliethoff, 1998). Sami *et al*. (2001) have reviewed other cofiring experiments. The review summarizes various biomass fuels, their properties, their combustion behavior, existing literature on co-firing, fundamental concepts related to coal: biomass blend combustion, and modeling studies. Apart from the disposal of waste, other advantages of cofiring biomass with coal are: i) energy conversion to useful form, ii) reduction of fossil fuel based CO_2, iii) reduction in NO_x, iv) reduction in fuel cost, v) minimization of waste and reduction in soil/water and air pollution, vi) possible use as reburn fuel, vii) improvement of hygienic conditions through reduction of pathogens, worm eggs, flies, environmental protection of soil, water, air and vegetation, viii) reduction of anaerobic release of CH_4, NH_3, H_2S, amides, volatile organic acids, mercaptans, esters, and other chemicals, ix) additional income sources, and x) great potential for immediate commercialization. Since the animal waste originates from feed ration (a biomass) and can be used as a fuel, the cattle waste will be henceforth re-termed as feedlot biomass (FB) and chicken and broiler waste as litter biomass (LB). However, FB (2-2.5 % N, 0.8-1 % P, and 1.5-2 % K on a dry weight basis) and LB (2.9 % N, 6.6 % P, and 5.5 % K on a dry weight basis) may cause emission and fouling problems. The LB, as seen later, may result in more problems compared to cattle manure. The melting point of the dissolved ash is also low which causes fouling and slagging problems. Table 1.1 presents melting point temperatures (TMP) and boiling point temperatures (TBP) of typical components of interest in ash.

Table 1.1: The TMP and TBP of Ash Components

Inorganic	TMP, K (°F)	TBP, K (°F)
Aluminum Al_2O_3	2303.15 K (3686 °F) 2318.15 K (3713 °F)	3253.15 K (5396 °F)
Calcium CaO	2843.15 K (4658 °F) (2853.15 K (4676 °F))	3123.15 K (5162 °F)
Iron Fe_2O_3	1811.15 K (2800.4 °F) (1838.15 K (2849 °F))	
Magnesium MgO	3073.15 K (5072 °F)	3873.15 K (6512 °F)
Manganese MnO	1353.15 K (1976 °F)	
Phosphorus P_2O_5	613.15 K (644 °F) Subl. Temp – 633.15 K (680 ºF)	
Potassium K_2O Volatile oxide	decomposes at 623.15 K (662 °F)	< 1373.15 K (2012 °F)
Potassium carbonate K_2CO_3	1164.15 K (1635.8 ºF)	
Silicon SiO_2	1983.15 K (3110 °F)	2503.15 K (4046 °F)
Sodium Na_2O Volatile oxide	Decomposed > 673.15 K (752 °F) Sublimated at 1548.15 K (2327 °F)	< 1373.15 K (2012 °F)
Sodium Carbonate, Na_2CO_3	1124.15 K (1563.8 °F)	
Sulfur SO_3	289.95 K (62.24 °F)	317.95 K (112.64 °F)
Titanium oxide	1973.15 K (3092 °F)	> 3273.15 K (5432 °F)

(www.chemfinder.com, www.abcr.de, Merck Index)

Reburn

The NO_x generated from fuel N is called fuel NO_x, and NO_x formed from the N_2 in air is called thermal NO_x. Typically, 75 % of NO_x in boiler burners is from fuel N. Since NO_x, is a precursor of smog, it is regulated to be reduced to 0.172-0.198 kg/GJ (0.40-0.46 lb/mmBtu) for wall fired and tangentially fired units under the Clean Air Act Amendments (CAAA). In Sweden and in some states in the U.S.A. (e.g., California), the standards are even more stringent, limiting the emissions to 0.05 kg/GJ (0.116 lb/mmBtu). The current technologies developed for reducing NO_x include: combustion controls (e.g. staged combustion, low NO_x burners or LNB, reburn) and post combustion controls (e.g. Selective Non-Catalytic Reduction, SNCR using urea, etc.). In reburning, additional fuel (coal or natural gas) is injected down stream from the primary combustion zone to create a fuel rich zone where NO_x is reduced through reactions with hydrocarbons. The nitrogen in the reburn fuel then recombines with oxygen to form NO_x, or combines with N to form N_2. After the reburn zone, additional air is injected in the burnout zone to complete the combustion process. A diagram of the reburn process with the different combustion zones is shown in figure 1.4. The reburn process is somewhat similar to air staging where the fuel is first burnt in a rich primary zone to minimize the production of NO_x, and later air is injected to complete the combustion process.

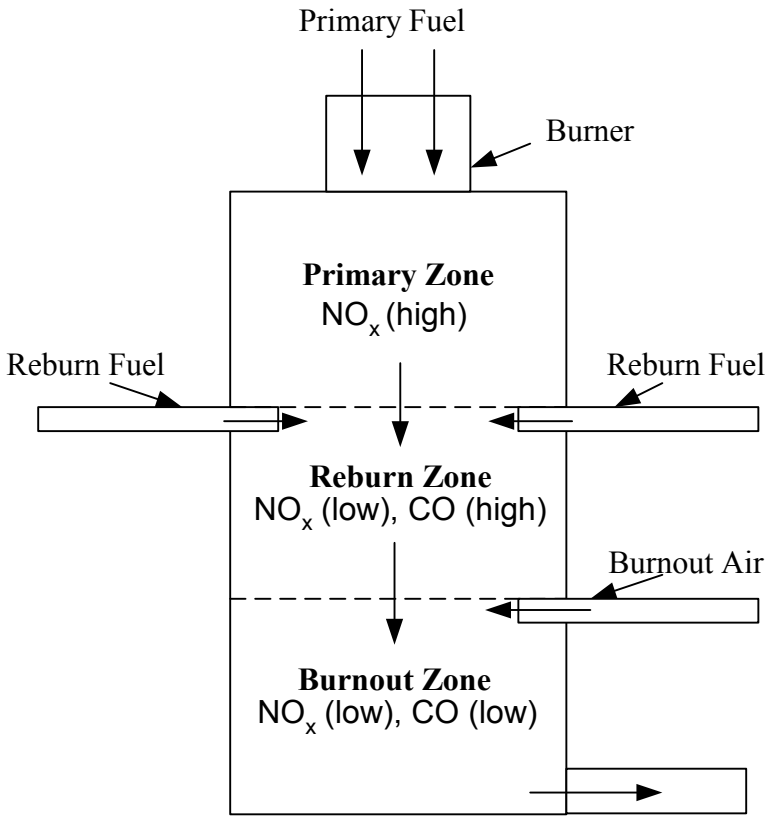

Figure 1.4: Reburn for Downward Fired Units

Table 1.2 provides an overview of some of the selected literature on co-firing, and table 1.3 shows an overview of current pilot data on degree of NO_x reduction achieved with various fuels. It is seen that there is no literature on using FB and LB as reburn fuels. Thus this project has explored FB, LB, blends of coal with FB (CFB), and blends of coal with LB (CLB) as reburn fuels for reduction of NO_x.

Gasification

The cofiring approach in existing suspension fired burners and as reburn fuel requires grinding of high ash, high moisture, and fibrous biomass almost to the same fineness as coal. The gasification approach does not require fine grinding and further the gases can be used as fuel either in boilers or in gas turbines. There is extensive literature on coal and biomass gasification.

Coal: Since commercial coal-gasification has been in use since 1830 (Stassen, 1995) an extensive experimental and simulation work has been done in this area (Cooper, *et al.*, 1984, Smoot, *et al.*, 1985, Nowacki 1980, and Hobbs, 1990). However, the study of particle sizes in the fixed bed gasification range (10-100 mm (0.4-4.0") particle size) is scarce (Hobbs, *et al*., 1990), as most of the study has been done for fluidized bed gasification of coal.

Biomass: Fixed bed gasification studies on a small scale have been conducted for various biomasses like beech wood, nutshells, olive husks (Blasi, *et al.*, 1999), cotton stalks (Patil, *et al.*, 1993), rice husk (Jain, *et al.*, 2000, Fang, *et al.*, 1998), pigeon pea stalk (Katyal, *et, al.*, 2000), wood chips, coconut fiber, dried leaves (Krishnamoorthy, *et al.*, 1989), and bundled jute sticks (Kayal, *et al.*, 1994).

Although active research is being done on fixed bed gasification of biomass, there is very little open literature data on fixed bed air gasification of feedlot biomass and chicken litter biomass. Krishnamoorthy, *et al.*, (1989) have studied the gasification of cattle waste briquettes in 6.0 kg/hr (13.2 lb/hr) and 25.0 kg/hr (55.1 lb/hr) fuel feed rate updraft gasifiers. There is no data about the product-gas species composition and the temperature variation along the fuel bed. Jones, *et al*., (1999) have studied the catalytic steam gasification of broiler litter at high pressure, in which steam is used as a source of oxygen and an alkali metal is used as a catalyst for gasification process. Since, the main goal of the study was to determine the technical feasibility of the process for using LB as the fuel there is no fundamental data, which can be used to understand the behavior of the fuel under gasification conditions.

Table 1.2: Literature Review on Reburn using fossil and biomass fuels

Author	Reburn Fuel	Reburn Min Stoichiometric Ratio (SR)	Particle size	Temp	Residence time	Burnout zone	Max Reduction	Conclusion
Adams *et al*, 1998	Wood	0.9	0.8-1.6 mm (1/32-1/16“)	1643 K (2498 °F)	0.4 to 1.2 s	YES	55%	Wood can successfully used a reburn fuel in a cyclone combustor
Bilbao *et al*, 1994	Natural Gas	N/A	Gas	1473-1773 K (2192-2732 °F)	98-280 ms	NO	<90%	Found that high temperature and low oxygen are good for NO reduction
Bilbao *et al*, 1995	Natural Gas	0.94	Gas	1473-1773 K (2192-2732 °F)	95-280 ms	YES	95%	Successful reburn at temperatures above 1200°C
Bilbao *et al*, 1997	Natural gas, methane, ethane	0.93	Gas	1373 K (2012 °F)	220 ms	NO	87.5%	Reburning with natural gas most effective at 0.93 SR
Chen *et al* 1996	Coal, and coal char	0.8 for those that reached a min	NA	1373 K (2012 °F)	0.2 s	NO	80-95%	Heterogeneous mechanisms accounted for the majority of the NO_x reduction, chars can be used in reburning
Kicherer *et al*. 1993	Coal, natural gas straw, light fuel oil	Min at 0.76, but little change after 0.85~0.9	2, 15, 30, 40 wt % <90 µm	NA	0.5 to 1.3 s, NO continually decreasing	YES	77.6%	To maximize NO reduction: small particles, high volatile fuel, long residence time, good mixing
Malay, P. *et al*, 1999	Natural gas, coal, pond fines, Refuge Derived Fuel (RDF), Orimulsion, and wood		~200 µm	1703.15 K (2606 °F)	0.2 to 0.9 s	YES	70-95%	Alternate fuels can be more effective than reburning with natural gas
Miller *et al*, 1996	Tire Derived Fuel TDF), and Natural gas	NA	< 6.4 mm (0.25”)	1093-1533 K (1508-2300 °F)	NA	YES	63%	TDF can be used successfully as a reburn fuel
Smart, J. *et al* 1994	Coal, Fuel oil, natural gas, and Coke oven gas	0.81	95% < 75 µm	1423-1523 K (2102-2282 °F)	NA	YES	88.7%	NOx reduction and the burnout were not greatly affected by the fuel type
Spliethoff *et al*, 1996	Coal, pyrolysis gas, and methane	0.8~.85	0.5% > 90 µm	1273-1673 K (1832-2552 °F)	0.2 to 2	YES	87.5%	Pyrolysis gas the best, longer residence time a lower NO_x concentration
Yang *et al* 1997	Coal	< 0.92	75% < 63 µm and 100%< 63 µm	1598 K (2417 °F)	120-840 ms, no effect beyond 450 ms	YES	65%	The reburn stoichiometry is the most important factor, fuel N content does not have a large effect on burn out NO

Table 1.3: % Reduction in NOx: Demonstration and/or Operating Reburn Installations on Coal-Fired Boilers in the United States (DOE, 1999)

#	Type of Burner	% Reburn Heat in	% Reduction	NO_x with Reburn kg/GJ (lb/mmBtu)
1	Gas Reburning			
	Tangential	18	50-67	0.11 (0.26)
	Cyclone	20-23	58-60	0.17-0.24 (0.4-0.56)
	Wall without LNB	18	63	0.16 (0.37)
2	Coal Reburning			
	Cyclone(micronized)	30 (17)	52 (57)	0.39 (0.91)
	Tangential(micron)with LNB	14	28	0.11 (0.26)

Coal and biomass blends**:** Updraft gasifiers capable of handling peat and biomass (wood and municipal sludge waste (MSW)) have already reached commercial levels (Kurkela *et al*., 1989). Collot *et al.* (1999) have studied the high pressure fixed bed co-gasification of 50:50 (%w/w) mixture of coal and silver birch wood in CO_2 and suggested that the mineral matter in biomass can play a catalytic role in coal char combustion. On the contrary, there is no open literature data available regarding the gasification of coal: feedlot biomass blends (CFB), and coal and chicken litter: biomass blends (CLB). Thus, it is hoped that the fundamental research conducted for the above-mentioned fuels shall be able to generate sufficient data to have a better understanding about the gasification characteristics of these fuels.

Loison (1966) has given the typical volatile matter release from the devolatilization of coal. Raman *et al*. (1981b) have given the devolatilization product distribution for FB at 983 K (1309.73 ºF). The results are shown in table 1.4. In table 1.4, the case for feedlot biomass, the product distribution consists mainly of the primary devolatilization reaction. The secondary reactions involving tar and char are low because of the low peak temperature during the devolatilization process. From table 1.4 it can be observed that for feedlot biomass the CO_2 release is much higher than that observed for coal, but at the same time for coal the CH_4 release seems to high compared to feedlot biomass. This might affect the product composition of the gas leaving the gasifier.

Objectives:

The review revealed that there is limited data on cofiring with FB and LB, gasification with FB and LB, no data on reburn with FB and LB. The overall objectives of the Texas A&M University project is to address the research aspects of combustion of feedlot biomass (FB) and litter biomass (LB) with coal and generate a data base on the thermo-chemical energy conversion technology for FB and LB fuels as, a) co-fired fuel, b) reburn fuel for reduction of NO_x, and c) fuel in fixed bed gasifiers. In order to achieve the overall objective, the following experimental and theoretical tasks were performed:

Task 1: Fundamental experiments on fuel characterization and combustion studies

Task 2: Boiler burner experiments for cofiring of CFB and CLB fuels and reburn tests

Task 3: Fixed bed studies on CFL and CLB fuels

Task 4: Numerical modeling of pulverized fuel (pf) fired burners and reburn systems

Task 5: Fuel collection, transportation, and economic analyses of FB and LB fuels

Table 1.4: Pyrolysis product distribution for coal and feedlot biomass

Species	Coal (% wt)	Feedlot biomass (% wt)
Water	23	59.4 (water + tar + oil)
Tar + Oil	20	
Gas	57	40.6
Dry gas composition	Coal (% vol.)	Feedlot biomass (% vol.)
CO	20.0	16.0
CO_2	6.1	38.9
H_2	13.1	8.6
CH_4	50.3	12.9
C_2H_4	--	0.3
C_2H_6	--	1.8
$H_2S + NH_3$	9.9	--
		--
N_2	--	10.9

The report is organized as follows. An executive summary will be given followed by experimental set-up for all tasks, results and discussion for the tasks completed, and summary of findings.

2. Executive Summary

Totally, about 910 million wet (excreta) tons of collectible animal manure (cattle, poultry, hogs, sheep) are produced annually in the U.S., whereas approximately 110 million wet tons of animal manure are produced in Texas (http://www.scorecard.org). Approximately 90 % of this manure are water and the rest dry solids. The overall goal of the project by Texas A&M University is to address the research aspects of combustion of feedlot biomass (FB) and litter biomass (LB) with coal and generate a data base on the thermo-chemical energy conversion technology for FB and LB fuels as a) co-fired fuel, b) reburn fuel for reduction of NO_x, and c) fuel in fixed bed gasifiers. The report presents data on fuel characteristics, emission data on co-firing generated by 30 kW_t (100,000 Btu/hr) pulverized fuel (pf) fired boiler burner facility, reburn results in the modified 30 kW_t (100,000 Btu/hr) facility, data on gasification of LB and FB, and numerical results obtained for cofiring of coal: LB blends using the PCGC2 combustion code and for reburn generated with zero dimensional reburn model.

Fuel Properties: The FB can be classified as raw manure (RM, 1 day old), partially composted (PC, 30 days old) and finished composted (FiC, 120 days old). It was found that FB-PC has approximately half the Btu content of coal, twice the volatile matter of coal on a dry ash free basis, four times the N content of coal on heat basis, and due to soil contamination during collection the ash content is almost 9-10 times that of low ash (5 %) coal. The energy potential of FB diminished with composting time and storage; but the DAF HHV is almost constant for ration, FB-raw, PC, and FiC at about 19,500 kJ/kg (8,400 Btu/lb) while that for Wyoming coal DAF heating value of 30140 kJ/kg (12,960 Btu/lb). The N and S contents increase from 1.8 to 2.4 kg/GJ (4.2 to 5.6 lb/mmBtu) and 0.6 to 0.9 kg/GJ (1.4 to 2.1 lb/mmBtu) with composting of FB while for coal the N and S contents are 0.4 kg/GJ (0.9 lb per mmBtu) and 0.2 kg/GJ (0.4 lb per mmBtu) respectively. Based on heating values and alkaline oxides, FB-PC seems preferable compared to RM and FiC. The TGA analyses indicate that FB starts pyrolysis at about 273 °C (523 °F) while coal pyrolyses at a higher temperature of 377 °C (711 °F). While coal sample ignited in air at 325 ºC (617 ºF) due to high char content, the biomass did not ignite under TGA conditions. The parallel reaction model and single reaction pyrolysis model were used to obtain kinetics of pyrolysis. Compared to SPS Wyoming coal ash, mineral analysis of feedlot biomass ash showed the latter is higher in Na, Mg, Si, and K, but is lower in Al, S, Ca, Ti, and Fe.

Analyses were performed on as excreted broiler manure (EM), cleanout litter (CL), and dry litter (DL), to determine fuel quality and characteristics. CL typically has moisture content of 26 % and they are dried to about 11 % and called DL. The heating values ranged from 9,550 kJ/kg (4,105 Btu/lb) for EM, 14269 kJ/kg (6130 Btu/lb) for CL, 19600 kJ/kg (5187 Btu/lb) for DL while dry ash free (DAF) heating values remained at about from 19350 kJ/kg (8300 Btu/lb). The DAF heating value of LB is comparable to FB but lower compared to DAF heating value of Wyoming coal. The N and S content in DL are 2.5 kg/GJ (5.8 lb/mmBtu). The ash composition indicates likely fouling and corrosion problems in burners due to higher volatile oxide composition as compared to coal.

Cofiring Data: The cofiring experiments were performed with 90:10 coal: FB blend (96:4 on a heat basis) using 30 kW_t (100,000 Btu/hr) boiler burner facility. The results revealed that the blend burns more completely in the boiler, due to the earlier release of biomass volatiles and higher amount of volatile matter. The NO_x emission for the short reactor for coal was 290 ppm, 0.16 kg/GJ (0.38 lb/mmBtu) and 260 ppm, 0.15 kg/GJ (0.34 lb/mmBtu) for the 90:10 coal: FB blends at 10 % excess air. Even though the effective N content of the blend increased by 18 %, compared to coal, the NO_x emission decreased, it could be attributed to the higher VM of FB and more N in the form of NH_3. The NO_x emission for 90:10 coals: LB blend remained at about 0.15 kg/GJ (0.34 lb/mmBtu) for the 90:10 blends at 10 % excess air. Further the effects of swirl number, simulated moisture content, FB and LB particle size, and fuel loading ratio on the transport line were investigated.

Reburn Data: the 30 kW_t boiler burner was finally modified with a NH_3 doped propane flame with 5 % excess air in order to produce a NO_x level of 600 ppm in the primary flame. The results

indicated a 75 % reduction when using pure biomass vs. 30 % for coal at reburn equivalence ratio of 1.05. Both FB and LB are more effective reburn fuels than coal, potentially due to their high volatile matter content, and fuel nitrogen dominantly in the form of urea/NH_3. Further the results are almost independent of reburn zone stoichiometry from SR =1 to 0.9. Due to lower P content, the FB could serve as an effective reburn fuel.

Gasification Studies: A 10 kW_t (34,000 Btu/hr), fixed-bed gasifier (reactor internal diameter 0.15 m (6"), reactor height 0.30 m (12")) facility was built and fired with a) coal, b) advanced feedlot biomass (AFB), c) chicken litter biomass (LB), d) high ash feedlot biomass (HFB), and e) coal: FB blend (CFB). The parametric studies include the effect of fuel particle size (0.52 mm (0.02") and 9.5 mm (0.37")), and the air flow rate (1.28 and 1.70 SCMH (45 and 60 SCFH)) on the gasification characteristics of the fuels. A summary of the results is as follows: the peak temperature in the bed was about 1500 K (2240.33 ºF) for coal (4.28 % ash), 1350 K (1970.33 ºF) for FB (14.83 % ash), and 1200 K (1700°F) for LB (43.85 % ash), correlating the decreased peak temperature with increased ash content. The gasification of coal, FB, and LB yielded the gas composition as CH_4 (%): 2.5, 1.8, 1.0; CO (%): 27.9, 29.1, 29.1; and H_2: 8.5, 8.0, 7.0. The heating value of the product gas was about 5.0 MJ/m^3 (135 Btu/SCF) for coal, 4.8 MJ/m^3 (130 Btu/SCF) for FB, and 4.5 MJ/m^3 (120 Btu/SCF) for LB. The LB (18.9 % (Na_2O + K_2O) in ash) showed consistent bed agglomeration, while FB (7.03 %) showed a reduced tendency for agglomeration, and coal (1.98 %) exhibited no agglomeration in the bed. Based on the current gasification study FB is preferred compared to LB, since the former has a lesser tendency to agglomerate.

Modeling of pulverized fuel (pf) fired burners: Numerical computations were carried out by modifying axisymmetric 2 Dimensional PCGC2 with moisture and P oxidation models and 3 mixture fraction (primary air, fuel off gas, moisture) to simulate co-firing of coal:LB blends. At temperatures less than 1400 K (2060.33 ºF), phosphorus mainly takes the form of P_4O_{10}. At high temperature around 2000 K (3140.33 ºF), P_4O_{10} is negligible while PO_2 is the main phosphorous product. PO_2 is unimportant in pre-flame region but has high concentration in post flame region. The exit PO_2 level is high (e.g., around 300 ppm for 90:10 coal-LB blend) while P_4O_{10} is negligible (less than 10 ppm for 90:10 coal-LB blend). The increasing in moisture content delays pyrolysis and char combustion causing longer flame length and lower burnout. The increase of swirl number from 0.7 to 1 leads to stronger flow recirculation and air-fuel mixing, a shorter flame length, decreased CO emission and increased NO due to better air-fuel mixing. As excess air increases, burnout increases in post-flame region, NO increases, CO decreases P_4O_{10} increases and PO_2 decreases.

A simplified **zero-dimensional reburn model** has been developed for estimating the NO_x reduction with any solid fuel as reburn fuel, along with more detailed heterogeneous char reactions and homogeneous global reactions. The experimental reburn data has been compared with predictions from zero dimensional model.

Economic Analyses: The economic analysis included cost of FB collection and transportation, cost saving for the plant, and ash produced for disposal or utilization. Collected manure from unpaved feedlots (UPFB or FB) and from flyash-paved feedlots (PFB or called as advanced feedlot biomass, AFB) was assumed to have 10 % moisture in both cases and ash contents of 47.4 % and 15 %, respectively. Results showed that the use of UPFB resulted in a fuel cost reduction of 1.7 % as compared to coal firing only, whereas PFB reduced annual fuel cost by 4.7 %. The CO_2 emissions were projected to be 5.7 % less for the UPFB blend than for coal as the only fuel. Economical hauling distance was estimated to be about double for the FB (~ 193 km (120 miles)) than for the AFB (~ 100 km (62 miles)). The results of the LB analysis show that the use of the 90:10 coal: LB blend is similar in cost as compared to coal due to increased cleaning cost of the broiler house and truck transportation cost.

3. Experimental

The different experimental set ups located in the boiler burner laboratory at Texas A&M University are (a) cofiring (30 kW_t or 100,000 Btu/hr), (b) reburn (30 kW_t or 100,000 Btu/hr), (c) fixed bed gasification (10 kW_t or 34,000 Btu/hr), and (d) TGA analyzer. This section describes a brief overview of the various experimental set ups used to conduct the experimental studies. In addition, the biomass procurements and protocols for collection and sampling are also discussed.

3.1. Fundamental experiments on fuel characterization and combustion

Fundamental data on fuel properties were generated using ultimate and proximate analyses and thermo-gravimetric analyses (TGA) in N_2 and air for FB and LB. Since FB promises to be a better fuel compared to LB, extensive analyses on FB were performed including the effects of composting process. More details are provided in Sweeten *et al*. (2003).

3.1.1. Feedlot Biomass for Cofiring and Reburn Applications

3.1.1a. Fuel Procurement

Arrangements were made with a commercial cattle feedlot and an adjacent commercial manure composting operation near Hereford, TX, to collect manure from two pens using wheel loaders, and to then compost the manure in two windrows of 136 Mg (150 tons) each with a Scarab composting unit. One windrow was prepared containing < 5 % admixed crop residues (cotton burs and hay on a volumetric ratio) and another windrow was prepared without added crop residues. Large 0.9 Mg (1 ton) samples of these materials were collected from each windrow on day-1 (raw FB or unprocessed manure, following an initial mixing only), day-31 (PC or FB-32), and day-125 (finished composted, or FiC or FB-125). Two bulk samples (three loader buckets equally spaced along the windrow) were extracted, loaded into a partitioned bobtail truck, hauled, and unloaded in storage under a shed.

3.1.1b. Fuel Protocol for Fuel Collection and Sampling

The protocol for manure collection and sampling was as follows:

Manure source. Typical well-drained feed-pens were selected at the commercial feed-yards in which cattle had been on a normal finishing ration. Relatively dry manure was harvested from the top 1/2 to 2/3 of the existing manure pack, with an effort to maintain an undisturbed manure pack of approximately 12.5-25 mm (1/2-1") to minimize ash (soil) entrainment. The pen numbers used for the source manure were recorded, along with animal numbers, weight, time of occupancy since last collection, and a printout of finishing ration.

Windrows. Upon removal, the manure was placed in two parallel windrows of normal cross-sectional size and at least 45 m (150 ft) long. One of the windrows was mixed with organic matter i.e. crops as a carbon source while the other windrow was mixed without crop residues. For the manure/carbon source windrow, the mixture was made following commercial compostor standard practice which involves ~5 % crop residue by volume. Crop residues included a small amount of cotton gin trash and forage sorghum straw but no inoculants were used. The estimated weight of manure in the windrows was about 3 Mg/m (1 ton/ft) running length.

Manure with crop residues. Manure that came out of two pens was placed into one windrow. The 45 m (150 ft) test section of the windrow had about 3/4 of a wheel loader bucket of cotton burs and 1/4 of a loader bucket of forage sorghum straw.

Manure with no crop residues. The manure-only windrow (45 m (150 ft)) contained manure from two adjacent pens.

Initial sampling. Within 24–48 hr of placement, both windrows were mixed once, and sampled by extracting a minimum of 15 sub-samples, mixing them, and then removing three composite sub-samples. Then a 1.9–2.3 m^3 (67-81 ft^3) sample weighing approximately 1.4 Mg (1 ton) was taken from each windrow by wheel loader. The large samples were taken with the wheel loader at three places equally spaced along the 45 m (150 ft) windrow section. The large bulk samples were placed in a bobtail truck with a partition to separate the two manure bulk samples and transported to the Texas Agricultural Experiment Station (TAES), James Bush Research Farm, Bushland, near Amarillo, for storage in a wooden bin inside an equipment shed.

Interim sampling. Both windrows were turned according to established practice by the commercial compostor. Immediately following the fourth turning, the windrows were again sampled.

Final sampling. When the compost site manager determined the two windrows ready for the final turning, he notified project personnel who sampled each windrow within 24 hr after the final turning.

Sample analysis. Manure sub-samples were analyzed for the following parameters: moisture, ash, higher heating value (HHV), total carbon, total nitrogen, sulfur, potassium, and sodium.

Shipment for combustion tests. Manure from the bulk samples stored at Bush Farm was reloaded in small drums for shipment to Vortec Industries for grinding and then to the National Energy Technology Laboratory (NETL), US Department of Energy, Pittsburgh, PA for pilot scale testing.

The 0.9 metric ton (1 ton) samples hauled to Bushland, TX, were stored in pallet bins under equipment shed at TAES–Bush Farm, Bushland, TX. Sub-samples were taken and sent to two laboratories: Southwestern Public Service Company (SPS)/New Century Energies, Amarillo, TX, which conducted proximate and elemental analyses and to Commercial Testing and Engineering Co., (CTE), Denver, which provided the ultimate analyses.

Larger sub samples of 4.5 kg (10 lb) were collected and shipped periodically, from the bin-stored materials, for combustion testing at the 30 kW_t (100,000 Btu/hr) small-scale (150 mm (6 in) diameter) Texas A&M University Boiler Burner Laboratory, College Station and to USDOE–NETL for material handling and feeding tests leading to pilot test burn in the 0.480 m (19 in) diameter 150 kW_t (500,000 Btu/hr) pilot plant combustor at Pittsburgh.

The moisture content of the PC bulk manure samples at 30–32 % moisture were reduced by thin-bed drying in a greenhouse at USDA–ARS in Bushland. Previous records showed that the drying of FB does not cause significant loss in heating values (Rodriguez *et al*., 1998).

A 570 kg (1260 lb) sample of the PC manure without crop residues was prepared for the test burn at TAMU and DOE–NETL by (a) solar drying to 3 % (wb) moisture in a stirred thin-bed on a concrete floor of a greenhouse at Bushland, (b) containerized shipment to Vortek Industries, Long Beach, CA, (c) grinding to -50 mesh particle size, and (d) reshipment in metal drums to NETL in Pittsburgh. Similar steps in handling, preparation, and grinding (< 20 mesh) were applied to the Wyoming coal materials supplied by SPS, Amarillo. About 80 % of coal particles and 75 % of FB passed through a 74-μm (200 mesh) sieve. After arrival of the coal and manure samples at NETL, they were blended together in a 90:10 ratio (as-received weight basis) and mixed in a cement mixer. The blend was sealed in plastic bags and stored in sealed barrels prior to test firing during the pilot plant tests (Co-fire results from the NETL tests will not be reported in this report).

3.1.1c. Proximate and Ultimate Analyses of Ration and Fuel

Proximate analyses were conducted by SPS on feed bunk ration for cattle and 3 sub-samples taken from a composite of 20 or more random probes into the 150-ton windrows of test manure that were collected from typical, adjacent cattle pens. These initial samples were taken immediately after the first mixing with the Scarab composter (Day-1), but before pronounced heating occurred with the onset of composting. Ultimate analyses on FB were provided by CTE, which analyzed only one composite sample of the three sub samples submitted to SPS. Results are presented in Section 4.

3.1.2. Litter Biomass

3.1.2a. Fuel Procurement

A large broiler integrator was contacted in the study area in east central Texas to gather information on broiler production systems and to procure broiler litter and wood shaving samples for physical and chemical analyses. An interview with the firm personnel was arranged to learn the following details of the integrated operation and litter management practices.

Figure 3.1 shows components of an integrated broiler production system and the role of a firm in producing broiler meat for consumers. The firm owns breeder flocks, a hatchery, chicks, and a feed mill and is responsible for processing and marketing of a grown out flock. Contract growers receive hatched chicks, feed from the firm owned feed mill, bedding martial (pine shavings etc.), and any medication needed during a 7-week period of growing chickens to marketable weight in grower-owned broiler houses. Each broiler house with 2045 m^2 (22,000 ft^2) floor area is populated with 27,500 birds providing 0.24 m^2 (0.8 ft^2) per bird. A total of six flocks per year are grown in a broiler house. The bedding material (litter) used in these broiler houses is wood shavings from pine trees. Initially, litter (wood shavings) is placed on the dirt floor at a depth of about 150 mm (6”). The birds are then raised on the litter that accumulates excreta, feathers, water from the drinkers, and spilled feed. Complete clean out of the litter biomass (defined as litter plus excreta, moisture, feathers, and feed) is conducted once a year. Between flocks, the top 50 mm (2”) layer of litter biomass is scraped to remove “cake”, the excessively moist material around drinkers and feeders. Therefore, the physical and chemical properties of litter biomass may vary considerably with age, moisture content, amount of excreta, spilled feed, feathers, and any other waste material such as dirt from scraped floors during total cleanout.

Based upon the above information, it was decided to sample freshly-excreted manure (EM) without bedding, bedding material (wood shavings), cake, and cleaned out litter (CL), cleaned out litter dried to around 10 % moisture (DL), coal and a blend of 90 % coal and 10 % ground DL (C90:DL10) on a mass basis. DL was dried (to about 10 % moisture) for ease in grinding to a size less than 1 mm. Samples of all but cake and wood shavings were analyzed to determine heating values, moisture, ash, and proximate and ultimate analyses for these materials. Both cake and wood shavings were analyzed for moisture content only. Pine tree wood shavings were collected from the firm’s storage and distribution house and cake was collected from several recently removed piles between flocks. The CL was collected from a broiler house after removal of the caked material. The EM was collected at the Texas A&M University Poultry Science Research Center. The collection was performed by isolating chickens in a plastic bin without the bedding material and then collecting freshly excreted manure from the bin floor. The coal samples used in this project were Powder River basin coal from Wyoming, which is fired, in local power plants (TMPA, Excel Energy) due to its low sulfur content.

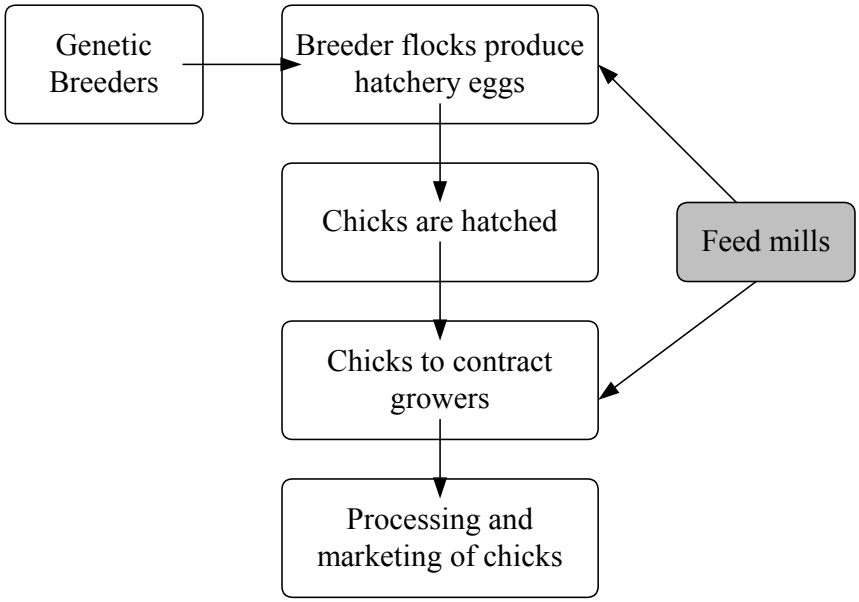

Figure 3.1: Components of a vertically integrated broiler production system

3.1.1b. Proximate and Ultimate Analyses of Ration and Fuel

CTE conducted the heating value, ash analysis, and ultimate and proximate analyses for all the fuels. All samples were air dried for 24-36 hr before delivery to the lab. Standard American Society for Testing and Materials (ASTM) methods were used by this laboratory for all analyses. The relevant standards are summarized in Table 3.1.

Table 3.1. ASTM coal and broiler litter analysis standards

Drying	D3173
C and H	D5373
N	D5373
S	D4239
ASH	D3174
Volatile matter	D3175
HHV	D5865
Ash analysis	Measured with atomic emission spectroscopy

Samples were ashed in air at 1023.15 K (1382 ºF) and ash constituents, sulfur (S), and metals were analyzed and reported as oxides. The higher or gross heating value (HHV) was determined with an adiabatic bomb calorimeter. Carbon (C), Hydrogen (H), Nitrogen (N), and Sulfur (S) were determined by combusting the sample at high temperature (1273.15-1623.15 K (1832-2462 ºF), depending upon the element) and measuring the off gases using analyzers specific to each element. Oxygen (O) was determined by difference (100-sum of % C, H, N, S, ash, and moisture). Moisture content of wood shavings, cake, and clean out litter was measured by drying to 378.15 °C (712.67 ºF), and then weighing using Standard Methods (APHA, 1995). Results are presented in Section 4.

3.1.3. Fuel Grinding and Sizing for Cofiring and Reburn

All of the fuels were ground by Vortek in Long Beach, California, and then shipped to Texas A&M in sealed barrels. Coal and biomass were size classified using a sieve shaker. The samples (45-55 g (0.09-0.11 lb)) were placed in the top sieve and the sieve shaker was run for 10 minutes. The sieve shaker used was a CE Tyler Roto-Tap model B. After 10 minutes the particles in the bottom collection pan were collected, the bottom of the bottom screen brushed off, and the sieves replaced. After 5 minutes of shaking, the particles in the bottom pan were weighted, and then combined with the previously collected particles. If the samples collected after 5 minutes were less than 0.5 g (0.001 lb), the sieving was stopped. If the collection pan contained more than 0.5 g (0.001 lb), the test was continued in 2 minutes intervals until less than 0.2 g (0.0004 lb) was collected in the bottom pan in a 2 minutes interval. When the sieving was completed, the contents of all the sieves were weighed to an accuracy of better than 0.01 g (0.00002 lb). The difference between the starting weight and the total weight at the end was added to the amount collected in the bottom pan as suggested by ASTM standards.

3.1.4. Fuel Procurement and properties of FB and LB for Gasification Studies

Excel Energy, Amarillo, Texas, supplied the Wyoming coal in 0.2 m^3 (5 gallon) capacity barrels in uncrushed form. The coal had to be crushed and sized into the two particle size ranges as described previously. Partially composted manure is the manure that has been collected from the cattle pens, processed, and matured for 30-45 days (Sweeten *et al*., 2003, Chen, 2001). The processing involved is the turning of the manure in the windrow using a rotating-drum compost turning machine at weekly or bi-weekly intervals. The fly ash surfaced feedlot biomass is the manure collected from feedlots which are fly ash surfaced, and this is a specially prepared manure as the ash constant in the manure is lower when compared to the soil surfaced feedlots (Annamalai *et al*., 2001). The feedlot biomass, both AFB (low ash, 15 %) and SFB (soil surfaced feedlot biomass, 56 %) were partially composted feedlot biomass and had to be specially dried in greenhouses to reduce the moisture content to about 10-12 % on weight basis. The manure was then sealed in metallic drum and shipped in uncrushed form to the laboratory at Texas A&M University. The manure had to be manually crushed and segregated into the size ranges.

The chicken litter biomass was collected from a local poultry farm located in Bryan Texas. Since the wet cake (litter around waterers) collected from the barn had very high moisture content, it had to be dried in a green house to reduce the moisture content to about 10 % on weight basis. In order to dry, the litter was shipped in sealed drums to Texas Agricultural Experiment Station (TAES), Amarillo, Texas, where they were dried in the green houses for three weeks. The dried chicken litter was crushed and sized in the same manner as the feedlot biomass. All the prepared and sized fuels were stored in sealed drums ready to be used for the experiments for studying their gasification characteristics.

Before using the fuels for gasification studies, it was essential to know the properties of the same. The fuels were analyzed and the proximate analysis, ultimate analyses were obtained. Results are presented in Section 4.

3.1.5. Thermo-Gravimetric Analysis

The TGA analyzer used was a TA instrument's 2960 Simultaneous DTA/TGA a schematic of which is shown in figure 3.2. The unit is equipped with a digital scale capable of measuring up to 0.35 kg (0.7 lb) to with 1 % accuracy, including the alumina sample cups. The heater is capable of variable heating rates from to 373.15 to 1273.15 K/min (671.67 to 2291.67 ºF/min), and air, oxygen, helium, or argon purge gas can be applied at rates up to 80 cm^3/min (4.88 in^3/min). The thermocouple was built into the metal bar supporting the sample cup holder.

The samples were pulverized, characterized, and sieved using a sieve shaker and divided into three size groups: $d_p < 45$ μm (0.0017"), 45 μm (0.0017") $< d_p < 75$ μm (0.0029") and $d_p > 75$ μm

(0.0029”), and an unsieved fourth group containing a distributed size as fired in a boiler burner. Samples of 25 mg (0.00005 lb) of specified size group were loaded into the TGA analyzer and the controller was programmed to the heat the sample from the ambient temperature at the rate of 283.15 to 1273.15 K/min (509.67 to 2291.67 ºF/min). Nitrogen was used as the purge gas. The mass-temperature vs. time traces were then recorded by the TGA analyzer. The analysis was repeated for the three size groups and finally on the unsieved fuels for coal, FB, and a 90:10 Coal:FB blend. Under identical conditions experiments were repeated using air as purging gas. The TGA experiments were run at a heating rate of 10 K/min (18 ºF/min).

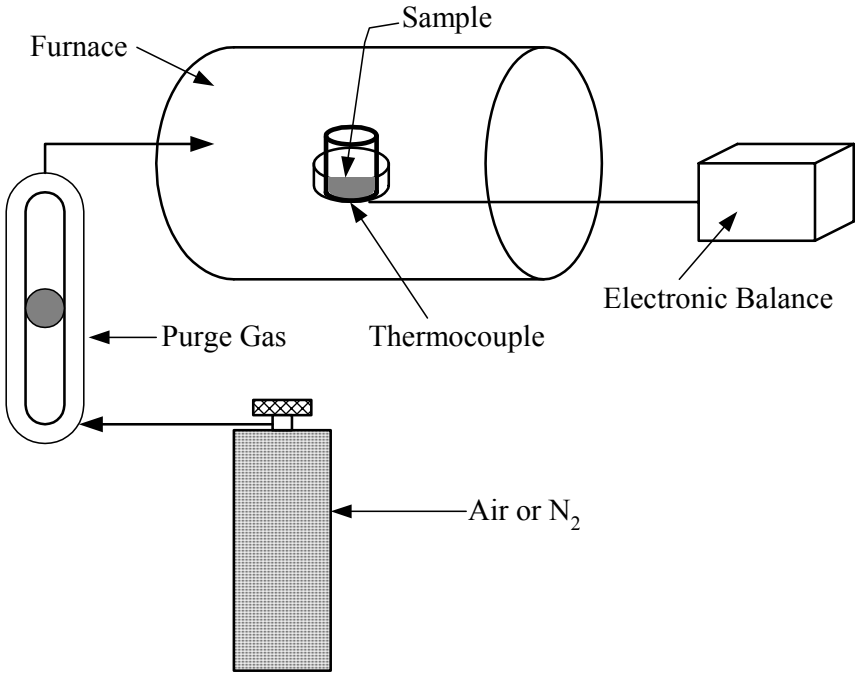

Figure 3.2: Schematic of the TGA setup

3.2. Boiler burner experimental set up

3.2.1. The 30 kW_t (100,000 Btu/hr) Cofired Boiler Burner Facility

The boiler burner facility used was a modified form of the previous boiler burner facility (Frazitta *et al.*, 1999). The previous boiler burner, made of a steel shell was modified with a ceramic walled refractory for higher temperature operation (Annamalai *et al* 2000a). The current boiler burner facility (TAMU, thermal rating of 30 kW (100,000 Btu/hr)) for firing either coal or coal:feedlot biomass fuel blends is shown in figure 3.3. The combustion air was supplied to the boiler burner (1) by a secondary air blower (2). The secondary air (80-90 % of total air) was preheated to a minimum of 473.15 K (392 ºF) with the use of a circulation heater (720 W (2456.7 Btu/hr)), (3), before it entered the boiler through a swirler (4). The fuel feed system was modified with a commercial Acrison volumetric feeding system (5), accurate to within 2 % for samples taken over a one-minute interval. The primary air (6) transports the fine fuel suspension injected through a Fox Venturi valve into the quarl (7) of the boiler burner. Dual water jets (8) injected water into the boiler to catch particulates and ash. The entire facility was operated from a central control panel (9). Gas analyses have been used to determine the combustion efficiency. The burner was fitted with two propane torches, which serve to preheat the boiler and initiate combustion.

The torch rating was approximately 1 % of the total burner rating, which ensured that the influence of the propane torch was negligible. The main furnace is 0.1524 m (6") in diameter, and is made of a 0.0508 m (2") silica ceramic shell surrounded by a 0.0508 m (2") thick silica fiber blanket and a 6.35 mm (0.25") steel shell. Temperature and species concentrations are obtained every 0.1526 m (6"). After the furnace gases have passed all of the sampling ports they are cooled by a water spray, and pumped out of the building through the exhaust system. The cooling water is drained off into a sump.

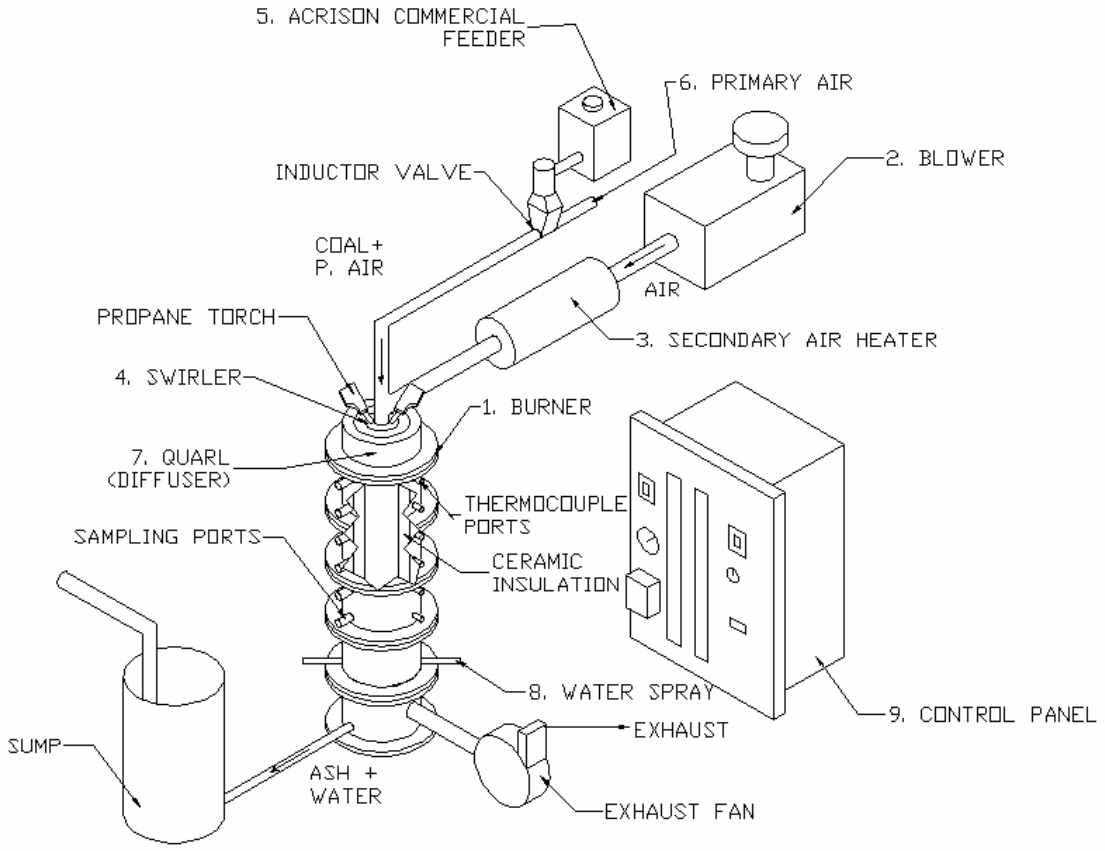

Figure 3.3: Pulverized fuel Boiler Burner Facility for Cofiring Coal: Feedlot/Litter Biomass fuels

Secondary air is injected co-axially with the primary air and the fuel but with a swirl motion. The formula suggested by Lawn (1987) was use to obtain a swirl number of 1.4 for this burner. A swirl number of 1.4 indicates a stable, well-defined recirculation zone inside the boiler burner. In addition to the swirler, a ceramic diffuser, or quarl is used to stabilize the flame. The quarl is made of silica ceramic and has a l/d ratio of 1.8 and a half angle of 24°.

The diagnostic system consisted of an orifice plate for measuring the secondary airflow rate, sheathed "type K" and "type S" thermocouples, in the boiler, the secondary air stream, and in the exhaust. A rotameter was employed to measure the primary airflow rate. Emission measurements were performed using an ENERAC 3000, and a Lancom 6500 emission measuring system, which use electrochemical cells as sensors. The system can measure five gases including SO_2, NO, NO_2, CO, and O_2. The probe also contained a "type K" thermocouple mounted at the tip for temperature measurements. Calibration gases were used to check the accuracy of the gas analyzer.

The experiments were conducted by first preheating the furnace with the secondary air preheater and propane torches for about 1 hour, and then firing the fuel. The secondary air heater was run for an

hour before the experiment was started. Once the secondary air reached a steady temperature (approximately 500 K (440.33 ºF)) the propane torches were ignited, and the cooling water was started. When the burner reached a steady temperature, usually about 15 minutes, the fuel was fed into the furnace. The furnace was allowed to run for 30 minutes before the first readings were taken. After 30 minutes of firing fuel, additional fuel was added to the hopper, and gas readings were taken. The readings were taken over 5 minutes intervals in each port, starting with the top port. At the bottom port, readings were taken for 10 minutes at 30 s intervals. After readings have been taken in all of the ports, the fuel flow was shut off, and the propane torches were purged of all remaining gas. Then the water-cooling spray was shut off, and ash samples were collected from the bottom of the furnace. Finally, all remaining equipment was turned off and exhaust fans set on high to cool the furnace.

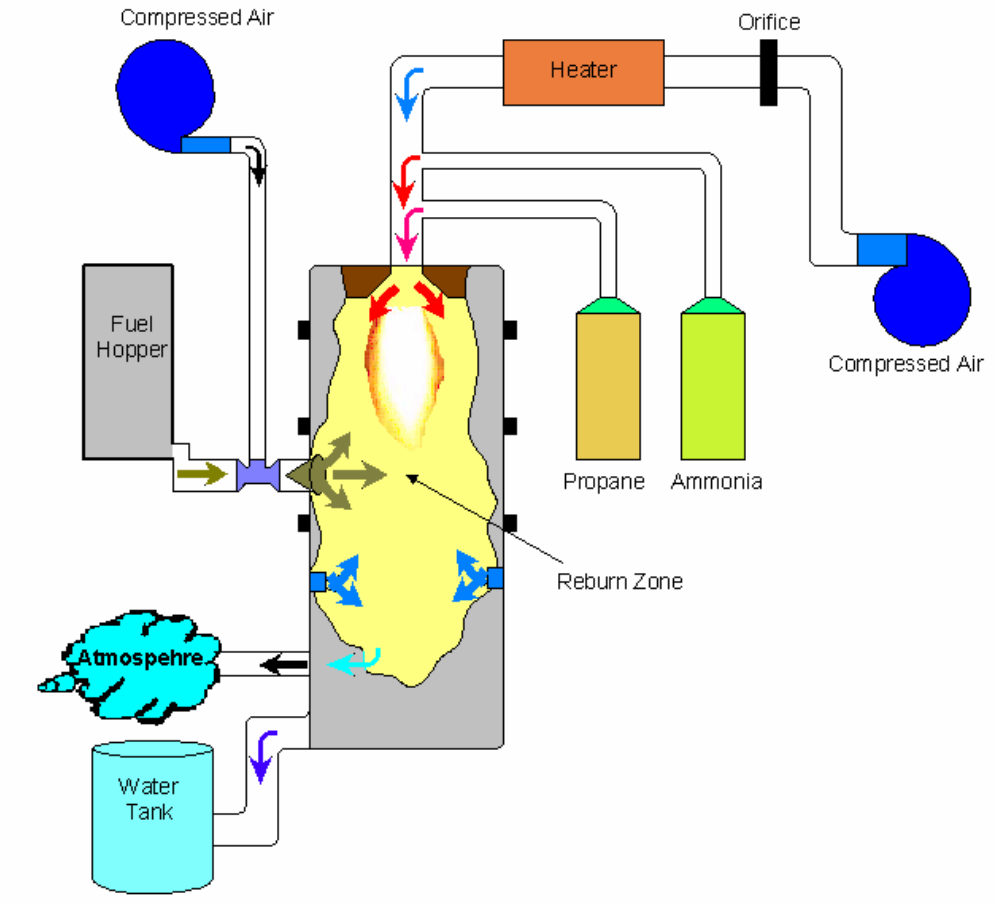

Figure 3.4: Reburn Schematic

3.2.2. The 30 kW_t (100,000 Btu/hr) A&M Reburn Facility

The experiments were conducted in the Texas A&M laboratory scale boiler burner that was modified for reburn experiments. Figures 3.4 shows the schematic of the reburn setup used for the experiments. A premixed propane burner is mounted at the top of the furnace to produce hot furnace gases to simulate the products of coal combustion. Ammonia is injected into the premixed propane fuel stream and burnt in the primary zone. The reburn fuel is fed from a dry-solid feeder (Acrison volumetric feeding system), via a venturi inductor value, and injected into the reburn boiler burner through the reburn

ports. The reburn injection ports are located below the tip of the premixed propane flame, after all of the NO has been formed in the primary zone. An Enerac 3000E gas analyzer is then used to measure the concentration of oxygen and NO in the final sampling port. After passing by the gas sampling port, the furnace gases are cooled by a water spray and exhausted out of the building. There is no burnout zone in the current boiler burner configuration.

For all of the experiments, the furnace was first allowed to preheat for one hour before the experiments were conducted. Then, the reburn air was adjusted to yield the appropriate exhaust O_2 percentage, and the ammonia was adjusted to yield 600 ppm NO in the furnace gases. When the air and the ammonia were adjusted to appropriate levels, the feeder was turned on and reburn fuel was injected into the furnace. When the NO reading leveled off (usually 5-10 min), it was then recorded. The reburning experiments were performed with coal, FB, LB, a 50:50 blend, and a 90:10 blend of each fuel (Thien *et al*., 2001b).

Results and discussion are presented in Section 4.

3.4. The 10 kW_t (30,000 Btu/hr) Gasification Facility

The development of the gasification facility required both designing, and fabrication of the whole unit. The setup contains a number of sub-systems like the gasifier (reactor), fuel storage and feeding system, heat recovery and cooling unit, gas sampling system, and control panel. The schematic layout of the setup is shown in figure 3.5 while detailed sectional view of the gasifier is shown in figure 3.6.

The entire system consists of the following sections:

a) Fuel storage and feeding system
b) Heat recovery and cooling unit
c) Gasifier
d) Control panel

A 10 kW_t fixed bed counter current atmospheric pressure gasifier was designed and fabricated which could gasify a range of biomass fuels. Figure 3.5 shows the schematic of the gasification set up. The core of the setup is an updraft gasifier. The total height of the gasifier is 0.75 m (29-5/8”). The gasifier is a cylindrical tube having an internal diameter of 0.343 m (13-1/2”). It is divided into 4 sections of 0.24 m (9-1/2”), 0.19 m (7-1/2”), 0.14 m (5-1/2”), and 0.15 m (6”) each. A two-stage insulation reduces the heat loss from the gasification zone. The inner insulation lining having a thickness of 50.8 mm (2”), (i.e. an inner and outer diameter of 139 mm (6”) and 179.8 m (10”) respectively) was made of castable alumna refractory. External to the inner layer is the layer of insulating blankets, which are wrapped around the inner layer and have a thickness of 44.5 mm (1-3/4”).

The grate, which supports the fuel in the bed, was made of high alumina castable refractory resistant to severe abrasion and resistant up to 1900 K (3400 ^oF) operating temperatures. The holes in the grate are 7.1 mm (0.281”) in diameter and are arranged in concentric circles for allowing the primary air to be fed into the reactor. The grate mounting mechanism enabled the grate to be easily removed and cleaned after every experiment. The plenum chamber is the zone under the grate. The primary air for gasification is supplied via a flow meter to the plenum chamber, from where it flows through the grate and into the combustion zone. The secondary air injection location is 641.4 mm (25-1/4”) above the base, where the excess or secondary air could be tangentially fed into the reactor. The fuel for gasification is stored in a hopper, and manually fed into the gasifier with the help of two sliding orifice gate valves. The fuel bed height inside the gasifier is maintained constant at around 171.5 mm ± 6.4 mm (6.75” ± 0.5”) above the grate throughout the operation. An induced suction blower located down stream of the exhaust enabled to maintain a slight vacuum pressure inside the gasifier preventing the leak of product gas from the gasifier into the laboratory.

Temperature profiles are measured by K type thermocouples at seven axial locations in the gasifier. There are six gas-sampling ports located axially above the grate of the gasifier. The product gas

was thoroughly cleaned and conditioned before being sent to the GC for analysis. The sample gas was cleaned by two disposable particle filter traps, cooled by two heat exchangers to condense the tar, and then dried by using nafion tubes before being stored for analysis. A HP 6980 gas chromatograph equipped with a TCD having a Carboxen-1000 stainless steel packed column was used for analyzing the product gas for the presence of permanent gases (CO, CO_2, H_2, N_2) and light hydrocarbons gases (CH_4, C_2H_4, C_2H_6).

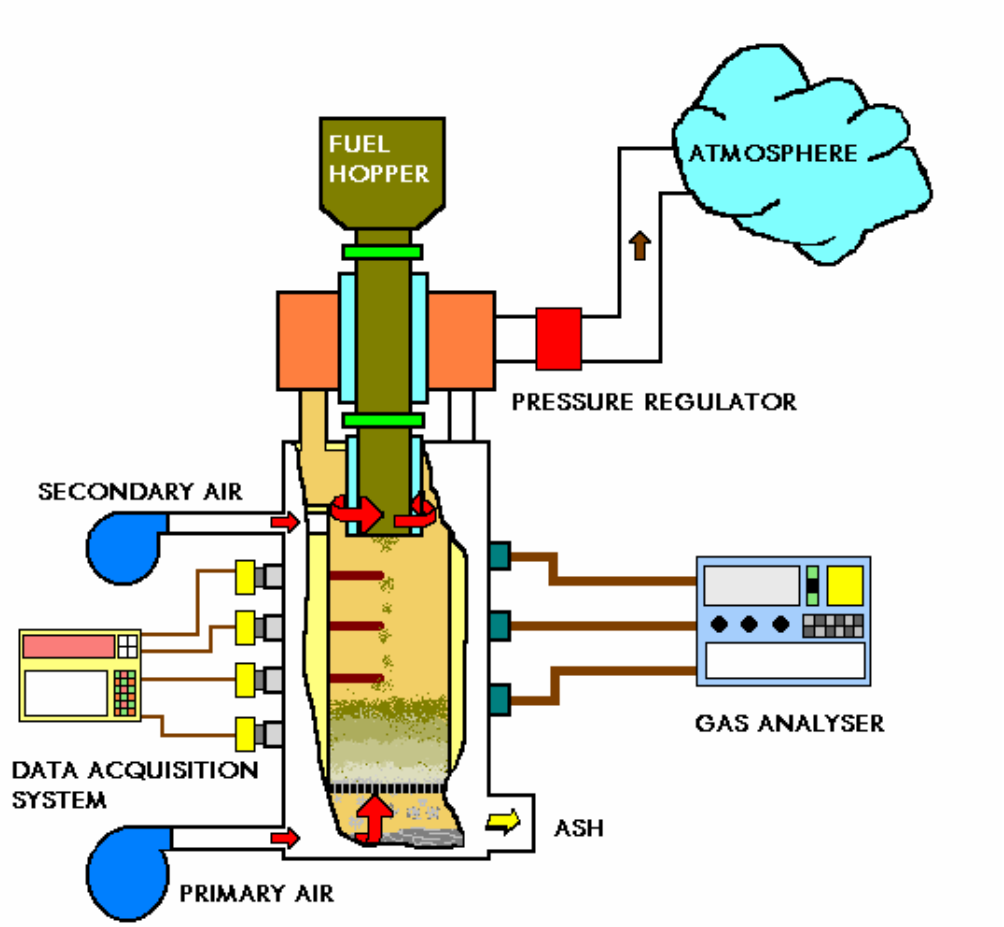

Figure 3.5: Schematic of the Gasification Setup

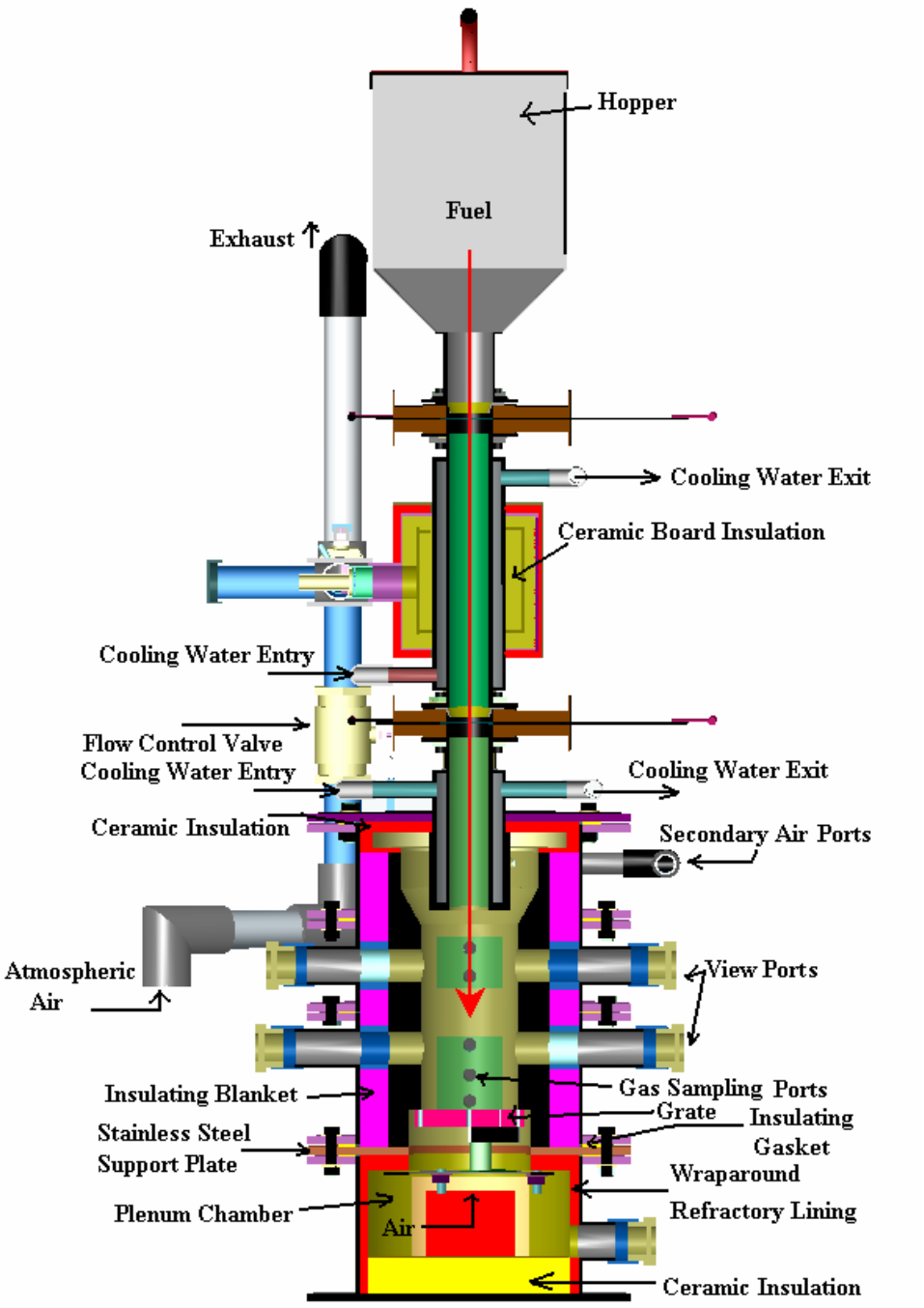

Figure 3.6: A Sectional View of the Gasification Setup

The gasification experiments were conducted in batch mode under two primary air flow rates: 1.27 and 1.70 m^3/hr (45 and 60 SCFH). Initially the fuel bed was empty and after regulating the required air flow into the system, the empty bed was heated up to 533.15 K (500 ºF), after which approximately 0.3 kg (0.66 lb) of the feedlot biomass was added to the bed, and the heating continued until the feedlot biomass ignited and the temperature of the feedlot biomass in the bed (0.3 kg (0.66 lb) initially added) reached approximately 1080.71 K (1500 ºF). After that the external heating was stopped and fuel was added in batches of 0.5 kg (1.1 lb) every five minutes until the required bed height of 171.5 mm (6.75”)

was reached. At that point, the clock timer was set to zero. Beyond that, the temperatures at different locations were recorded simultaneously by the seven thermocouples at every three-minute interval. Then the gas samples were collected from the five gas sampling ports. The gas sampling was started at approximately five minutes into the run, and collected from the gas sampling ports from 1 through to 5. Length of each sampling lasted over 3 minutes. Only one batch of sample-gas (one batch is three samples collected for more accurate gas analysis) was collected from each gas sampling port during the entire run.

Due to the small size of the holes in the grate, the ash did not fall through the grate into the plenum chamber; instead, it accumulated inside the gasifier. Therefore, the runs were always under batch mode operation, as steady state was not achievable due to ash accumulation in the bed except for low ash coal. The experiment was run for approximately 1 hour after attaining the initial bed height. Longer runs were not possible as the ash accumulation in the bed caused the flame front to move towards the free surface. The important fact to keep in mind is that the operator cannot control the air fuel ratio, as the fuel feed-rate is controlled by the bed height. The fuel feed rate is adjusted to keep the bed height constant at 171.5 mm (6.75”) above the grate. At the end of the experiments, the average air fuel ratio for the entire experiment was calculated based on the air flow rate and the total fuel gasified during the course of the entire experiment. The same procedure was repeated for coal: feedlot biomass blends and coal: litter biomass blends.

3.5. Economic analysis

Experimental work not undertaken.

4. Results and Discussion

4.1. Properties of fuels

4.1.1. Feedlot Biomass

4.1.1.1 Proximate and Ultimate Analyses of Ration and Fuel:

The FB analyses in Table 4.1 show the results of the proximate and elemental ash analyses provided by SPS on feed bunk ration and 3 sub-samples taken from a composite of 20 or more random probes into the 136 Mg (150 ton) windrows of test FB that were collected from typical, adjacent cattle pens. These initial samples were taken immediately after the first mixing with the Scarab composter (day-1), but before pronounced heating occurred with the onset of composting. Ultimate analyses were provided by the Commercial Testing and Engineering Company (CTE), which analyzed only one composite sample of the three sub-samples submitted to SPS. According to SPS results, FB moisture contents were about 4 % higher and ash content about 4 % lower for the FB only than for windrow with crop residues. Similarly, initial volatile matter, VM (dry basis) and fixed carbon, FC (dry basis) were slightly higher for the FB-only windrow than for the < 5 % crop residue windrow. The CTE data corroborated the SPS findings of higher ash and lower moisture for the crop residue windrow, and showed identical initial carbon contents. Because crop residues generally have higher VM and lower ash than FB, the differences between FB with crop residue and without crop residue in the experiment are more likely due to the variations in properties of the FB harvested from the feed-pens, including any entrained soil or debris, resulting from FB collection, than to any effects of incorporating the crop residues. More properties are given in section 4.2 when discussing the results of cofiring experiments.

4.1.1.2. Higher Heating Values (HHV):

The cattle ration samples taken from feed-bunks adjacent to three pens from which FB had been removed showed much lower ash and much higher values of total carbon, FC, VM, and heating values than either FB windrow (Table 4.1). The ration had a much higher HHV value (as-received and dry-basis) compared to FB-raw due to its reduced moisture and ash content (HHV as-received, Fig.4.1). However, on a dry-ash free (DAF) basis, the heating value was similar for ration 19,500 kJ/kg (8,390 Btu/lb), FB-only 20,900 kJ/kg (8,990 Btu/lb), and FB/crop residue 19,800 kJ/kg (8,500 Btu/lb). Dry ash percentage of ration was only 4.5 %. If a metabolic efficiency of 20 % is assumed, then the ash content is expected to increase slightly. However, the ash percentage on a dry basis is 40 % in FB indicating a large collection of soil from the feedlots and/or substantial degradation in situ in the feedlot; therefore, resulting in the loss of VM with time before collection (120-150 days typical).

After 32 days of composting, the windrows were re-sampled following the same protocol as before. In order to determine the extent of loss of combustibles, the ash percentage on dry basis was determined. Results of the PC FB (without crops) analysis (Table 4.2) indicated that moisture decreased from 39 % (Table 4.1) to about 32 % (Table 4.2) for both windrows while ash content increased from 40 % (dry basis) to 45 %. The moisture reduction should increase the heat value. The ash increased with composting time (Fig. 4.2), indicating a loss of combustibles and hence a reduction in HHV on dry basis (See HHV-Dry in Fig. 4.1). However, the HHV-DAF remained almost constant at about 19,500 kJ/kg (8,400 Btu/lb) for ration, FB, and PC and 19,800 kJ/kg (8,500 Btu/lb) for FB mixed with crop residue. The HHV decreased by 19 % for the FB-only windrow and 8 % for the FB/crop residue windrow, to a level of about 10,900 kJ/kg (4,700 Btu/lb) dry basis for both windrows.

After 125 days of composting (Table 4.3), ash content was higher for finished compost (FiC) biomass than at Days 1 and 32 (Fig.4.2), moisture was slightly lower, and the heating value was 7-9% lower 10,000 and 9,930 kJ/kg (4,310 and 4,270 Btu/lb) dry basis, respectively) for the FB-only and FB-crop residue compost. Volatiles were lower as well, along with total carbon, but fixed carbon was slightly lower for the FB-only windrow and higher for FB with crop residue.

There was a large variation in HHV on an as-received basis, but the HHV on a DAF basis was approximately constant. After 125 days, the DAF-HHV decreased slightly indicating a loss of the high heating value components of the combustibles. The DAF heating values of raw FB-raw (1 day), PC (32 days), and FiC (125 days) is compared in Fig. 4.1.

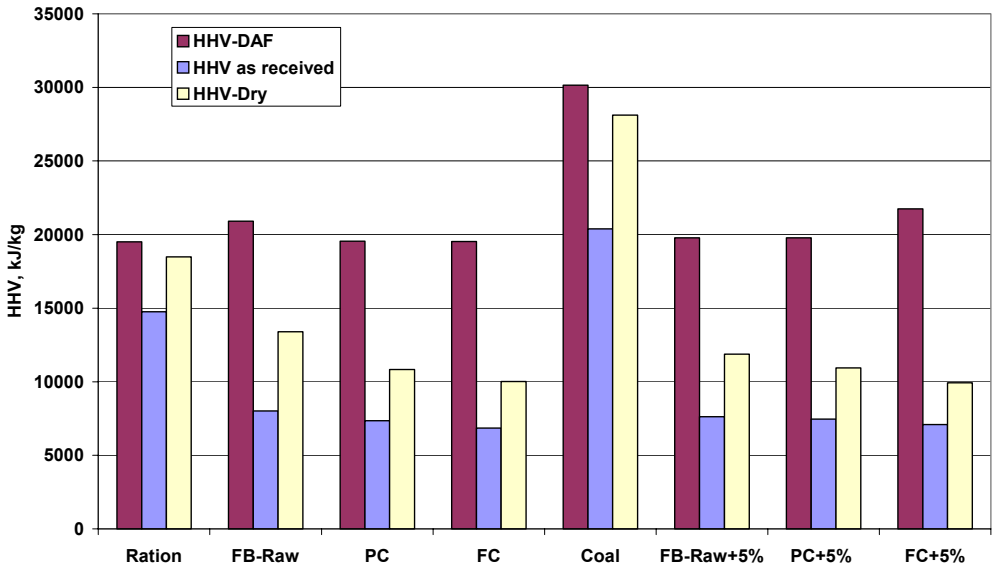

Figure 4.1: Higher Heating Values (HHV) of Ration and Animal Based Biomass Fuels (multiply HHV by 0.4299 to obtain Btu/lb)

Table 4.1. Analysis Summary for Initial Raw/Feedlot biomass (RM) and Feed Ration Samples, Day-1

	Feedlot biomass		Feedlot biomass + 5 % Crop Residues		Feedbunk Ration	
I. Ultimate Analysis by Commercial Testing and Engineering Co. (CTE), Denver, Colorado						
Parameter	As Received	Dry Basis	As Received	Dry Basis	As Received	Dry Basis
% Moisture	38.6	xxx	36.2	xxx	19.8	xxx
% Carbon	18.2	29.6	18.9	29.6	35.9	44.8
% Hydrogen	2.06	3.35	2.19	3.43	4.96	6.18
% Nitrogen	1.57	2.55	1.48	2.32	1.63	2.03
% Sulfur	0.5	0.81	0.51	0.8	0.08	0.1
% Ash	24.8	40.4	27.3	42.8	3.6	4.5
% Oxygen (Diff.)	14.3	23.3	13.5	21.1	34	42.4
Total	100	100	100	100	100	100
II. Proximate and Elemental Ash Analysis by Southwestern Public Service Co. (SPS), Amarillo, TX						
Parameter	Mean ± SD	Mean ± SD	Mean ± SD	Mean ± SD	Mean ± SD	Mean ± SD
Moisture %	40.2 ± 1.0	--	35.8 ± 0.2	--	20.2 ± 0.2	--
Ash %	21.5 ± 0.4	35.9 ± 0.1	25.6 ± 0.1	40.0 ± 0.01	4.2 ± 0.4	5.2 ± 0.5
Sulfur %	0.45 ± 0.02	0.76 ± 0.03	0.47 ± 0.02	0.73 ± 0.04	0.26 ± 0.0	0.33 ± 0.01
Heat of Combust. kJ/kg	8,010 ± 200	13,400 ± 500	7,620 ± 120	11,900 ± 200	14,700 ± 100	18,500 ± 100
Btu/lb	3,450 ± 90	5,760 ± 220	3,280 ± 50	5,100 ± 70	6,340 ± 40	7,950 ± 40
Sodium % of Ash	--	2.93 ± 0.12	--	3.30 ± 0.11	--	2.12 ± 0.06
Magnesium % of Ash	--	5.08 ± 0.02	--	4.34 ± 0.15	--	7.19 ± 0.09
Potassium % of Ash	--	11.7 ± 0.2	--	10.7 ± 0.3	--	13.5 ± 0.4
Calcium % of Ash	--	13.6 ± 0.4	--	11.7 ± 0.0	--	23.0 ± 0.2
Subtotal		33.3 ± 0.5		30.0 ± 0.60		45.8 ± 0.3
Ash % db (above)	--	35.9 ± 0.1	--	40.0 ± 0.1	--	5.2 ± 0.5
Volatiles % db	--	50.2 ± 0.9	--	47.6 ± 1.1	--	72.9 ± 0.1

Table 4.2: Analysis Summary for Partially Composted (PC) Feedlot Biomass (32 days after composting)[*]

	Feedlot biomass		Feedlot biomass + 5 % Crop Residues	
I. Ultimate Analysis by Commercial Testing and Engineering Co. (CTE), Denver, Colorado				
Parameter	As Received	Dry Basis	As Received	Dry Basis
% Moisture	32.0	xxxx	30.7	xxxx
% Carbon	19.8	29.0	20.0	28.8
% Hydrogen	2.20	3.23	2.16	3.12
% Nitrogen	1.67	2.46	1.62	2.34
% Sulfur	0.56	0.82	0.53	0.76
% Ash	30.7	45.1	28.5	41.2
% Oxygen (Diff.)	13.1	19.3	16.5	23.8
Total	100.0	100.0	100.0	100.0

II. Proximate and Elemental Analysis by Southwestern Public Service Co. (SPS), Amarillo, Texas				
Parameter	Mean ± SD	Mean ± SD	Mean ± SD	Mean ± SD
Moisture %	32.5 ± 3.7	--	31.7 ± 2.5	
Ash %	30.3 ± 2.1	44.6 ± 1.2	30.6 ± 2.6	44.7 ± 2.3
Sulfur %	0.51 ± 0.03	0.75 ± 0.03	0.49 ± 0.06	0.71 ± 0.02
Heat of Combust., KJ/kg	7,350 ± 380	10,800 ± 90	7,450 ± 380	10,900 ± 900
Btu/lb.	(3,160 ± 160)	(4,660 ± 90)	(3,200 ± 160)	(4,700 ± 390)
Sodium % of Ash	--	2.18 ± 0.03	--	2.55 ± 0.17
Magnesium % of Ash	--	4.40 ± 0.36	--	4.53 ± 0.09
Potassium % of Ash	--	8.95 ± 0.27	--	8.90 ± 0.48
Calcium % of Ash	--	12.3 ± 0.5	--	11.6 ± 0.4
Subtotal	--	27.8 ± 0.7	--	27.6 ± 0.6
Ash % db (above)	--	44.6 ± 1.2	--	44.7 ± 2.3
Volatiles % db	--	42.3 ± 1.3	--	42.8 ± 0.5
Fixed Carbon % db	--	10.1 ± 0.2	--	9.4 ± 0.2
Total	--	97.0 ± 0.6	--	96.9 ± 1.7

[*] P content could be as high as 1.4 % for FB-PC and could be reduced to as low as 0.7 % and Cl content of FB is 1.2 % and coal is < 0.1 % (Sweeten *et. al*., 2003)

Table 4.3. Analysis Summary for Finished Feedlot biomass Compost (FiC) (125 days of composting)

	Finished Compost (FiC) Manure Only		Finished Compost (FiC), Manure + 5 % v/v Crop Res.		SPS Coal (Sampled 6/7/99)	
Parameter	As-Received	Dry Basis	As-Received	Dry Basis	As-Received	Dry Basis
I. Ultimate Analysis by Commercial Testing and Engineering Co. (CTE), Denver, Colorado						
Moisture %	31.2	0	27.3	0	26.9	0
Carbon %	16.8	24.4	17.6	24.2	50.8	69.5
Hydrogen %	1.65	2.4	1.82	2.5	3.33	4.56
Nitrogen %	1.61	2.34	1.69	2.33	0.75	1.03
Sulfur %	0.6	0.87	0.6	0.83	0.31	0.42
Ash %	33.4	48.5	38.1	52.5	5.3	7.3
Oxygen (Diff.) %	14.8	21.5	12.9	17.7	12.6	17.2
Totals	100	100	100	100	100	100
II. Proximate and Elemental Analysis, Southwestern Public Service Co. (SPS), Amarillo, TX						
	(n = 3 sub-samples)		(n = 3 sub-samples)		(n = 1 sub-samples)	
Parameter	As-Received Mean (SD)	Dry Basis Mean (SD)	As-Received Mean (SD)	Dry Basis Mean (SD)	As-Received	Dry Basis
Moisture %	32.4 (0.3)	0 (0)	28.5 (1.8)	0 (0)	27.5	0
Ash %	32.9 (0.98)	48.7 (1.64)	38.9 (2.41)	54.4 (2.3)	4.89	6.74
Sulfur %	0.51 (0.01)	0.75 (0.01)	0.49 (0.02)	0.68 (0.01)	0.35	0.48
Heat Combust., KJ/kg	6,850 (390)	10,000 (360)	7,100 (30)	9,930 (270)	20,400	28,100
Btu/lb	2,940 (170))	4,310 (160)	3,050 (10)	4,270 (120)	8,760	12,100
Ash % db (above)		48.7 (1.6)		54.4 (2.3)	4.89	6.74
Volatiles % db		39.1 (0.6)		37.9 (0.5)	30.7	42.3
Fixed Carbon % db		9.45 (0.43)		9.70 (0.58)	36.9	50.9
Sodium % of Ash		2.44 (0.07)		2.20 (0.11)		
Magnesium % of Ash		4.53 (0.19)		4.00 (0.13)		
Potassium % of Ash		8.66 (0.03)		8.18 (0.36)		
Calcium % of Ash		12.8 (0.4)		13.2 (0.8)		
Subtotals		28.5 (0.5)		27.6 (0.4)		
Totals		97.3 (0.7)		102.0 (1.8)		

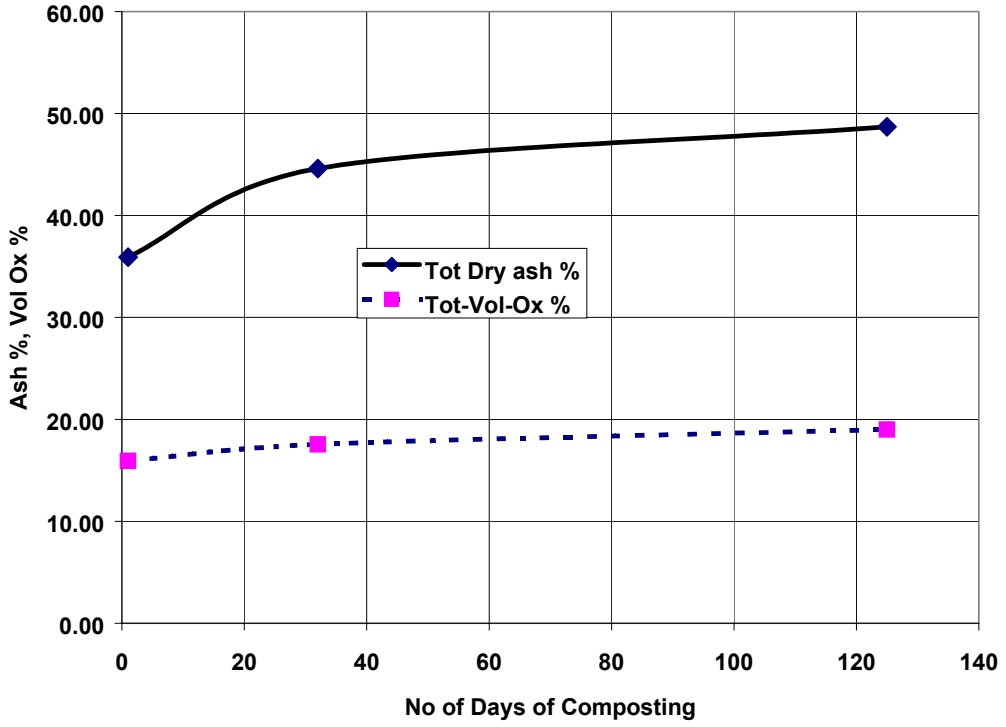

Figure 4.2: Variation of Ash and Total Volatile Oxide matter with composting time

4.1.1.3.Effect of Composting on Fuel Analyses

A direct comparison of ultimate analysis of composted FB after 1, 32, and 125 days is provided in Table 4.4 (ultimate analysis, CTE) and Table 4.5 (proximate and elemental analysis, SPS). The higher H/C ratio, lower O/C ratio, and lower ash content likely were responsible for the higher HHV in FB-raw fuels (Fig. 4.3). The trends toward decreasing moisture, carbon (total and fixed), hydrogen, volatiles, and heating value with increasing composting time are readily evident. Simultaneously, on a dry basis, ash content increased (both as-received and dry basis) while nitrogen and oxygen slightly decreased or remained constant. However, the H/C ratio decreased monotonically while the O/C ratio first decreased and then increased (Figures 4.3 and 4.4) with composting. Thus, the DAF heating value of PC was almost the same as 1-day FB. The DAF heating value of FiC had a slightly lower value as compared to PC and FB, indicating that the volatile components of high heat content were lost.

It is seen that there is very little S and low N per mmBtu in the ration. After metabolism in the cattle, both the N and S jump to a high value (figure 4.5). The N % increases on dry basis while C and H % decreases indicating loss of combustibles. Thus, the N/C and S/C continue to increase with composting. On a DAF basis, both the N/C and S/C ratios increase which indicates that S and N losses are not lost with the volatile losses. Since DAF heating values are approximately constant, the S and N contents per mmBtu must show an increase as shown in figure 4.6.

4.1.1.4. Effect of Storage:

After cessation of windrow composting, the one-ton lots of finished compost (FiC) were stored under roof in open bins. The lots were stored alongside the similar batches taken under roof on Day-1 and Day-32. During this period of storage, further chemical and physical changes occurred in the FB.

The analyses for samples taken are shown in Table 4.6 (ultimate and proximate analysis) and Table 4.7 (elemental analysis of ash from FB samples). As compared to data for Day 125 in Tables 4.4 and 4.5, data in Table 4.6 for bin-stored FB or compost showed large reduction in moisture (below 23% wb), similar carbon and volatiles, lower heating values (9,630 and 8,340 kJ/kg (4,140 and 3,756 Btu/lb), db), slightly higher ash (dry basis), slightly higher sulfur, and similar nitrogen. The ash analyses revealed very small differences between mineral oxide values as a function either of time in storage or the addition of crop residue. Table 4.8 shows the results of ultimate and proximate analyses on 90:10 (mass) coal: PC FB blends.

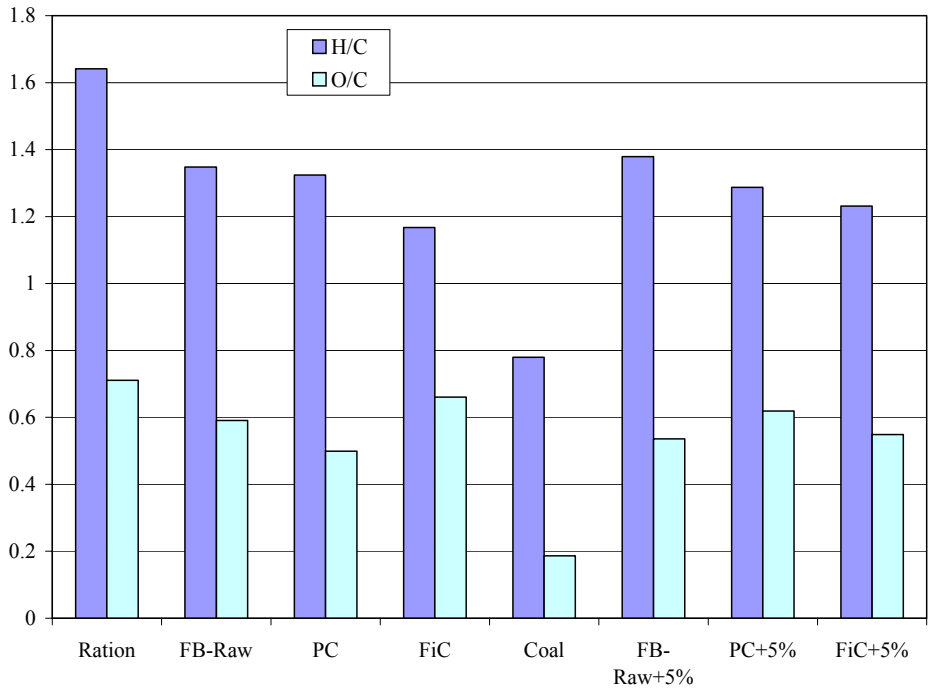

Figure 4.3: Variation of hydrogen to carbon and oxygen to carbon ratios for ration and Feedlot Biomass (FB or manure) with composting time.

Table 4.4: Comparison of Proximate and Elemental Analyses of Composted Feedlot Biomass after 1, 32, and 125 days of composting

		Finished Compost (FiC) FB Only		Finished Compost (FiC) FB + 5 % v/v Crop Res.	
		Concentration		Concentration	
Parameter	No. Days Composting	As-Received n = 1	Dry Basis n = 1	As-Received n = 1	Dry Basis n = 1
I. Ultimate Analysis by Commercial Testing and Engineering Co. (CTE), Denver, Colorado					
Moisture %	1	38.6	0	36.2	0
	32	32.0	0	30.7	0
	125	31.2	0	27.3	0
Carbon %	1	18.2	29.6	18.9	29.6
	32	19.8	29.0	20.0	28.8
	125	16.8	24.4	17.6	24.2
Hydrogen %	1	2.06	3.35	2.19	3.43
	32	2.20	3.23	2.16	3.12
	125	1.65	2.40	1.82	2.50
Nitrogen %	1	1.57	2.55	1.48	2.32
	32	1.67	2.46	1.62	2.34
	125	1.61	2.34	1.69	2.33
Sulfur %	1	0.50	0.81	0.51	0.80
	32	0.56	0.82	0.53	0.76
	125	0.60	0.87	0.60	0.83
Ash %	1	24.8	40.4	27.3	42.8
	32	30.7	45.1	28.5	41.2
	125	33.4	48.5	38.1	52.5
Oxygen % (Diff.)	1	14.3	23.3	13.5	21.1
	32	13.1	19.3	16.5	23.8
	125	14.8	21.5	12.9	17.7

Table 4.5: Comparison of Proximate and Elemental Analyses of Composted Feedlot Biomass after 1, 32, and 125 days of composting

		Concentration (n = 3)		Concentration (n = 3)	
Parameter	No. Days Composting	As-Received Mean (SD)	Dry Basis Mean (SD)	As-Received Mean (SD)	Dry Basis Mean (SD)
I. Proximate and Elemental Analysis, Southwestern Public Service Co. (SPS), Amarillo, TX					
Moisture %	1	40.2 (1.0)	0.0 (0)	35.8 (0.2)	0.0 (0)
	32	32.5 (3.71)	0.0 (0)	31.7 (2.5)	0.0 (0)
	125	32.4 (0.3)	0.0 (0)	28.5 (1.8)	0.0 (0)
Ash %	1	21.5 (0.4)	35.9 (0.1)	25.6 (0.1)	40.0 (0.1)
	32	30.3 (2.1)	44.6 (1.2)	30.6 (2.6)	44.7 (2.3)
	125	32.9 (1.0)	48.7 (1.6)	38.9 (2.4)	54.4 (2.3)
Sulfur %	1	0.45 (0.02)	0.76 (0.03)	0.47 (0.02)	0.73 (0.04)
	32	0.51 (0.03)	0.75 (0.03)	0.49 (0.06)	0.71 (0.02)
	125	0.51 (0.01)	0.75 (0.01)	0.49 (0.02)	0.68 (0.01)
Heat Combust., kJ/kg	1	8025	13400	7630	11860
	32	7350	10840	7445	10930
	125	6840	10025	7095	9930
Sodium % of Ash	1		2.93 (0.12)		3.30 (0.11)
	32		2.18 (0.03)		2.55 (0.17)
	125		2.44 (0.07)		2.20 (0.11)
Magnesium % of Ash	1		5.08 (0.02)		4.34 (0.15)
	32		4.40 (0.36)		4.53 (0.09)
	125		4.53 (0.19)		4.00 (0.13)
Potassium % of Ash	1		11.7 (0.2)		10.7 (0.3)
	32		8.95 (0.27)		8.90 (0.48)
	125		8.66 (0.03)		8.18 (0.36)
Calcium % of Ash	1		13.6 (0.4)		11.7 (0.0)
	32		12.3 (0.5)		11.6 (0.4)
	125		12.8 (0.4)		13.2 (0.8)
Volatiles % db	1		50.2 (0.9)		47.6 (1.1)
	32		42.3 (1.3)		42.8 (0.5)
	125		39.1 (0.6)		37.9 (0.5)
Fixed Carbon % db	1		11.3 (0.3)		10.4 (0.2)
	32		10.1 (0.2)		9.4 (0.2)
	125		9.5 (0.4)		9.7 (0.6)

Table 4.6. Uncomposted, Partially Composted (PC), and Finished Compost (FiC) Following 6-11 Months of Bin-Storage Under Roof

Parameter	Uncomposted FB				Partially Composted FB (PC)				Finished Compost (FiC)			
	(Day 1)				(Day 32)				(Day 125)			
	0% Crop Residues		<5% Crop Residues		<5% Crop Residues		0% Crop Residues		0% Crop Residues		5% Crop Residues	
	As-Received	Dry Basis	As-Received	Dry Basis	As-Received	Dry Basis	As-Received	Dry Basis	As-Received	Dry Basis	As-Received	Dry Basis
I. Ultimate Analysis by Commercial Testing and Engineering Co. (CTE), Denver, Colorado												
Moisture %	23	--	10.8	--	9.1	--	17.9	--	20.9	--	20.1	--
Carbon, Fixed %	23.7	30.8	26.4	29.6	23.9	26.3	21.9	26.7	21.9	27.6	19.6	24.6
Hydrogen %	2.6	3.37	3.04	3.41	2.58	2.84	2.41	2.93	2.35	2.97	2.03	2.54
Nitrogen %	2.21	2.87	1.98	2.22	2.03	2.23	1.86	2.26	2	2.53	1.81	2.27
Sulfur %	0.72	0.94	0.73	0.83	0.73	0.8	0.65	0.79	0.68	0.86	0.63	0.79
Ash %	33	42.8	39.8	44.7	45	49.5	40.1	48.8	39.4	49.8	42.5	53.3
Oxygen (Diff.) %	14.8	19.2	17.2	19.3	16.7	18.4	15.2	18.5	12.8	16.2	13.2	16.6
Totals	100	100	100	100	100	100	100	100	100	100	100	100
II. Proximate and Elemental Analysis, SPS Co., Amarillo, Texas												
Moisture %	23.3	--	10.9	--	9.3	--	18.1	--	20.9	--	20.5	--
Ash %	32.3	42.1	39.6	44.5	44.6	49.2	40.1	49	40.2	50.8	41.2	51.8
Sulfur %	0.61	0.79	0.54	0.61	0.64	0.7	0.57	0.7	0.68	0.86	0.64	0.81
Heating Value, kJ/kg	9,040	11,800	9,570	10,740	8,710	9,600	8,060	9,840	7,620	9,640	6,940	8,740
Btu/lb	-3,890	-5,060	-4,120	-4,620	-3,740	-4,130	-3,460	-4,230	-3,280	-4,140	-2,990	-3,760
Ash % db (above)	--	42.1	--	44.5	--	49.2	--	49	--	50.8	--	51.8
Volatiles % db	--	46.5	--	45	--	41.3	--	41.3	--	39.9	--	38.8
Fixed Carbon % db	--	11.4	--	10.5	--	9.5	--	9.7	--	9.3	--	9.4
Totals	--	100	--	100	--	100	--	100	--	100	--	100

Table 4.7: Mineral Analysis* of FB Ash (% dry basis) After Composting and Bin Storage vs. Coal Ash

Mineral Analysis % dry basis:	Uncomposted FB (Day 1)		Partially Composted FB (PC) (Day 32)		Finished Compost (FiC) (Day 125)		Mean (± SD)		Mean (± SD)	SPS Coal Sample
	0% Crop Residues	5% Crop Residues	0% Crop Residues	5% Crop Residues	0% Crop Residues	5% Crop Residues	0% Crop Residues	5% Crop Residues	Combined 0% & 5% Crop Residues	6/7/99 n=1
Sodium oxide, %	4.26	4.09	3.71	4.13	4.26	3.39	4.08 (0.32)	3.87 (0.42)	3.97 (0.35)	0.94
Magnesium oxide, %	8.63	7.72	7.16	7.05	7.19	6.47	7.66 (0.84)	7.08 (0.63)	7.37 (0.73)	5.53
Aluminum oxide, %	8.67	9.29	9.84	9.68	9.64	9.57	9.38 (0.63)	9.51 (0.20)	9.45 (0.42)	19.08
Silica, %	41.80	45.78	45.58	47.51	46.16	48.02	44.51 (2.37)	47.10 (1.17)	45.81 (2.19)	28.67
Sulfur trioxide, %	3.62	3.34	3.20	2.77	3.19	3.09	3.34(0.25)	3.07 (0.29)	3.20 (0.28)	9.86
Potassium oxide, %	13.61	11.96	11.09	11.41	11.60	10.50	12.10 (1.33)	11.29 (0.74)	11.70 (1.06)	0.46
Calcium oxide, %	17.84	16.15	17.37	15.62	15.99	16.95	17.07 (0.96)	16.24 (0.67)	16.65 (0.87)	27.93
Titanium oxide, %	0.43	0.48	0.49	0.48	0.49	0.48	0.47 (0.03)	0.48 (0.00)	0.48 (0.02)	1.34
Ferric oxide, %	0.95	1.02	1.35	1.20	1.27	1.35	1.19 (0.21)	1.19 (0.17)	1.19 (0.17)	5.58
Strontium oxide, %	0.10	0.09	0.11	0.09	0.10	0.09	0.10 (0.01)	0.09 (0.00)	0.10 (0.01)	--
Barium oxide, %	0.08	0.08	0.10	0.07	0.10	0.08	0.09 (0.01)	0.08 (0.01)	0.09 (0.01)	--
Total	99.99	100.00	100.00	100.01	99.99	99.99	99.99	100.00	100.01	99.39

* Analysis provided by Southwestern Public Service Co., Amarillo, Texas.

Table 4.8: Analysis of Coal (90%) and FB (10%) Mixture

Parameter	As-Received (n = 5)		Dry Basis (n = 5)	
	Mean	SD	Mean	SD
I. Ultimate Analysis by Commercial Testing and Engineering Co. (CTE), Denver, Colorado				
Moisture %	7.86	0.27	--	--
Carbon %	60.1	0.6	65.2	0.6
Hydrogen %	4.31	0.02	4.67	0.02
Nitrogen %	1.06	0.01	1.15	0.01
Sulfur %	0.50	0.01	0.54	0.01
Ash %	11.4	0.2	12.3	0.2
Oxygen (Diff.) %	14.8	0.4	16.1	0.5
Totals	100.0	--	100.0	--
II. Proximate and Elemental Analysis, SPS Co., Amarillo, Texas				
Moisture %	8.40	0.16	--	--
Ash %	10.8	0.11	11.8	0.11
Sulfur %	0.48	0.02	0.52	0.02
Heat Combust., kJ/kg	23,600	300	25,800	300
Btu/lb	(10,200)	(100)	(11,100)	(100)
Volatiles % db	37.8	0.4	41.2	0.5
Fixed Carbon % db	43.0	0.6	46.9	0.6
Totals	100.5	--	100.4	--

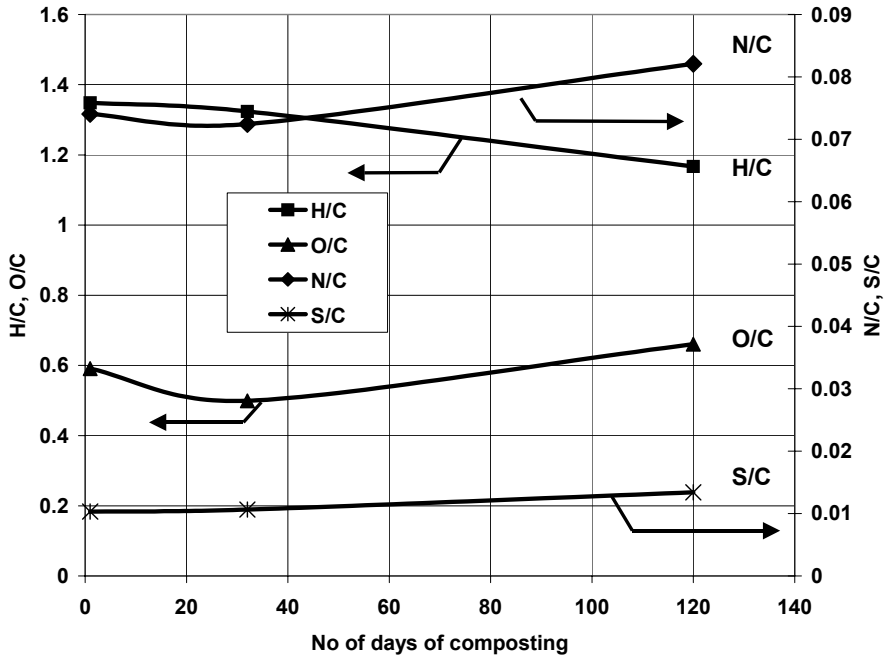

Figure 4.4: Variation of hydrogen to carbon (H/C) and oxygen to carbon (O/C), nitrogen to carbon (N/C), and sulfur to carbon (S/C) ratios of FB with composting time

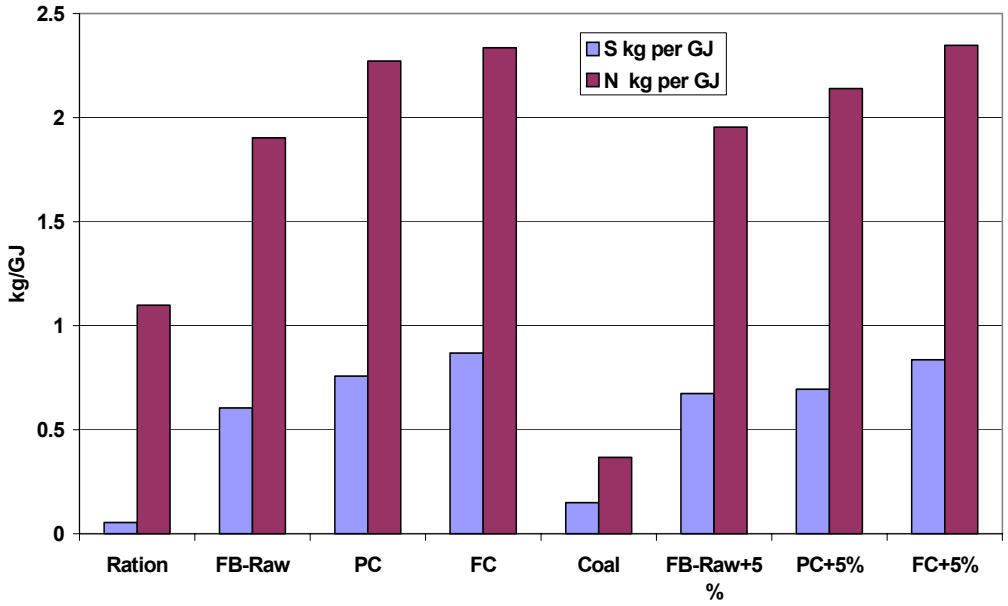

Figure 4.5: Nitrogen and Sulfur contents on a heat basis vs. fuel type (divide ordinate by 0.4299 to obtain lb. per mmBtu)

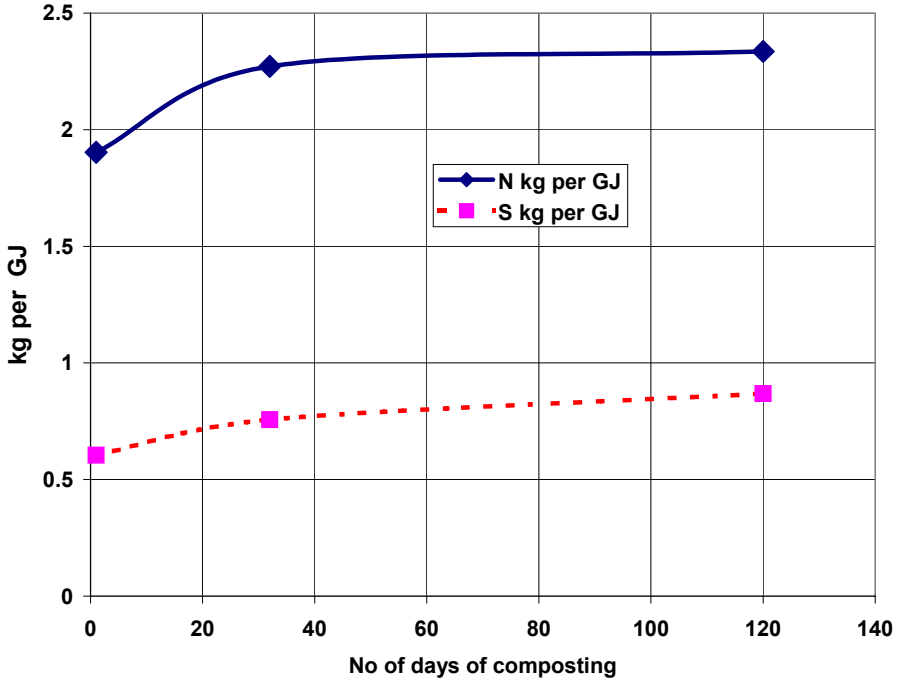

Figure 4.6: Change in Nitrogen and Sulfur contents on a heat basis with composting (divide ordinate by 0.4299 to obtain lb. per mmBtu)

4.1.1.5. Volatile Matter and Higher Heating Values of Volatile Matter:

On DAF basis, the VM percentage remained between 75-83 % (Figure 4.7). If the heat of pyrolysis is negligible (about –420 kJ/kg (–181 Btu/lb) of volatiles) (Annamalai and Ryan, 1992). Table 4.8 shows the results of ultimate and proximate analyses on 90:10 (mass) coal:PC FB blends. For DAF fuel,

$$HHV_{Fuel} = HHV_{vol} * VM + (1\text{-}VM)* HV_{FC} \quad (4.1.1)$$

Where HHV_{Fuel} and HHV_{Vol} are the higher heating values for the fuel and volatiles, respectively. Knowing HHV_{Fuel}, VM, and HV_{FC} = 32,800 kJ/kg (14,100 Btu/lb), then one can estimate the HHV_{vol} for FB, PC, FiC, and coal as shown in Figure 4.8. It is seen that the heating values of volatiles ranged from 17,400 kJ/kg (7,500 Btu/lb) to 15,100 kJ/kg (6,500 Btu/lb) as FB is composted, while the HHV_{vol} of coal is (figure 4.8) about 26,700 kJ/kg (11,500 Btu/lb). One can estimate the % heat contribution by volatiles using the following relation:

$$\%\ \text{Heat contribution by volatiles} = VM * HHV_{Vol} / HHV_{Fuel} \quad (4.1.2)$$

While the VM of FB is almost twice that of coal, the percentage of heat contributed by volatiles from FB ranges from 60-70 % while in coal it contributes only 40 % of total heating value (Figure 4.9). The volatiles, from FB, are released more rapidly at lower temperatures compared to coal, the flame is expected to be more stable when firing a coal: FB blend.

4.1.1.6. Adiabatic Flame Temperatures

The HHV on a DAF basis was almost constant $\left(\approx 20{,}000\,\frac{kJ}{kg}\right)$ for raw-FB, ration, and PC (Figure 4.1 and 4.9). Heat contents are linearly related to ash and moisture contents (Sweeten *et al*, 1985) and their results are plotted in figure 4.10. The DAF heating value when extrapolated to zero ash percentage yields 21,900 kJ/kg (9,350 Btu/lb), which is 1,800 kJ/kg (780 Btu/lb) higher than the current data shown in Figure 4.1. Most biomass fuels including FB fuel have varying amounts of oxygen accompanied by variations in heating value and stoichiometric air. It has been reported that the DAF higher heating value per unit of stoichiometric air is roughly constant for most biomass fuels at 3800 kJ/m^3 (1300-1600 Btu/lb) (Sami *et. al*, 2001). Thus, if DAF biomass fuels are fired into a boiler, they will all have similar adiabatic flame temperatures. Hence variations in flame temperatures for biomass fuels are essentially due to variation in the ash and moisture contents of the biomass fuels. From simple theory on adiabatic combustion of stoichiometric air:fuel (with ash and moisture) mixtures, it can be shown that if HV_{DAF} per unit stoichiometric air is constant for most of the fuels then the adiabatic flame temp should have the following approximate correlation:

$$\text{Temp (K)} = A + B*(\%\text{ moisture}) + C*(\%\text{ ash}) + D*(\%\text{ moisture})*(\%\text{ ash})^2 + E*(\%\text{ moisture})^2 + F*(\%\text{ ash})^2 \quad (4.1.3)$$

A THERMOLAB spreadsheet based combustion program assuming equilibrium concentrations was run for many agricultural and animal based biomass fuels with varying, moisture and ash (Annamalai and Puri, 2001). The curve fit for many different biomass fuels with moisture ranging from 0 % to 45 % and ash percentage ranging from 0 % to 40 %yields the following correlation:

$$T(C)=2012 - 1.8864*H_2O + 5.0571*\text{Ash} - 0.3089*H_2O*\text{Ash} - 0.1802*H_2O^2 - 0.1076*\text{ASH}^2 \quad (4.1.4)$$

$$T(F)=3653 - 3.3955*H_2O + 9.1027*\text{Ash} - 0.5560*H_2O*\text{Ash} - 0.3244*H_2O^2 - 0.1937*\text{ASH}^2 \quad (4.1.5)$$

Where H_2O and ash are given on a mass % basis. Figure 4.11 shows a comparison of the exact results (points) from the program and the curves obtained by the above correlation. The R squared value for the curve fit is 0.9906 and as such, 99.06 % of the variation in temperature is explained by the curve fit. The figure readily yields the allowable moisture and ash contents of biomass fuels for any specified flame temperature.

4.1.1.7. Mineral Matter

The mineral matter (mm) analyses are extremely important for high ash FB since the mm affects the deposition, corrosion, and erosion rates of heat transfer tubes. The FB contains almost 45 % ash while coal contains only 5 % ash. Thus a 90:10 blend will double the ash output compared to coal. Alkaline matter such as Na, K, etc are believed to vaporize, react with SO_2, and form Na_2SO_4,

K_2SO_4, etc, which become sticky around 750 K (890.33 ºF). Higher alkaline oxide content results in a higher probability of fouling. Once a small amount of ash sticks to a metal surface, the oxide layers grow, and are accompanied by an increase in surface temperature (as much as 1000 K (1340.33 ºF)), which will accelerate the deposition process. The mineral analysis of ash (Table 4.9) for the coal-FB blend (dry basis) contained consistent levels of 11 minerals, especially silica (39.2 ± 0.8 %), aluminum oxide (19.6 ± 0.5 %), and calcium oxide (17.8 ± 0.7 %). Lower levels (2-6 %) were present of sulfur > magnesium > iron > potassium > sodium. The remaining mineral oxides (titanium > strontium > barium) represented less than 1 % each. While the total ash percentage increased (figure 4.2), the K, Na, and Mg as percentage of ash decreased during composting (Table 4.9, see Volatile oxides in figure 4.12) possibly due to leaching from the outer layers of the windrow surface. Thus, PC FB is preferable compared to FB-raw. Note that the total volatile oxide percentage in the fuel still increases due to an increased ash percentage in fuel, as shown in figure 4.2.

Ash fusion temperatures (AFT) have been tabulated in Table 1.1 for selected compounds in ash; fusion temperature of ash (a mixture) depends upon the percent of ash acid (SiO_2, Al_2O_3, TiO_2 etc) vs. the percent basic (Fe_2O_3, and alkaline oxides CaO, MgO, Na_2O and K_2O). Figure 4.13 plots the percentage of acidic vs. basic oxides in ash as FB is composted. Conventionally, the higher the basic percentage higher is the AFT that is typically lower than the flame temperatures. It is seen that volatile oxides range around 40-44 % for 0 % crops residues with dominant component being CaO and K_2O, while for coal it is about 35 % with the dominate compound being CaO. More ash analysis of FB is presented in section 4.4.

Table 4.9: Mineral Analysis of Ash From Coal: FB (90: 10%) Blend, % db

Mineral Analysis % db	Mean	SD
Sodium Oxide %	2.39	0.28
Magnesium Oxide %	4.64	0.33
Aluminum Oxide %	19.6	0.5
Silica %	39.2	0.8
Sulfur Trioxide %	6.36	0.27
Potassium Oxide %	4.23	0.30
Calcium Oxide %	17.8	0.7
Titanium Oxide %	0.99	0.03
Ferric Oxide %	4.43	0.21
Strontium Oxide %	0.20	0.00
Barium Oxide %	0.18	0.01
Total	100.0	

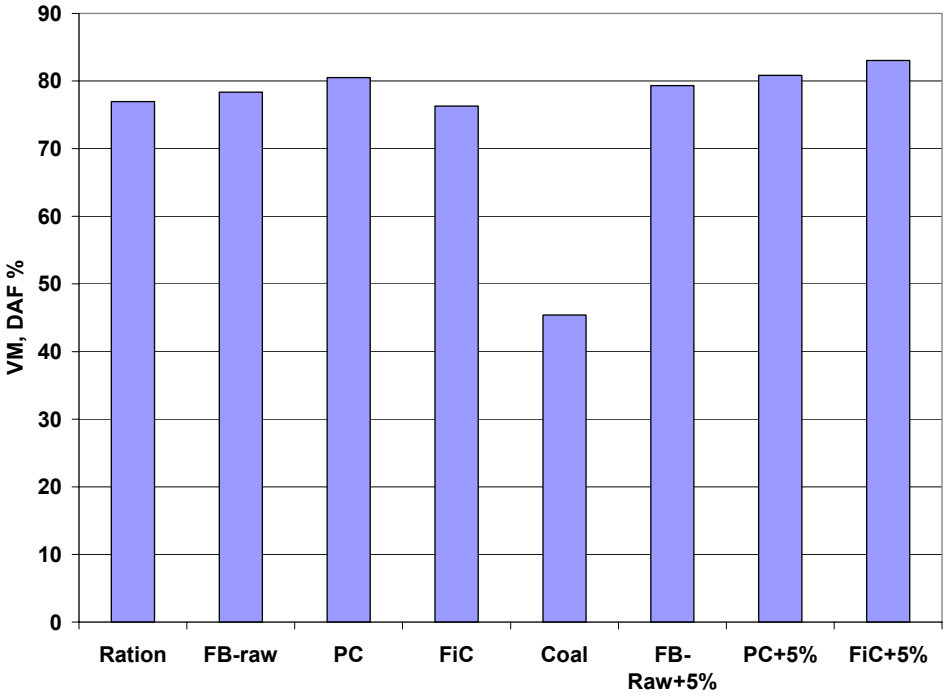

Figure 4.7: Volatile Matter percentage on DAF basis

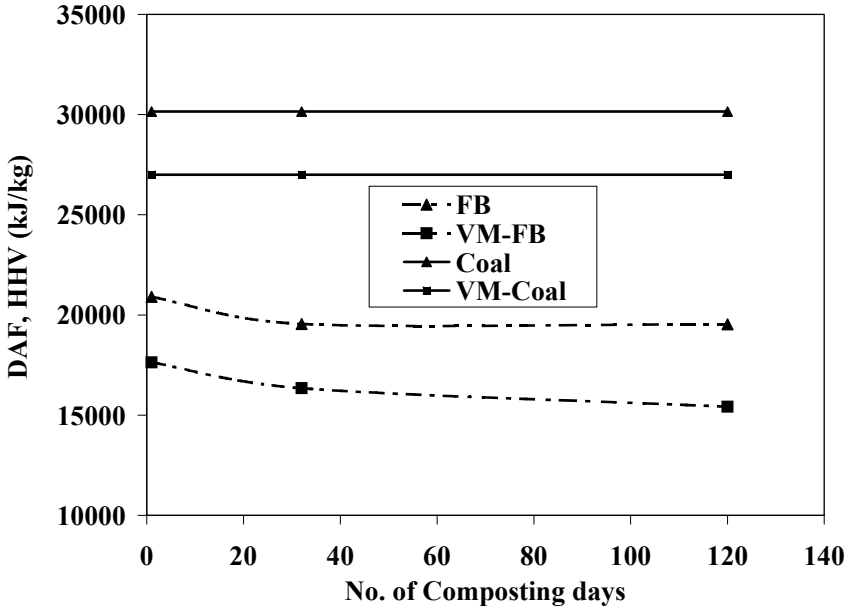

Figure 4.8: Variation of Heating Values of Volatiles (multiply ordinate by 0.4299 to obtain Btu/lb)

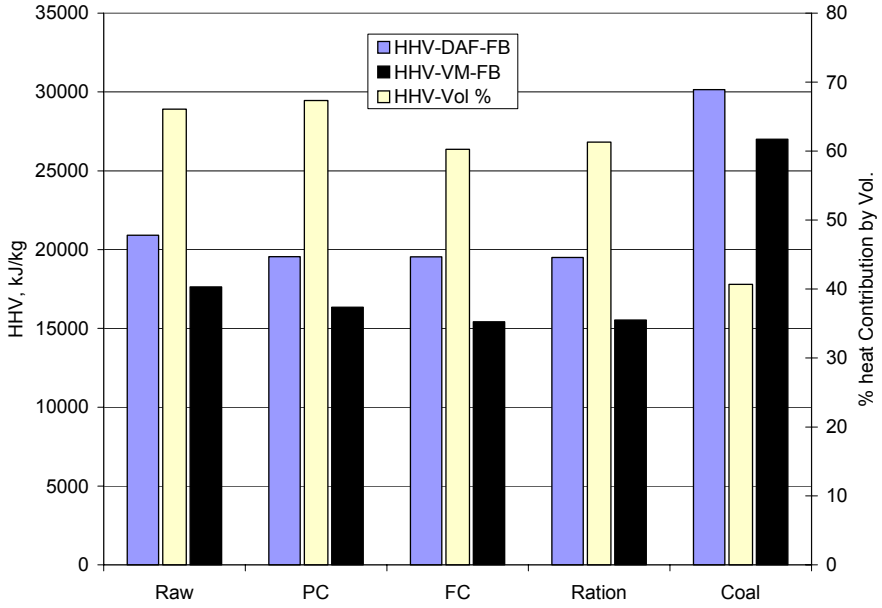

Figure 4.9: Estimated Heating Values of Volatiles and the % Heat Contribution by Volatiles (Multiply heating values by 0.4299 to obtain Btu/lb)

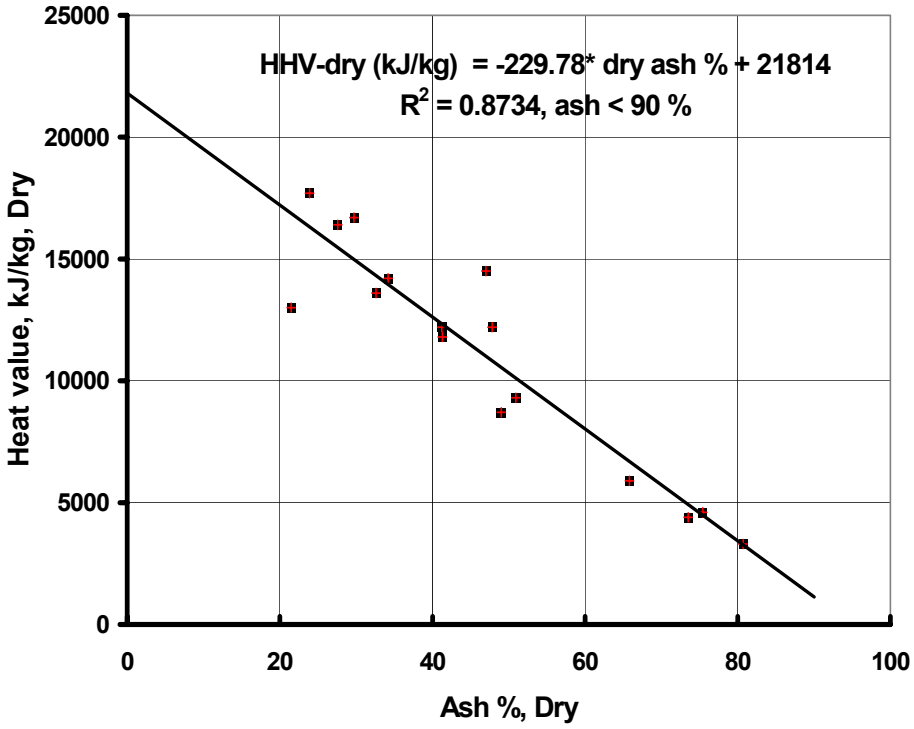

Figure 4.10: Variation of Dry Heating Values of FB with Ash contents (Multiply ordinate by 0.4299 to obtain BTU/lb; HHV-dry [BTU/lb] = -98.87* dry ash % + 9380, ash < 90 % (Sweeten *et al*, 1985)

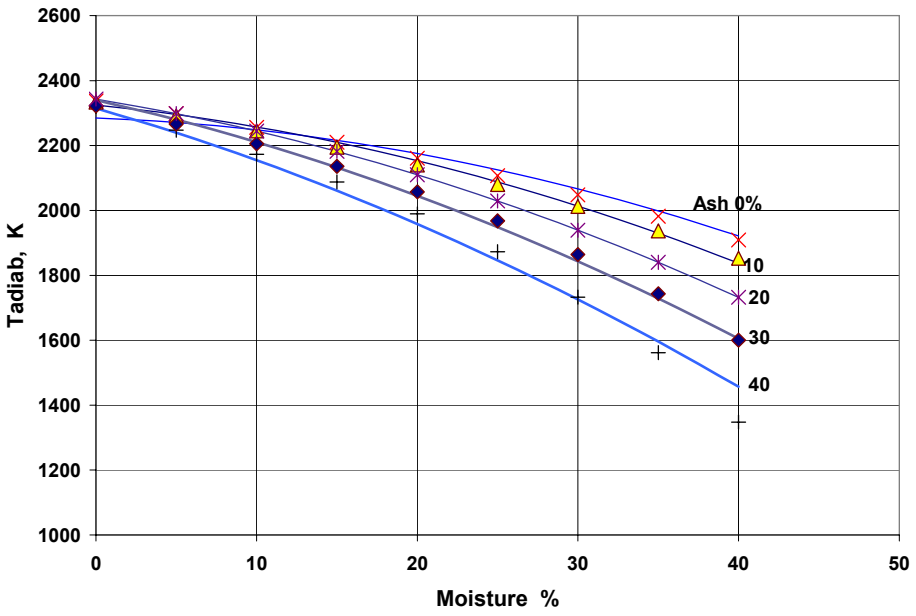

Figure 4.11: Correlation of Adiabatic Flame Temperature with Moisture and Ash contents; T (K) =2285 - 1.8864*H_20 + 5.0571*Ash - 0.3089*H_2O*Ash - 0.1802 * H_2O^2 -0.1076*ASH^2; T (F) = ordinate *1.8-460; T (F)=3653 - 3.3952*H_20 + 9.1028*Ash - 0.5560*H_2O*Ash - 0.3244 * H_2O^2 - 0.1937*ASH^2

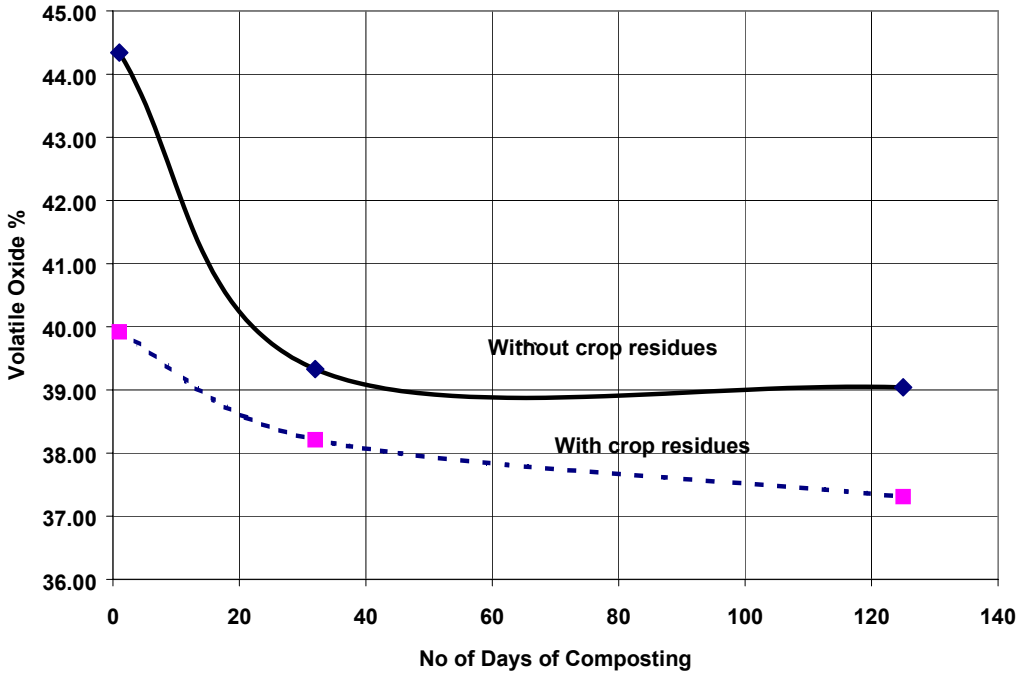

Figure 4.12: Variation of Alkaline Oxide % in ash with composting time

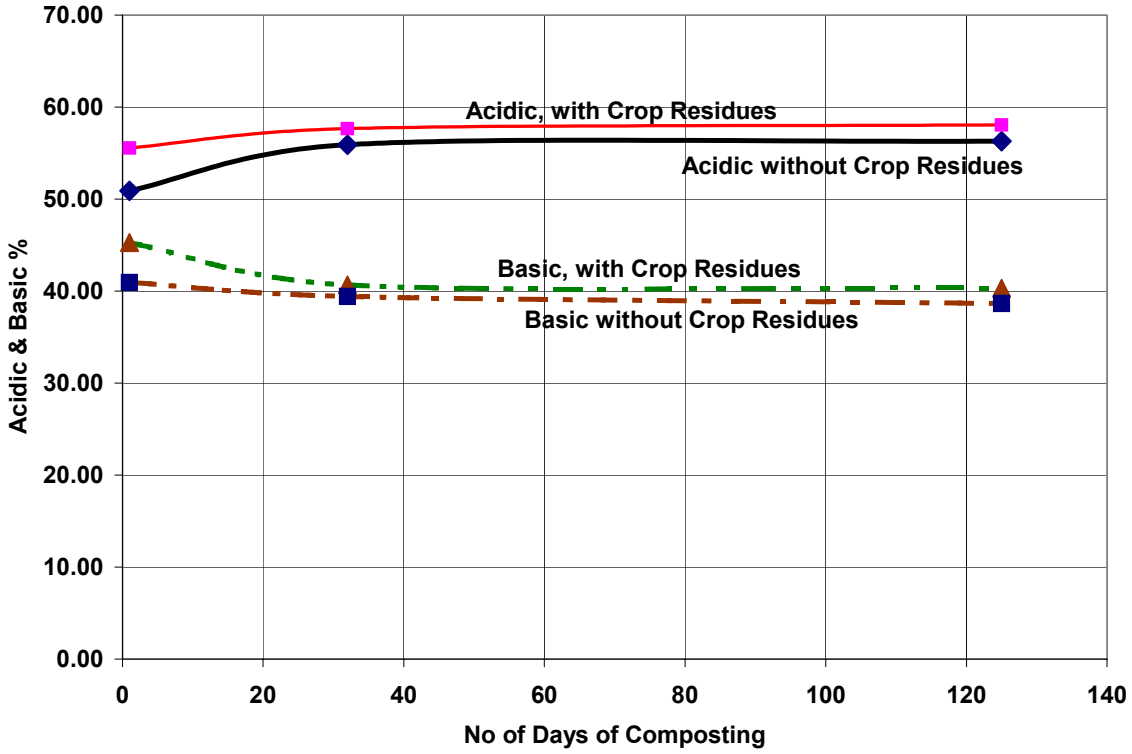

Figure 4.13: Ash acidic and Basic Percentage vs. composting time

4.1.2. Fuel Analyses on Litter Biomass

Samples were ashed in air at 750 °C (1382 ºF) and ash constituents, sulfur (S), and metals were analyzed and reported as oxides (Table 4.13). The higher or gross heating value (HHV) was determined with an adiabatic bomb calorimeter. Carbon (C), Hydrogen (H), Nitrogen (N), and Sulfur (S) were determined by combusting the sample at high temperature (1273.15-1623.15 K (1832-2462 °F)), depending upon the element) and measuring the off gases using analyzers specific to each element. Oxygen (O) was determined by difference (100-sum of % C, H, N, S, ash and moisture). Moisture content of wood shavings, cake, and clean out litter was measured by drying to 378.15 K (221 °F), and then weighing using Standard Methods (APHA, 1995, Table 3.1).

4.1.2.1. Moisture Content

Moisture contents of wood shavings, cake and (clean-out litter) CL biomass are presented in Table4.10. Average moisture contents were 45.32, 53.65, and 26.42 % for pine shavings, cake, and CL, respectively. Average moisture content values for cake and clean out litter biomass were higher than the published values of 40 and 21 % (NRAES, 1999) for cake and CL, respectively. As indicated by range and standard deviations, all materials sampled had highly variable moisture contents.

4.1.2.2. Ultimate and Proximate Analyses

Ultimate and proximate analyses were conducted on different fuels relating to broiler litter combustion to determine the most basic fuel properties. Five different fuels were investigated in the project: (excreted manure) EM, CL, (dried litter) DL, Coal, and the coal and DL blend (C90: DL10).

A (C90: DL10) proportion by mass was chosen to minimize the change in fuel properties from the original fuel, thereby reducing the amount of modification that may have to be made before the blended fuel can be fired in existing boiler burners.

The results of the ultimate and proximate analyses for the five fuels are shown in Table 4.11. O and H are given as the amount of organic O and H in the fuel. Organic O refers to the O that is part of the combustible fuel but does not include the part that is found in the moisture loss. The results show that all litter-based fuels have a higher ash, higher S, higher N, and a lower heating value than coal. Higher S and N will lead to significant pollutants such as oxides of sulfur (SO_x) and nitrogen (NO_x) which cause acid rain and ozone depletion. Higher moisture and ash will result in a lower heating value and a lower flame temperature during combustion. The heating value is reduced with high ash and moisture because these components reduce the combustible portion of the fuel. A lower flame temperature reduces the reaction rates and hence the completeness of combustion within a limited residence time and may result in loss of fuel energy due to unburnt fuel. Additional thermal energy is required to heat the moisture and ash while at the same time the heating value is reduced due to dilution. The change in dry ash % for CL compared to EM is possibly due to, (a) addition of bedding material and (b) loss in combustible matter.

Large moisture and ash content differences among various fuels make it difficult to compare the combustible portions of the fuels. To allow for this comparison, the results are presented on a dry ash free (DAF) basis in Table 4.12. The results show that all of the litter-based fuels are very similar in regards to the combustible portion of the fuel. The main change in the properties as the fuel is processed, is the increase in ash and the decrease in dry loss which have a corresponding effect on the heating value. The one exception is the amount of nitrogen. The addition of the bedding materials to the excreted manure results in a reduction of nitrogen when the clean out litter is formed. The bedding material that is mixed with the EM is lower in nitrogen than the EM and decreases the total nitrogen of the overall mixture. Some additional nitrogen is also lost through volatilization as the litter remains on the floor of the broiler house. It is also important to note that the broiler litter has a much higher percentage of its combustibles in the form of volatile matter as compared to coal. During combustion the volatile matter gasifies and burns more readily than the fixed carbon. The increase in volatile matter has the potential to enhance combustion when using the biomass fuels. Boiler burner testing is needed to fully determine the effect of increased volatile content.

Nitrogen and sulfur in the fuel can combine with O_2 during combustion to form nitrogen oxides (NO_x) and sulfur oxides (SO_x) that are recognized air pollutants. Of particular interest to boiler operators is the amount of nitrogen, sulfur, and ash in the fuel. High levels of ash in the fuel decrease the flame temperature, decrease the heating value, foul the boiler tubes inside the furnace, and lead to boiler tube corrosion. Fouling refers to the build up of ash deposits on the boiler tubes, which can lead to decrease in heat transfer and boiler tube corrosion. The ash per heat value for the studied fuels is given in Figure 4.14. The results are reported on a heat basis as the amount of fuel that is fired is determined by how much energy is desired. If a boiler operator switches to a lower heating value fuel with the same amount of nitrogen by mass, more fuel must be fired resulting in a higher throughput of nitrogen. The results show that the amount of ash in the litter fuels is higher than the coal. It is not known what the impact of the additional ash will be, and fouling studies must be conducted in a future using a pilot scale burner. Thus, the contents of S and N are expressed in kg/GJ (figures 4.15 and 4.16). Figure 4.15 shows the amount of N on a heat basis for different fuels. Again, the results show that there is a much greater nitrogen content in the biomass fuels and a slight increase in the nitrogen in the blended fuel. To determine if the higher fuel nitrogen will result in higher NO_x emissions, boiler burner testing need to be performed. Finally the sulfur content on a heat basis is shown in Figure 4.16. The additional sulfur in the litter fuels has the potential to produce SO_x during combustion, and boiler burner testing is necessary to determine the rate of conversion during combustion.

The ash of EM, CL, and Coal was analyzed for its constituents with the results shown in Table 4.13. Coal ash consists mainly of calcium (Ca) and silicon (Si), while the EM and CL consist mainly of calcium, phosphorus, and potassium. The ash appears as fly ash, partially fused ash, which, can stick to boiler tubes, and volatized material that can condense later and form hard deposits. The volatile constituents in ash are CaO, K_2O, MgO, and Na_2O. As shown in Table 4.13, concentrations of these volatile oxides for EM and CL are nearly twice the concentration of volatile oxides for coal. These higher amounts of volatile oxides may result in increased boiler fouling and corrosion (the metal loss is typically measured as 200 nm to 1000 nm per hour in coal fired plants). Corrosion can be caused by high amounts of Hydrogen Sulfide under reducing conditions (oxygen starved zones) and hydrochloric acid (HCl) near furnace tube walls. For example, up to 200 ppm of HCl can occur when chlorine is about 0.25 % in the fuel (Lawn, 1987), and ash deposits can accelerate the metal loss. Further testing in an operating boiler burner is necessary to fully assess the fouling performance of these LB fuels.

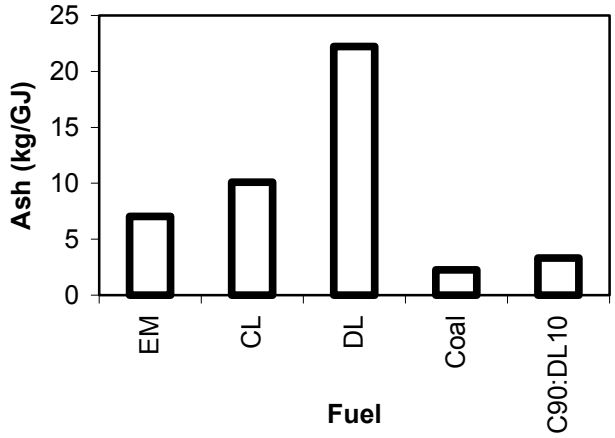

Figure 4.14: Fuel ash content on a kg/GJ basis (multiply ordinate by 2.32 to get lb/mmBtu)

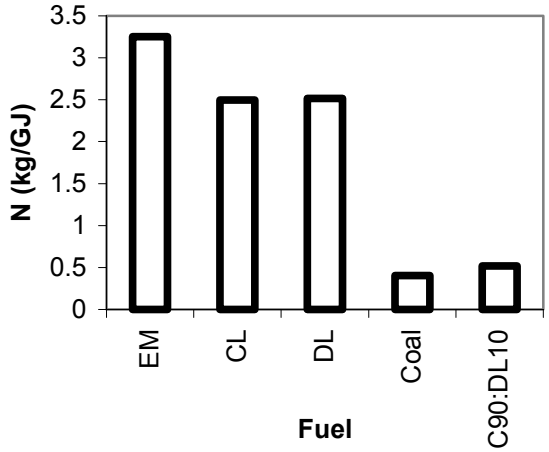

Figure 4.15: Fuel nitrogen contents on a kg/GJ basis (multiply ordinate by 2.32 to get lb/mmBtu)

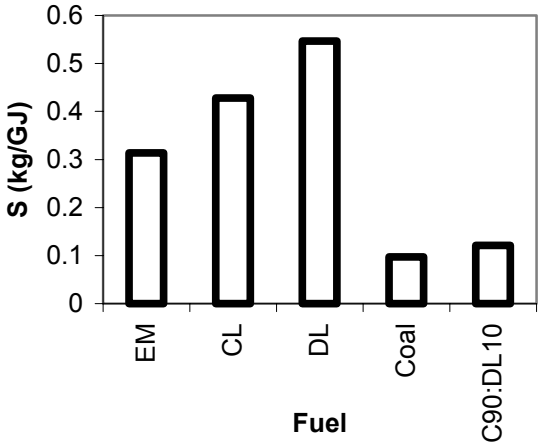

Figure 4.16: Fuel sulfur content on a kg/GJ basis (multiply ordinate by 2.32 to get lb/mmBtu)

Table 4.10: Moisture contents for pine shavings, cake, and clean out litter biomass

Material	Average Moisture Contents*, wet basis (%)	Range (%) Min-max	Standard Deviation (%)
Pine Shavings	45.32	36.26-55.14	7.36
Cake	53.65	39.43-62.84	6.47
Clean out	26.42	22.89-32.25	3.74

* Average of 10 samples per material.

Table 4.11: Ultimate and proximate analysis (as received)[*]

	EM	Coal	DL	(C90:DL10)
Parameter	n=5	n=2	n=2	n=2
C, %	23.62	60.30	28.44	57.10
H, %	3.16	3.62	3.71	3.63
O, %	19.02	14.50	22.80	15.33
N, %	3.11	0.96	3.04	1.17
S, %	0.30	0.23	0.66	0.27
Dry loss, %	44.07	15.12	11.62	14.77
Fixed C, %	8.02	42.38	10.92	39.23
Volatile Matter, %	41.20	37.17	50.65	38.51
Ash, %	6.72	5.33	26.82	7.47
HHV (kJ/kg)	9545	23709.80	12065.70	22545.39
HHV (Btu/lb)	4143	10219	5200	9717

[*] P, % could be as high as 3.2 for DL

Table 4.12: Dry ash free ultimate and proximate analysis

	EM	CL	Coal	DL	(C90:DL10)
Parameter	n=5	n=3	n=2	n=2	n=2
C, %	48.00	47.30	75.80	46.20	73.43
H, %	6.42	5.93	4.55	6.03	4.67
O, %	38.65	40.81	18.23	37.03	19.71
N, %	6.32	4.77	1.21	4.93	1.50
S, %	0.61	0.82	0.29	1.07	0.35
Dry loss, %	0.00	0.00	0.00	0.00	0.00
FC, %	16.29	19.41	53.27	17.73	50.45
VM, %	83.72	80.76	46.73	82.27	49.52
Ash, %	0.00	0.00	0.00	0.00	0.00
HHV (kJ/kg)	19396	19090	29805	19598	28994

Table 4.13: Ash analysis

	EM	CL	Coal
Parameter	n=5	n=3	n=2
Aluminum, % as AL_2O_3	0.79	1.23	16.785
Calcium, % as CaO	15.084	21.50	23.08
Iron, % as Fe_2O_3	1.484	1.06	4.33
Magnesium, % as MgO	7.472	5.9	3.625
Manganese, % as MnO	0.626	0.22	0.055
Phosphorous, % P_2O_5	24.798	25.12	0.9
Potassium, % as K_2O	26.944	16.51	0.485
Silicone, % as SiO_2	3.686	6.34	33.275
Sodium, % as Na_2O	3.724	6.52	1.725
Sulfur, %SO_3	8.326	7.23	13.19
Titanium, % as TiO_2	0.122	0.10	1.305
Total Volatile Oxides (%) CaO+ MgO+ K_2O+ Na_2O	53.22	50.40	28.90

4.1.3. Size Analyses

The size analyses of the pulverized coal, FB and LB fuels are presented in Figure 4.17 and Table 4.14. The Rosin-Rammler distribution is a probability distribution used to analyze the distribution of ground coal. It has also been reported that the analysis can be applied accurately to cement, gypsum, flint, clay, and others (Herdan, 1960). The distribution is based on the assumption that the probability density function is:

$$y = 100 n_p b x^{n_p - 1} e^{-b x^{n_p}} \qquad (4.1.6)$$

where y: probability distribution function, n_p and b: Rosin-Rammler parameters, and x: particle size.

Integrating $\int_o^x y dx$ gives:

$$D_p = 100\left(1 - e^{-bx^{n_p}}\right) \tag{4.1.7}$$

Where D_p: % mass having isze $0 < d_p < x$

Eq (4.1.7) gives the percentage D_p, which can pass through a sieve of size less than x. The percent retained is given as:

$$R_p = 100 - D_p = 100e^{-bx^{n_p}} \tag{4.1.8}$$

Taking the log of both sides yields:

$$\log\left(\frac{R_p}{100}\right) = -bx^{n_p}\log e \tag{4.1.9}$$

Taking the log of both sides again yields:

$$\log\log\left(\frac{R_p}{100}\right) = \log b + \log\log e + n\log x \tag{4.1.10}$$

Now the above equation has linear parameters and can be curve fit using standard linear regression to find n_p and b. The results of the size analysis are show in the Rosin Rammler plot in figure 4.17, and the curve fit parameters are given in table 4.14. Coal A and FB A are the fuels used in the TGA analysis, and for the first set of cofiring experiments. Coal B and FB B are the fuels used in the second set of cofiring experiments, and for the reburning experiments. The particle size distribution is shown in table 4.14b. About 90 % of mass passes through 40 μm for coal A, 45 % for coal B, 75 % for FB A, 62 % for FB B, and 60 % for LB. The results show that FB is not ground as finely as the coal. This is due to hay fibers in the manure that were not broken up during grinding, but instead compressed. To better visualize the size distributions, the distributions are graphed in a bar graph in figure 4.18. Similarly there is only 3 % of coal A greater than 100 μm, while for FB B there is 30 % greater than 100 μm. The results show the FB and LB samples were ground to a very similar size, and that coal sample A contained a larger fraction less than 45 microns, than in coal sample B.

Table 4.14a: Rosin Rammler parameters

Value	Coal A	FB A	Coal B	FB B	LB
n	1.6765	.7683	4.1559	1.0007	1.0751
b	.001544	.026140	1.637E-8	.00601	.0189

Table 4.14b: Particle size distribution of fuels used in cofiring and reburn experiments

Fuel type	Percentage mass < 40 μm
Coal A	90
Coal B	45
FB A	75
FB B	62
LB	60

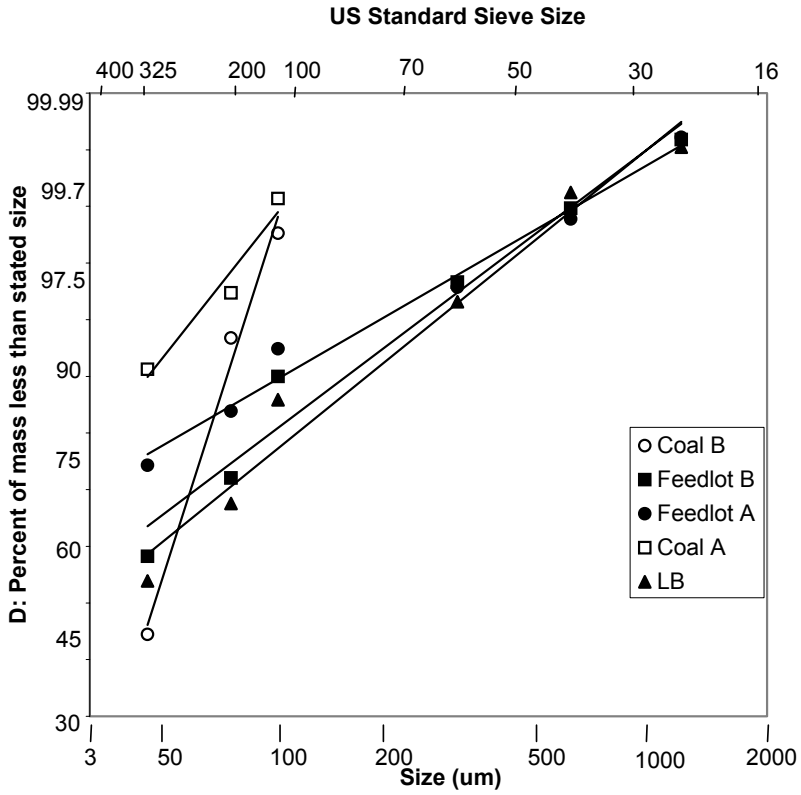

Figure 4.17: Rosin Rammler plot

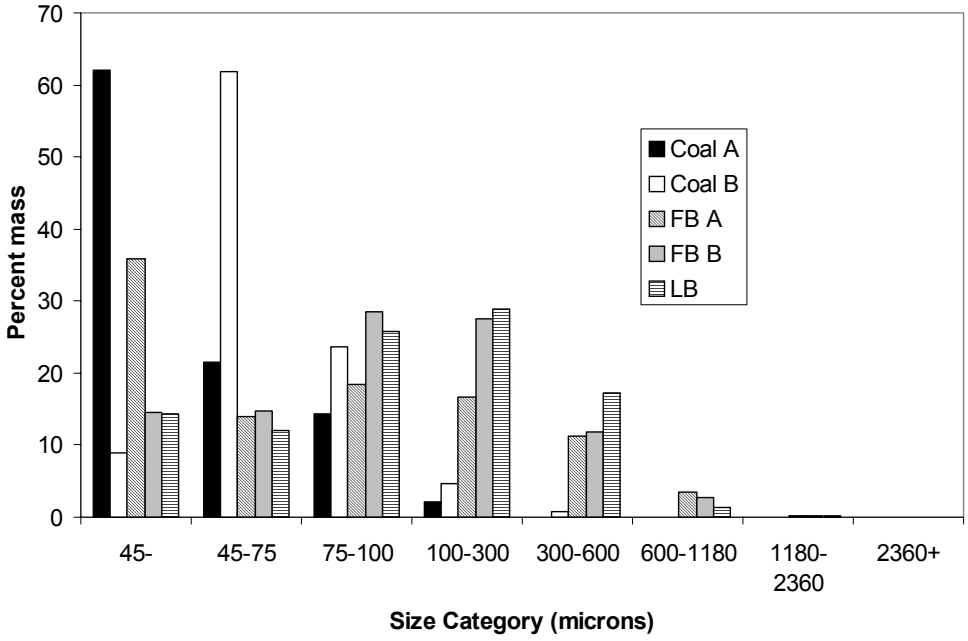

Figure 4.18: Size distribution bar graph

4.1.4. TGA Studies:

4.1.4.1. TGA Fuel Properties

Experiments in fuel properties were conducted on coal, FB, and LB. "Coal-A" (Table 4.15) and "FB-A" (Table 4.16) were used in the TGA experiments, and the initial short-length boiler burner experiments. "Coal-B" and "FB-B" (Table 4.17) were used in the reburn experiments, and the extended boiler burner experiments, which included SO_2 measurements. The fuel B has a moisture level of 15.12 % while fuel A has a moisture level of 22.5 %. FB A has a moisture percentage of 5.5 % vs. and 54 % ash and FB B has 7.7 % moisture and 44 % ash with a corresponding change in HHV. The fuel referred as LB is Litter biomass that was used in the co-firing and reburning experiments. The properties of LB and 90: 10 LB blend fuel are shown in table 4.18. For fuel samples labeled "A", two samples of fuel were analyzed, and the results were averaged. Table 4.19 shows properties of the 90:10 blend for "A fuels". All of the blends were analyzed on a mass basis, and all the blend properties were obtained through the law of mixtures from the coal and biomass analyses. The results are given on an as received basis, except for the oxygen and hydrogen that are given as organic hydrogen and oxygen in the as received sample.

Additional calculated fuel parameters, including the adiabatic flame temperature, ash in kg/GJ, etc. are shown in tables 4.20 to 4.23. The adiabatic flame temperature given in the tables is a theoretical flame temperature based on stoichiometric air and equilibrium gas concentrations. Figure 4.19 shows the amount of ash in kg/GJ for the different fuels. It is apparent that FB is an ash heavy fuel. The adiabatic flame temperatures indicate that the coal will burn hotter than the FB or LB due to lower ash and moisture. The heating values of FB and LB are much lower than coal (figure 4.20), so the mass flow of fuel has to be increased in order to maintain the same heat throughput when firing blends. Even more troubling is the increased Sulfur (figure 4.21) and Nitrogen (figure 4.22) in FB. When the fuel burns N and S in the fuel will combine with O_2 from the air to form NO and SO_2, which are recognized air pollutants.

The results show that FB has a greater ash content, lower carbon content higher volatile matter on DAF (dry ash free) basis and a lower heating value than coal. On a heat basis, FB contains 4 times more Nitrogen than coal. Figure 4.11 shows the effect of different moisture and ash levels on the adiabatic flame temperature of coal A. The results show that the ash and moisture content in a fuel can have a large effect on the flame temperature, and therefore should be carefully controlled. On a dry ash free basis, the FB will consist of almost only volatile matter, with very little fixed carbon, while the combustible portion of the coal is made up of equal parts fixed carbon and volatiles. A comparison of the FB fuel to the LB fuels shows that the both the biomass fuels have similar properties, with the FB having more ash.

Table 4.15: "Coal A" Analysis

Parameter	Sample 1	Sample 2	Avg.
Dry Loss	22.53	23.08	22.805
Ash	5.42	5.47	5.445
C	54.34	53.79	54.065
O	13.43	12.72	13.075
H	3.81	3.06	3.435
N	.81	.81	0.81
S	.39	.38	0.385
Total	100.73	99.31	100.02
HHV	21475 kJ/kg (9233 Btu/lb)	21294 kJ/kg (9155 Btu/lb)	21384 kJ/kg (9194 Btu/lb)
FC	36.85	37.65	37.25
VM	35.20	33.80	34.5

Table 4.16 FB-A properties

Parameter	Sample 1	Sample 2	Avg.
Dry Loss	6.8	6.78	6.79
Ash	41.91	42.67	42.29
C	24.39	23.4	23.895
O	20.07	20.45	20.26
H	3.61	3.52	3.565
N	2.31	2.29	2.3
S	0.91	0.89	0.9
Total	100	100	100
HHV	9571 kJ/kg (4115 Btu/lb)	9552 kJ/kg (4107 Btu/lb)	9561.5 kJ/kg (4111 Btu/lb)
FC	41.62	39.18	40.4
VM	9.67	11.37	10.52

Table 4.17: FB-B and Coal B properties

	Coal	Feedlot	Feedlot 90-10
C	60.3	23.6	56.6
H	3.62	2.9	3.55
O	14.5	19.1	15.0
N	0.96	1.78	1.04
S	0.23	0.5	0.26
Cl	<.1	1.85	NA
DL	15.12	7.7	14.4
FC	42.38	6.5	38.8
VM	37.17	41.4	37.6
Ash	5.33	44.2	9.21
HHV kJ/kg (Btu/lb)	23709.8 (10219)	9423 (4061)	22281 (9603)

Table 4.18: Properties of LB, and a 90:10 LB coal: LB blend

	Coal	Litter	LB:Coal 90:10
C	60.3	28.44	57.1
H	3.62	3.71	3.629
O	14.5	22.796	15.329
N	0.96	3.035	1.167
S	0.23	0.66	0.273
Cl	<.1	0.93	NA
Dry loss	15.12	11.62	14.77
FC	42.38	10.915	39.23
VM	37.17	50.65	38.51
Ash	5.33	26.815	7.47
HHV kJ/kg (Btu/lb)	23709.8 (10219)	12065.7 (5120)	22545.39 (9717)
P	NA	1.965	NA

Table 4.19: "90:10" blend properties for coal A and FB A

Parameter	Value
Dry Loss	20.551
Ash	9.1295
C	51.048
O	13.7935
H	3.4525
N	0.959
S	0.4365
Total	99.37
HHV	20202 kJ/kg (8685 Btu/lb)
FC	37.565
VM	32.102

Table 4.20: Coal A Calculated properties

Parameter	Value
Adiabatic Flame Temperature	2200 K (3500.33 ºF)
DAF formula	$CH_{0.7589}O_{0.1816}N_{0.0128}S_{0.00267}$
MW of DAF fuel	15.95
$A:F_{DAF}$	9.57
$A:F_{as\ received}$	6.866
Ash kg/MJ (lb/mmBtu)	0.0025 (5.8)
N kg/GJ (lb/mmBtu)	0.379 (0.879)
S kg/GJ (lb/mmBtu)	0.18 (0.418)
CO_2 kg/MJ (lb/mmBtu)	0.084 (194.9)

Table 4.21: FB A calculated properties

Parameter	Value
Adiabatic Flame Temperature	2012 K (3161.93 ºF)
DAF formula	$CH_{1.7795}O_{.6365}N_{.0825}S_{.01411}$
MW of DAF fuel	25.59
$A:F_{DAF}$	3.129
$A:F_{as\ received}$	6.1458
Ash kg/MJ (lb/mmBtu)	0.044 (106.54)
N kg/GJ (lb/mmBtu)	2.41 (5.59)
S kg/GJ (lb/mmBtu)	0.941 (2.18)
CO_2 kg/MJ (lb/mmBtu)	0.082 (190.26)

Table 4.22: Coal B calculated properties

Parameter	Value
Adiabatic Flame Temperature	2178 K (3460.73 ºF)
DAF formula	$CH_{.7162}O_{.1800}N_{.0137}S_{.0014}$
MW of DAF fuel	15.85
$A:F_{DAF}$	9.49
$A:F_{as\ received}$	8.14
Ash kg/MJ (lb/mmBtu)	0.0022 (5.33)
N kg/GJ (lb/mmBtu)	0.405 (0.94)
S kg/GJ (lb/mmBtu)	0.097 (0.225)
CO_2 kg/MJ (lb/mmBtu)	0.084 (194.9)

Table 4.23 FB-B calculated properties

Parameter	Value
Adiabatic Flame Temperature	2178 K (3460.73 ºF)
DAF formula	$CH_{1.4732}O_{0.6070}N_{0.0647}S_{.0113}$
MW of DAF fuel	24.47
$A:F_{DAF}$	24.47
$A:F_{as\ received}$	8.14
Ash kg/MJ (lb/mmBtu)	0.047 (109.05)
N kg/GJ (lb/mmBtu)	1.89 (4.39)
S kg/GJ (lb/mmBtu)	0.531 (1.23)
CO_2 kg/MJ (lb/mmBtu)	0.084 (194.9)

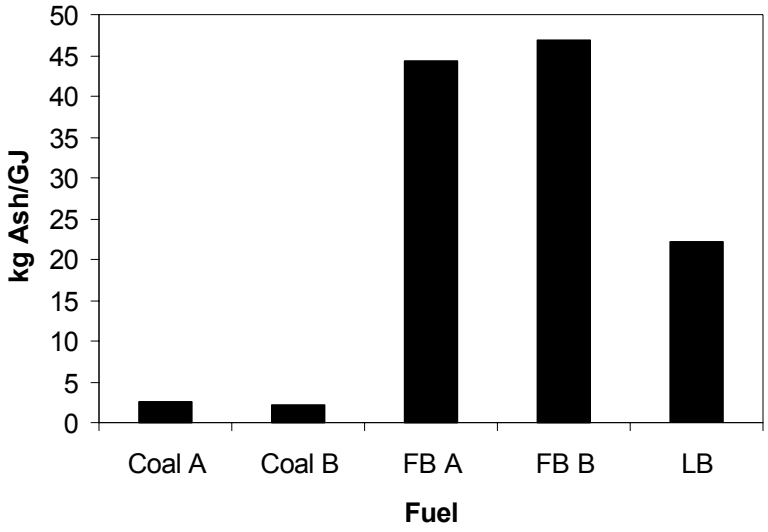

Figure 4.19: Ash content on a heat basis

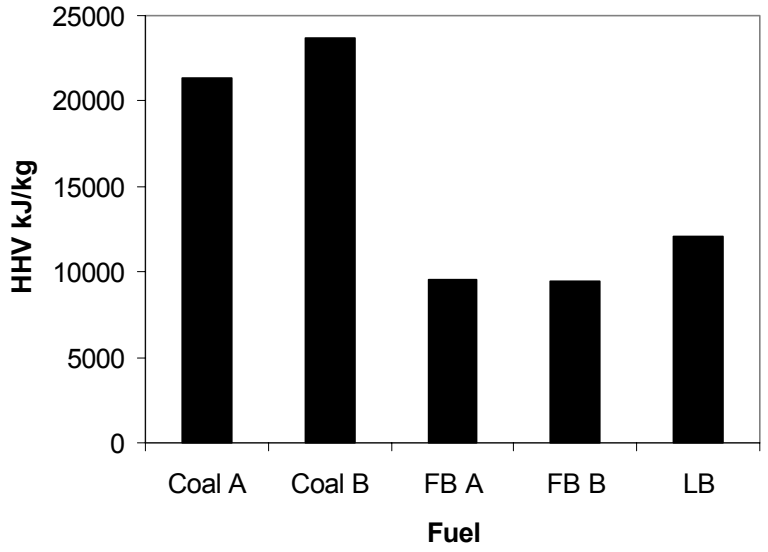

Figure 4.20: Heating values for the different fuels

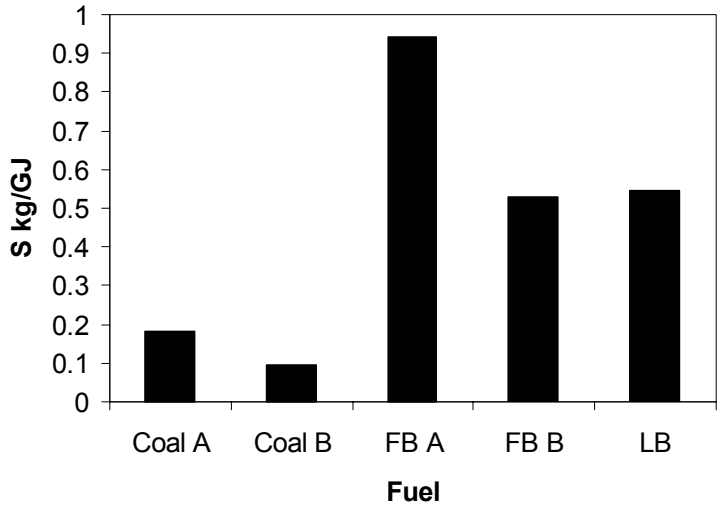

Figure 4.21: Sulfur content on a heat basis

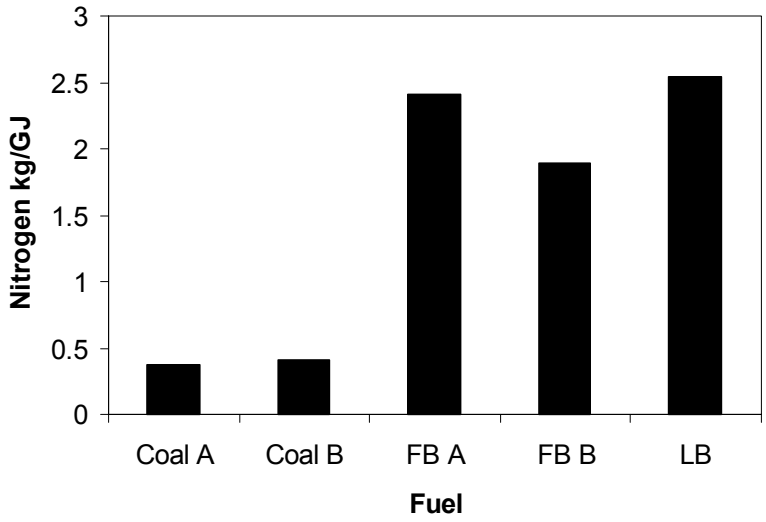

Figure 4.22: Nitrogen content on a heat basis

In addition to the ultimate and proximate analyses, the detailed ash compositions of "coal A" and "FB A" were analyzed. The results are shown in table 4.24 for coal and table 4.25 for FB-A. The results indicate that both of the ashes are composed primarily of silicon, with silicon making up 50% of the FB ash content. The composition of the FB ash will render it more alkaline than coal, with a lower ash fusion temperature, resulting in increased fouling problems. Also, note that both the FB and coal ash are high in CaO, which can capture SO_2 under the proper conditions.

Table 4.24: Coal A ash analysis

	Sample 1	Sample 2	Average
Aluminum , Al_2O_3	17.06	16.51	16.785
Calcium, CaO	23.09	23.07	23.08
Iron, Fe_2O_3	4.34	4.32	4.33
Magnesium, MgO	3.63	3.62	3.625
Manganese, MnO	0.05	0.06	0.055
Phosphorus, P_2O_5	0.81	0.99	0.9
Potassium, K_2O	0.51	0.46	0.485
Silicon, SiO_2	33.91	32.64	33.275
Sodium, Na_2O	1.74	1.71	1.725
Sulfur, SO_3	13.18	13.20	13.19
Titanium oxide	1.31	1.30	1.305
Total	99.63	97.88	98.755

Table 4.25: Analysis of FB A ash

	Sample 1	Sample 2	Average
Aluminum , Al_2O_3	5.27	5.38	5.325
Calcium, CaO	17.57	17.49	17.53
Iron, Fe_2O_3	1.73	1.76	1.745
Magnesium, MgO	3.45	3.48	3.465
Manganese, MnO	0.08	0.07	0.075
Phosphorus, P_2O_5	5.14	5.02	5.08
Potassium, K_2O	8.30	8.05	8.175
Silicon, SiO_2	50.35	50.70	50.525
Sodium, Na_2O	3.36	3.48	3.42
Sulfur, SO_3	4.59	4.42	4.505
Titanium oxide	.29	30	15.145
Total	100.13	129.85	114.99

4.1.4.2. Characteristics of pyrolysis and particle ignition

The previous section presented the VM for coal, FB, and LB, while pyrolysis and ignition characteristics are presented in this section. TGA experiments were conducted to determine the kinetics of pyrolysis and ignition behavior for coal, FB, LB, and 90:10 blends. The fuels designated FB A, Coal A, and LB were used for the TGA analyses, after being sieve classified as described in the experimental procedure (Thien *et al*., 2001a). For the TGA analysis, samples were pulverized, characterized, sieved using a sieve shaker, and divided into three size groups: $d_p < 45$ μm (0.0017"), 45 μm (0.0017") < d_p < 75 μm (0.0029") and $d_p > 75$ μm (0.0029"), and an unsieved fourth group containing a distributed size as fired in a boiler burner. The TGA analysis was repeated for the three size groups and finally on the unsieved fuels for coal, FB, LB, and 90:10 blends of both biomass types with coal. Under identical conditions, experiments were repeated using air as a purge gas. A matrix of the TGA experiments is shown in table 4.26. The number in the matrix shows the number of experimental runs that were conducted, and the base case, which is considered the full size fraction coal in nitrogen.

A typical TGA trace (heating rate of 10 K/min (18 ºF/min)) showing both the sample temperature and the mass is shown in Figure 4.23. Within about 10 min, the temperature rises to

about 370 K (206.33 ºF), releasing all the moisture. The sample gets heated up to 600 K (620.33 ºF) at t≈30 min without any significant mass loss, then the evolution of VM starts and is completed at t≈100 min. Figure 4.24 is a qualitative replot of figure 4.23 with temperature as the abscissa, which indicates the relationship between mass and temperature. Figure 4.25 shows the actual trace vs. temperature. Typical TGA traces for the full size group coal, FB, and a 90:10 blends are shown in figure 4.26. The first stage of the pyrolysis (figure 4.24) is the moisture loss portion, the second stage is a relatively flat portion where little mass is driven off as the samples continue to be heated, and the third stage is the pyrolysis portion of the curve as seen in figure 4.24. In order to better understand and compare the pyrolysis behavior of the fuels, the moisture loss portion of the curve was assumed to be any mass lost before 450 K (350.33 ºF). The TGA traces with the moisture loss portion of the curve removed to allow comparison is shown in figure 4.27. The final fourth stage is the heating of the FC and ash with little mass loss when N_2 is used as a carrier gas. The traces show that the biomass begins to loose volatiles at a lower temperature (≈ 520 K (477.66 ºF) for coal as compared to ≈ 620 K (656.33 ºF) for FB), and at a faster rate than coal. The behavior of the 90:10 blend is dominated by the behavior of the coal, which is to be expected as the blended fuel is 90 percent coal by mass, but still falls between the behavior of the two component fuels. Similar TGA traces were obtained for LB fuels.

Table 4.26: Matrix of TGA experiments, Base case - Full size distribution in N_2

	Air	Nitrogen
>45 μm Coal	1	1
45-75 μm Coal	1	1
<75 μm Coal	1	1
Full size Coal	1	1*
>45 μm FB	1	1
45-75 μm FB	1	1
<75 μm FB	1	1
Full size FB	1	1
>45 μm LB	1	1
45-75 μm LB	1	1
<75 μm LB	1	1
Full size LB	1	1
>45 μm 90:10 coal:FB blend	1	1
45-75 μm coal:FB blend	1	1
<75 μm coal:FB blend	1	1
Full size coal:FB blend	1	1
>45 μm coal:LB blend	1	1
45-75 μm coal:LB blend	1	1
<75 μm coal:LB blend	1	1
Full size coal:LB blend	1	1

Number indicates number of experiments, * is base case

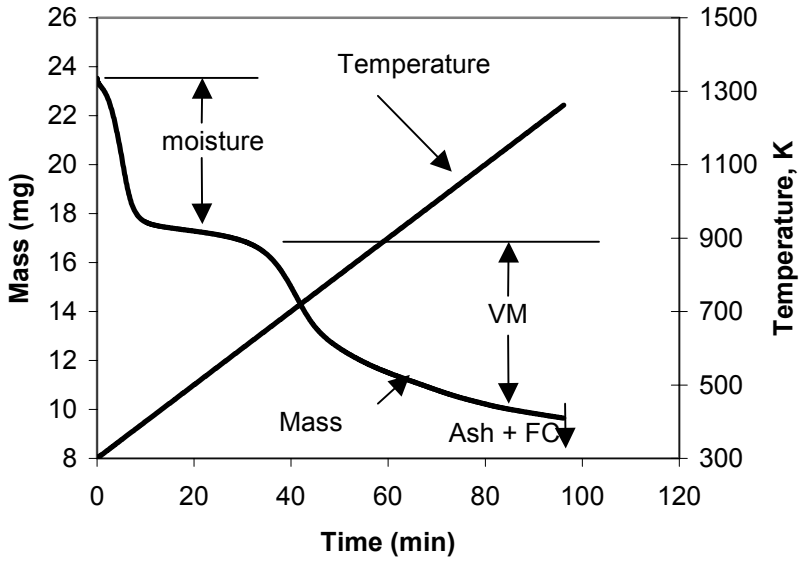

Figure 4.23: Typical TGA traces for coal A (Full size)

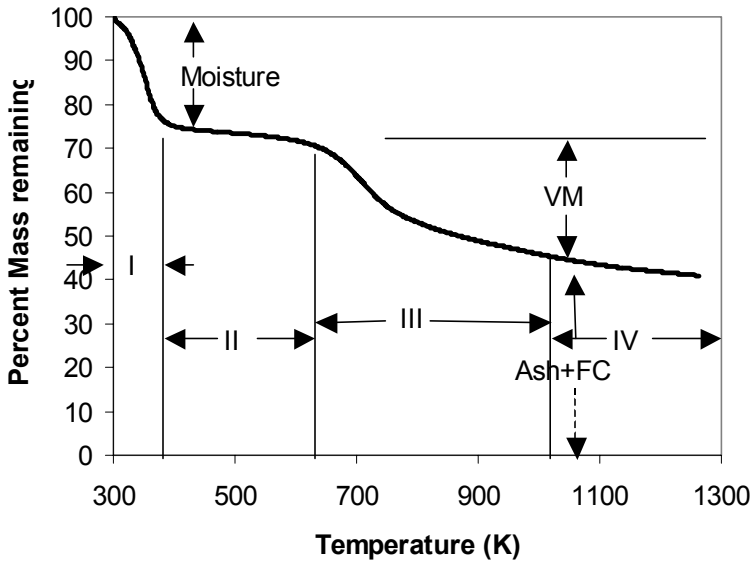

Figure 4.24: TGA trace as plotted with temperature as abscissa.

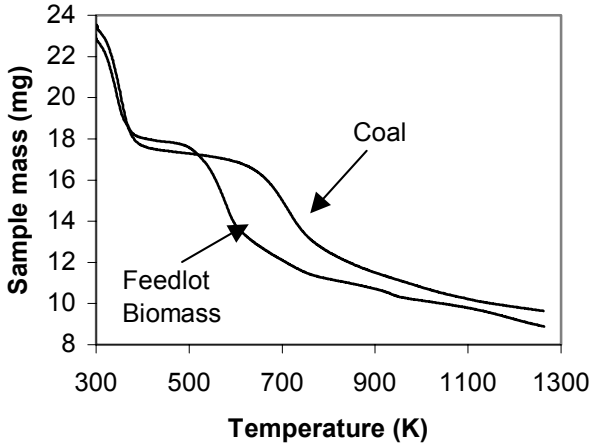

Figure 4.25: Actual Mass loss vs Temperature trace

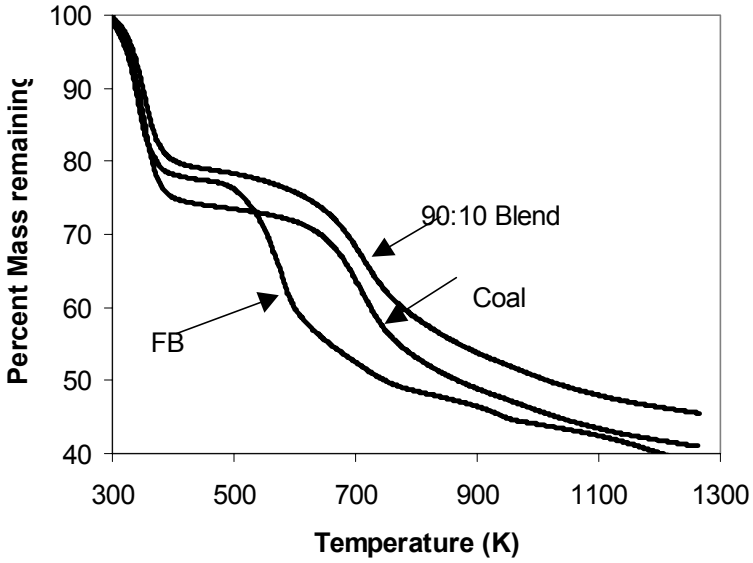

Figure 4.26: TGA traces for coal-A, FB-A, and 90:10 blend, full size fraction.

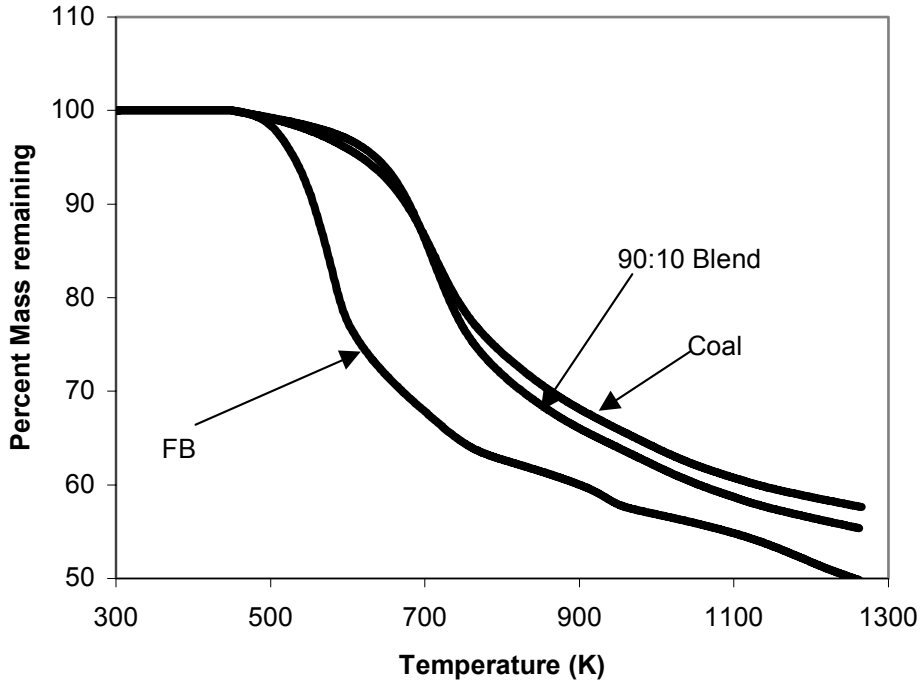

Figure 4.27: TGA traces, with moisture loss removed, full size fraction.

4.1.4.3. Parallel reaction model

The TGA traces were fit to the parallel reaction, to determine the average activation energy and standard deviation of activation energies as seen in the literature review. A FORTRAN program was developed to numerically integrate the integrals, and determine the best-fit values of E_m and σ. The integrals were evaluated using Simpson's formula for numerical integration. The best fit values of E_m and σ were found by minimizing the squared error. Various values of E_m and σ were tried by the program until a minimum value could be found. The value 1.002×10^{15} 1/min was chosen for k_o under the recommendation of Raman *et al*., (1981a), and Anthony *et al*., (1974).

Figure 4.28 shows a TGA trace of coal, and the parallel reaction curve fit to the TGA data. The parallel reaction model is described elsewhere (Anthony *et al.,* 1994) and more details are provided in Thien (2002). The average activation energy for all size classes is shown in figure 4.29, with the standard deviations shown in figure 4.30. A comparison of the results between FB A, LB, and Coal A is found in figure 4.31. The numerical results from the parallel reaction model analysis are available in table 4.27. The curve fits were performed over the entire mass loss, but different values of E and σ are found in the literature. The TGA parallel reaction curve fits reveal that the activation energy of FB is lower than the average activation energy of the coal, and slightly greater than the activation energy of LB. The lower activation energy in the biomass leads to a faster release of volatiles, at a lower temperature. The TGA curve fits also reveals that the standard deviation of activation energies is larger in FB than in coal. A larger standard deviation translates into a greater spread of activation energies, and indicates FB is a less homogeneous substance than coal. The geologic process that convert organic matter to coal underground have a homogenizing effect, while such a scheme is not available for FB and LB.

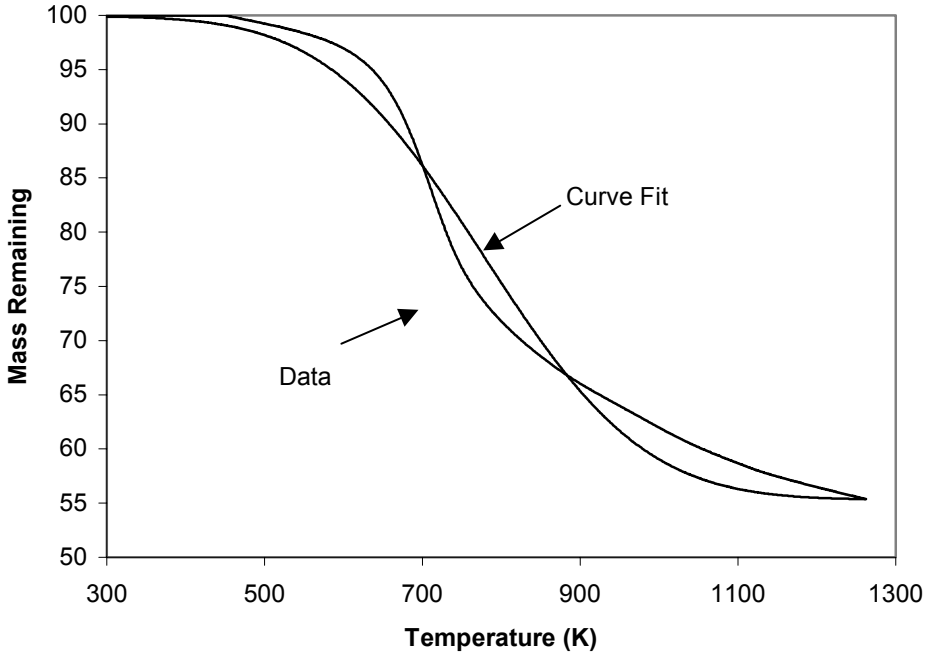

Figure 4.28: TGA parallel reaction model fit to coal, full size fractions.

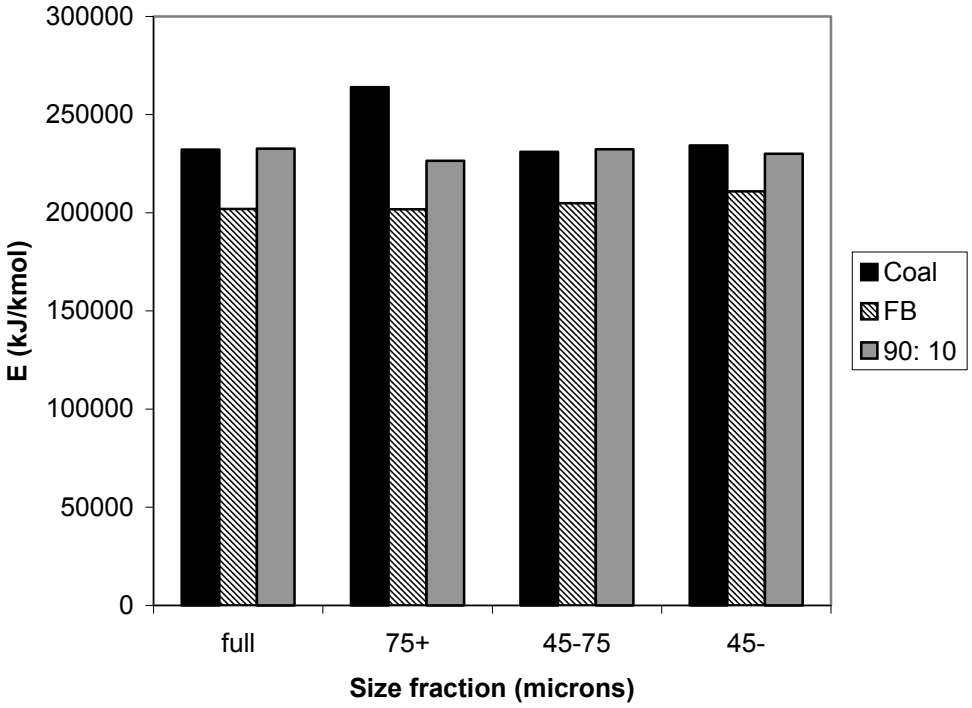

Figure 4.29: Parallel reaction model E_m values, for all size classes.

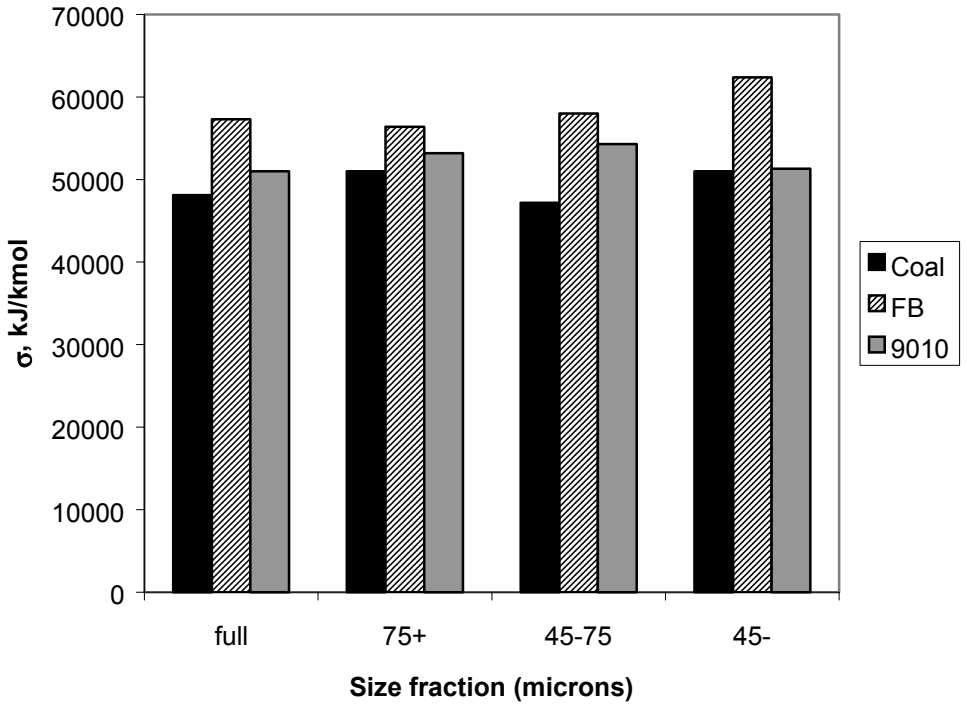

Figure 4.30: Parallel reaction model σ values for all size classes

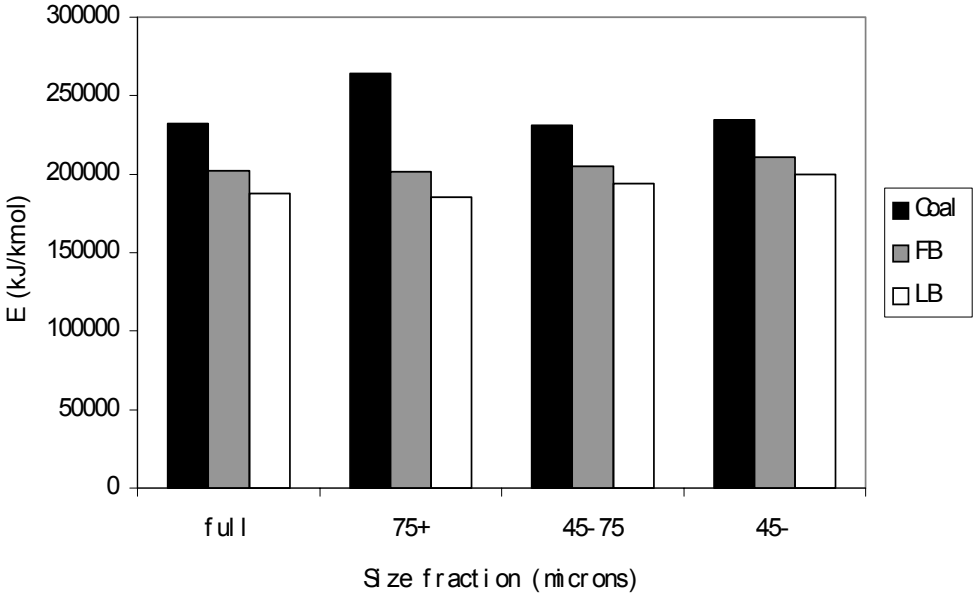

Figure 4.31: Comparison of Coal, LB and FB activation energies

Table 4.27: Parallel reaction parameters for fuels tested

E (kJ/kmol)					
	Coal	FB	FB 90:10	LB	LB 90:10
full	232200	202000	232700	187700	222600
75+	264000	201800	226500	185100	215000
45-75	231000	204900	232300	193900	226300
45-	234300	210800	230100	199900	231100
σ (kJ/kmol)					
	Coal	FB	90:10	Litter	90:10
full	48100	57300	51000	39300	47500
75+	51000	56400	53200	35400	47600
45-75	47200	58000	54300	47000	49500
45-	51000	62400	51300	53300	53900

4.1.4.4. Single reaction model

The PCGC-2 combustion code, which is used in modeling the combustion behavior of coal: biomass fuel blends, requires kinetic parameters for the pyrolysis of biomass. The parallel reaction model is useful for describing the underlying physics of biomass pyrolysis, but it is too complicated to be used in a practical combustion code, as it requires the evaluation of two numerical integrals. To model the pyrolysis of biomass fuels for computer modeling, the TGA trace of FB was curve was also curve fitted with the single reaction model. The computer code used for simulation runs allows either the competing reaction model or the single reaction model for the pyrolysis of fuel. Thus in addition to the parallel reaction model, the single reaction model was also used for the modeling of pyrolysis. The single reaction model of pyrolysis describes pyrolysis with the following Arrhenius rate equation:

$$\frac{dm_v}{dt} = -Bm_v \exp\left(\frac{-E}{RT}\right) \qquad (4.1.11)$$

Appendix 3 provides the details of deduction of B and E for the single reaction model.

The first attempts to the fit the FB to the single reaction model yielded activation energies and pre-exponential factors that were much lower than expected. It was observed that as less of the mass loss was used to curve fit the data, the closer the values came to resemble commonly accepted values. Figure 4.32 shows single reaction model curve fits for the full size group of FB, with each succeeding graph covering more of the mass loss. The temperature on each of the graphs indicates the ending temperature of the curve fit, when the starting temperature was taken as 300 K (80.33 ºF). The values of B and E that were obtained for each of these curve fits are show in table 4.28. The results show that the curve up to 600 K (620.33 ºF) follows the fit portion of the curve very closely, and as the portion fit increases, the fit follows the data less closely. The results also indicate that the values obtained for the 600 K (620.33 ºF) curve fit come closest to the values usually expected for an activation energy and pre-exponential factor. The problem with the curve fits lies in the second half of the pyrolysis, where the slope appears to change, and slowly levels off. The change in slope indicates that there may be a second reaction occurring during the pyrolysis process, and that a model that includes two different reactions may be more appropriate.

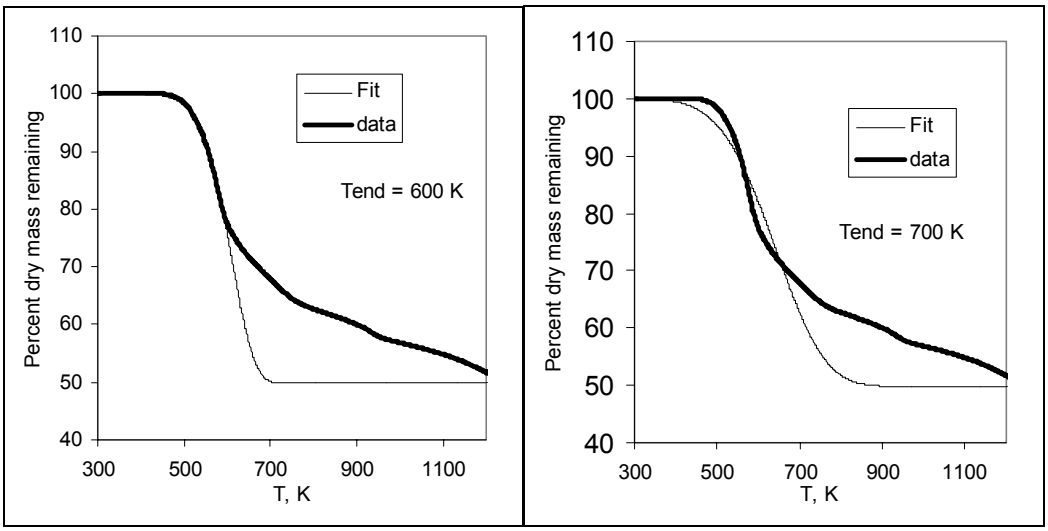
Percent dry mass remaining
T, K
Fit
data
Tend = 600 K

Percent dry mass remaining
T, K
Fit
data
Tend = 700 K

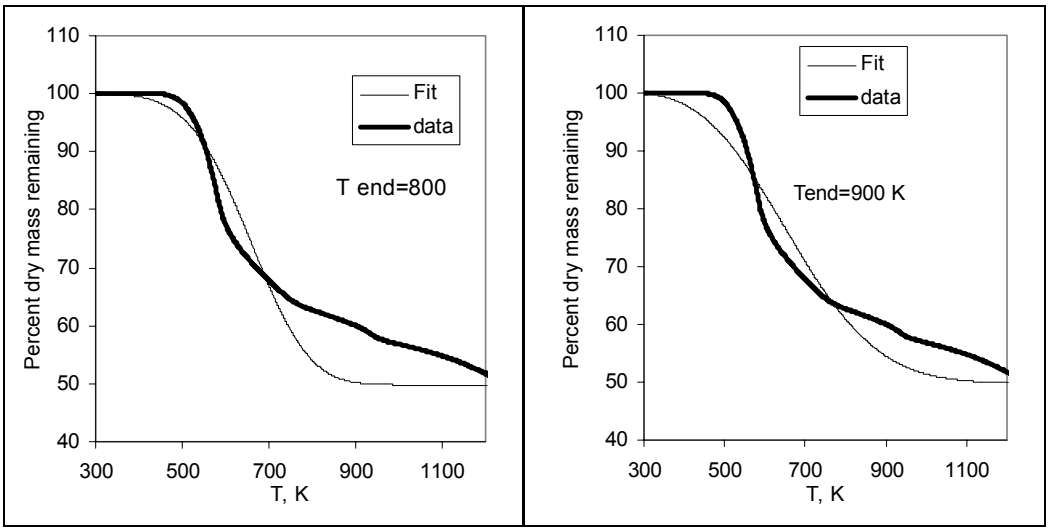
Percent dry mass remaining
T, K
Fit
data
T end=800

Percent dry mass remaining
T, K
Fit
data
Tend=900 K

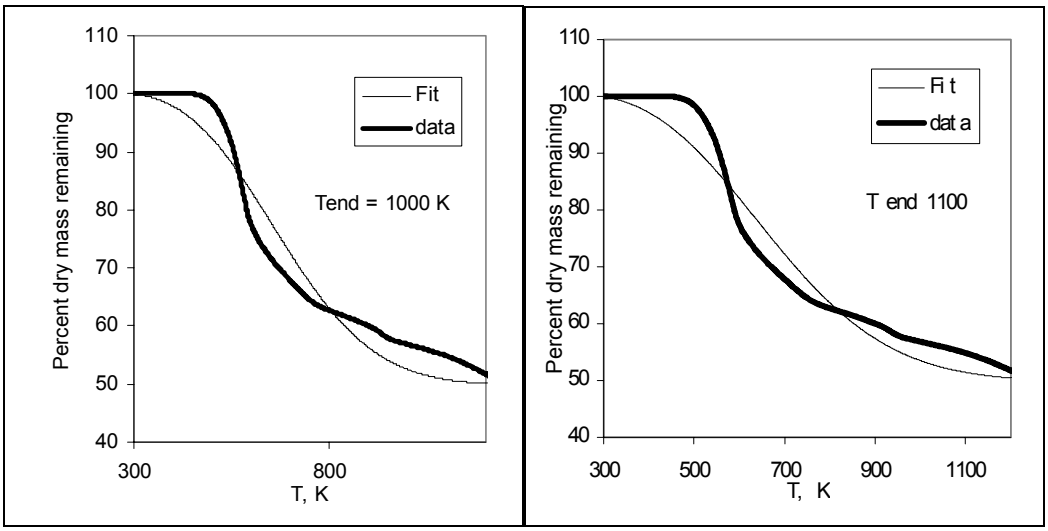
Percent dry mass remaining
T, K
Fit
data
Tend = 1000 K

Percent dry mass remaining
T, K
Fit
data
T end 1100

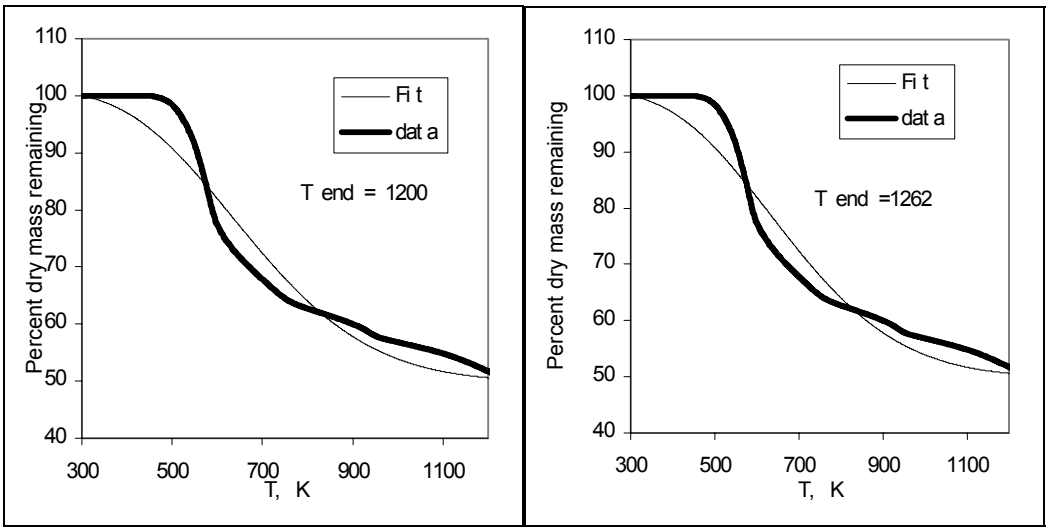

Figure 4.32: TGA curves over part of mass loss for coal, T_{start} = 300 K (80.33 ºF)

Table 4.28: Single Reaction Parameters for a curve fit over part of the full size fraction FB TGA curve for coal T_{start} = 300 K (80.33 ºF)

Ending Temp (K)	E (KJ/kmol)	B (1/min)	% mass loss covered	Ending mass (% of total)
600	60811	30038	45.1	77.36
700	29528	21.25	64.44	67.65
800	27940	12.23	62.69	62.69
900	15367	0.753	79.76	59.96
1000	14000	0.5133	86	56.83
1100	11697	0.3156	90.19	54.81
1200	11157	0.277	96.14	51.74
1262	11125	0.2758	100	49.80

4.1.4.5. Ignition Characteristics

The TGA experiments were then repeated using air as a purge gas, for all fuels, and size fractions in order to determine the ignition behavior. Using the same method as Tognotti *et al* (1985), the ignition temperature of the fuels was found graphically as the point where the nitrogen and air traces diverged, as shown in figure 4.33 for coal. The circled point where the curves diverged was taken as the ignition temperature. The ignition analysis was repeated for FB and LB, but the results did not clearly indicate an ignition temperature, as seen in figure 4.34. The higher volatile matter of the biomass, lower release temperature and the reduced O_2 concentration due to blowing effect may interfere with ignition, as the volatiles carry away thermal energy when released from carbon oxidation, and may keep the biomass from reaching a clear ignition temperature. The coal ignition temperatures were analyzed with a group ignition theory, with the results shown in figure 4.35 (Thien *et al.*, 2001, Thien *et al.*, 2003). The x-axis is the mass mean diameter of the particles in the sample, and the y axis is the observed ignition temperature. The values E = 86530 kJ/kmol (81844 Btu/kmol) and B = 662 m/s (2034 ft/s) for the group ignition temperature model were found to be the best fit for the ignition data. As the particle size in the sample increases, the ignition temperature increases. This is in agreement with Hertzberg *et al* (1981), who also found an increasing ignition temperature with increasing particle size for groups of particles. The trend of increasing temperature with

increasing particle size is typically reversed for single particles, where a smaller particle size results in greater heat loss, and a lower ignition temperature.

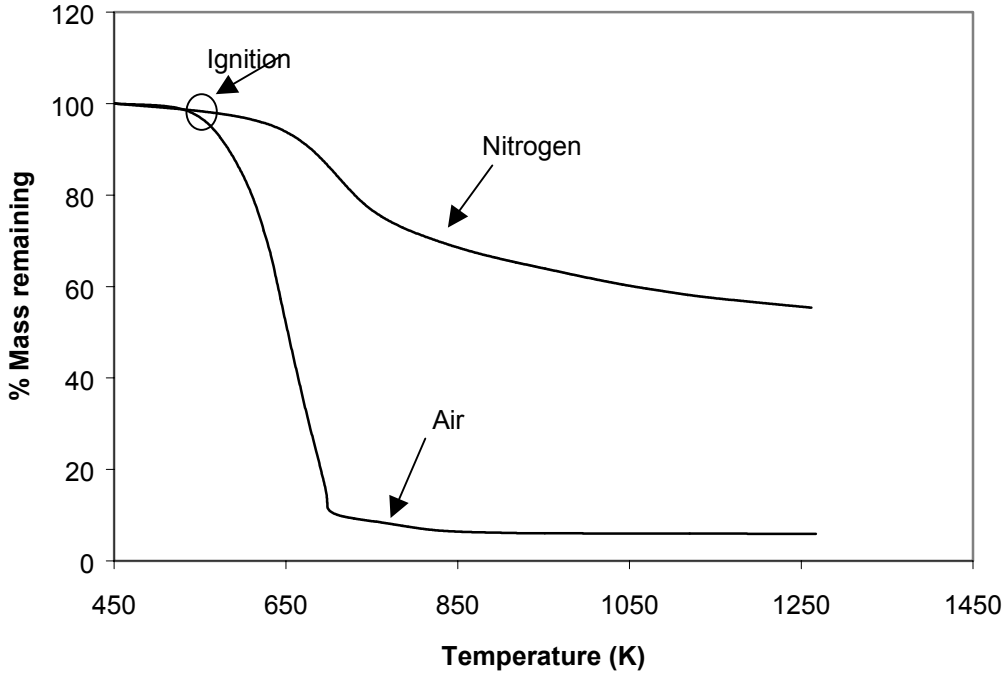

Figure 4.33: Determination of ignition temperature for coal (full size).

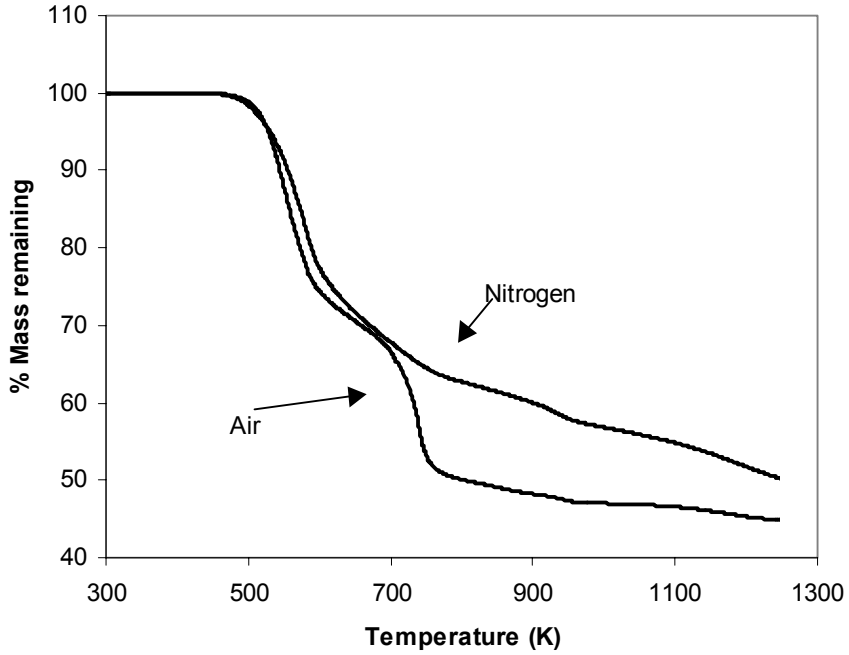

Figure 4.34: FB TGA in nitrogen and air, full size group

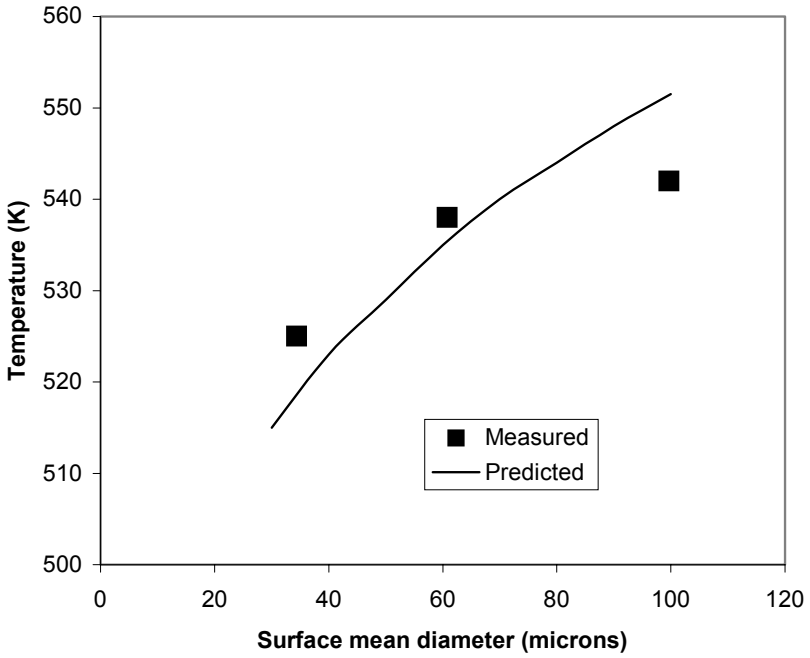

Figure 4.35: Ignition temperature vs. particle size of coal

4.2. Boiler Burner Experiments for Cofiring of CFB and CLB fuels and Reburn Test

4.2.1. Cofiring Results with Coal: FB Blends

The FB used in the experiments was placed on tarps, and allowed to dry in a greenhouse until < 8% moisture was obtained. Then the FB was placed in sealed barrels, shipped to California, and ground. The first series of experiments were conducted with coal and FB "A", while the second series of experiments was conducted with coal and FB "B" (Annamalai *et al.,* 2001, Annamalai *et al*., 2002). The properties of both the "A" and "B" fuels are detailed in tables 4.15 to 4.17. Table 4.29 is a matrix showing the experiments that were conducted in the furnace. Coal at 10 % excess air is considered the base case for the co-firing experiments. Table 4.30 shows the cofiring parameters for the experiments.

Table 4.29: Cofiring experimental matrix

	Excess air			
Fuel:	5	10*	15	20
Coal	2	2*	2	2
90:10 Coal: FB blend	2	2	2	2
90:10 Coal: LB blend	2	2	2	2

Number indicates number of experiment, * base case

Table 4.30: Cofiring parameters for the furnace

Parameter	Value
Primary air	0.059 m^3/min (108 SCFH)
Fuel flow rate	~80 g/min
Primary air loading ratio (air/fuel)	1.33
Secondary air	0.497-0.578 m^3/min (1054-1225 SCFH)
Primary air % or total air	9%
Secondary air Temp	380 K (224.33 ºF)
Residence time	~4 s cold, ~1 s cold
Heat throughput	30 kW_t (100,000 Btu/hr)

Results of experiments in the unmodified reactor (shorter reactor length) particularly the high CO concentration (Frazitta et al., 1999) illustrated, the need for a longer residence time and verification of the calculated equivalence ratio, an adjustment for the action of the propane torches which lowered the O_2 concentration, and an error analysis. The furnace was run without coal to measure the oxygen percentage from the propane torches. The oxygen concentration was found to be 19 %, and for the second set of experiments in the extended furnace, the excess air percentages were calculated by assuming the ambient air contained only 19 % oxygen on a dry basis instead of the 20.9 % normally present in air. To address the possibility of air leaking into the furnace, any visible cracks in the furnace were sealed with silicon sealant, and then the furnace was tested for leaks with a propane burner. The coal burner was replaced with a propane burner, which was run at 30 kW_t (100,000 Btu/hr) with the propane igniter torches off, and the oxygen concentration was recorded at a variety of different furnace pressure settings, with and without the probe sealed into the furnace with

electrical tape. At first, the results indicated a leak of 0.85 m^3/hr (30 SCFH) into the furnace with the damper set to 2.54 mm (0.1") of water column and the secondary air was adjusted to account for the difference. Later it was found to be correct without correction, as the expected oxygen concentration was calculated on a wet gas analysis while the gas analyzer provides a dry gas analysis. The initial results indicated the furnace was not leaking, and the results have been altered to account for the 30 SCFH difference and the results have been adjusted to indicate the correct excess air percentage, which are no longer are 0, 5, 10, and 15 % as originally intended.

An error analysis was conducted to quantify the error in the calculated parameters. Table 4.31 gives the errors for the equipment used in the experiments, with values provided by the manufactures, and table 4.32 shows the errors for the calculated experimental parameters, based on a standard error analysis. The reported errors in the table are the maximum errors encountered over the range of values encountered in the results. Typical values for all of the parameters were chosen and used to calculate a percent error to give the reader a better feel for the magnitude of the errors. The biggest error occurred in the calculation of the excess air, as it is closely related to the equivalence ratio, but its magnitude is increased, as it must be subtracted from one during the calculation. The error bars shown on the co-firing results, and on the reburning results, are calculated from the error analysis.

Table 4.31: Given instrument error

Parameter	Error	Typical Value	Percent error
O_2 Concentration	± 0.2 %	3%	± 6.66%
CO Concentration	±4% of reading	500 ppm	± 4%
CO_2 Concentration	± 0.1%	12%	± 0.83%
NO	±4% of reading	420 ppm	± 4%
NO_2	±4% of reading	0	± 4%
SO_2	±4% of reading	60 ppm	± 4%
Combustibles	±10% of reading	1.33	± 10%
Primary air Gauge	± 3 SCFH	70 SCFH	± 4.2%
Secondary Air Manometer	± 0.05 in	5.8 in	± 0.86%
Solids feeder	± 2 g/min	80.7 g/min	± 2.48%
DL	± 0.03%	23.60	± 0.13%
C	± 0.03%	2.91	± 1.03%
H	± 0.03%	19.08889	± 0.16%
O	± 0.03%	1.78	± 1.7%
N	± 0.03%	0.71	± 4.2%
S	± 0.03%	7.73	± 0.39%
Ash	± 0.03%	44.16	± 0.068%
Heating value	± 221 kJ/kg	9421.9 kJ/kg	± 2.34%
Digital scale	± 2 g	250 g	± 0.8%
Package Scale	± 0.25lb	18 lb.	± 1.39%
Secondary air	±6% of reading	1100 SCFH	± 2%

Table 4.32: Derived errors

Parameter	Error	Typical Value	Percent error
Fraction manure mixed	± 0.0026	0.1	± 2.6
Primary air SCFH	± 5.3	108	± 4.907
Equivalence Ratio	±0.027	0.909	± 2.970
Excess air	±3.925	10%	± 39.25
BF	±0.031	0.95	± 3.263
X_{CO2}	±0.006	0.11	± 5.454
Nconv	±0.016	0.16	± 10
NO kJ/kg	±0.014	0.17	± 8.235
NO normalized ppm	±21.95	381	± 5.761
% Reburn reduction	± 5%	50 %	± 2.6

4.2.1.1. Size effects

The effect of different biomass particle sizes was investigated by size classifying the biomass into 3 size groups: a 0-75 μm size group, a 75-150 μm size group, and a 150+ μm size group. Biomass can be harder to grind than coal, and experience a larger variation of size. The effect of different sizes must be investigated before larger scale co-firing can be attempted. The fuels were fired at 10 % excess air using the same experimental parameters. Figure 4.36 shows the effect of the difference particle sizes on the CO emissions. The CO emissions are the same for all of the size classes except for the largest size class. The larger particles take longer to burn, resulting in less complete combustion and a higher CO emissions level. The effect of biomass particle size on O_2 % emissions is shown in figure 4.37. Since coal constitutes 90 % of the blend, the different size groups do not appear to have different O_2 levels, but the full size group appears to have a slightly higher O_2 level due to variations in the experiments. The burnt mass fraction is shown in figure 4.38 for the different size groups. The level of combustion seems to be fairly constant for all of the size groups, expect for the full size group, because of its higher oxygen concentration. Now the NO emissions are seen on an uncorrected ppm basis in figure 4.39. The results again show similar level across all of the different size groups. Finally, the NO emissions are shown in figure 4.40 on a kg/GJ basis. Again, it is seen that there are no large differences between the different size groups. Smaller sized particle heat up rapidly and release gases and N compounds rapidly. Thus the BF is higher, lesser CO and hence more NO.

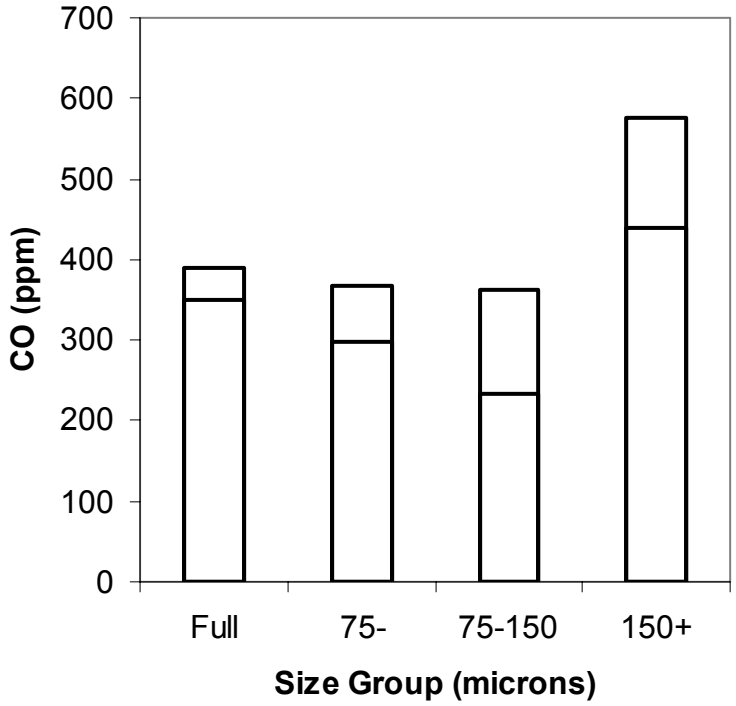

Figure 4.36: Effect of biomass particle size on CO emissions

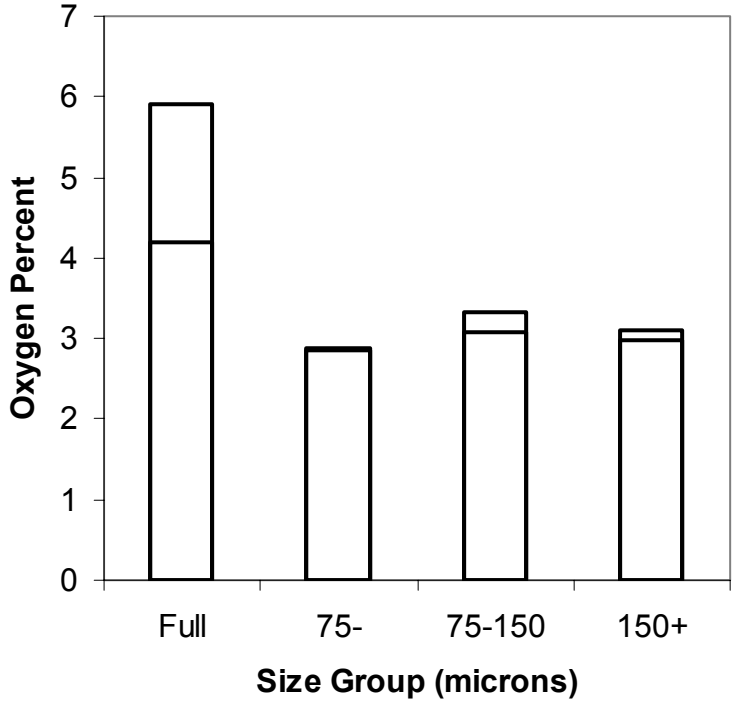

Figure 4.37: Effect of biomass particle size on O_2 emissions

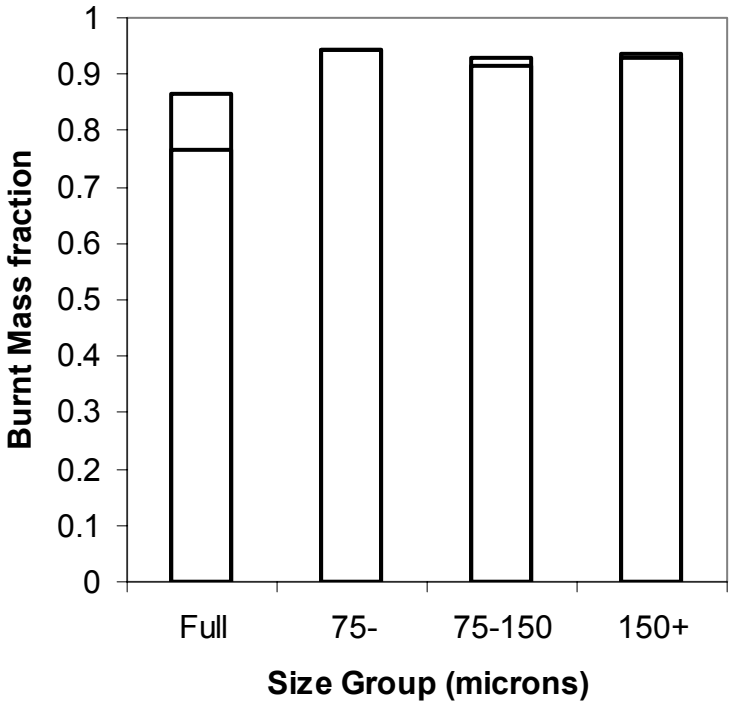

Figure 4.38: Effect of biomass particle size on burnt mass fraction

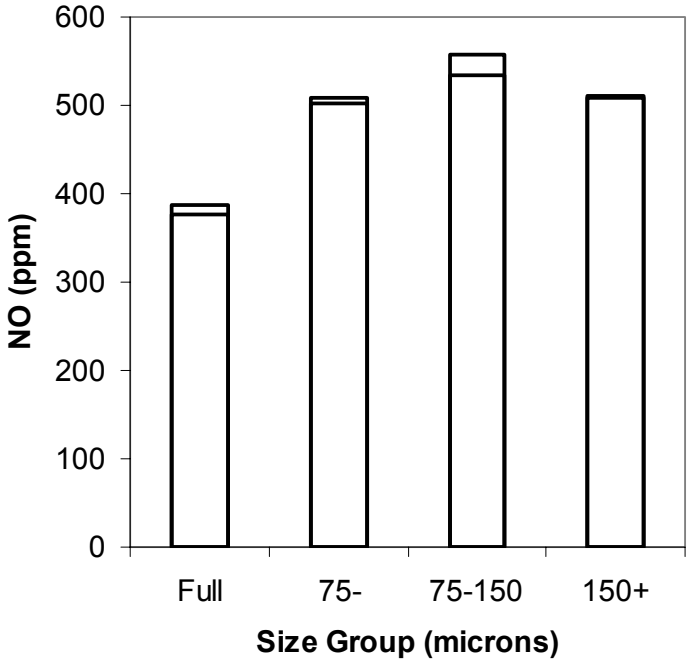

Figure 4.39: Effect of biomass particle size on NO emissions (uncorrected)

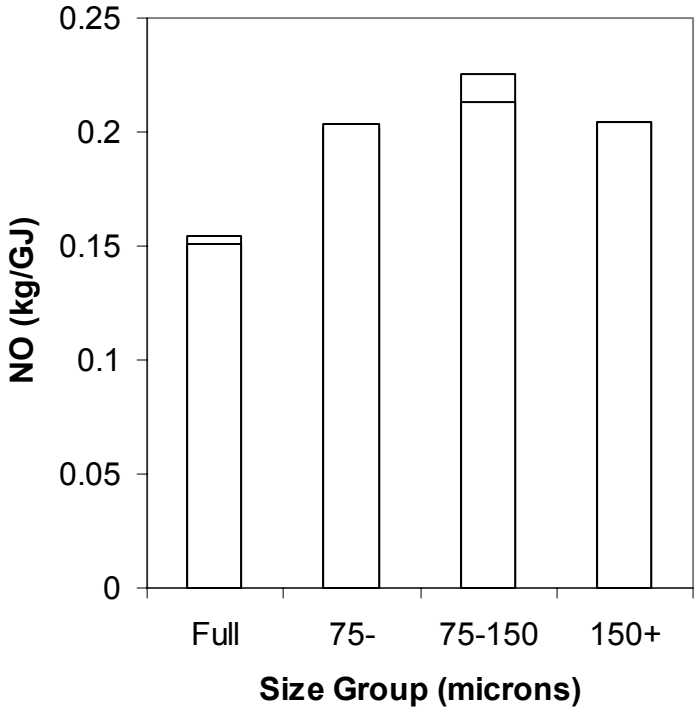

Figure 4.40: Effect of biomass particle size on NO emissions on a heat basis

4.2.1.1. Swirl Effects

The effect of changing the swirl number was also investigated. The swirl at the top of the furnace was removed and replaced with a swirler with a fin angle of 55° to get a secondary air swirl number of 1. The original swirl burner had a secondary air swirl number of 0.7 and a swirl angle or 45°. The effect of the altered swirl number on CO emissions is shown in figure 4.41. There is little change between the high swirl and the low swirl burner. The effect of changing swirl on the O_2 emissions is shown in figure 4.42. The higher swirl results in a lower oxygen concentration. The high swirl number results in greater turbulence, and a faster mixing of fuel and air, and hence rapid combustion which results in lowering O_2 %. The effect of swirl number on the burnt mass fraction is shown in figure 4.43. The result of greater mixing in again seen in the burnt mass fraction, where the greater mixing results in a greater burnt mass fraction. The swirl also influences the NO emissions, seen on a ppm basis in figure 4.44, and on a kg/GJ basis in figure 4.45. The greater swirl and mixing translates to higher levels of NO emissions. The fuels are mixed faster, bringing the fuel N and Oxygen together sooner, and allowing more time for NO formation.

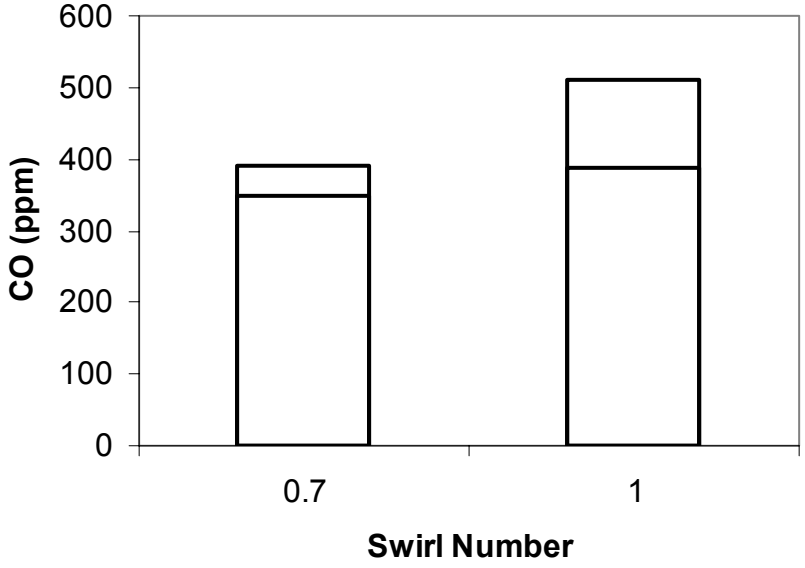

Figure 4.41: Effect of swirl number on CO emissions

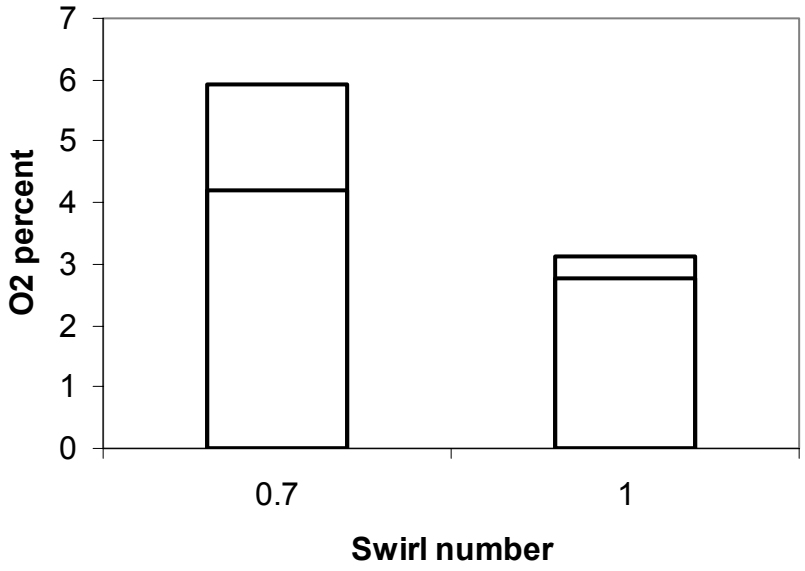

Figure 4.42: Effect of Swirl number on O_2 emissions

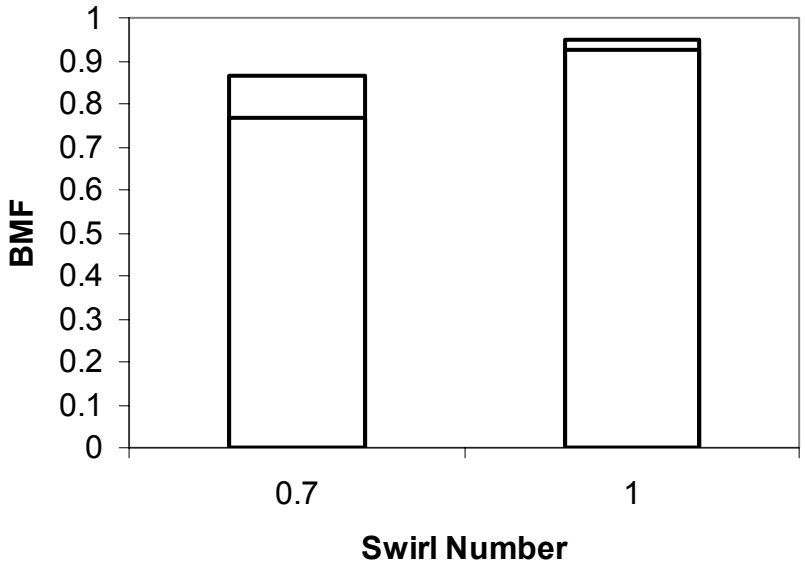

Figure 4.43: Effect of Swirl number on BMF

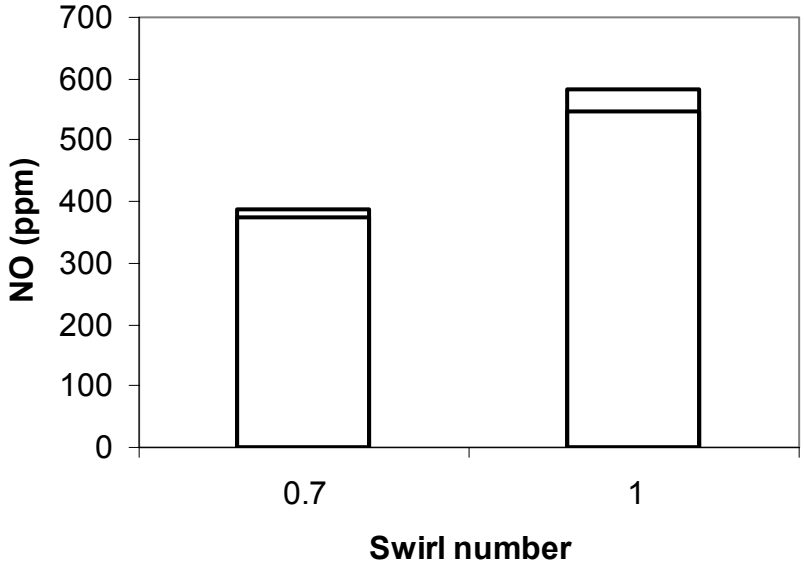

Figure 4.44: Effect of swirl number on NO

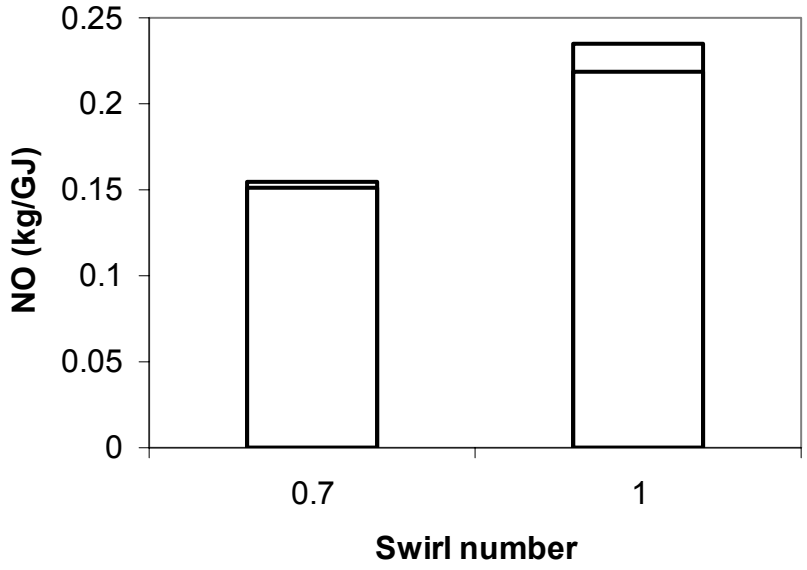

Figure 4.45: Effect of swirl number on NO emission (heat basis)

4.2.1.3. FB moisture effects

Next, the effects of different manure moisture contents were investigated. The biomass used in these experiments was dried to allow for grinding and easier handling. In an industrial setting, drying to a low moisture level of the order of 10 % may not be possible, and it is necessary to investigate the effect that a high level of biomass moisture will have on the combustion parameters. For these experiments, water was mixed with the coal and the biomass to simulate biomass moisture with 30 % dry loss. The resulting CO emissions are given in figure 4.46. The results show that the higher biomass moisture will translate into high CO emissions by creating more CO through reaction between steam and the fuel char. Similar results were obtained by Chen et al when they injected water along with fuel in a boiler burner (Chen *et al.*, 2001). The O_2 emissions for high and low biomass moisture levels are given in figure 4.47 and the burnt mass fraction are shown in figure 4.48. The burnt mass fractions appear similar in both cases. The reduction in heating value caused by the addition of water is made up by faster reaction with steam, which allows the fuels to achieve similar level of burnt mass fraction. Finally, the NO emissions are shown on a ppm basis in figure 4.49, and on a heat basis in figure 4.50. Lower levels of NO emission were obtained with the low moisture fuel. The higher water content will result in lower flame temperatures, and a corresponding drop in the formation of thermal NO_x from atmospheric nitrogen.

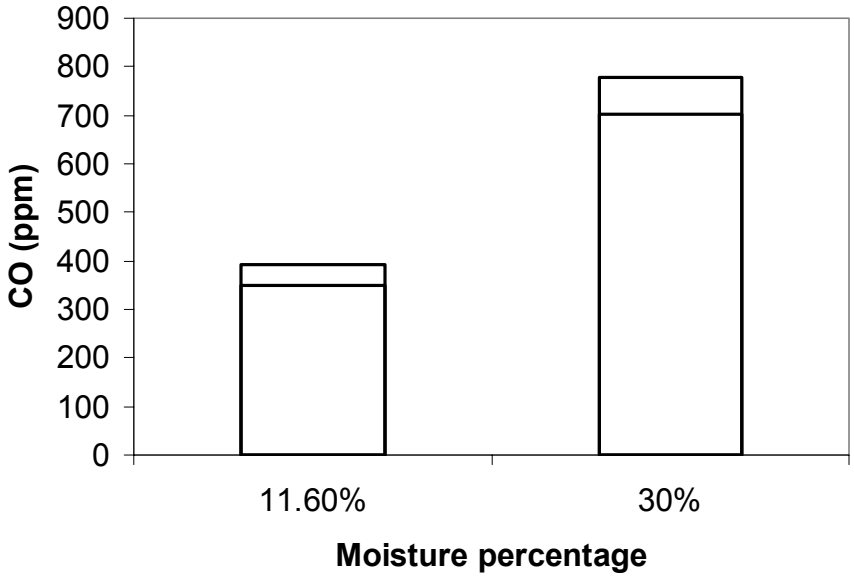

Figure 4.46: Effect of biomass moisture percentage on CO emissions

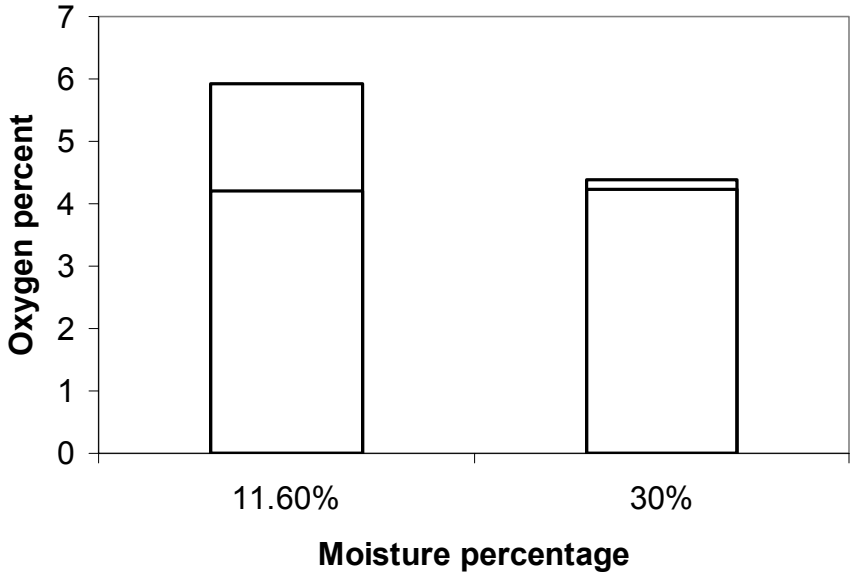

Figure 4.47: Effect of biomass moisture percentage on O_2 emissions

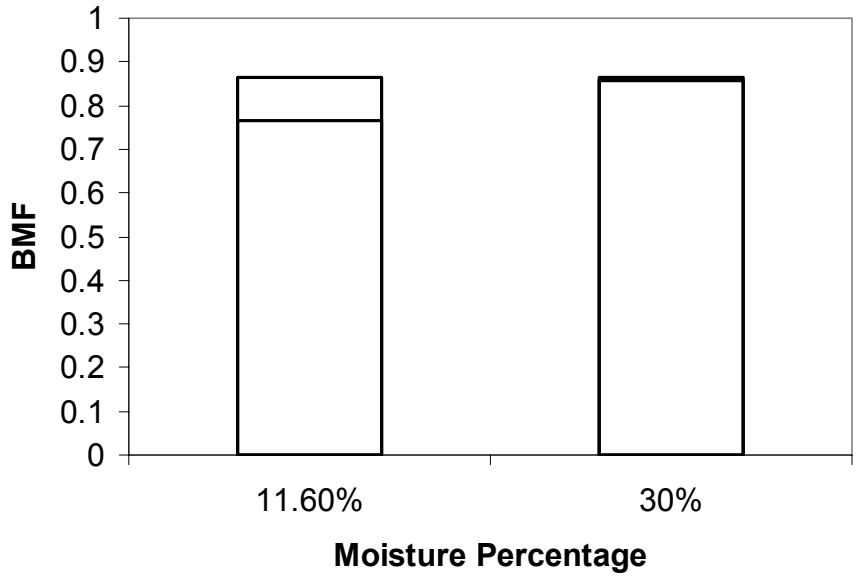

Figure 4.48: Effect of biomass moisture percentage on burnt mass fraction

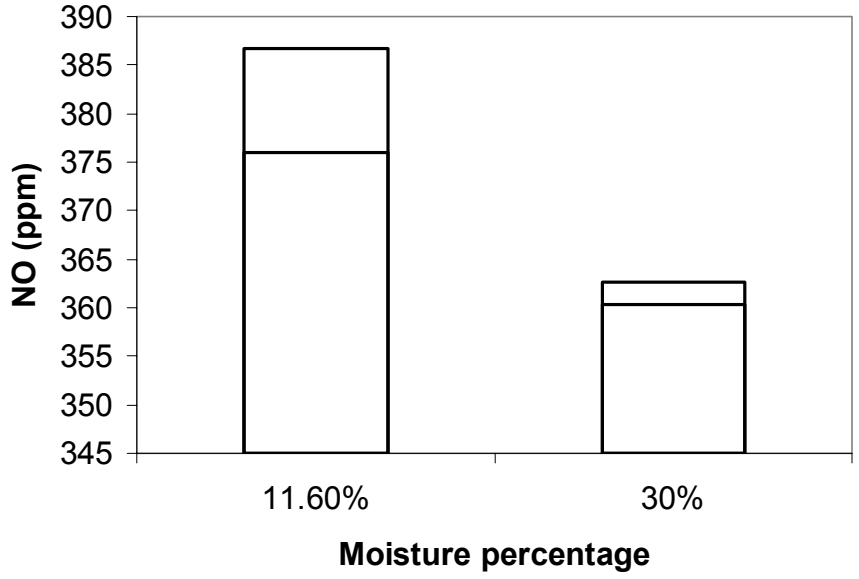

Figure 4.49: Effect of biomass moisture percentage on NO emissions

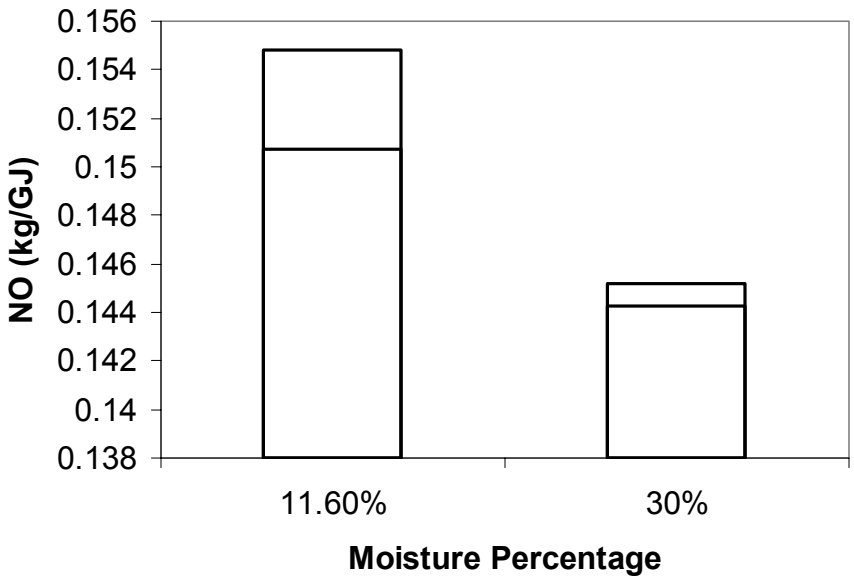

Figure 4.50: Effect of biomass moisture percentage on NO emissions (heat basis)

4.2.1.4. Loading ratio

The effect of different loading ratios on the combustion performance was also investigated. The loading ratio is the mass of fuel in the primary air stream divided by the mass of air in the primary air stream. When a higher loading ratio was tried, with more fuel in the stream, the greater fuel density caused frequent clogging in the venturi, and sometimes uneven combustion results were obtained. The variation of CO with loading ratio is shown in figure 4.51, and the variation of O_2 with loading ration is shown in figure 4.52. The clogging of the fuel feeder created burst of fuel, which resulted in the high CO and lower O_2 levels, as burst of fuel would cause spikes of high CO and low oxygen. The effect of the primary air-loading ratio on the burnt mass fraction is shown in figure 4.53. Finally, the NO emissions on a ppm basis and on a heat basis are shown in figures 4.54 and 4.55. The higher loading ration resulted in a higher NO emissions, but the results are unreliable due to the problems with feeding the fuel at the higher loading ratio.

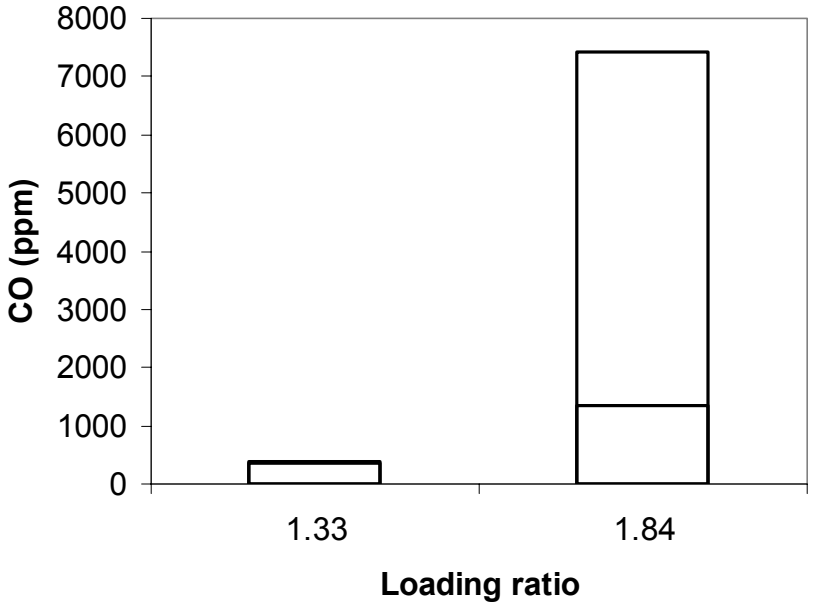

Figure 4.51: Effect of primary air loading ratio on CO emissions

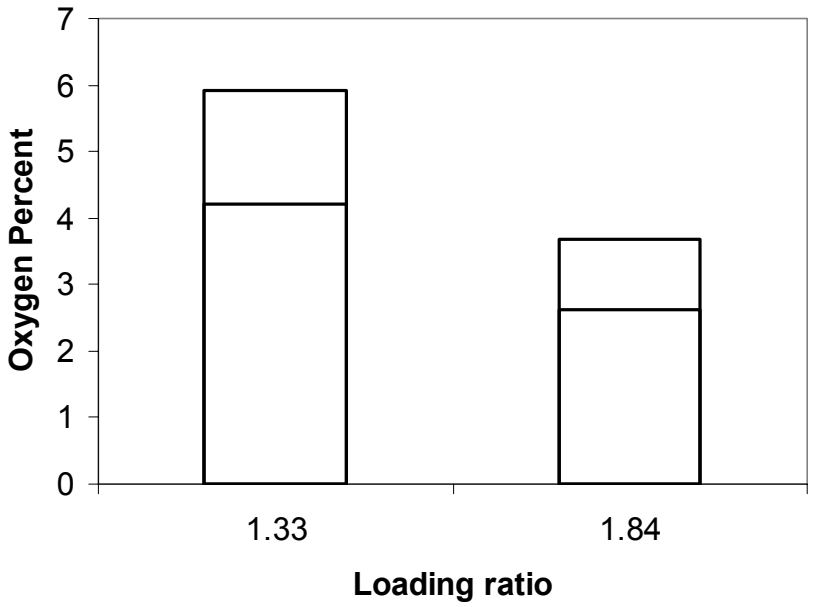

Figure 4.52: Effect of primary air loading ratio on O_2 emissions

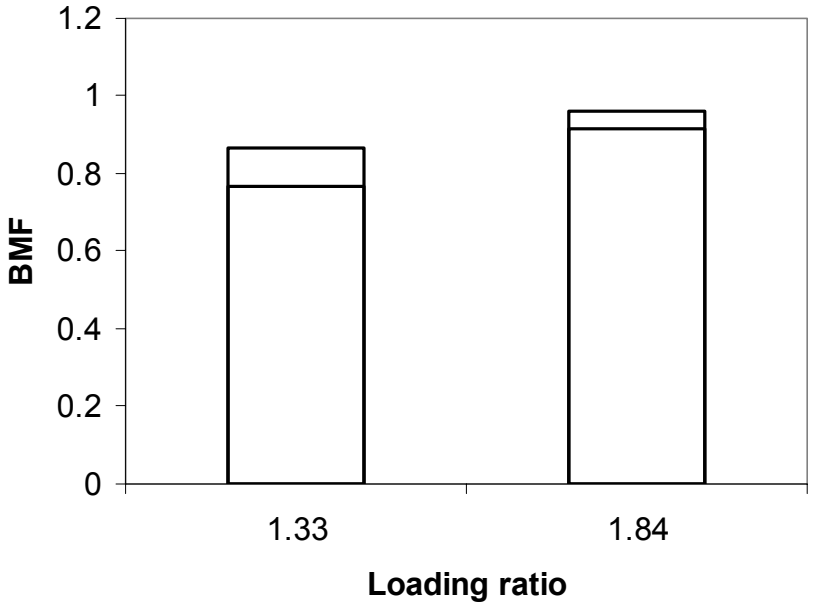

Figure 4.53: Effect of primary air loading ratio on burnt mass fraction

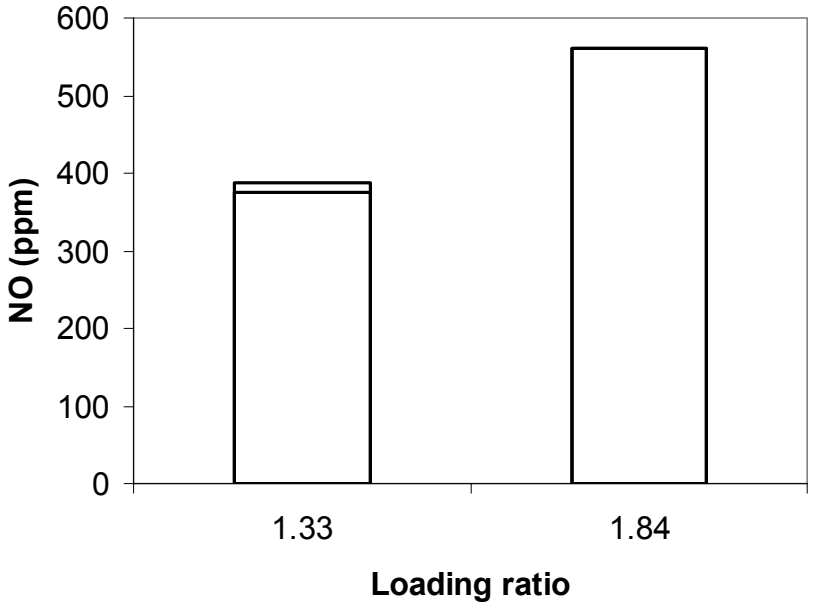

Figure 4.54: Effect of primary air loading ratio on NO emissions

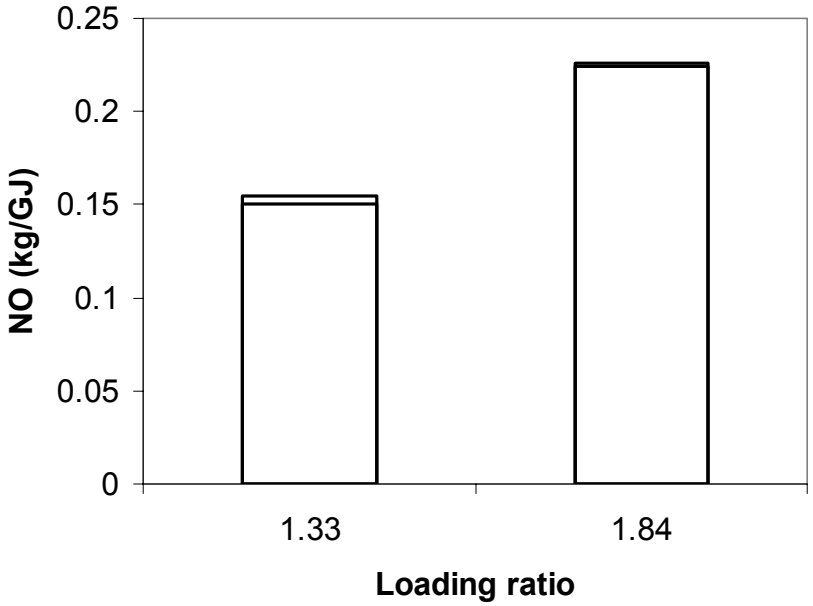

Figure 4.55: Effect of primary air loading ratio on NO emissions (heat basis)

4.2.2. Cofiring Results with Coal: LB Blends

4.2.2.1. Size effects

The effect of different biomass particle sizes was investigated by size classifying the litter biomass into 3 size groups: a 0-75 μm size group, a 75-150 μm size group, and a 150+ μm size group. Biomass can be harder to grind than coal, and experience a larger variation of size. The effect of different sizes must be investigated before larger scale co-firing can be attempted. The fuels were fired at 10 % excess air using the same experimental parameters. Figure 4.56 shows the effect of the difference particle sizes on the CO emissions. The CO emissions are the same for all of the size classes except for the largest size class. The larger particles take longer to burn, resulting in less complete combustion and a higher CO emissions level. The effect of biomass particle size on O_2 emissions is show in figure 4.57. The different size groups do not appear to have different O_2 emissions levels, but the full size group appears to have a slightly higher O_2 level due to variations in the experiments. The burnt mass fraction is shown in figure 4.58 for the different size groups. The level of combustion seems to be fairly constant for all of the size groups, expect for the full size group, because of its lower oxygen concentration. Now the NO emissions are seen on a uncorrected ppm basis in figure 4.59. The results again show similar level across all of the different size groups. Finally, the NO emissions are show in figure 4.60 on a kg/GJ basis. Again, it is seen that there are no large differences between the different size groups.

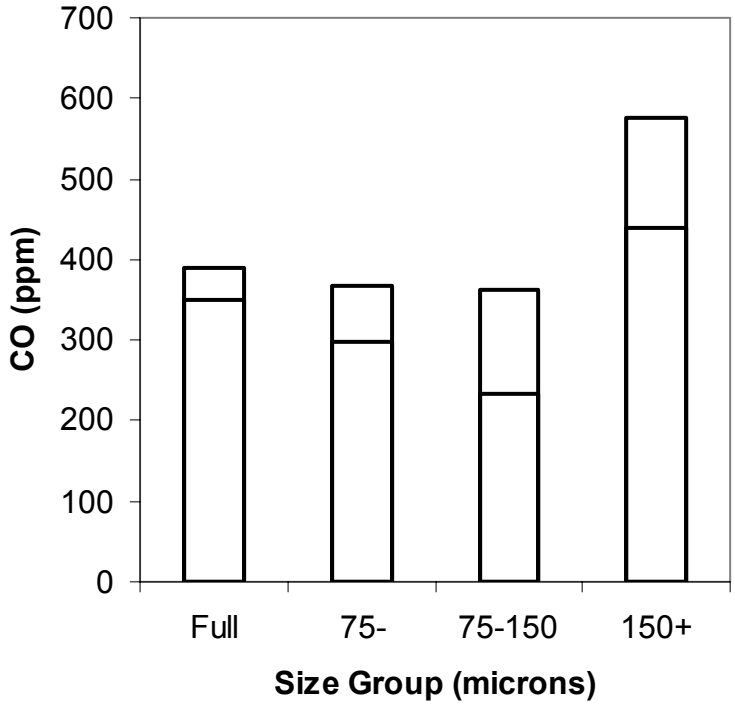

Figure 4.56: Effect of Litter biomass particle size on CO emissions

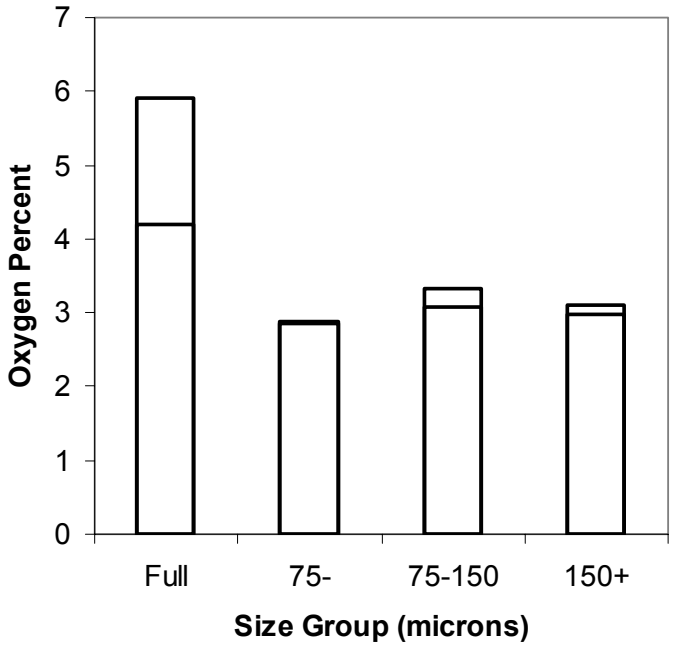

Figure 4.57: Effect of Litter biomass particle size on O_2 emissions

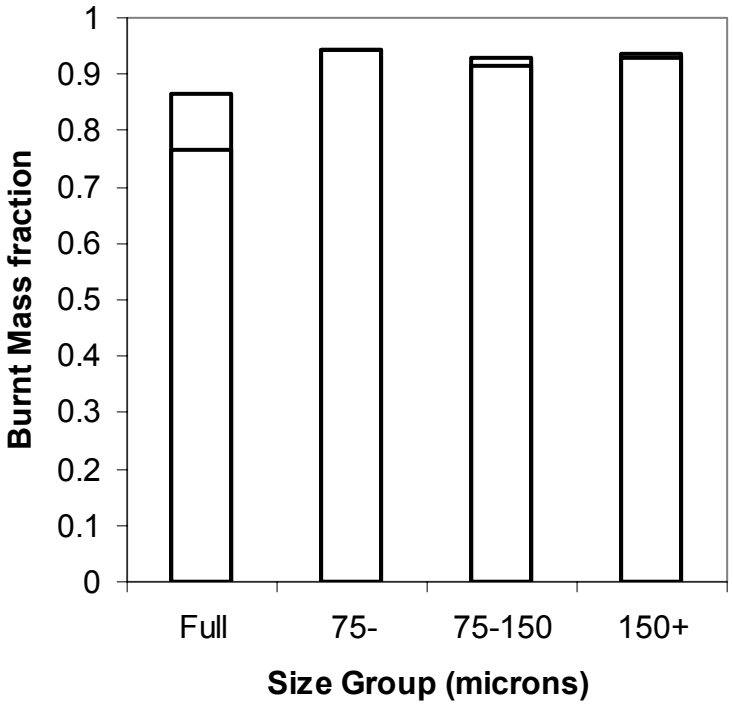

Figure 4.58: Effect of Litter biomass particle size on burnt mass fraction

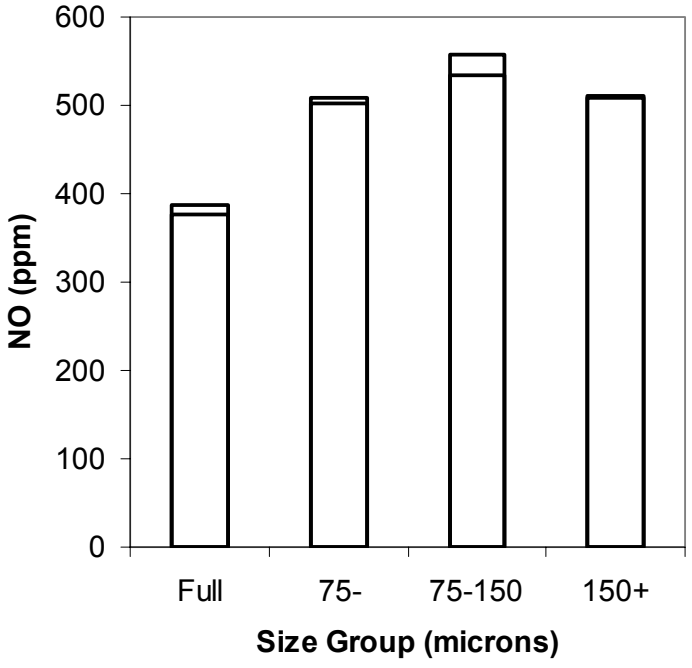

Figure 4.59: Effect of Litter biomass particle size on NO emissions (uncorrected)

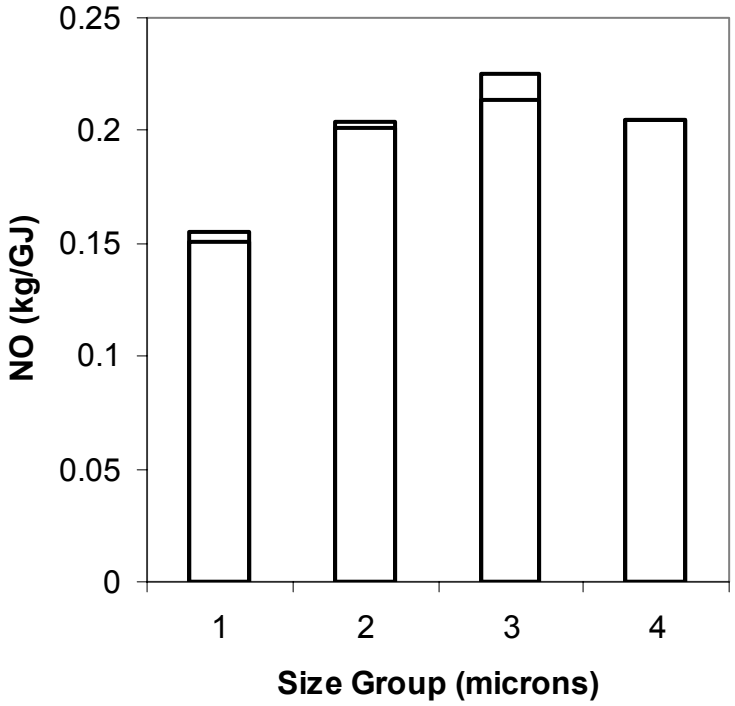

Figure 4.60: Effect of Litter biomass particle size on NO emissions on a heat basis

4.2.2.2. Swirl Effects

The effect of changing the swirl number was also investigated. The swirl at the top of the furnace was removed and replaced with a swirler with a fin angle of 55° to get a secondary air swirl number of 1. The original swirl burner had a secondary air swirl number of 0.7 and a swirl angle or 45°. The effect of the altered swirl number on CO emissions is shown in figure 4.61. There is little change between the high swirl and the low swirl burner. The effect of changing swirl on the O_2 emissions is shown in figure 4.62. The higher swirl results in a lower oxygen concentration. The high swirl number results in greater turbulence, and a faster mixing of fuel and air, which lowers the oxygen concentration. The effect of swirl number on the burnt mass fraction is shown in figure 4.63. The result of greater mixing in again seen in the burnt mass fraction, where the greater mixing results in a greater burnt mass fraction. The swirl also influences the NO emissions, seen on a ppm basis in figure 4.64, and on a kg/GJ basis in figure 4.65. The greater swirl and mixing translates to higher levels of NO emissions. The fuels are mixed faster, bringing the fuel N and Oxygen together sooner, and allowing more time for NO formation.

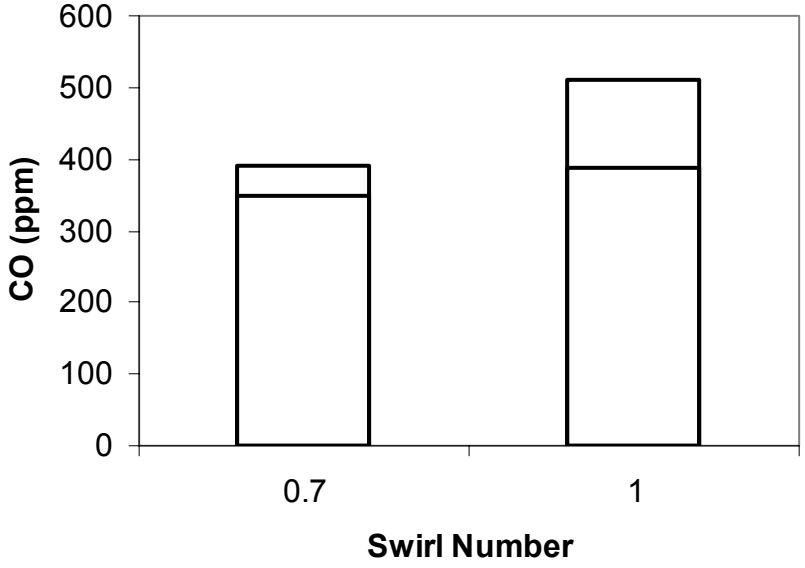

Figure 4.61: Effect of swirl number on CO emissions: CLB

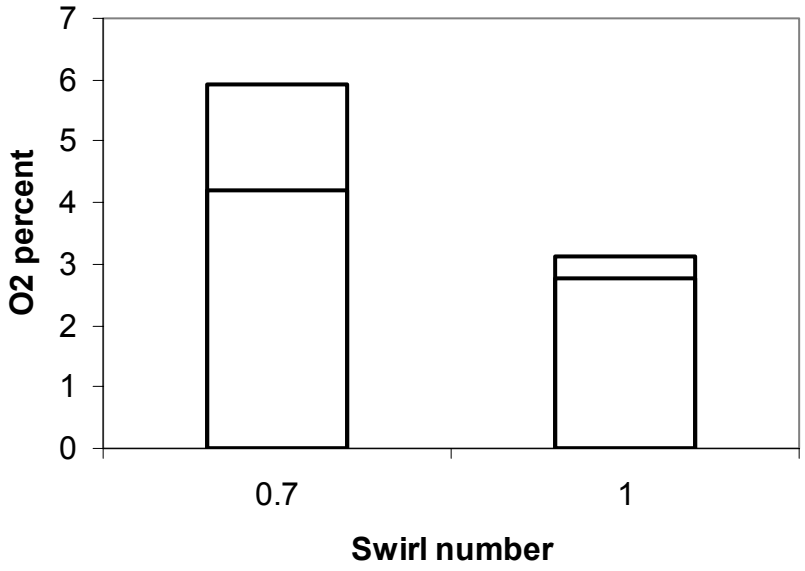

Figure 4.62: Effect of Swirl number on O_2 emissions: CLB

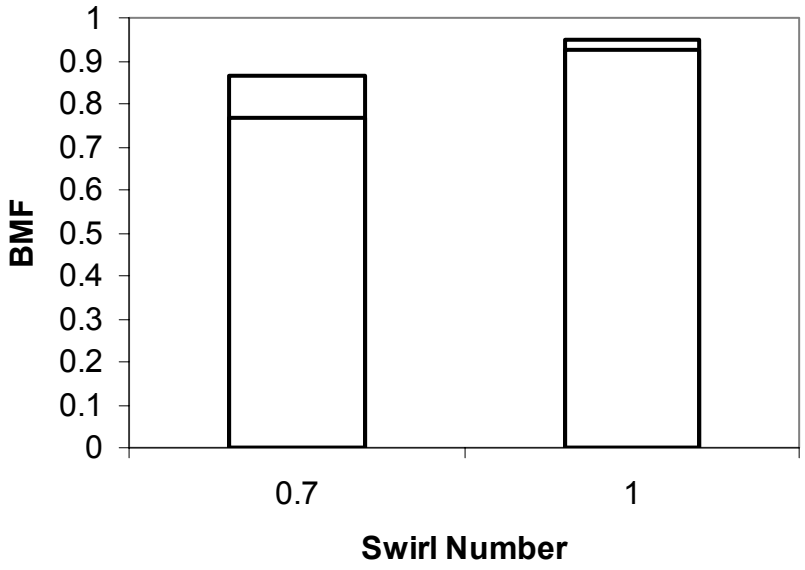

Figure 4.63: Effect of Swirl number on BMF: CLB

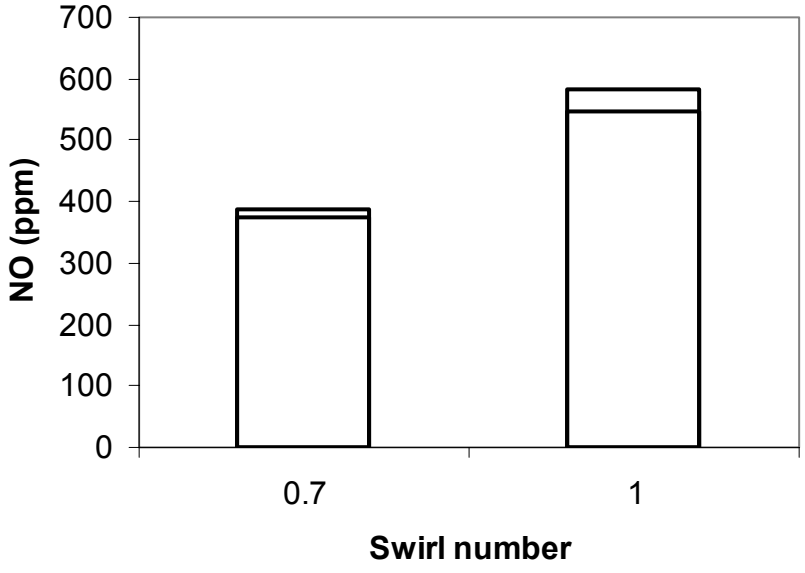

Figure 4.64: Effect of swirl number on NO: CLB

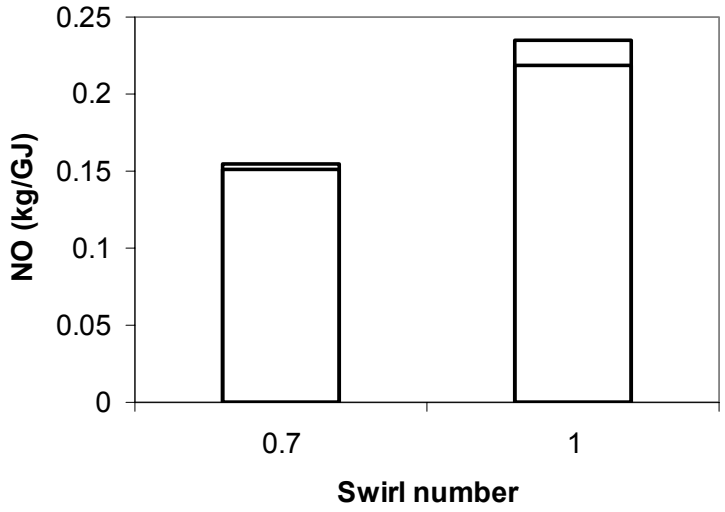

Figure 4.65: Effect of swirl number on NO emission (heat basis): CLB

4.2.2.3. Biomass moisture effects

Next, the effects of different manure moisture contents were investigated. The biomass used in these experiments was dried to allow for grinding and easier handling. For these experiments, water was mixed with the coal and the biomass to simulate biomass moisture with 30 % dry loss. The resulting CO emissions are given in figure 4.66. O_2 emissions for high and low biomass moisture levels are given in figure 4.67 and the burnt mass fraction are shown in figure 4.68. The burnt mass fractions appear similar in both cases. Finally, the NO emissions are shown on a ppm basis in figure 4.69, and on a heat basis in figure 4.70. The results are similar to those of coal: FB blends.

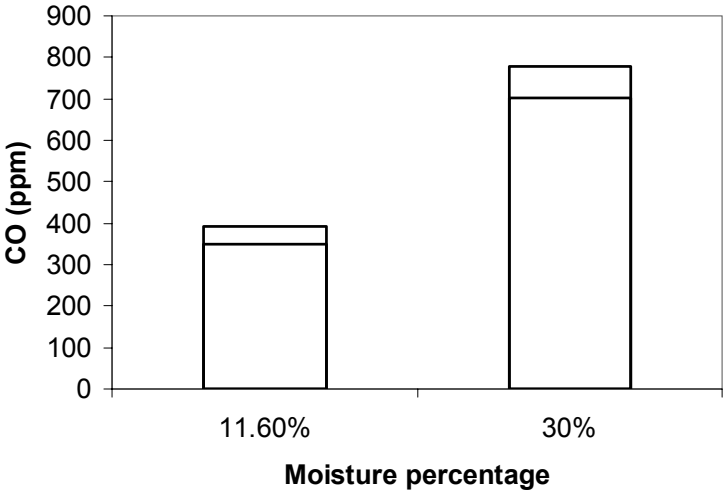

Figure 4.66: Effect of biomass moisture percentage on CO emissions: CLB

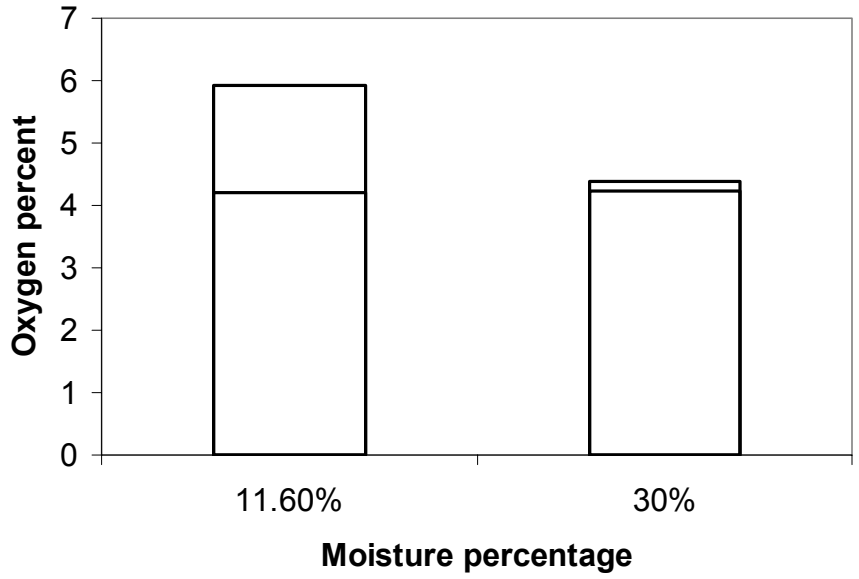

Figure 4.67: Effect of biomass moisture percentage on O_2 emissions: CLB

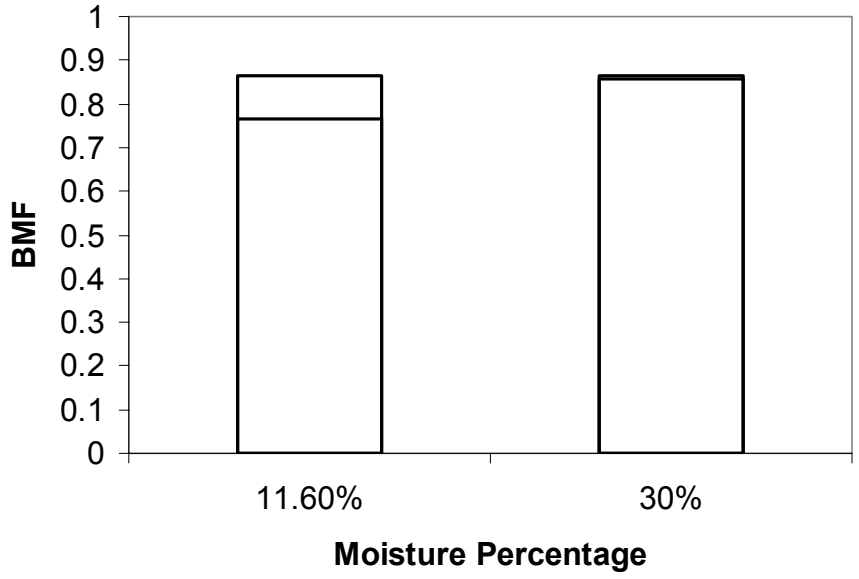

Figure 4.68: Effect of biomass moisture percentage on burnt mass fraction: CLB

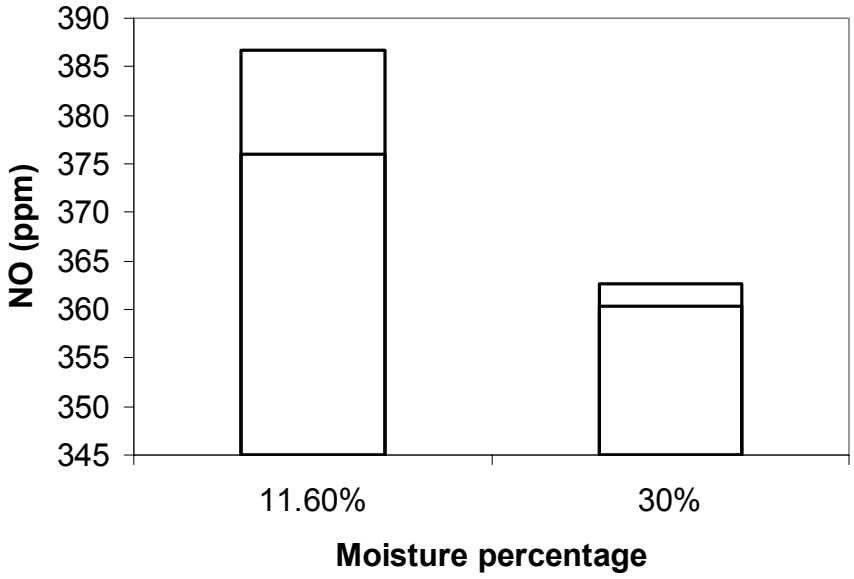

Figure 4.69: Effect of biomass moisture percentage on NO emissions: CLB

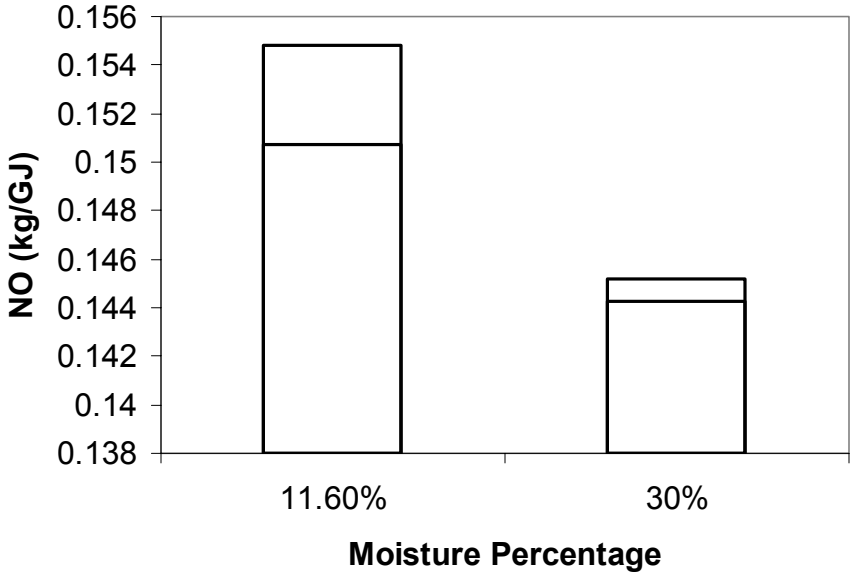

Figure 4.70: Effect of biomass moisture percentage on NO emissions (heat basis): CLB

4.2.2.4. Loading ratio

The effect of different loading ratios on the combustion performance was also investigated. The variation of CO with loading ratio is shown in figure 4.71, and the variation of O_2 with loading ration is shown in figure 4.72. The effect of the primary air-loading ratio on the burnt mass fraction is shown in figure 4.73. Finally, the NO emissions on a ppm basis and on a heat basis are shown in figures 4.74 and 4.75.

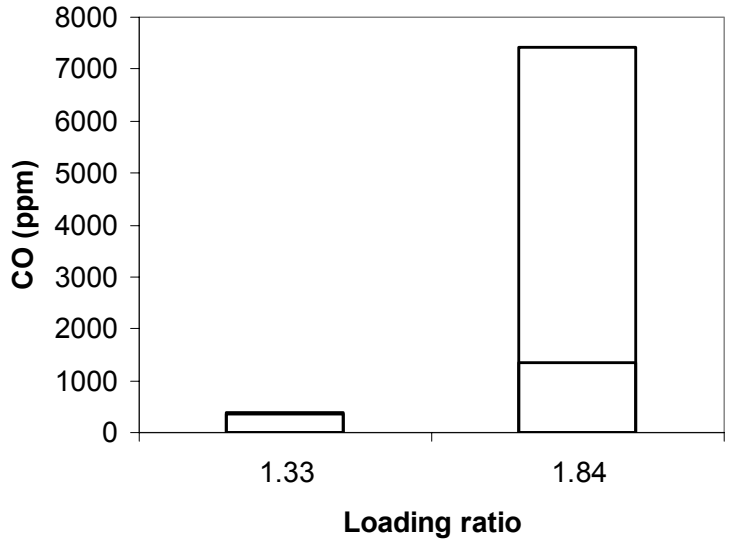

Figure 4.71: Effect of primary air loading ratio on CO emissions: CLB

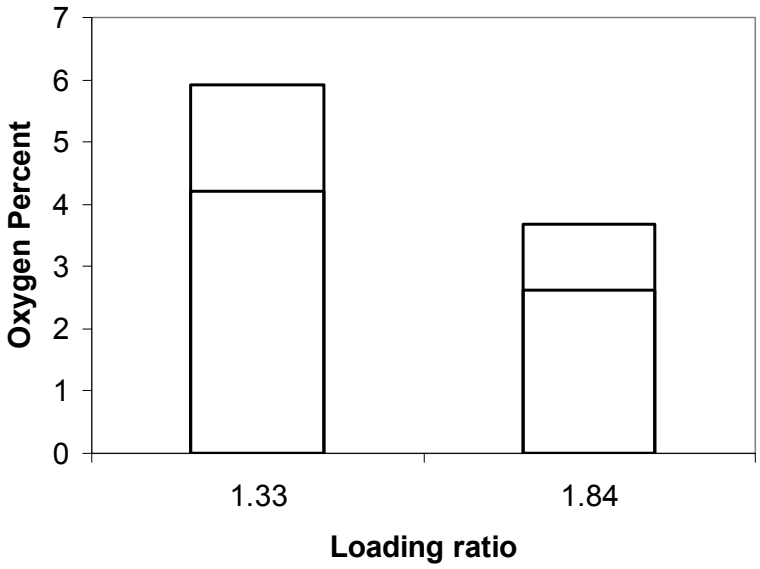

Figure 4.72: Effect of primary air loading ratio on O_2 emissions

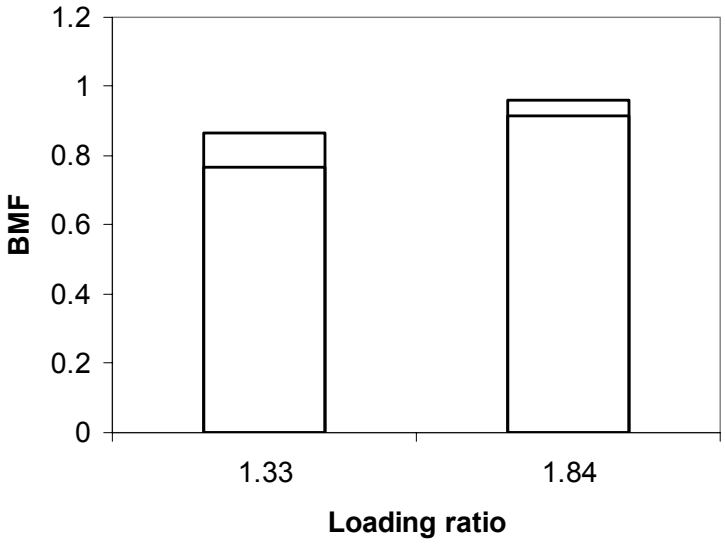

Figure 4.73: Effect of primary air loading ratio on burnt mass fraction

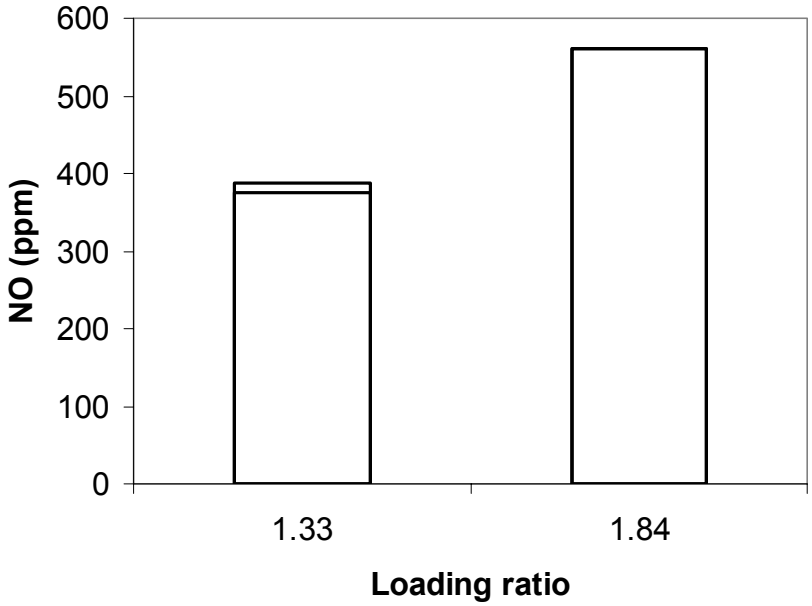

Figure 4.74: Effect of primary air loading ratio on NO emissions

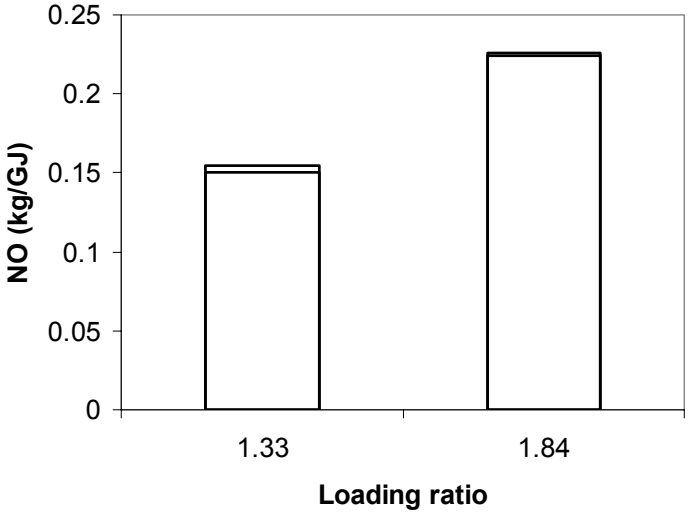

Figure 4.75: Effect of primary air loading ratio on NO emissions (heat basis)

4.2.3. Reburning results with Coal, CFB and CLB Blends

The reburning experiments were performed with coal, FB, LB, a 50:50 blend, and a 90:10 blend of each fuel (Thien *et al*., 2001b). A matrix showing the experiments performed is shown in table 4.33, with coal at a 1.05 equivalence ratio considered to be the base case. The high amount of unburnt particles, short residence time, and uncondensed hydrocarbons in the reburn gases broke both of the gas analyzers, and there were difficulties in repeating the data for a few reburning experiments. Table 4.34 shows the reburn injection equivalence ratios for coal and biomass. The equivalence ratio is the ratio of the stoichiometric air fuel ratio to the actual air fuel ratio. The injection equivalence ratios are similar, and therefore, a higher injection equivalence ratio at one of the injection nozzles is not causing the greater NO_x reduction. Figure 4.76 shows the reburn fuel injection velocities when using coal and FB as a reburn fuel. Typical time scale reach the middle of reactor is estimated to range from 4 ms to 7.5 ms. It is seen that the injection velocities for the two fuels are very similar, and therefore the mixing rate of the two fuels can be assumed similar.

Table 4.33: Reburning experimental matrix

Fuel	Equivalence ratio		
	1	1.05	1.1
Coal	2	2*	2
FB	2	1	2
50:50 Blend Coal:FB	1	1	1
90:10 Blend Coal:FB	1	1	1
LB	1	1	1
50:50 Blend Coal:LB	1	1	1
90:10 Blend Coal:LB	1	1	1

Number indicates number of experiment, * base case

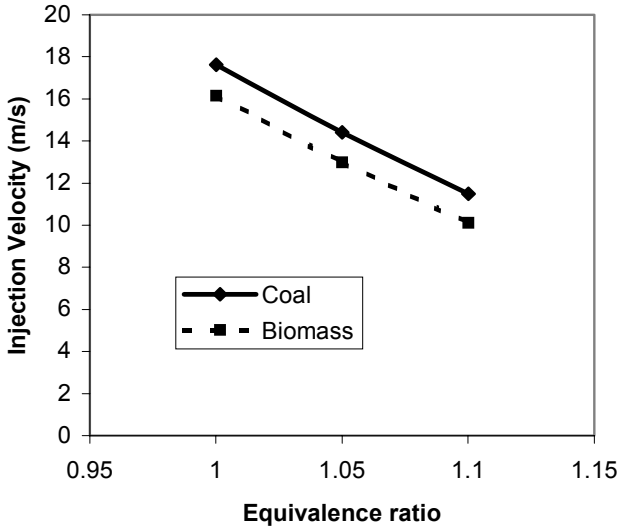

Figure 4.76: Reburn injection velocity

Table 4.34: Reburn injection equivalence ratios

Reburn ϕ	Coal Injection ϕ	Feedlot Injection ϕ
1	1.15	1.15
1.05	1.45	1.4
1.1	1.8	1.8

The results of the reburning experiments were conducted with the operating parameters listed in table 4.35 with FB-B and blends (figure 4.77) with coal-B and for LB and blends with coal (figure 4.78). Pure biomass fuels, a 50-50 blend of coal and biomass, a 90-10 blend of coal and biomass, and pure coal was tested. All of the results shown are the percent reduction from the initial level of 600 ppm NO. A reduction of 80% was achieved for reburning with FB-B or LB, while a reduction of 10-40 % was achieved with coal, depending on the equivalence ratio. The reduction obtained with the 50:50 fuel blend and the 90:10 fuel blend fell in between the behavior of the pure coal and the biomass. A greater reduction in NO was achieved with coal at higher equivalence ratios, but with biomass the reduction, using FB-B or LB appeared to be fairly constant at all equivalence ratios. The percentage reduction NO did not reach a minimum with respect to the equivalence ratio as reported in the literature, but only equivalence ratios up to 1.1 were tested. High levels of CO and combustibles were encountered during the reburn experiments, and over ranged the sensors of the gas analyzer, resulting in sensor damage, and inaccurate CO and combustible readings. Note that CO emissions are expected to be comparable to real boiler concentrations with reburning. The gas analyzer detected no O_2 while the reburn fuel was fed. The greater effectiveness of biomass in reburning is an unexpected result, as both of the biomass fuels are higher in nitrogen than coal. It is believed the greater effectiveness is probably due to its high volatile content (Zhou *et al*., 2000) and the release of fuel nitrogen in the form of NH_3. The biomass fuels release more volatiles at a faster rate than coal, and are able to more rapidly produce very fuel rich areas where NO is reduced. Reactions involving the NH_3 released by the biomass will proceed faster then reactions involving HCN released by coal. The kinetics of several reaction that involve nitrogen were reviewed by Sami (2000):

$HCN+O_2 \rightarrow NO + \ldots$ **(4.2.I)**

$HCN+NO \rightarrow N_2 + \ldots$ **(4.2.II)**

$NO+char \rightarrow N_2 + \ldots$ **(4.2.III)**

$NH_3+O_2 \rightarrow NO + \ldots$ **(4.2.IV)**

$NH_3+NO \rightarrow N_2 + \ldots$ **(4.2.V)**

The characteristics reaction time of these reactions are shown in figure 4.79, and reactions involving NH_3 proceed at a faster rate than reactions involving HCN for temperature < 1600 K (2420.33 ºF).

Table 4.35: Summary of reburn experimental parameters

Propane flowrate	70,000 Btu/hr
Primary airflow rate	800 SCFH
Total burner rating	100 kW
Reburn Percentage	30%
Reburn injection velocity	10-16 m/s
Primary equivalence ratio	0.95
Reburn equivalence ratio	1.00 – 1.1
Residence time (cold)	~4 s
Residence time (hot)	~1 s
Propane Flowrate	0.014 m^3/min (30.2 SCFH)
Initial NO concentration measured at 183 cm from burner	600 ppm
O_2 concentration in Primary zone	0.96
O_2 concentration before application of reburn fuel	4.1-5.7

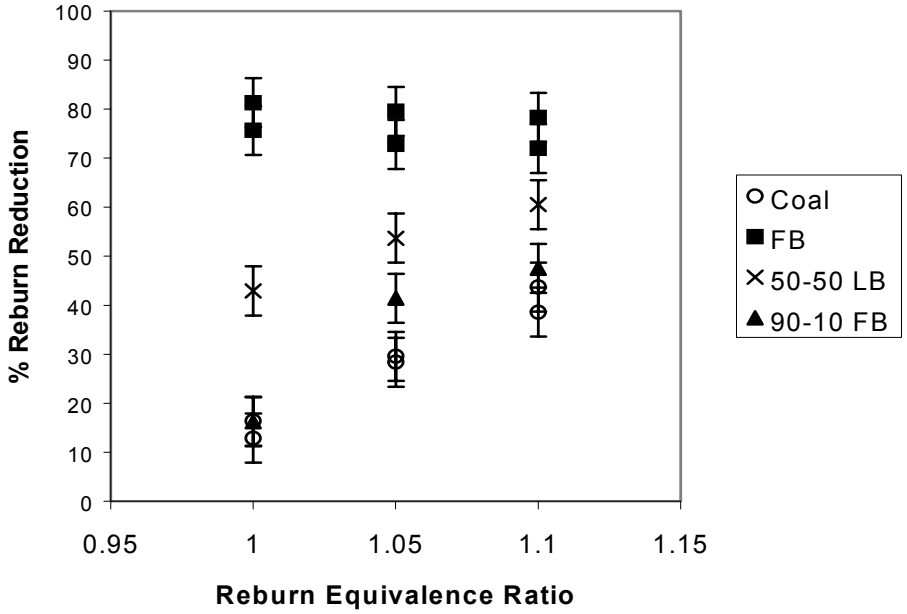

Figure 4.77: Reburning results with coal and FB (US patent under Review)

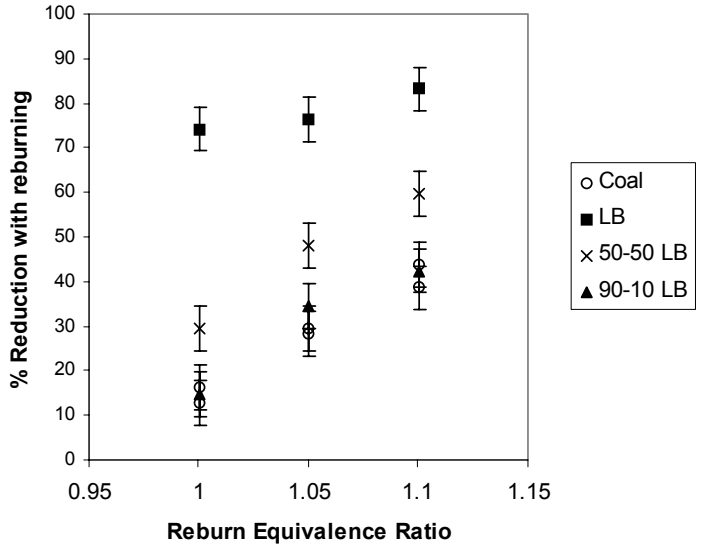

Figure 4.78: Reburning results with LB

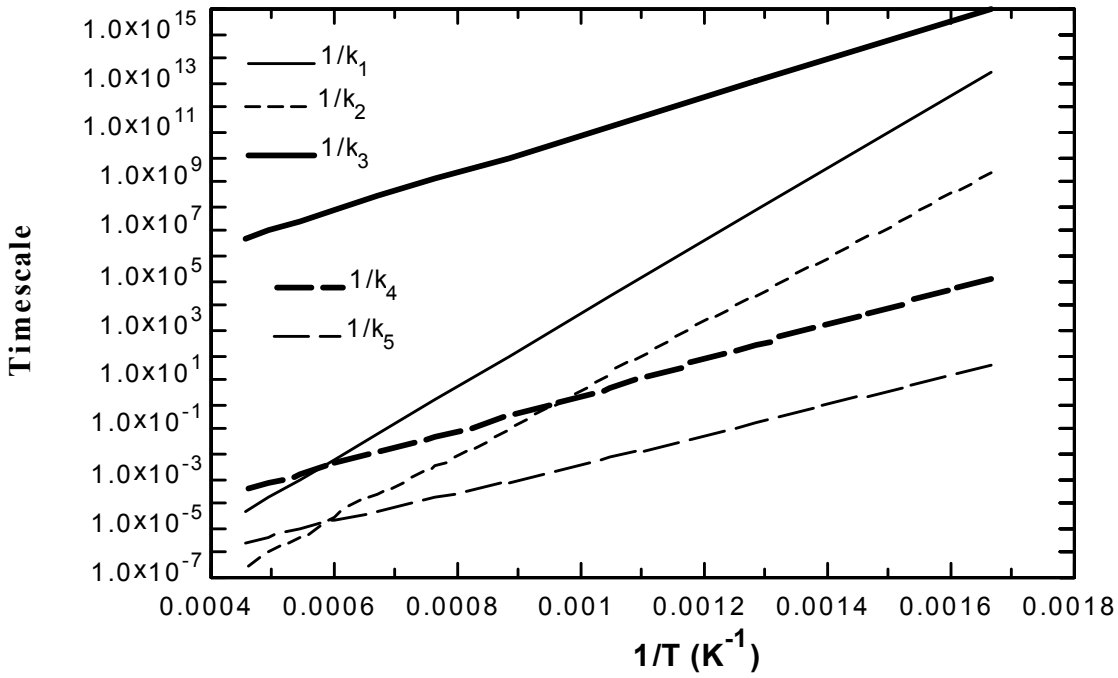

Figure 4.79: Reaction rates for reactions involving NO: (k_1: HCN oxidation, k_2: NO reduction on HCN, k_3: NO reduction on char, k_4: NH_3 oxidation and k_5: NO reduction on NH_3). (Sami, 2000)

4.3. Fixed Bed studies on CFB and CLB fuels

In this section, results of gasifying coal, feedlot biomass, chicken litter biomass, and their blends are presented. It includes the fuel properties and data on temperature and concentration profiles of various gas species. During the experiment, ash seemed to play a major role in the gasification process and shall be discussed in detail along with references to the ash fusion temperatures of the fuels. Figure 4.80 shows the photographic view of the setup, and figure 4.81 shows the various zones in an updraft fixed bed gasifier. For details about the design and construction of the gasifier, refer to Section 3.

Table 4.36 shows the experiments conducted using different fuels with different particle sizes, and under air flow rates.

Table 4.36: Experiment matrix for fixed bed studies

S.No.	Fuel Type	No. of Experiments	
		PA = 1.27 m^3/hr (45 SCFH), SA = 0 m^3/hr (0 SCFH)	PA = 1.70 m^3/hr (60 SCFH), SA = 0 m^3/hr (0 SCFH)
1	$Coal_1$*	1	1
2	$Coal_2$*	1	1
3	AFB_1*	1	1
4	AFB_2*	1	1
5	LB_1*	1	1
6	LB_2*	1	1
7	$CAFB_1$*	1	1
8	$CAFB_2$*	1	1
9	CLB_1*	1	1
10	CLB_2*	1	1
Total Experiments		10	10

*The subscript denotes the range of the fuel particle size fired into the gasifier.

$_1$ denotes particle sizes in the range of 6.4 mm (0.25") < d_p < 12.7 mm (0.50")

$_2$ denotes particle sizes in the range of 4.0 mm (0.157") < d_p < 6.4 mm (0.25")

Using the analyses the empirical formulas, molecular weights (based on empirical formulas), and the stoichiometric air fuel ratios were calculated, and the results are shown in table 4.37. The values reported for hydrogen and oxygen weight fractions in the ultimate analysis (as received basis) included both the moisture bound and organically bound hydrogen and oxygen. Figure 4.82 shows the comparative proximate analyses of the fuels on as received basis. It can be observed that the fixed carbon in coal is the highest and the ash content lowest amongst all the tabulated fuels. However, the volatile matter of the coal is lower compared to AFB and LB, implying that on a mass basis the pyrolysis products evolved per unit mass of DAF fuel shall be higher for LB and AFB. The volatile matter content of (on as received basis) soil-surfaced FB (SFB) is lowest due to the high ash content of the fuel. Figure 4.83 shows the ultimate analyses of the fuels in which the organically bound

hydrogen and oxygen have been separated from the hydrogen and oxygen contained in the form of moisture in the fuel. The organic hydrogen and sulfur in all the fuels is comparable, but the carbon content of coal is very high compared to the other fuels. The high carbon and low ash content of the coal indicate that the stoichiometric air fuel ratio (on mass basis) shall be higher as compared to the rest of the fuels. The higher carbon content also translates into a higher heating value as compared to other fuels, this is observed in figure 4.84.

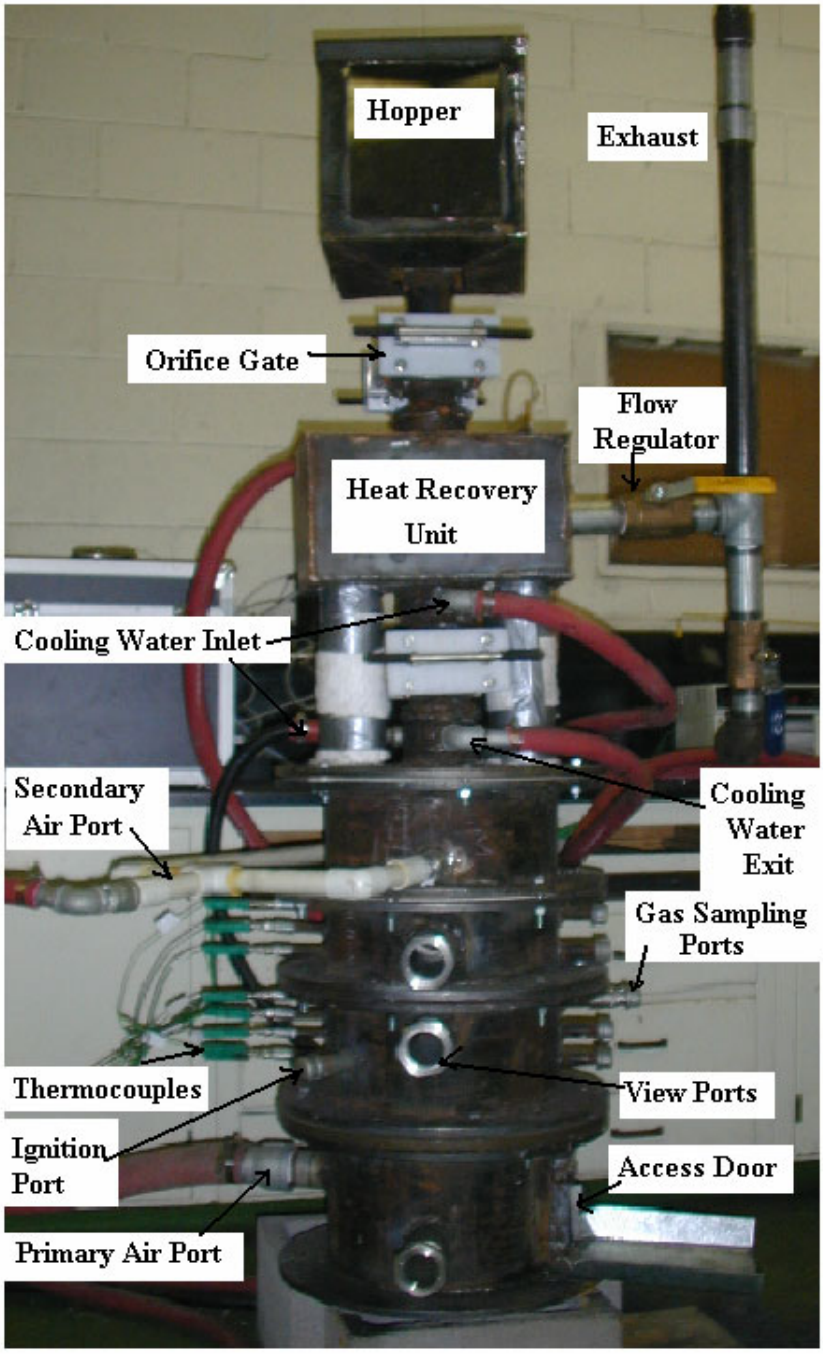

Figure 4.80: Photographic view of the Gasifier setup

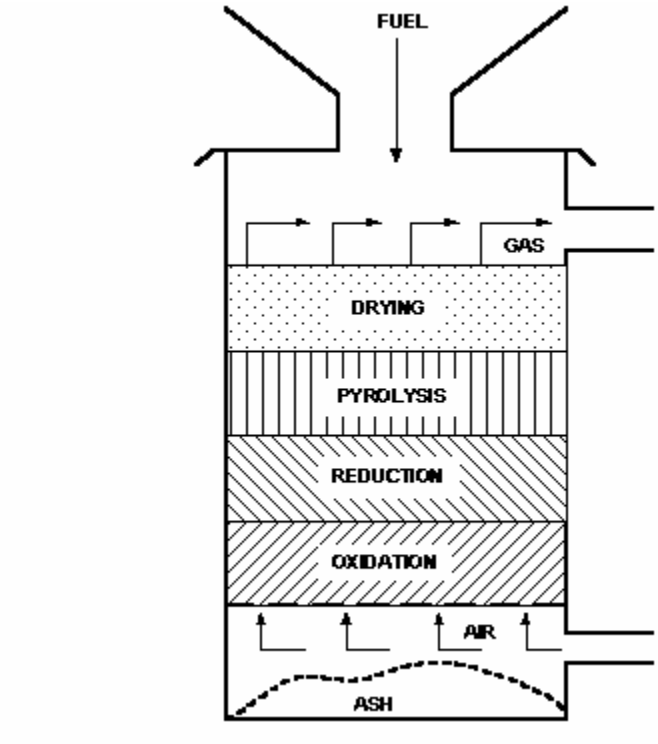

Figure 4.81: Different zones in an updraft gasifier

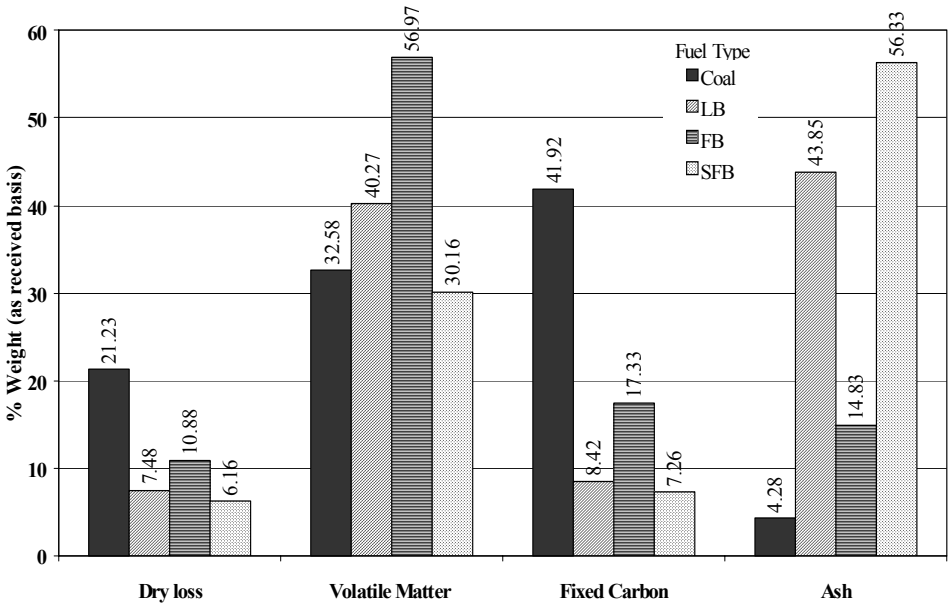

Figure 4.82: Comparative proximate analysis of the fuels

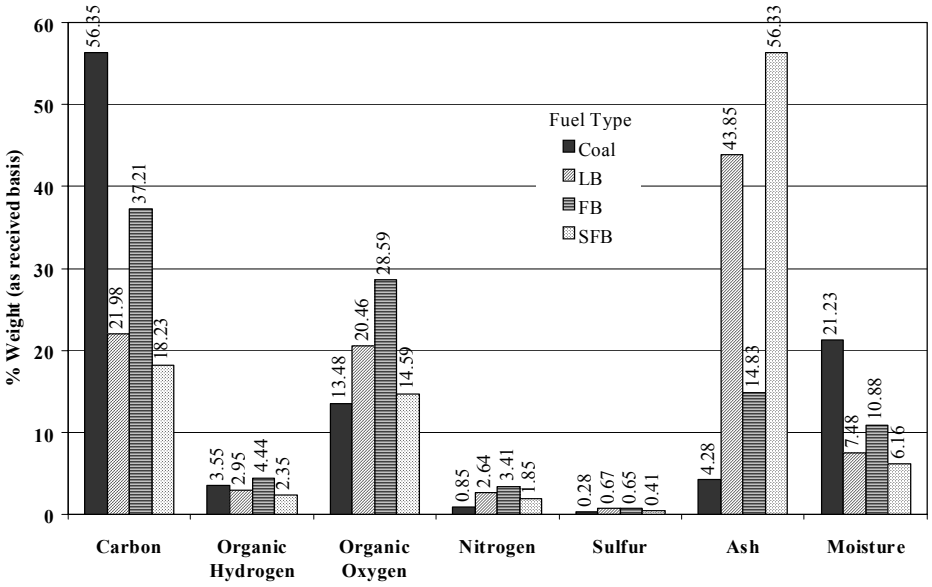

Figure 4.83: Comparative ultimate analysis of the fuels

Table 4.37: Comparative fuel characteristic

Parameter		Wyoming Coal	Feedlot Biomass (AFB)	Soil Surfaced FB	Chicken Litter (LB)	CAFB	CLB
Proximate Analyses (as received)	Dry loss	21.23	10.88	6.16	7.48	16.05	14.35
	Volatile Matter	32.58	56.97	30.16	40.27	44.77	36.42
	Fixed Carbon	41.92	17.33	7.26	8.42	29.63	25.17
	Ash	4.28	14.83	56.33	43.85	9.55	24.06
Ultimate Analysis (DAF Basis)	Carbon	75.63	50.08	48.58	45.14	62.87	63.58
	Hydrogen	4.76	5.98	6.25	6.06	5.37	5.27
	Oxygen	18.10	38.49	38.89	42.02	28.28	27.55
	Nitrogen	1.14	4.58	4.92	5.41	2.86	2.83
	Sulfur	0.37	0.87	1.09	1.37	0.62	0.76
Empirical formula (DAF) [1]		$CH_{0.75}O_{0.18}N_{0.013}S_{0.0018}$	$CH_{1.42}O_{0.58}N_{0.078}S_{0.0066}$	$CH_{1.53}O_{0.60}N_{0.086}S_{0.0084}$	$CH_{1.59}O_{0.69}N_{0.10}S_{0.011}$	$CH_{1.02}O_{0.34}N_{0.039}S_{0.0037}$	$CH_{0.99}O_{0.33}N_{0.038}S_{0.0045}$
Molecular Weight [2] (kg/kmole)		20.39	27.47	28.69	30.66	23.2	23.27
Molecular Weight (DAF) [2] (kg/kmole)		15.87	23.96	24.64	26.58	19.09	18.87
Heating Value for complete combustion (kJ/kg, as received basis)		21809	14983	6941	9235	18396	15522
$A:F_{stiochiomatric}$ (as received) [2]		7.39	5.36	5.21	4.74	6.43	6.41
$A:F_{stiochiomatric}$ (DAF) [2]		9.51	6.15	6.08	5.48	7.83	7.92
$A:F_{stiochiomatric}$ (DAF) [2] for complete gasification, i.e. C to CO, and H to H_2		7.87	4.08	3.90	3.36	5.98	6.09
HV for complete gasification (kJ/kg, DAF basis)		5746	1198	333	1073	3475	3889

[1] Determined from ultimate analysis
[2] Calculated from empirical formula
[3] Includes moisture in the fuel

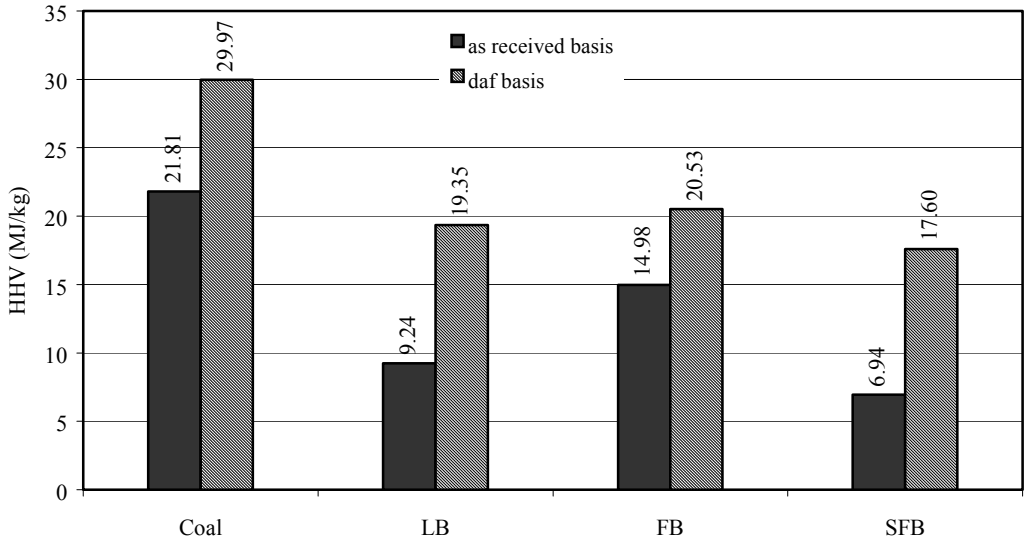

Figure 4.84: Comparative Heating Values of the fuels

4.3.1. Gasification Reactions

During the gasification process, there are both heterogeneous and homogeneous reactions taking place. The rates of these reactions may be functions of temperature, particle size, gas species concentration, pressure, etc. Since the gasification process conducted in the laboratory were under nearly atmospheric pressure conditions, it becomes imperative to study the effect of temperature on the reaction rates. There are two types of reactions taking place: the homogeneous and the heterogeneous reactions. The time scales for heterogeneous reactions are much larger as compared to the homogeneous reactions. A brief overview of the heterogeneous reactions is as follows:

a) O_2 - C reactions

$$C + \frac{1}{2} O_2 \rightarrow CO \qquad \textbf{(4.3.I)}$$

Where the reaction rate per unit volume (kg/m^3 s) and the heating value of the reaction is given by: (Annamalai and Puri, 2004)

$$\dot{m}'''_{C,I} = \rho_{O2} A V \left(\frac{2\,MW\,C}{MW\,O2} \right) k_I \frac{ShD_I}{d_P} \left[\frac{1}{\frac{ShD_I}{d_P} + k_I} \right] \qquad \textbf{(4.3.1)}$$

where D_I - Diffusion coefficient

HV_I = 9.25 MJ/kg (3985.18 Btu/lb) of fuel consumed. **(4.3.2)**

The above reaction equation includes the effect of diffusion and chemical kinetics. The chemical kinetic rate constant is expressed in the modified Arrhenius form as (Evans *et al*., 1977):

$$k_I = 1.74 T_S \exp\left(-9x10^3 / T_S \right) \qquad \textbf{(4.3.3)}$$

$$C + O_2 \rightarrow CO_2 \qquad \textbf{(4.3.II)}$$

where the reaction rate per unit volume (kg/m^3 s) and the heating value of the reaction is given by:

$$\dot{m}'''_{C,II} = \rho_{O2} A V \left(\frac{MW\,C}{MW\,O2} \right) k\,II \frac{ShD\,II}{d\,P} \left[\frac{1}{\frac{ShD\,II}{d\,P} + k\,II} \right] \qquad \textbf{(4.3.4)}$$

HV_{II} = 32.83 MJ/kg (14144.15 Btu/lb) of fuel consumed. **(4.3.5)**

The chemical kinetic rate constant is expressed as (Annamalai *et al*., 1993):

$$k_{II} = 1.6x10^5 \exp\left(-20000 / T_S\right) \qquad \textbf{(4.3.6)}$$

Ratio of CO to CO2 in C-O2 reactions:

Walker *et al*. (1959) have shown that for heterogeneous reactions under combustion and gasification conditions both CO and CO_2 are the primary products and the ratio of the primary products CO/CO_2 increases with increasing temperature. Further Arthur *et al*. (1951) have cited that the ratio of the reaction rates of CO/CO_2 could be expressed as (refer figure 4.85):

$$\frac{\dot{m}_{CO}}{\dot{m}_{CO2}} = 2500 \exp(-6240 / T) \qquad \textbf{(4.3.7)}$$

The above expression is applicable for temperatures between 730 K (854.33 ºF) and 1170 K (1646.33 ºF), and the ratio increases as the temperature increases.

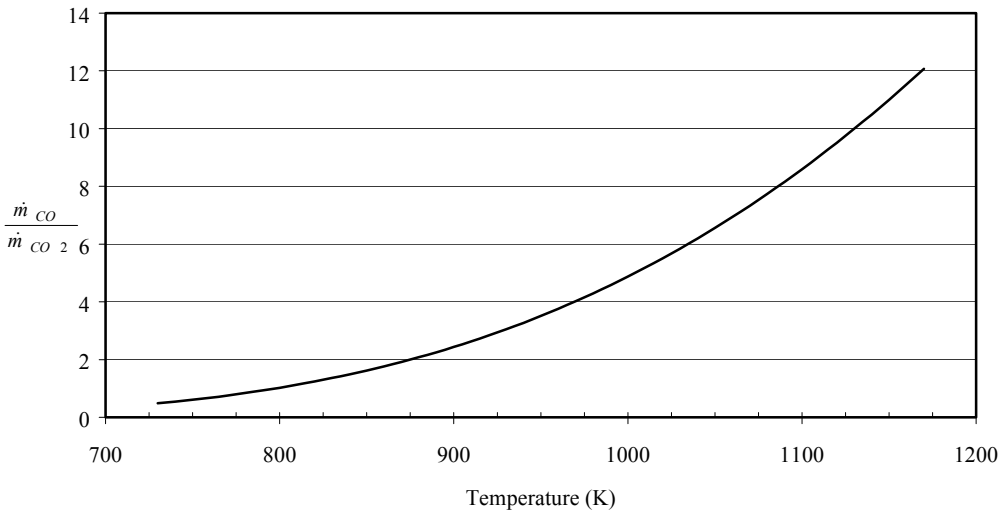

Figure 4.85: Reaction rate ratio of CO/CO_2 (between 730-1170 K (854.33-1646.33 ºF))

b) Boudouard reaction

$$C + CO_2 \rightarrow 2CO \qquad \textbf{(4.3.III)}$$

Where the reaction rate per unit volume (kg/m^3 s) and the heating value of the reaction is given by:

$$\dot{m}'''_{C,III} = \rho_{CO2}\, A_V \left(\frac{2\,MW_C}{MW_{CO2}}\right) k_{III} \frac{Sh D_{III}}{d_P} \left[\frac{1}{\frac{Sh D_{III}}{d_P} + k_{III}}\right] \qquad \textbf{(4.3.8)}$$

HV_{III} = -14.42 MJ/kg (-6212.57 Btu/lb) of fuel consumed **(4.3.9)**

The chemical kinetic rate constant is expressed as: (Bryden *et al*., 1996)

$$k_{III} = 3.42 T_S \exp\left(-1.56x10^4 / T_S\right) \qquad \textbf{(4.3.10)}$$

c) Steam carbon reaction

$$C + H_2O \rightarrow CO + H_2 \qquad \textbf{(4.3.IV)}$$

Where the reaction rate per unit volume (kg/m^3 s) and the heating value of the reaction is given by:

$$\dot{m}'''_{C,IV} = \rho_{H20}\, A_V \left(\frac{MW_C}{MW_{H_2O}}\right) k_{IV} \frac{Sh D_{IV}}{d_P} \left[\frac{1}{\frac{Sh D_{IV}}{d_P} + k_{IV}}\right] \qquad \textbf{(4.3.11)}$$

HV_{IV} = -10.92 MJ/kg (-4704.66 Btu/lb) of fuel consumed **(4.3.12)**

The chemical kinetic rate constant is expressed as (Yoon *et al*., 1978):

$$k_{IV} = 5.71 T_S \exp\left(-1.56x10^4 / T_S\right) \qquad \textbf{(4.3.13)}$$

d) Hydrogasification reaction

$$C + 2H_2 \rightarrow CH_4 \qquad \textbf{(4.3.V)}$$

Where the reaction rate per unit volume (kg/m^3 s) and the heating value of the reaction is given by:

$$\dot{m}'''_{C,V} = \rho_{H2}\, A_V \left(\frac{MW_C}{2MW_{H2}}\right) k_V \frac{Sh D_V}{d_P} \left[\frac{1}{\frac{Sh D_V}{d_P} + k_V}\right] \qquad \textbf{(4.3.14)}$$

HV_V = 6.25 MJ/kg (2692.69 Btu/lb) of fuel consumed. **(4.3.15)**

The chemical kinetic rate constant is expressed as (Raman *et al*., 1981b):

$$k_V = 0.75x10^7 \exp\left(-27697 / T_S\right) \qquad \textbf{(4.3.16)}$$

Since primary products of carbon oxidation in air are CO and CO_2, so reactions I and II can be represented by the following reaction (Hobbs *et al*., 1992):

$$C + \lambda' O_2 \rightarrow 2(1-\lambda')CO + (2\lambda' - 1)CO_2, \qquad \frac{1}{2} \le \lambda' \le 1 \qquad \textbf{(4.3.17)}$$

Laurendeau (1978) has correlated the ratio CO/CO_2 as:

$$\frac{CO}{CO_2} = A\exp\left(-\frac{E}{RT}\right) = \frac{2(\lambda - 1)}{(2 - \lambda)} \qquad \lambda' = \frac{1}{\lambda} \qquad \textbf{(4.3.18)}$$

where A ≈ $10^{2.5}$ and E ≈ 25-38 kJ/mol (23.7-36.0 Btu/kmol) for low pressure (applicable to our case of 100 kPa (1 bar)). Therefore using the above equation, the value of λ can be calculated as:

$$\lambda = \frac{2\left[A\exp\left(-\frac{E}{RT}\right)+1\right]}{A\exp\left(-\frac{E}{RT}\right)+2} \qquad \textbf{(4.3.19)}$$

According to Arthur's equations the values of λ' at 500, 1000, and 1500 K (440.33, 1340.33, 2240.33 ºF) as 0.926, 0.562, and 0.518 respectively. Thus at high temperatures or under normal combustion conditions CO is the predominating reaction taking place. However, under gasification conditions, the concentration of oxygen reduces immensely and the concentrations of CO, CO_2, and H_2O become significant. Under these conditions, reactions 4.3.III and 4.3.IV may become significant especially at high temperatures.

The homogeneous reactions that can occur during gasification are:

$$CO + \frac{1}{2}O_2 \rightarrow CO_2 \qquad \textbf{(4.3.VI)}$$

$$H_2 + \frac{1}{2}O_2 \rightarrow H_2O \qquad \textbf{(4.3.VII)}$$

$$CO + H_2O \rightarrow CO_2 + H_2 \qquad \textbf{(4.3.VIII)}$$

The reactions 4.3.VI, 4.3.VII, and 4.3.VIII are exothermic. Reaction 4.3.VIII has an overall effect on the over all CO/H_2 ratio. The heating values of the reactions are 283 MJ/kmole (268233 Btu/kmol) (4.3.VI), 241.85 MJ/kmole (229230 Bu/kmol) (4.3.VII), and 41.16 MJ/kmole (39012 Btu/kmol) (4.3.VIII). It can be seen that reaction 4.3.VIII is slightly exothermic when compared to reactions 4.3.VI, and 4.3.VII. Figure 4.86 shows the logarithmic values of the equilibrium constants for the above-mentioned reactions at different temperatures. It can be observed that the equilibrium constants for reactions 4.3.VI, and 4.3.VII are large even a around 1500 K (1340.33 ºF) implying that the reverse reaction rates for reactions 4.3.VI, and 4.3.VII are still negligible at this temperature. But for reaction 4.3.VIII, at 1500 K (1340.33 ºF) the equilibrium constant has negative value implying that the reverse reaction is also significant, thus at T > 1500 K (1340.33 ºF) the reverse reaction may become significant, and CO and steam are the preferred products whereas for low temperatures, the water shift reaction 4.3.VIII favors the production of H_2. Tabatabaie-Rasi (1987) have cited that reaction 4.3.VIII is catalyzed by ash or minerals in the fuel so that a thermodynamic equilibrium exists at the high reaction zone temperatures given as:

$$\frac{[CO_2][H_2]}{[CO][H_2O]} = K(T) \qquad \textbf{(4.3.22)}$$

Kosky *et al*. (1980) have reported the formulation of the thermodynamic equilibrium constant as:

$$K(T) = 0.0265\exp\left(\frac{7860}{RT}\right) \qquad \textbf{(4.3.23)}$$

Thus, at high temperatures the presence of excess moisture (which might result due to moisture release of the fuel) shall tend to decrease the concentration of CO in the mixture thereby

increasing the concentrations of CO_2, and H_2. However, the high temperature in the oxidation zone shall favor the production of CO and steam.

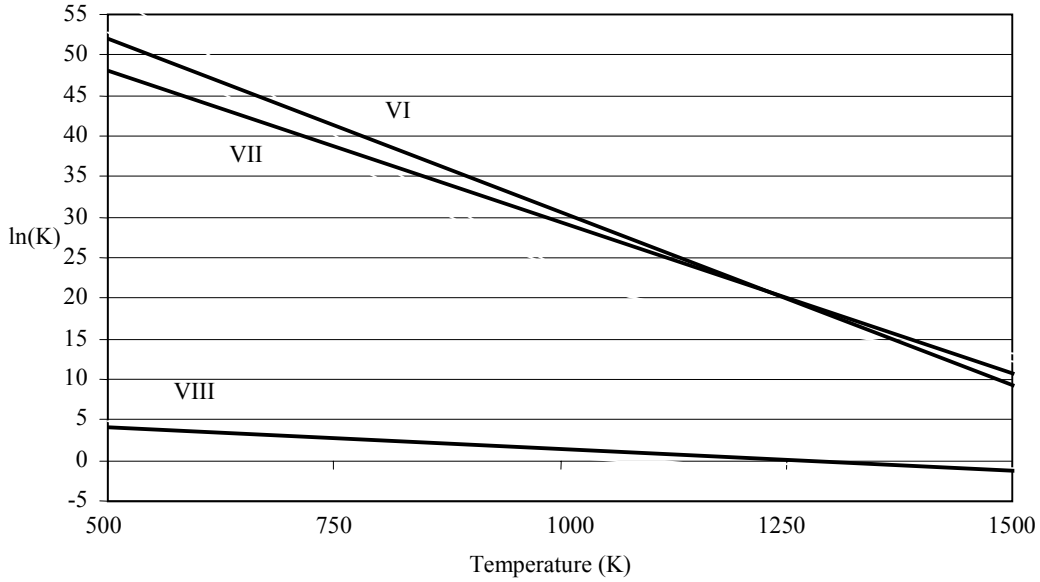

Figure 4.86: Equilibrium constant Vs. Temperature for homogeneous gasification reactions

4.3.2. Bed Temperature Profiles

In this section of the chapter, the temperature profiles in the bed for different fuels shall be discussed. The temperature profiles in the bed during the gasification process can help to qualitatively predict the various zones inside the bed, thus enabling to understand the temperature dynamics for the various fuels. Preceding the discussion for each individual fuel shall be a general discussion on the factors affecting the temperature profiles in the bed.

The oxidation and gasification zones are regions of chemical reaction, where as the drying and devolatilization zones are more physical in nature. The temperature gradients are much higher in the oxidation and gasification zones as compared to the other two remaining zones. The temperature in the bed is affected by a galore of factors, each having its own effect on the temperature in the bed.

From the previous discussion on gasification reactions, and it was concluded that char oxidation is diffusion controlled, where as char gasification with H_2O and CO_2 is kinetic controlled. However, the char oxidation rate is dependent upon the availability of O_2 in the free stream, and if the free stream gas is severely depleted in O_2, then char oxidation by O_2 rate is reduced and under such circumstances, reactions 4.3.III and 4.3.IV become significant. At the same time if the rate of depletion of O_2 is very vigorous, then the oxidation zone in the gasifier is rather thin (figure 4.81) and there is an overlap in the exothermic oxidation and endothermic gasification zone. This is further supported by Walker *et al*. (1959), who observed that, during gasification O_2 was consumed within 10 ms of entering the reactor and CO and H_2 were found within 3 ms due to non-oxidized pyrolysis products. Hunt *et al*. (1951) have reported that even at high temperatures of 1150 K (1610.33 ºF), the char-steam reaction is kinetic controlled. Hobbs *et al*. (1992) has also reported that there are simultaneous oxidation and gasification reactions occurring in the oxidation zone. Therefore, under high temperatures in the oxidation zone, the char consumption may also be due to the endothermic

gasification reactions. In addition, to further complicate the matter, the endothermic gasification reactions in the oxidation zone reduces the peak temperature and under some conditions, even the char oxidation reaction with O_2 could become kinetic controlled.

The air flow rate is an important variable influencing the temperature profile in the bed. Increasing the air flow rate increases the availability of O_2 to the fuel, and the diffusion rate increases as the thickness of the boundary layer around the particle decreases at high velocity enabling higher mass and heat transfer rates which results in an increase in the peak temperature in the bed. However, at the same time the fuel feed rate also increases, so higher amount sensible energy is required to heat the particles to the higher temperature, so the temperature in the bed could also decrease. A lower air flow rate results in a higher spatial temperature gradient in the bed, due to lower convective heat and mass transfer into the bed, and also due to lower combustion peak temperatures due to reduced O_2 availability. But Blasi *et al*. (1999) have reported that under low flow rates the air flow rate does not significantly effect the temperature profile in the bed. A higher air flow rate results in higher convective heat and mass transfer into the bed, thus affecting the devolatilization rate of the fuel in the bed. The devolatilization increases with temperature, which increases due to hotter bed at higher air flow rates. As the devolatilization rate increases the total volatile yield increases (tar, volatile gases). The increased release results in more of the bed with char, but char also get oxidized. The increased volatilization rate in the upper part of the bed results in higher mass transfer loss from the fuel particle and cooling of the particle due to energy lost (carried) by the pyrolyzing gases. Simultaneously the devolatilization of fuel causes a decrease in density of the fuel and the heat capacity of the fuel, which implies that lower amount of sensible energy is required to raise the temperature of the pyrolyzed fuel through one degree temperature rise. Therefore, the temperature in the devolatilization and drying zone can increase due to decrease in heat capacity of the pyrolyzed fuel and increased char oxidation at higher air flow rate. Thus, it is obvious that there are a number of both acting and counter acting effects on the temperature in the bed caused due to a variation in the air flow rate into the gasifier.

Under steady state conditions if the fuel feed rate is increased, the temperature shift is slower and the peak temperature tends to be confined to the bottom of the gasifier. The pressure also affects the temperature profile, but since the experiments were conducted at near atmospheric pressures, its effect is negligible.

The maximum temperature in the bed is partially determined by the particle size in the oxidation zone, the extent of gas phase oxidation of CO and H_2, ash behavior, axial thermal diffusion in the bed, and void fraction in the bed.

Finally, in transient studies, the history of the experiment also affects the temperature profile in the bed. It can be clearly concluded that temperature in the bed is affected by a number of factors, and depending on which factor dominates, the temperature profile changes for different fuels.

The temperature profiles shall be studied individually for each fuel. Since coal is treated as the base fuel it shall be studied first and the rest shall be compared to it.

4.3.2.1. Coal

For coal-particle size range between 6.4 mm (0.25”) and 12.7 mm (0.5”), figures 4.87, and 4.88 show the temperature profiles in the bed for coal under air flow rates of 1.27 and 1.70 m^3/hr (45 and 60 SCFH) respectively. From figures 4.87, and 4.88, the different regions in the bed can be qualitatively identified. It should be noted that though the temperature data was collected at seven locations along the gasifier, the points were connected to present a more lucid view of the temperature. However, the connecting line may not always show the correct temperature profile, as there may be a peak in-between the two consecutive points that might not be reflected in the graph. Under such conditions, a note shall be made about the actual temperature profile.

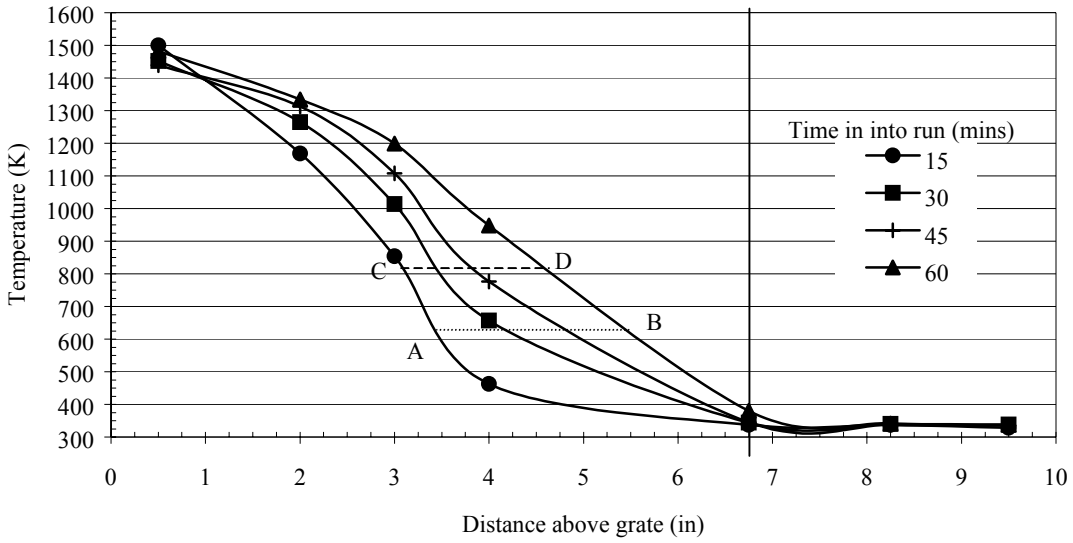

Figure 4.87: Temperature profile for Coal (6.4 mm (0.25") – 12.7 mm (0.5")) under air flow rate of 1.27 m^3/hr 1.27 m^3/hr (45 SCFH) (Average fuel feed rate 1.39 kg/hr (3.05 lb/hr), SR = 0.16)

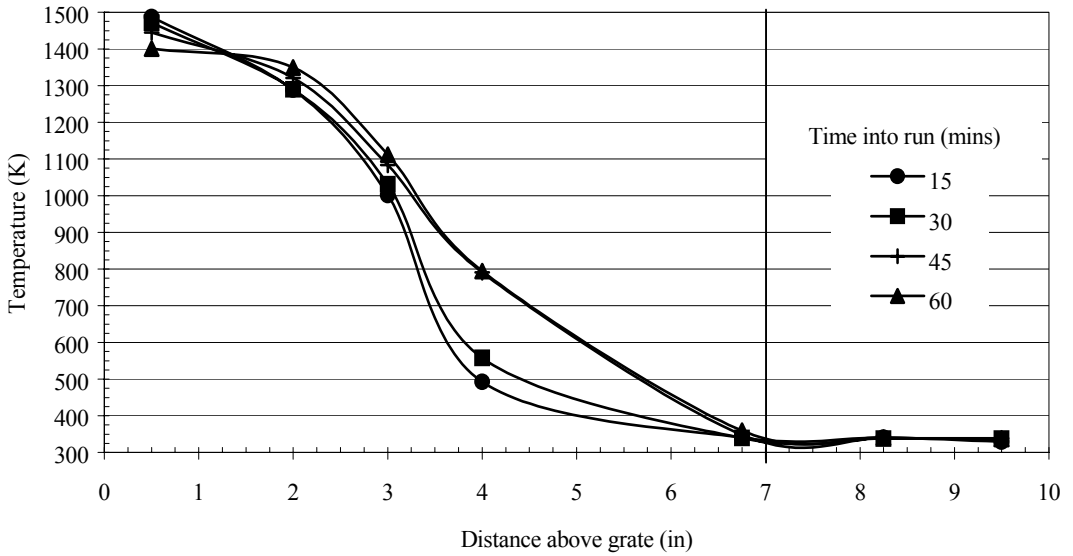

Figure 4.88: Temperature profile for Coal (6.4 mm (0.25") – 12.7 mm (0.5")) under air flow rate of 1.7 m^3/hr (60 SCFH) (Average fuel feed rate 1.2 kg/hr (2.64 lb/hr), SR = 0.23)

From the above figure 4.87, the general trend of the temperature profile for coal is observed. Initially at 15 minutes into the run, the peak temperature is at the base of the gasifier where O_2 is available for oxidation of char, but as time progresses the temperature at the base (25.4 mm (1") above the grate) drops slightly. This is due to the ash accumulation at the base of the bed or in other

words, the combustible at the bottom decreases thus decreasing the temperature and/or the ash layer over the coal may reduce the reaction rate thus decreasing the peak temperature. The temperature at the other locations increases as time progresses, which shall be discussed in a detailed manner.

At 15 minutes into the run, the temperature in the bed decreases from a peak of about 1500 K (1340.33 ºF) at the bottom of the bed to about 350 K (170.33 ºF) at the top. The temperature gradient between 12.7 mm (0.5") and 44.45 mm (1.75") is about -890 K/mm (-1602 ºF/mm), whereas that between 44.5 mm (1.75") and 101.6 mm (4.0") is about -1320 K/mm (-2376 ºF/mm, steepest), and about -140 K/mm (-252 ºF/mm) between 101.6 mm (4.0") and 171.5 mm (6.75").

Table 4.38: Temperature gradients at different times during the experiment for Coal (6.4 mm (0.25") – 12.7 mm (0.5")) under an air flow rate of 1.27 m^3/hr (45 SCFH)

Time into run (minutes)	Temperature gradient (K/cm)	
	44.5 mm (1.75") – 101.6 mm (4.0")	101.6 mm (4.0") – 171.5 mm (6.75")
15	-132	-14
30	-108	-43
45	-105	-63
60	-66	-82

From table 4.38 it is clear that as the time into the experiment increases the temperature gradient between 44.5 – 101.6 mm (1.75" – 4.0") becomes more and more flat, but that between 101.6 – 171.5 mm (4.0" – 6.75") becomes more and more steep. The rapid temperature fall in the 44.5 – 101.6 mm (1.75" – 4.0") region may be due to the drying and devolatilization of the coal. The drying and devolatilization results in a rapid mass loss, which carries away the sensible heat from the coal thus decreasing its temperature. But as time progresses, the amount of drying and devolatilization decreases which results in lower mass loss thus the temperature drop becomes flatter. The flatness can also be attributed to the lower heat capacity of the dried and devolatilized coal (i.e. char with ash), as it requires lower sensible heat energy to heat it. The lower heat capacity also explains the temperature rise at 44.5, 76.2, and 101.6 mm (1.75", 3.0", and 4.0") above the bed as time progresses. So, the region between 44.5 and 101.6 mm (1.75" and 4.0") can be described as the drying devolatilization region in the bed. This can be concluded from the TGA results as shown in figure 4.89, for coal of 75+ μm in size reported by Thien (2002), which show that the pyrolysis of coal begins at about 630 K (674.33 ºF) in inert atmosphere of N_2. If the pyrolysis temperature is 630 K (674.33 ºF), then from figure 4.87, the pyrolysis front moves (see figure 4.81 for various regions in the fixed bed) from A to B which is 63.5 mm (2.5") in 45 minutes (figure. 4.87) i.e. the rate of propagation of char is approximately 83.82 mm (3.3") per hour. If the ignition temperature is approximately 800 K (980.33 ºF), then the char ignition layer moves from points C to D which is 38.1 mm (1.5") in 45 minutes, i.e. the rate of propagation of the char is 50.8 mm (2.0") per hour. But the temperature gradient between 101.6 and 171.5 mm (4.0" and 6.75") becomes steeper as time progresses due to the addition of fresh fuel to the top of the bed in order to maintain the bed height constant. Thus as the time progresses, the drying and devolatilization zone shifts towards the free surface, resulting in a steeper temperature drop in the region between 101.6 and 171.5 mm (4.0" and 6.75"). The drying and devolatilization process determines the fuel feed rate, as the rate of mass loss during this process is the highest amongst all the other processes known to occur during gasification of coal.

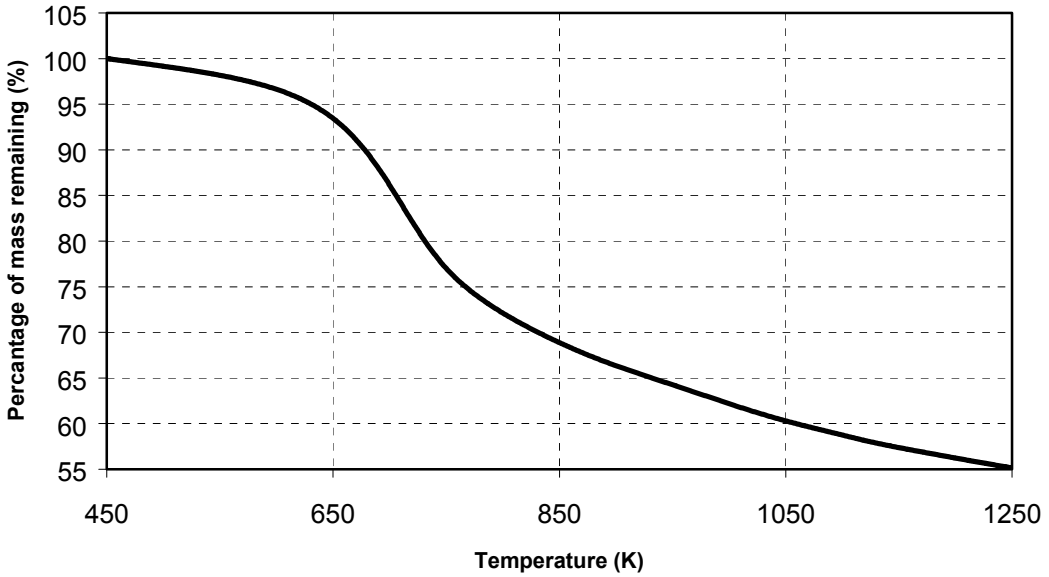

Figure 4.89: TGA of coal of 75+ μm in N_2 atmosphere

The temperature gradient between 12.7 and 44.5 mm (0.5" and 1.75") has not been discussed, as the true temperature gradient cannot be determined from the data at two points. This is because as time progresses though the temperature at 12.7 mm (0.5") decreases and is still the highest temperature in the bed as compared to the other measured locations, it is not the true peak temperature. The actual peak temperature lies somewhere between 12.7 and 44.5 mm (0.5" and 1.75") above the grate. This is due to a decrease in the burning rate at the base of the bed, which causes the peak temperature to shift towards the free surface and causes the oxidation zone to spread further into the bed. The burning rate per unit volume of the bed at the base decreases due to the accumulation of ash and/or the additional resistance to burning due to the ash layer formation on the coal. The ash acts as a heat sink as it absorbs a part of the sensible heat energy and causes the temperature to drop. The fact that the peak temperature shifts further towards the free surface can be safely concluded from the results obtained from another experiment which was conducted under similar conditions, but for a duration of 7 hours (Figure 4.90).

If the rate of coal feed rate is known then the ash accumulation rate in the bed can be determined as:

$$\dot{m}_{fuel} \times Y_{ash,in} = m_{bed} \frac{\partial Y_{ash,bed}}{\partial t} \qquad \textbf{(4.3.24)}$$

Assuming that the mass of the bed is almost fixed, the above equation reduces to

$$\dot{m}_{fuel} \times Y_{ash,in} \propto \frac{\partial Y_{ash,bed}}{\partial t} \qquad \textbf{(4.3.25)}$$

The ash increases linearly with time, which accumulates mostly at the bottom. From figure 4.90 it can be seen that after 2.0 hours into the run the temperature at 12.7 mm (0.5") above the grate has dropped by 150 K (270 ºF) from a high of 1500 K (2240.33 ºF) (at time = 0.0 hours) to 1350 K (1970.33 ºF) (at the end of 2.0 hours). The temperature at 12.7 mm (0.5") steadily drops to around 1050 K (1430.33 ºF) at the end of 7.0 hours, and at the same time, the temperature at 44.5 mm (1.75")

steadily rises from 1200 K (1700.33 ºF) (at time = 0.0 hours) to 1500 K (2240.33 ºF) (at the end of 7.0 hours). At around 7.0 hours into the run, the peak has shifted from 12.7 to 44.5 mm (0.5" to 1.75") above the grate. So, the data at 12.7 to 44.5 mm (0.5" to 1.75") cannot be used to compute the true temperature gradient in this region. The crux of the above discussion is that the ash in the fuel plays an influential role in determining the temperature profile and temperature dynamics in the oxidation zone of the gasifier and is responsible for the peak shift in the bed.

From figure 4.90 it can be further observed that the temperature profile gets flatter as time progresses, and at 7.0 hours into the run, the temperature at the top of the bed reaches to around 950 K (1250.33 ºF) from a low of 550 K (530.33 ºF) (at the start of the experiment). The temperature rise in the post 44.5 mm (1.75") region is because as the peak shifts further towards the free surface, the heat capacity of the fuel above the peak decreases (lower bed volume above the peak temperature), and the higher temperature results in drying and devolatilization beginning at a higher height in the bed, thus making the temperature profile flatter as time progresses.

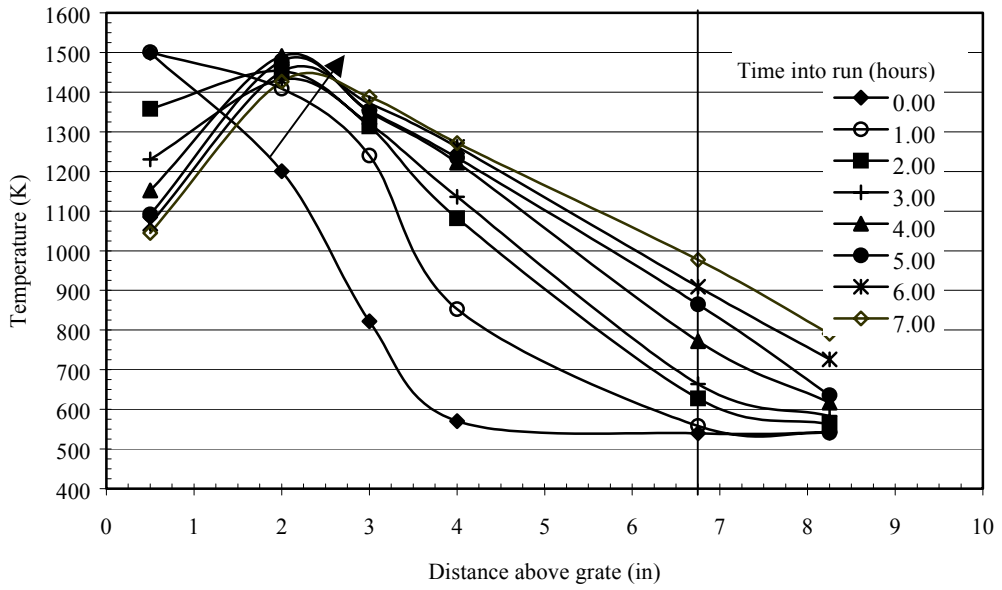

Figure 4.90: Temperature profile for Coal (12.7 mm (0.25") – 0.64 cm (0.5")) under air flow rate of 1.27 m^3/hr (45 SCFH) (experiment run for 7.00 hours)

For coal with air flow rate of 1.7 m^3/hr (60 SCFH), figure 4.88 shows that the temperature profile with a air flow rate of 1.7 m^3/hr (60 SCFH) is almost similar to that under a air flow rate of 1.27 m^3/hr (45 SCFH). Initially the peak temperature occurs at the base and as time progresses the peak shifts. In this case, the temperature at 12.7 mm (0.5") drops from about 1500 K (2240.33 ºF) to 1400 K (2060.33 ºF) after 1 hour into the experiment. This drop is about 50 K (90 ºF) more than that for air flow rate of 1.27 m^3/hr (45 SCFH). This shows that the higher air flow rate results in a higher burn rate at the base of the bed, which translates into a faster peak shift. The higher temperature drop at the base could also be due to the higher heat transfer associated with a higher air flow rate.

From 4.91, which shows the comparative temperature profiles for coal at different air flow rates, it is seen that the temperature profiles are almost similar. The temperature profiles in the 445-101.6 mm (1.75" – 4.0") interval is different for both at 15 minutes into the run because, the higher flow rate has caused a higher heating of the particles at 44.5 mm (1.75") due to higher convective heat transfer in the bed. This causes a higher temperature gradient between 44.5 and 101.5 mm

(1.75" and 4.0") for air flow rate of 1.7 m^3/hr (60 SCFH) as compared to that of 1.27 m^3/hr (45 SCFH). But after 45 minutes into the run, both the temperature profiles are very similar, showing that the change in air flow has not appreciably affected the temperature profile in the bed.

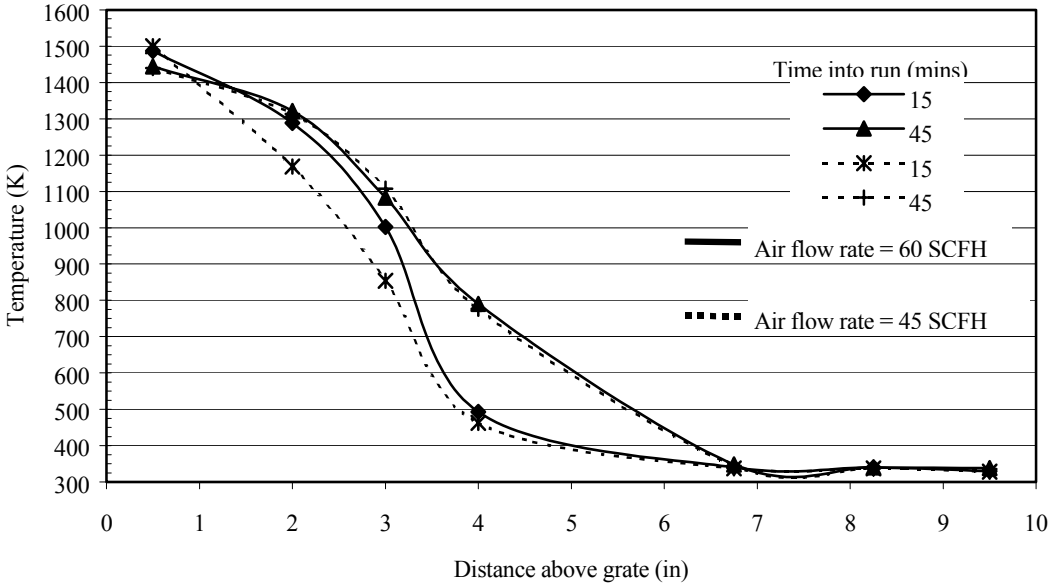

Figure 4.91: Comparative temperature profiles for Coal (12.7 mm (0.25") – 6.4 mm (0.5")) at air flow rates of 1.27 and 1.7 m^3/hr (45 and 60 SCFH)

For coal particles size ranged between 4 mm and 6.4 mm (0.157" and 0.25"), figure 4.92 shows the comparative temperature profiles under air flow rates of 1.27 and 1.7 m^3/hr (45 and 60 SCFH).

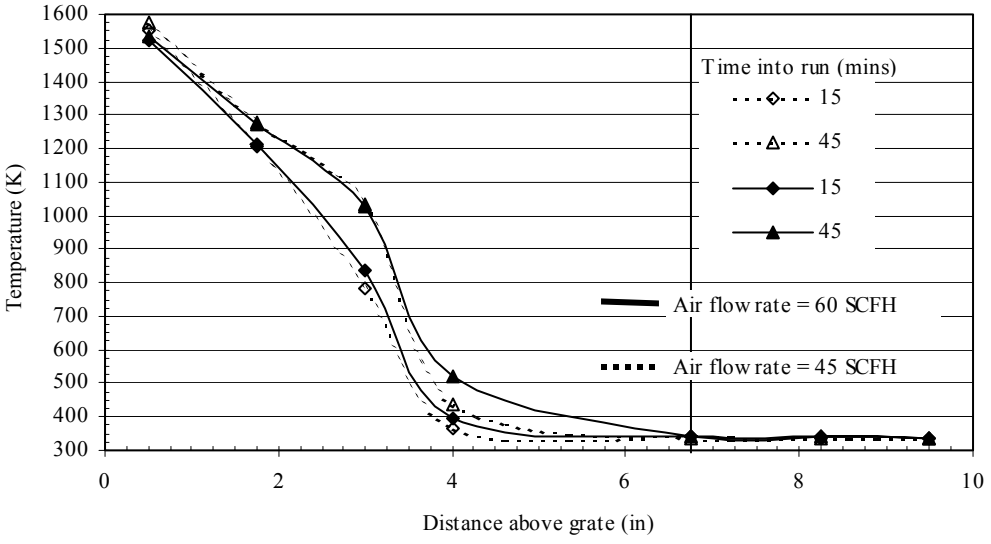

Figure 4.92: Comparative temperature profiles for Coal (4 mm (0.157") – 6.4 mm (0.25")) at air flow rates of 1.27 and 1.7 m^3/hr (45 and 60 SCFH)

Though at first the temperature profiles seem identical, there are subtle differences in the profiles. Firstly, the temperature at the base of the bed i.e. at 12.7 mm (0.5") above the grate is higher for air flow rate of 1.27 m^3/hr (45 SCFH) as compared to 1.7 m^3/hr (60 SCFH) by about 50 K (90 ºF). Since the particle size distribution is similar for both the cases, the void fraction almost identical, so the burning rate is almost identical (except for slight change in the Sherwood number which is dependent on the velocity of the flowing fluid, so the burning rate may be higher if the air flow rate is increased).

Now that the temperature profiles have been discussed separately for different particle sizes, it would be interesting to study the particle size effect on the gasification dynamics. Figure 4.93, shows the particle size effect on the gasification characteristics under air flow rates of 1.27 m^3/hr (45 SCFH).

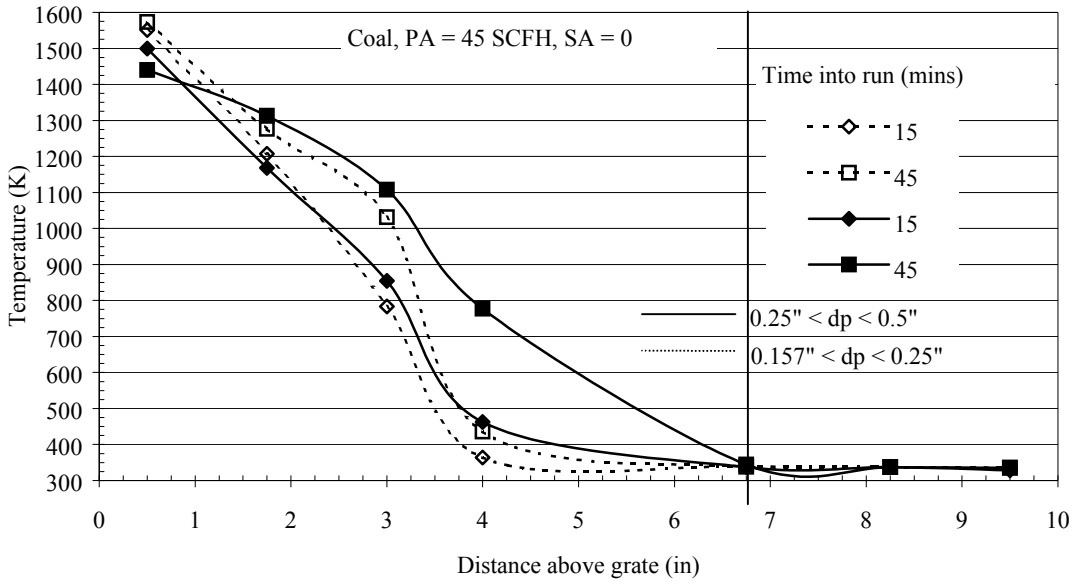

Figure 4.93: Particle size effect on the temperature profile in the bed under air flow rate of 1.27 m^3/hr (45 SCFH)

The temperature profiles for both the particle sizes are slightly different; it is important to discuss the reasons for such a deviation in behavior. Initially the peak temperature in the case of smaller sized particles is higher than their larger counterparts by about 60 K (108 ºF). This can be attributed to two main reasons, the first being the higher S_V in the case of smaller particles, and the second being the higher convective heat transfer per unit volume in the bed for smaller particles.

Since the S_V ratio increases as the particle size decreases the burn rate per unit volume of the bed increases. This is because the surface area available per unit volume of the bed increases as the particle size decreases. In addition, the higher burn rate translates into a higher heat generation in the oxidation zone leading to a higher temperature in the oxidation zone. As the particle size decreases, the particle number density increases, in other words the bulk density of coal increases, which may require higher sensible heat energy to heat it to a higher temperature. But from the above graph it is seen that the temperature rise effect due to higher heat generation is offset by the temperature decreasing effect caused due to a higher heat capacity in the oxidation zone and higher heat loss per unit volume.

The void fraction in the bed increases as the particle sizes increases. An increased void fraction leads to a higher convective heat transfer in the bed. Thus in case of larger particles, the temperature may not only be lower due to lower burn rate, but also may be lower due to higher rate of heat loss from the oxidation zone.

The temperature gradient in the 44.5-101.6 mm (1.75" – 4.0") region is always greater for smaller particles because of the higher heat capacity of the bed and lower convective heat transfer in the bed. It can be observed that even after 45 minutes into the run, the temperature gradient in the 76.2 – 101.6 mm (3.0" to 4.0") region is very high for the smaller particles as compared to the larger particles. The heat capacity for smaller particles is greater than the larger particles due to two main reasons; a) the higher bulk density because of the smaller particle size, and b) the lower heat transfer rate results in slower drying and devolatilization rate causing the heat capacity to decrease much slowly as compared to the larger particles. The lower heat transfer rate also implies that the oxidation zone is relatively thin, this can be concluded by comparing the temperatures at 762 – 101.6 mm (3.0" and 4.0") after 45 minutes into the run. Even though the peak temperature is higher for smaller particles, it is lower as compared to the larger particles at 76.2 and 101.6 cm (3.0" and 4.0").

The temperature drop at 12.7 mm (0.5") is greater for the larger sized particles as compared to the smaller particles. This is due to the fact that the larger sized particles results in a larger void fraction at the bottom, lower combustible per unit volume, thus enabling the O_2 penetration further into the bed, causing the peak temperature to shift faster. More over the combustion of larger particles seems to be effected by the formation of the ash layer over the surface causing the temperature to spread into the bed, no such effect is noticed for the smaller sized particles as the peak shift is rather slower when compared with the larger particles.

Figure 4.94, shows the comparative temperature profiles for different coal particle sizes under an air flow rate of 1.7 m^3/hr (60 SCFH). It can be concluded that the peak temperature is higher for smaller particles as compared to the larger ones. In fact, the previous discussion that was done for air flow rate of 1.27 m^3/hr (45 SCFH), is applicable even for air flow rate of 1.7 m^3/hr (60 SCFH). This goes on to show that the temperature profile in the bed is more influenced by the particle size.

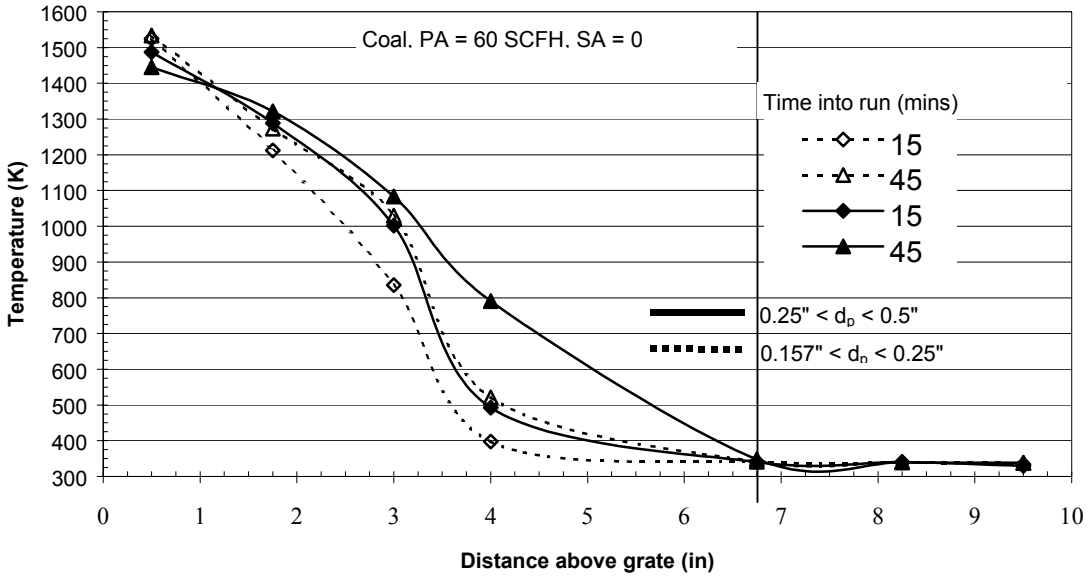

Figure 4.94: Particle size effect on the temperature profile in the bed under air flow rate of 1.7 m^3/hr (60 SCFH) (coal)

The figure 4.95 shows the comparative average coal feed rates for different experiments. It can be seen that for both the air flow rates of 1.27 and 1.7 m^3/hr (45 and 60 SCFH), the feed rate for the larger particles is always greater than that of the smaller particles. This is because the fastest process occurring during gasification is the drying and devolatilization process, during which there is rapid loss of mass and sensible energy from the fuel. Thus, over such short duration of the experiments, the conditions under which the drying and devolatilization processes are faster have the highest feed rate in order to maintain the required bed height. The higher the temperature in the drying and devolatilization zone, the faster is the process, so comparing the temperature in the drying and gasification zone for the different conditions as shown previously in figures 4.93, and 4.94, we see that for larger sized particles the temperature in the drying and devolatilization zone is always higher as compared to their smaller counter parts, thus leading to faster mass loss from the bed. Therefore, for larger particles a higher feed rate is required in order to maintain the required bed height of 171.5 mm (6.75") above the grate.

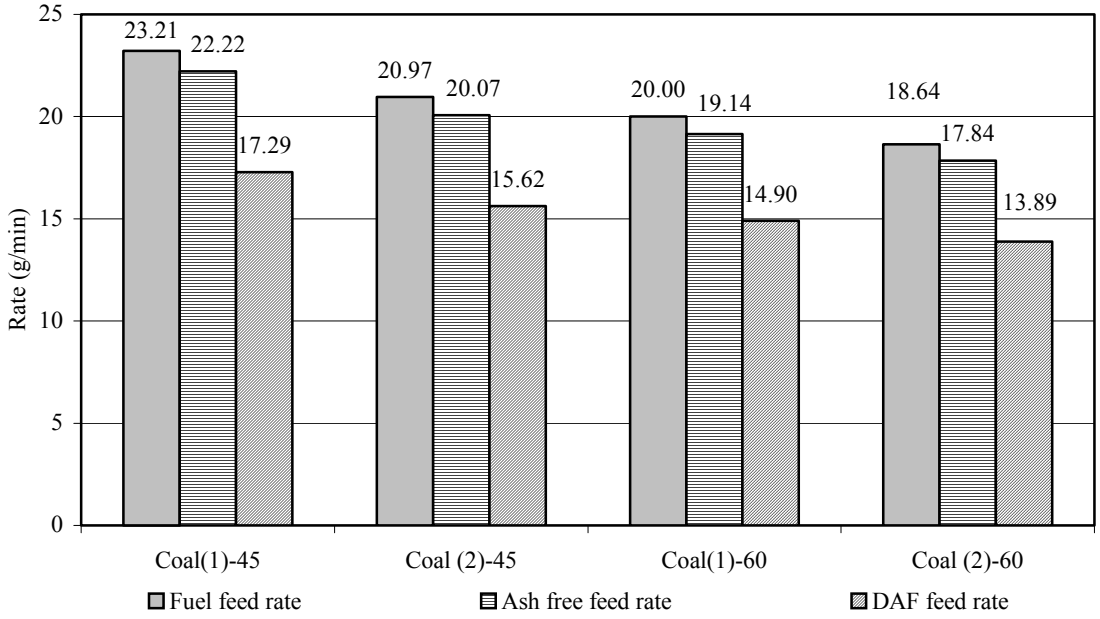

Figure 4.95: Comparative average coal feed rates for different experiments (Coal (1), 6.4-12.7 mm (0.25" –0.5"), Coal (2), 4-6.4 mm (0.157" – 0.25"))

From figure 4.96, it can be easily interpreted that, a higher feed rate for larger particles results in a lower average air fuel ratio and a higher stoichiometric ratio.

From the discussion about the gasification of coal the following conclusions can be drawn; 1) the smaller the particle size, smaller is the oxidation zone, the higher is the peak temperature, slower is the drying and devolatilization process, and lesser is the spatial temperature distribution, 2) ash seems to play an important role in the rate of char oxidation for larger sized particles, 3) the temperature profile is more adversely affected by the particle size rather than the air flow rate of the primary air, and 4) the drying and devolatilization rate determines the coal feed rate into the gasifier.

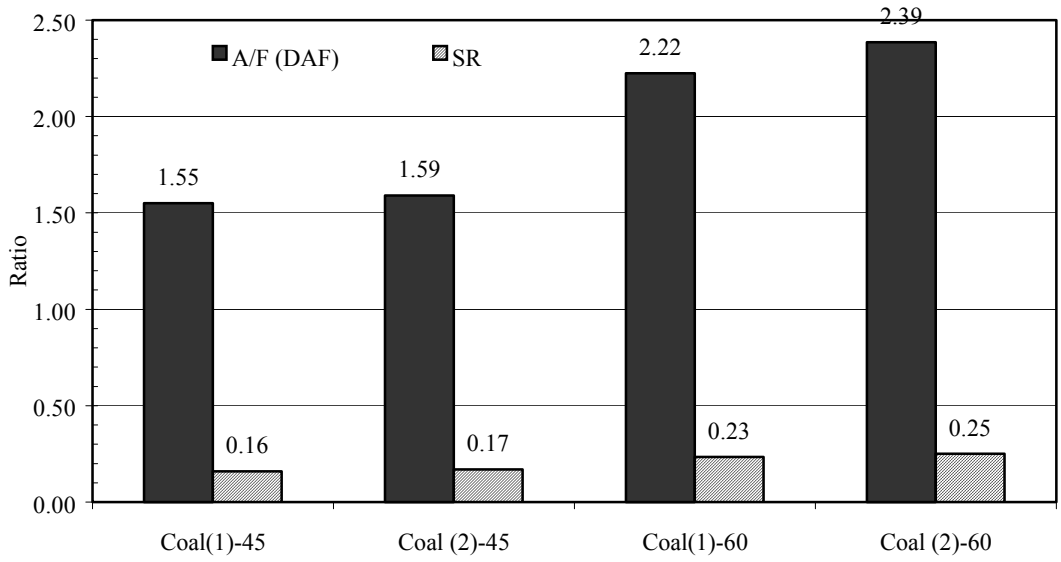

Figure 4.96: Comparative average $A/F_{(DAF)}$ and SR ratios for coal under different operating conditions (Coal (1), 6.4-12.7 mm (0.25" –0.5"), Coal (2), 4-6.4 mm (0.157" – 0.25"))

4.3.2.2. Fly ash surfaced Feedlot biomass (AFB)

As in the case of coal, the study shall include the effect of air flow rate and also the effect of particle size on the temperature profiles in the bed.

Before studying the temperature profiles, it is worthwhile to discuss the fuel properties of feedlot as compared to coal. From table 4.37, the fixed carbon in AFB is only 17.33 % as compared to 41.92 % for coal (as received basis). The sum of dry loss and volatile matter in AFB is 67.84 % while that of coal is 53.80 %, and finally the ash percent in AFB is about 3.5 times that present in coal. Since for every unit weight of AFB added there going to be only 17.33 % of char formed while for coal is 41.92 %, this shall play an important role in determining the temperature profile in the bed.

Another aspect of the fuels is the flow characteristics, while conducting the experiments, it was observed that coal was freely flowing, whereas AFB had a tendency to clump together due to fibrous material and not flow freely. This fuel characteristic also plays an important role in determining the temperature profile in the bed. Thus fuel flow down the bed may not be as smooth as coal.

Tar also plays an important role during gasification; it was observed that tar formation was more in the case of AFB as compared to coal. The tar was visible as a condensate in the bed, which implied that there was external condensation of tar, which could lead to ash agglomeration.

The porosity of the fuel affects the burning rate of the fuel. In case of AFB, which has a higher content of volatile matter as compared to coal, it is expected that the AFB char shall be more porous as compared to coal. The higher porosity shall make additional surface area available for reaction thus boosting the burning rate of the more porous char (fuel). This can be further qualitatively shown from the Thiele modulus (ϕ), which depends on the diffusivity in the pore, rate constant of reaction, pore dimension, and external surface concentration.

$$\phi = L_P \left(\frac{kCs^{m-1}}{V_p D} \right)^{1/2} \quad \textbf{(4.3.26)}$$

Where,

L_P = effective pore length = r/3 for spheres

k = reaction rate constant

C_S = external surface concentration

m = reaction order

V_P = pore volume

D = diffusivity

The average reaction rate within the particle (r_{avg}) may be related to the rate based on the surface concentrations ($r_{surface}$) in terms of the effectiveness factor, which is defined as follows:

$$\eta = \frac{\left(r_{avg}\right)}{\left(r_{surface}\right)} = \frac{Tanh\phi}{\phi} \quad \textbf{(4.3.27)}$$

The above expression is only valid for an isothermal particle. So when $\phi \rightarrow 0$ (i.e. reaction rate is extremely slow), $\eta \rightarrow 1$ meaning that $r_{avg} = r_{surface}$. Under these conditions, all the pore area is accessible for the reaction. But when $\phi \rightarrow \infty$ (extremely fast reaction rate), $\eta \rightarrow 0$ meaning that $r_{avg} << r_{surface}$ (note that reactant consumption rate at the surface is still finite), and the reaction is exclusively at the particle external surface and the reactant gas does not penetrate into the pores.

Assuming, that the particles at the bottom of the bed are mostly char in both cases for feedlot as well as for coal, and so the reaction rate constants are approximately equal for the two chars. Since the AFB has higher volatile matter than coal, so post pyrolysis the AFB char is more porous than the coal char, which means that the pore volume is higher in AFB than coal. This means that the reactivity of feedlot char is greater than that of coal, so feedlot char shall burn faster than coal char under similar conditions. In addition, the amount of fixed carbon in AFB char is almost half of that present in coal. Therefore, for a given amount of AFB char and coal char, AFB will gasify faster than coal, not only because of the higher char porosity and increased char burn rate, but also due to lower amount of fixed carbon in the AFB.

The specific heat of the char also shall affect the temperature profile. In case of coal, the char composition shall be 90 % fixed carbon, and 10 % ash, while that for AFB would be 54 %fixed carbon and 46 % ash. And as reported earlier literature review, the specific heat capacity of ash is around 6 % of that of fixed carbon, so the specific heat capacity of AFB char shall be almost half of that of coal char. This implies that a lower amount of sensible heat energy is required to heat the AFB char through one-degree rise in temperature as compared with coal char.

From figure 4.97, (Thien, 2002) it can be seen that the pyrolysis of AFB begins at about 500 K (440.33 ºF), which is about 120 K (216 ºF) lower than that of coal. Therefore, for AFB, the pyrolysis in the bed begins earlier as compared to coal, due lower activation energy for pyrolysis. The above-mentioned properties of the AFB affect the temperature profiles in the bed.

For fly ash surfaced AFB particle size range between 6.4 and 12.7 mm (0.25” and 0.5”), figure 4.98 shows the comparative temperature profiles under air flow rates of 1.27 and 1.7 m^3/hr (45 and 60 SCFH). It is seen that the temperature profile exhibited by AFB is entirely different from that exhibited by coal under similar operating conditions. In this case, there is a distinct peak in the temperature and the peak shift is clearly apparent during the short run of the experiment.

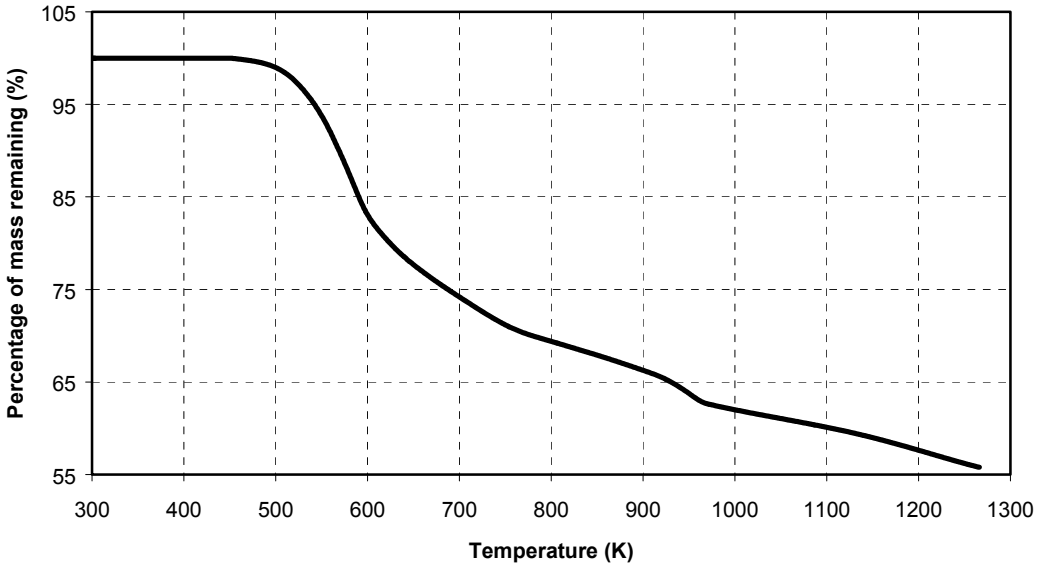

Figure 4.97: TGA of AFB of 45+ μm in N_2 atmosphere

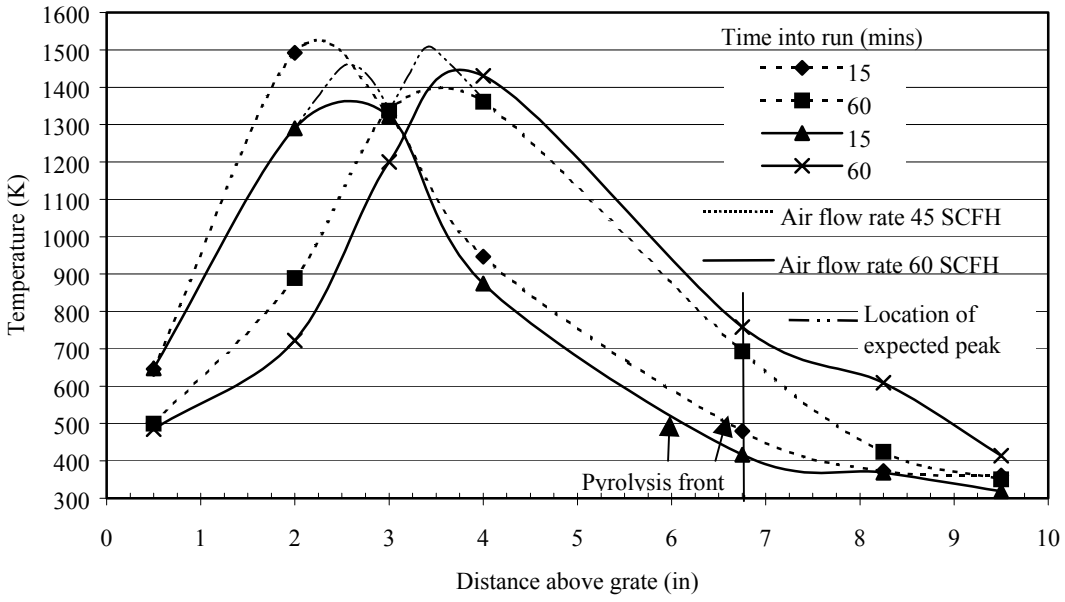

Figure 4.98: Comparative Temperature profiles for AFB (6.4-12.7 mm (0.25" – 0.5")) under air flow rates of 1.27 and 1.7 m^3/hr (45 and 60 SCFH0

Surprisingly after only 15 minutes into the run the temperature at 12.7 mm (0.5") above the grate is about 650 K (710.33 ºF). The pyrolysis front is closer to the free board since it occurs at a lower temperature (500 K (440.33 ºF)). This shows that the condition at that location is similar for

both the cases. Moving further into the bed, it is observed that at 44.5 mm (1.75") above the grate, the temperature is higher for the 1.27 m^3/hr (45 SCFH) case as compared to the 1.7 m^3/hr (60 SCFH) case, with the peak occurring at 50.8 mm (2.0") above the grate for 1.27 m^3/hr (45 SCFH) case, and at about 64 mm (2.5") for the 1.7 m^3/hr (60 SCFH) case. Interestingly the peak temperature for the 1.27 m^3/hr (45 SCFH) case is higher than the 1.7 m^3/hr (60 SCFH) case by about 100 K (180 ºF). Such a trend in the temperature profile can be explained as follows. Due to the high porosity and lower fixed carbon, the AFB burns rapidly so by 15 minutes into the run the composition of the bed at 12.7 mm (0.5") above the grate is mostly ash, this helps to explain the equal temperatures at 12.7 mm (0.5") for both the cases. The peak for 1.27 m^3/hr (45 SCFH) occurs at a lower height as compared to the 1.7 m^3/hr (60 SCFH) case because the higher air flow results in a higher convective heat transfer into the bed, thus causing the peak to move faster for the 1.7 m^3/hr (60 SCFH) case. The temperature at 1.75" is higher for the 1.27 m^3/hr (45 SCFH) case because the higher air flow rate also results in a higher reaction rate, so the AFB burns faster for the 1.7 m^3/hr (60 SCFH) case. In other words, if the bed composition between the base of the bed and 44.5 mm (1.75") were to be compared, the ash content would be higher for the 1.7 m^3/hr (60 SCFH) case, due to faster burning, thus reducing the combustible content in the bed, so resulting in a lower temperature. The lower temperature is also due to the higher convective heat transfer in the bed. The convective heat transfer also reduces the peak temperature in the bed for the 1.7 m^3/hr (60 SCFH) case, thus causing the peak temperature for the 1.7 m^3/hr (60 SCFH) case to be lower than the 1.27 m^3/hr (45 SCFH) case. Initially after 15 minutes into the run, the lower peak temperature translates into lower temperatures in the bed beyond the peak and the temperature differences at 101.6 and 171.5 mm (4.0" and 6.75") are small.

However, after 60 minutes into the run, the situation is entirely different. The temperature at 12.7 mm (0.5") has fallen to about 500 K (440.33 ºF) for both the cases, showing that the conditions in the bed at that location are similar for both the cases. The rate of peak shift for the 1.27 m^3/hr (45 SCFH) case is about 42.5 mm/hr (1.7"/hr), and about 51.0 mm/hr (2"/hr) for the 1.7 m^3/hr (60 SCFH) case. The temperatures at 101.6 and 171.5 mm (4.0" and 6.75") are slightly higher for the 1.7 m^3/hr (60 SCFH) case as compared to the 1.27 m^3/hr (45 SCFH) case. This is because of the proximity of the peak temperature to these locations and due to the higher convective heat transfer rate. In addition, the temperature is higher because, the higher convective heat transfer also facilitates a slightly higher drying and devolatilization rate, thereby decreasing the heat capacity of the fuel, thus helping in increasing the temperature at 101.6 and 171.5 mm (4.0" and 6.75") for the 1.7 m^3/hr (60 SCFH). Due to the similarity of the temperature profiles in the drying and devolatilization region, the feed rate is expected to be almost similar for both the cases, which can be concluded from, figure 4.101. Similar feed rate results in a higher air fuel ratio for the 1.7 m^3/hr (60 SCFH) case as compared to the 1.27 m^3/hr (45 SCFH) case and can be observed in figure 4.102.

The shift in peak temperature is due to the ash accumulation in the bed, the higher burning rate, and lower fixed carbon. The shift in temperature is more pronounced for AFB as it has a higher ash content, and lower fixed carbon as compared to coal. In order to verify that the ash was actually responsible for the temperature shift in the bed, a special experiment was conducted for AFB at an air flow rate of 1.27 m^3/hr (45 SCFH) over a 2.75 hour period. During this experiment, the temperature profiles were measured at regular intervals and are shown in figure 4.99.

In figure 4.99, it is observed that the peak temperature shifts, as time progresses. Some of the profiles are shown in dashed lines, as they do not show the actual peaks in the bed. However, it can be clearly observed that as the peak shifts, the temperature at the top of the bed increases. From equation 4.6.25, where it was observed that the ash accumulation in the bed is directly proportional to the ash feed rate into the gasifier. If instead of AFB, a high ash content coal is fed into the gasifier, then the temperature shifts in the bed for both the cases could be comparable. The same time, the temperature at 12.7 mm (0.5") above the grate seems to stabilize at 450 K (350.33 ºF) after about 60 minutes into the run, showing that the char at this location has almost completely burned, and the composition of the bed near the grate is primarily ash.

It is to be mentioned that though tar condensation was observed at about 101.6 mm (4.0") above the bed for both the cases, it did not cause appreciable agglomeration in the bed. However, the presence of moisture condensate causes the AFB to become sticky and not flow freely. This could aggravate the problem of agglomeration in the bed.

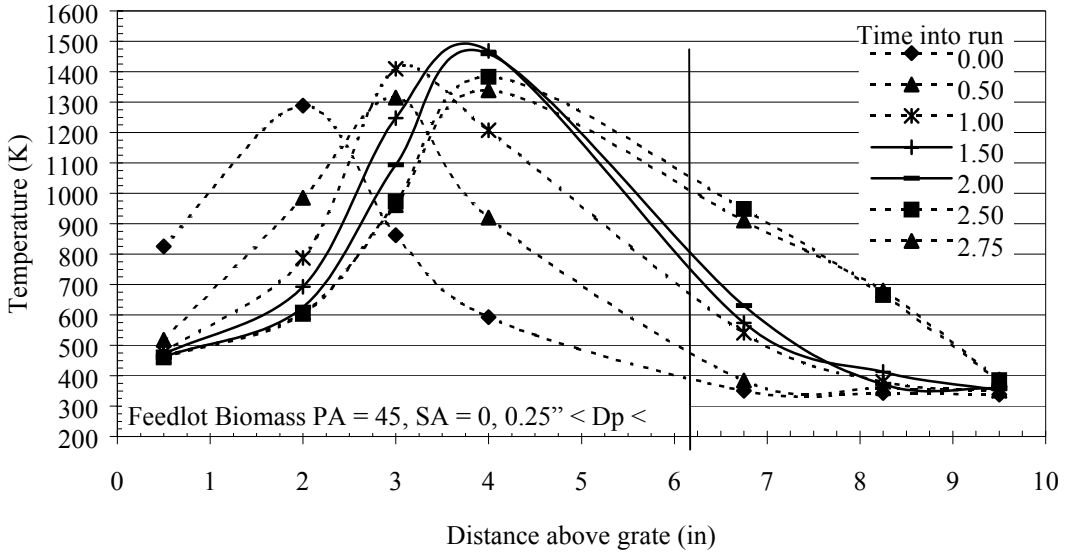

Figure 4.99: Temperature profile for AFB (6.4-12.7 mm (0.25" –0.5")) under air flow rate of 1.27 m^3/hr (45 SCFH) (experiment run for 2.75 hours)

For AFB particle size range between 0.157" and 0.25", figure 4.100 shows the comparative temperature profile for air flow rates of 1.27 and 1.7 m^3/hr (45 and 60 SCFH). As in the case of large sized AFB particles, the temperature profile look a bit similar, exhibiting a distinctive peak, which is evident even after only 15 minutes into the run. However, a difference is the formation of a plateau after one hour into the run for the 1.7 m^3/hr (60 SCFH) case. First discussing the temperature profiles at 15 minutes into the run shall enable to understand the difference between the behavior of smaller sized particles as compared to their larger counterparts.

After 15 minutes into the run, the temperature at 12.7 mm (0.5") above the grate is almost same for both the cases and is about 575 K (575.33 ºF). This temperature is about 75 K (135 ºF) lesser than those reported for the larger sized particle under similar condition (refer figure 4.98). This difference in temperature is due to the higher gasification rate associated with smaller sized particles, because of the higher S_V ratio for smaller particles, thus resulting in a higher concentration of ash at 12.7 mm (0.5") above the grate after 15 minutes into the run. Moving further into the bed it is observed that the peak temperatures for both the cases occur at about the same location. However, the peak temperature is higher for the 1.7 m^3/hr (60 SCFH) case as compared to the 1.27 m^3/hr (45 SCFH) case, by about 100 K (180 ºF). This is just the opposite to what was observed for the case of larger particles. In case of the smaller particles, the higher air flow rate results in a higher burning rate thus increasing the peak temperature, but interestingly due to the smaller particle size, the convective heat transfer in the bed associated with higher flow rates is not that effective as it was with the larger particles. The smaller sized particles result in a lower void fraction in the bed, i.e., increase the bulk density in the bed, reduce channeling in the bed and hence less hat loss through interstitial

gas flows. The higher peak temperature in the case of 1.7 m^3/hr (60 SCFH) case, results in higher temperatures at 76.2, 101.6 mm (3.0", 4.0") locations. The higher temperature in the upper portion of the bed, shall enhance the drying and pyrolysis process, thus increase the fuel feed rate into the gasifier.

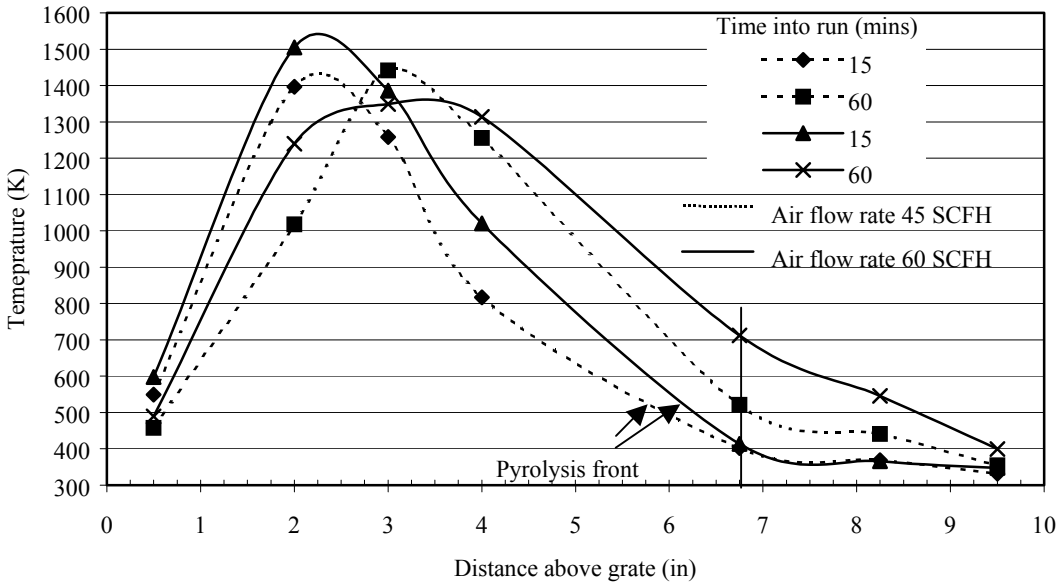

Figure 4.100: Comparative Temperature profiles for AFB (0.157" –0.25") under air flow rates of 1.27 and 1.7 m^3/hr (45 and 60 SCFH)

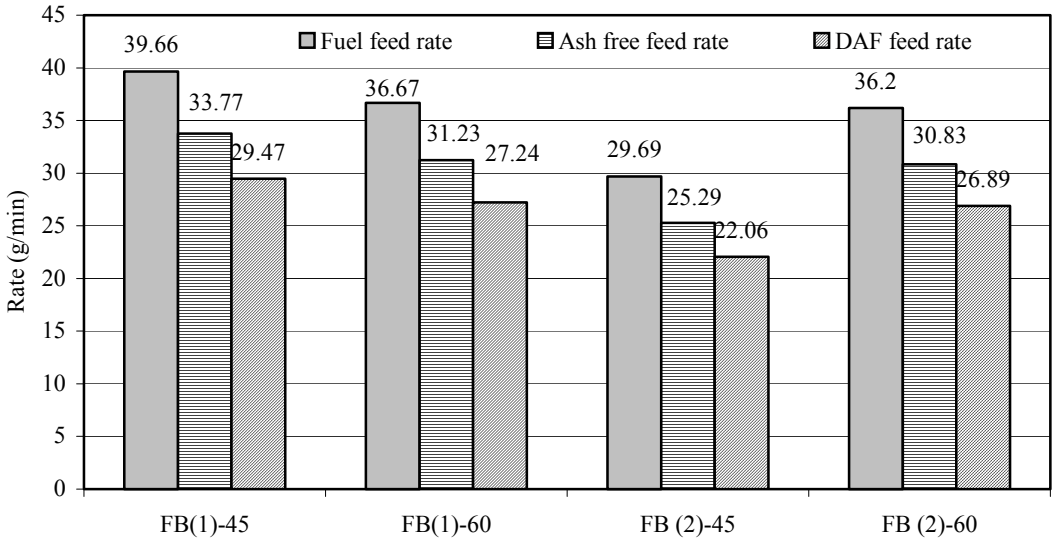

Figure 4.101: Comparative average AFB feed rates for different experiments (AFB (1), 6.4-12.7 mm (0.25" – 0.5"), AFB (2), 4-6.4 mm (0.157" – 0.25"))

Now studying the temperature profiles in the bed after 60 minutes into the run, the rate of peak shift in the 1.27 m^3/hr (45 SCFH) case is about 34 mm/hr, whereas the 1.7 m^3/hr (60 SCFH) case, exhibits a plateau between 2.0" and 4.0" above the grate. Beyond the peaks, the temperature for the 1.7 m^3/hr (60 SCFH) case is consistently higher as compared to the 1.27 m^3/hr (45 SCFH) case, this results in faster drying and devolatilization rates with the pyrolysis front moving towards the free board, and hence a higher feed rate for the 1.7 m^3/hr (60 SCFH) case (refer figure 4.101). Though the higher feed rate tends to decrease the air fuel ratio, the increase in the air flow rate tends to increase the air fuel ratio for the 1.7 m^3/hr (60 SCFH) case, and can be observed in figure 4.102.

After 60 minutes into the run, the peak exhibited by the 1.7 m^3/hr (60 SCFH) case is reduced to about 1350 K (1970.33 ºF). This is because as the fuel starts agglomerating, the surface area available for reaction reduces thus reducing the peak temperature. At the same time agglomeration, causes pronounced channeling in the bed causing enhanced convective heat transfer further in the bed. This is observed in the higher temperatures exhibited at 171.5 mm (6.75") above the bed. It shall be interesting to determine the ash fusion temperatures of the AFB. The ash fusion temperatures of the fuels shall be discussed at the end of this section. For the 1.27 m^3/hr (45 SCFH) case, the lower peak results in lower temperatures in the drying and volatilization regions and hence a lower feed rate as compared to the 1.7 m^3/hr (60 SCFH) case.

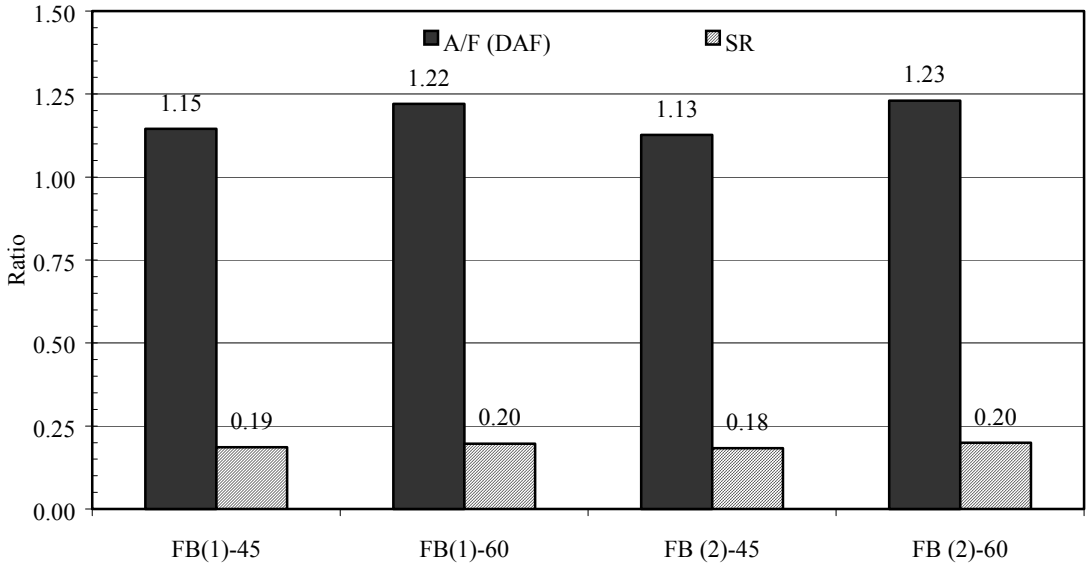

Figure 4.102: Comparative average A/F (DAF) and SR ratios for AFB under different operating conditions

Comparing the temperatures for both the cases of 1.27 and 1.7 m^3/hr (45 and 60 SCFH) at 12.7 mm (0.5") above the grate shows that, both the temperatures are similar and are equal to about 475 K (395.33 ºF), which is about 100 K (180 ºF) lower than that observed after 15 minutes into the run. This shows that there was some combustible at that location after 15 minutes into the run, but after 60 minutes into the run, the bottom of the base is almost ash. This has been already discussed in the case of larger sized particles.

Figure 4.103, shows a comparison of temperature profiles for different particle size fired into the gasifier under an air flow rate of 1.27 m^3/hr (45 SCFH).

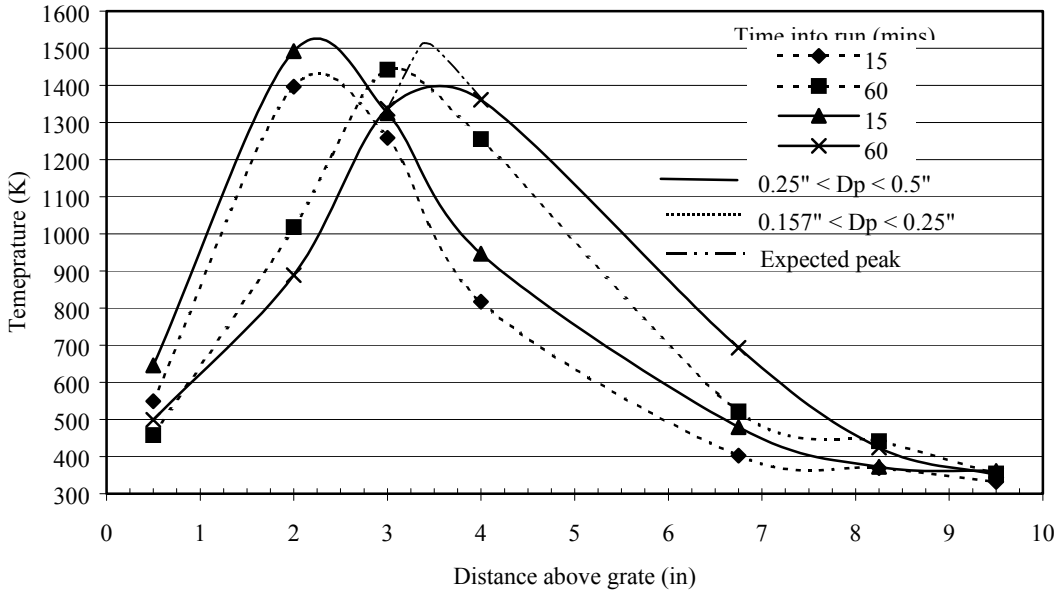

Figure 4.103: Particle size effect on the temperature profile in the bed under air flow rate of 1.27 m^3/hr (45 SCFH) (AFB)

The lower peak temperature in the smaller particle size case is unexpected, as for smaller particles, the S_V ratio is larger resulting in a higher burn rate, thus resulting in a higher peak temperature. On the other hand, the rapid combustion depletes O_2 rapidly. Therefore, at 1.27 m^3/hr (45 SCFH) the air flow rate is not enough to raise the peak temperature. This is also evident from the temperature at the bottom of the bed, since char is already consumed. Comparing the temperatures at 12.7 mm (0.5") above the grate, after 15 minutes into the run, it is seen that the temperature for the smaller particles is lower by about 100 K (180 ºF) than their larger counterparts. This shows that though the burning rate is higher for smaller particles, the higher amount of ash in that location due to rapid depletion of smaller sized char particles decrease the temperature to such an extent. The temperatures in the 101.6-171.5 mm (4.0" – 6.75") are higher for the larger particles, not only due to the faster spreading of peak, but also due to higher convective heat transfer in the bed. The higher temperature results in higher drying and pyrolysis rate, thus allowing increased feed rate for the larger particles. The lower void fraction for the smaller particles causes the peak temperature to move much slower in the bed as compared to the larger particles. Therefore, the void fraction clearly affects the temperature profile in the bed, by affecting the convective transport rates in the bed.

$$\frac{char\ mass}{Volume\ of\ bed} = \left(\frac{char\ mass}{bed\ mass}\right) \times \left(\frac{bed\ mass}{Volume\ of\ bed}\right) \propto Y_{char} \qquad \textbf{(4.3.28)}$$

and

$$S_V \propto \frac{1}{d_p} \qquad \textbf{(4.3.29)}$$

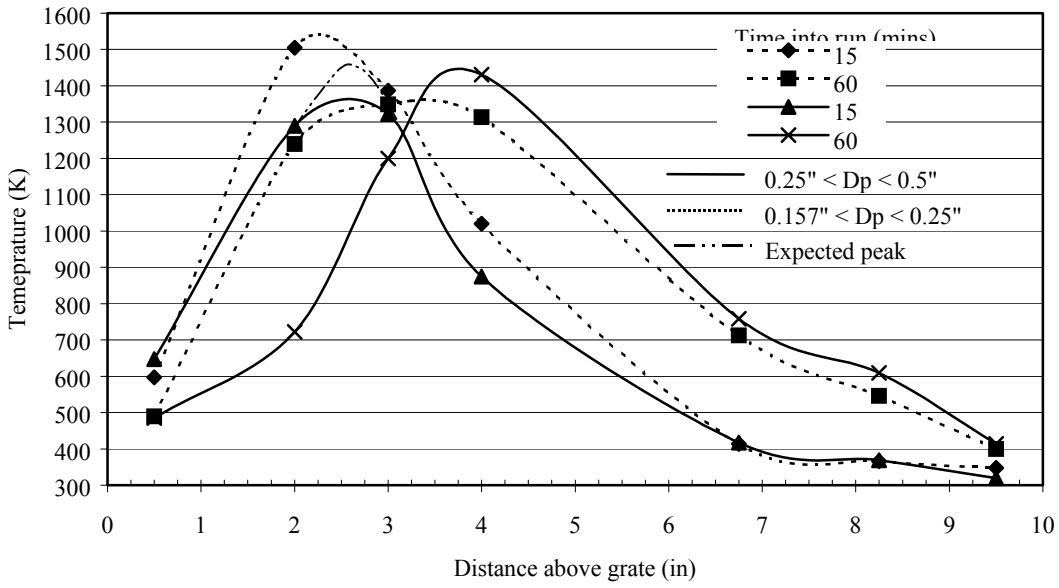

Figure 4.104: Particle size effect on the temperature profile in the bed under air flow rate of 1.7 m^3/hr (60 SCFH) (AFB)

Figure 4.104 shows the particle size effect on the temperature profiles in the bed under air flow rates of 1.7 m^3/hr (60 SCFH). It is interesting to note that in this case the peak temperature is higher for smaller particles, as the temperature increase caused due to higher burn rate seems to out weigh the temperature decrease caused due to the higher heat capacity of the bed. Thus, higher air flow rates for smaller particles seem to increase the peak temperature. However, the higher peak temperature associated with the smaller particles caused agglomeration in the bed. The ash agglomeration causes the temperature profile to be more flat, due to reasons already discussed. For larger particles, the higher flow rate seems to increase the convective heat transfer rate, causing the peak to shift faster as compared to the smaller particles, and decreases the peak temperature in the bed thus avoiding agglomeration in the bed. Since the temperature in the 101.6 to 171.5 mm (4.0" to 6.75") region is almost similar for both the particle sizes, the drying and devolatilization rates are also similar. The result, almost similar fuel feed rates, resulting in almost similar air fuel ratios.

Another interesting fact is that though the peak temperature achieved for large particles under an air flow rate of 1.27 m^3/kg (45 SCFH), and for smaller particles under an air flow rate of 1.7 m^3/hr (60 SCFH) is about 1500 K (2240.33 ºF), agglomeration occurs only in the later case. This may be because, for smaller particles they are more compactly packed and the contact surface area per unit volume of the bed is more as compared larger particles, so tar condensation in the 101.6 mm (4.0") region might cause the smaller particles to clump and fuse thus leading to agglomeration in the bed. For larger particles, the higher void fraction results in a lower contact surface area, so in spite of tar condensation there is not obvious agglomeration in the bed.

To conclude the discussion on temperature characteristics of AFB, it is seen that the peak temperature as well as the rate of peak shift in the bed is affected by the air flow rate, and the particle size. The air flow rate increases the convective heat transfer in the bed, while the smaller particle size increases the heat capacity of the bed. The smaller particles have a tendency to agglomerate, so it is advisable to fire larger particles into the gasifier. Since the ash content of the AFB is higher than that

of coal, the ash discharge at the gate has to done more frequently in order to minimize the temperature shift in the bed.

4.3.2.3. Coal: AFB blend (CAFB)

The blends of coal and AFB in a weight ratio of 50:50 were fired into the gasifier and the temperature profile studied. The proximate and ultimate analysis of the blend is shown in table 4.37. Ash and volatile matter content of the blend are less than that of the AFB but more than coal, while the vice-versa is true for fixed carbon. The ash is expected to play an important role in determining the temperature profile in the bed. The behavior of the blend is expected to be a mixture of both coal and AFB. It will be interesting to see, whether the blend shows any agglomeration tendencies or not?

For coal and fly ash surfaced FB blend (CAFB) particle size range between 6.4 mm (0.25") and 12.7 mm (0.5") figure 4.105 shows the comparative temperature profiles under 1.27 and 1.7 m^3/hr (45 and 60 SCFH) air flow rates. The blend exhibits a distinct peak in the bed, which is similar to that exhibited by the AFB.

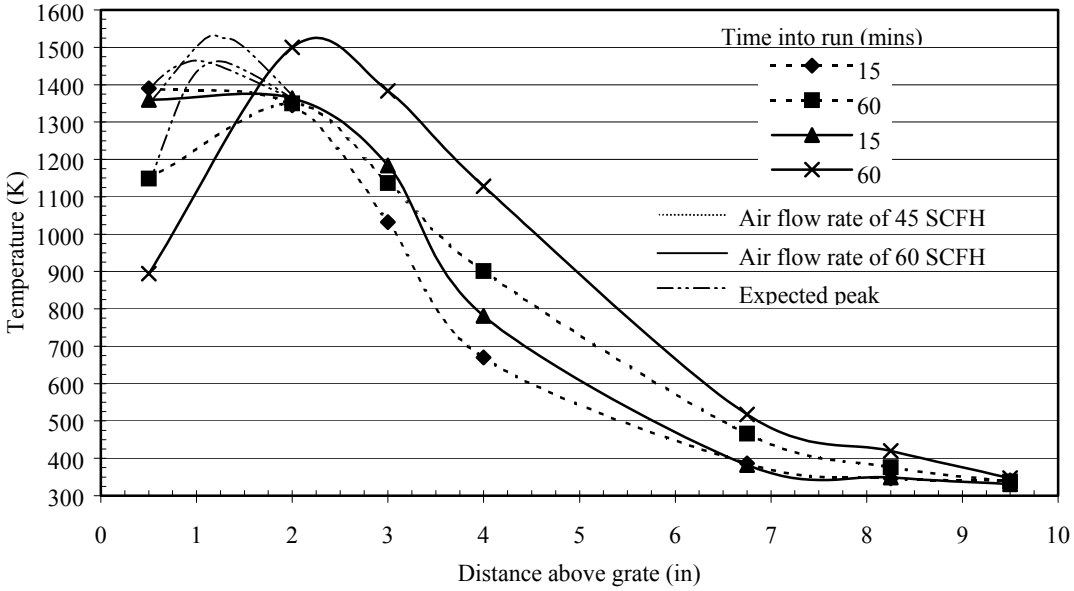

Figure 4.105: Comparative temperature profiles for CAFB (6.4-12.7 mm (0.25" – 0.5")) at air flow rates of 1.27 and 1.7 m^3/hr (45 and 60 SCFH)

After only 15 minutes into the run, there is a distinct temperature peak in the bed for both the cases. This behavior is similar to that exhibited by AFB. However, the temperature at 12.7 mm (0.5") above the grate is about 1300 K (1880.33 ºF) (where coal char is still burning), as compared to about 650 K (710.33 ºF) in the case of AFB (as most of the char has already gasified or burnt). This proves that, there is some reaction occurring at this location, and this behavior is along the expected lines. Since coal takes a much longer time to burn as compared to AFB (under similar conditions), the AFB has almost burned, where as the coal at this location is still under going oxidation. This oxidation helps to keep the temperature up at this location and is higher than that shown by AFB. However, the temperature exhibited by coal under such conditions is about 1500 K (2240.33 ºF), which is higher than those shown by the blend. This is because, of the higher ash content of the blend, coupled with the faster oxidation of AFB in the blend, which increases the ash content in the

lower portion of the bed, thus bringing the temperature down to about 1300 K (1880.33 ºF). The location of the peak temperatures is almost same for both the cases, and is located at about 25.4 mm (1.0") above the grate. The peak temperature for the 1.7 m^3/hr (60 SCFH) case is higher than the 1.27 m^3/hr (45 SCFH) case by about 50 K (90 ºF). This may be due to the higher burning rate associated with the higher air flow rate. The temperatures in the 76.2 to 171.5 mm (3.0" to 6.75") region are higher for the 1.7 m^3/hr (60 SCFH) case as compared to the 1.27 m^3/hr (45 SCFH) case, this is due to higher convective transfer rates associated with higher air flow rates. The higher temperatures in the upper portion region of the bed would result in a higher drying and devolatilization rate, thus requiring a higher fuel feed rate.

After 60 minutes into the run, the peak shift has occurred for both the cases, while for the 1.27 m^3/hr (45 SCFH) case the shift is not significant, but for the other case, it is about 1.0" further into the bed. The peak shift is faster for the 1.7 m^3/hr (60 SCFH) case, due to higher convective transfer rates in the bed, and due to higher burning rates. The conclusion of higher burn rates can be determined by comparing the temperatures at 12.7 mm (0.5") above the grate. For the 1.7 m^3/hr (60 SCFH) case it is about 900 K (1160.33 ºF), whereas for the other case it is about 1150 K (1610.33 ºF). This can only mean that the fuel in this location of the bed has higher ash content or lower combustible matter, and hence results in a lower temperature. The higher ash content is due to higher burning rates caused by the higher air flow rates. The temperatures in the 76.2 mm (3.0") to the 171.6 mm (6.75") region are much higher for the 1.7 m^3/hr (60 SCFH) case as compared to the 1.27 m^3/hr (45 SCFH) case. This is due to higher convective flow rates in the bed. The higher temperature should translate into a higher feed rate for the 1.7 m^3/hr (60 SCFH) case. However, on referring figure 4.107 it is seen that the feed rate for the 1.27 m^3/hr (45 SCFH) case is about 31 g/min and that for the 1.7 m^3/hr (60 SCFH) case is about 25 g/min. The higher burning rate for the 1.7 m^3/hr (60 SCFH) case, results in a faster accumulation of ash in the bed, so the volume of bed (as the height of the bed is fixed) available for the combustibles decreases, decreasing the feed rate. The lower feed rate results in a lower heat capacity of the bed, thus resulting in higher temperatures in the upper portion of the bed in the case of 1.7 m^3/hr (60 SCFH). The lower feed rate translates into t a higher air fuel ratio for the 1.7 m^3/hr (60 SCFH) case as compared to the 1.27 m^3/hr (45 SCFH) case. There was no agglomeration tendencies exhibited by the coal and AFB blend.

For coal and fly ash surfaced AFB blend (CAFB) particle size range between 4 and 6.4 mm (0.157" and 0.25"), figure 4.106 shows the comparative temperature profiles for the coal and AFB blends under different air flow rates. The smaller particles also exhibit a distinct peak in the bed as exhibited by their larger counterparts. The peak for the 1.7 m^3/hr (60 SCFH) case is higher than the 1.27 m^3/hr (45 SCFH) case by about 100 K (180 ºF).

After 15 minutes into the run, the peaks for both the cases are located at about the same location of 25.4 mm (1.0") above the bed. Initially the high flow rate does not seem to effect the location of the peak temperature in the bed, this could be due to the lower void fraction in the bed, inhibiting the convective heat transfer rates. The comparative temperatures at 12.7 mm (0.5") above the grate, show that the burn rate is clearly higher in the case of the 1.7 m^3/hr (60 SCFH) case. The higher burn rate results in lower combustible matter at this location, and higher ash content, which cause the temperature to decrease faster than the 1.27 m^3/hr (45 SCFH) case. The temperatures in the 76.2 to 171.5 mm (3.0" to 6.75") region seem to be almost similar for both the cases, with the 1.7 m^3/hr (60 SCFH) case showing a slightly higher temperature. This similar temperature distribution in the drying and devolatilization region would result in an almost similar fuel feed rates for both the cases.

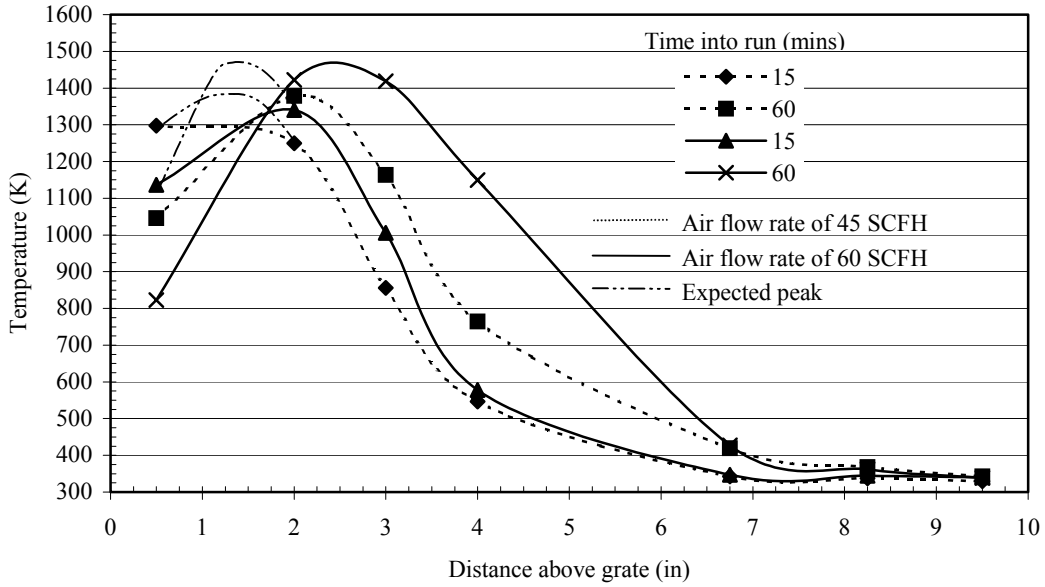

Figure 4.106: Comparative temperature profiles for CAFB (4-6.4 mm (0.157" – 0.25")) at air flow rates of 1.27 and 1.7 m^3/hr (45 and 60 SCFH)

After 60 minutes into the run, the rate of peak shift for the 1.7 m^3/hr (60 SCFH) case is much higher as compared to the 1.27 m^3/hr (45 SCFH) case. This is because of the higher burn rate and hence faster accumulation of ash in the bed. For smaller particles, the heat generation due to higher flow rates seems to out weigh the temperature decrease caused due to higher convective transfer rates in the bed. This is because, the void fraction in the bed does not allow appreciable convective heat transfer in the bed, as the flow is more distributed across the cross section of the bed. However, the comparative temperatures in the upper portion of the bed, show a much higher temperature distribution for the 1.7 m^3/hr (60 SCFH) case. This is because, the higher peak temperature at a higher location in the bed, causes some of the AFB to burn, and partially fuse with the coal to form a crude channeling phenomenon in the bed. The channeling results unless heat transfer in certain sections of the bed pushing the temperature in the bed much higher. This reason is established by referring figure 4.107, which shows that the fuel feed rates for both the case are close with the 1.7 m^3/hr (60 SCFH) case having a slightly higher feed rate. The higher air flow rate translates into a higher air fuel ratio which is reflected in figure 4.108.

The channeling in the bed results in agglomeration in the bed. Though the agglomeration was not as severe as in the case of AFB, there certainly was agglomeration in the bed in this case. This agglomeration is on a much smaller scale, because the AFB per unit volume in the bed is smaller as compared to the pure AFB case. Thus, the particle contact surface seems to play an important role in causing agglomeration in the bed. This could be because of external tar condensation in the bed might be causing the particles to fuse, and the presence of high temperatures might be accelerating the agglomeration process. Another important observation is that the smaller particles exhibit agglomeration tendencies, so the particle size could be playing an important role in the agglomeration in the bed. The particle size also affects the inter-particle contact surface area, with the inter-particle contact surface area increasing with a decrease in the particle size. Thus, it shall be interesting to determine the ash fusion temperatures of the AFB, then try, and correlate the obtained experimental results. The results of ash fusion temperatures shall be discussed concluding part of this section.

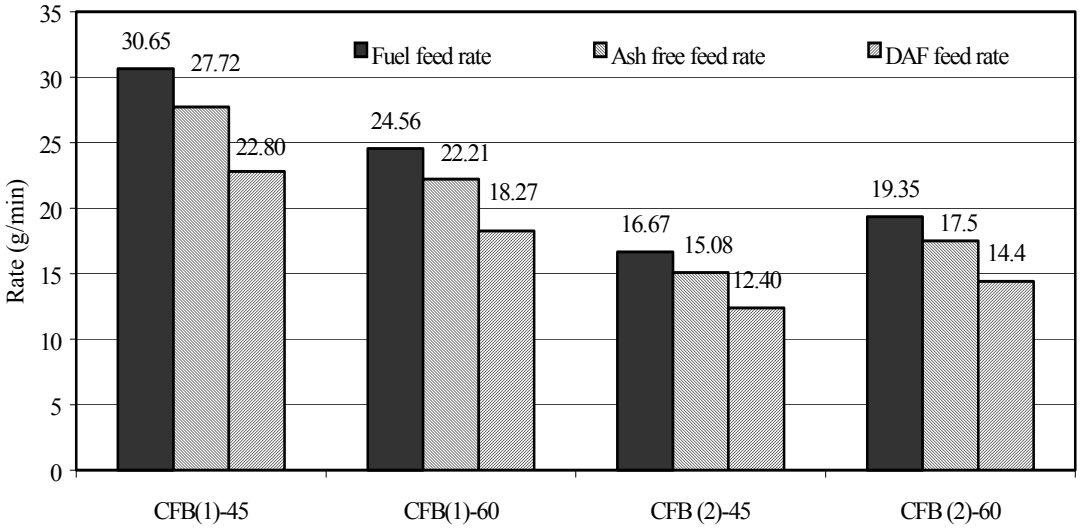

Figure 4.107: Comparative average coal and AFB blend (CAFB) feed rates for different experiments (CAFB (1), 6.4-12.7 mm (0.25" – 0.5"), CAFB (2), 4-6.4 mm (0.157" –0.25"))

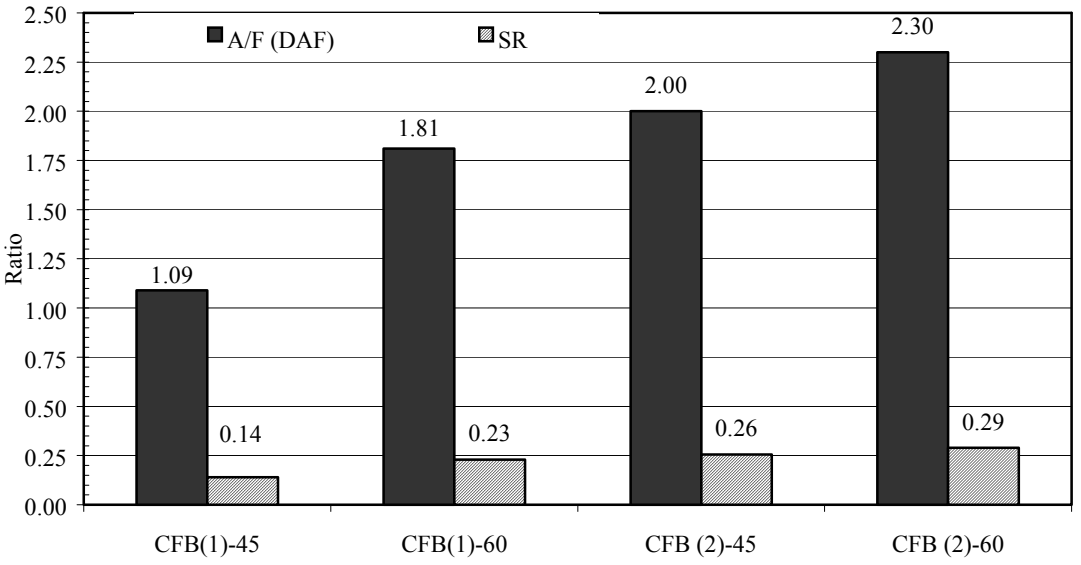

Figure 4.108: Comparative average A/F (DAF) and SR ratios for coal and AFB blends under different operating conditions (CAFB (1), 6.4-12.7 mm (0.25" – 0.5"), CAFB (2), 4-6.4 mm (0.157" –0.25"))

In case of coal and AFB blends, the air flow rate seems to effect the temperature profiles for the larger particles more than the smaller particles. The higher air flow rates also results in higher peak temperatures in the bed for both the cases. However, most importantly, the peak shift in the case of blends is not that fast as exhibited by only AFB case. Thus, a lesser frequent ash disposal shall be required for this case. The smaller particles tend to show agglomeration tendencies at higher air flow rates.

4.3.2.4. Chicken litter biomass (LB)

Referring table 4.37, it can bee seen that the ash content in the LB is almost 10 times as that in coal and almost thrice as that of fly ash surfaced AFB. This high ash content shall play the crucial role in determining the peak shift rates and the overall temperature profiles in the bed. At the same time the fixed carbon content in the LB is almost half of that in fly ash surfaced AFB and about a fifth of that of coal. Such low fixed carbon per unit volume in the bed, shall result in very high burn out rates, and it is expected that the for a given mass of all the three above mentioned fuels, the propagation rate of the peak (due to high stoichiometric ratio (SR), and high ash fraction for LB) for LB shall be the highest, followed by AFB and then finally coal. This shall also affect the temperature dynamics in the bed. Thus, the temperature dynamics of such a high ash content fuel shall help in further understanding the effect of ash on the temperature dynamics in the bed.

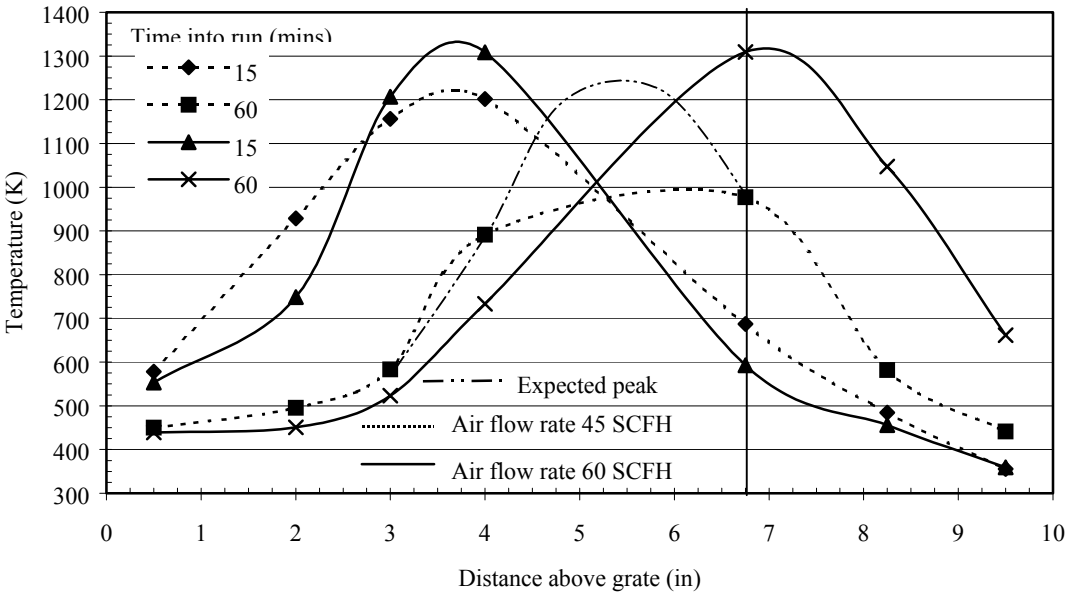

Figure 4.109: Comparative temperature profiles for LB (6.4-12.7 mm (0.25" – 0.5")) at air flow rates of 1.27 and 1.7 m^3/hr (45 and 60 SCFH)

For LB particle size range between 6.4 and 12.7 mm (0.25" and 0.5"), figure 4.109 shows the comparative temperature profiles in the bed under different air flow rates. As in the case of AFB, LB also displays a distinct peak in the bed, and the rate of peak shift is relatively high when compared to the AFB case. From the figure 4.109, it is evident that the ash seems to play the most determining factor in shaping the temperature profile in the bed.

After 15 minutes into the run, it is observed that the peak for both the cases occurs relatively at same locations i.e. at 88.9 mm (3.5") above the grate. The peak for the 1.7 m^3/hr (60 SCFH) case is about 100 K (180 ºF) higher than the 1.27 m^3/hr (45 SCFH) case. This is because of the higher burning rate associated with higher flow rates, but similar initial location of the peaks show the ineffectiveness of the convective heat transfer rates in the bed, at least in the initial stages. Comparing the temperatures at 12.7 mm (0.5") above the grate reveals, that the temperature at that

location is similar for both the cases. Beyond the 101.6 mm (4.0") towards the top of the bed, the temperature profiles are similar for both the cases.

After 60 minutes into the run, it is observed that the peak temperature in the case of 1.7 m^3/hr (60 SCFH) has reached the top of the bed, where as for the 1.27 m^3/hr (45 SCFH) case it lies around 139.7 mm (5.5") above the grate. Because of the higher burning rates, resulting in higher ash accumulation in the bed, and higher air flow rates, resulting in higher convective heat transfer rates in the bed, the temperature peak shift seems to be so fast for the 1.7 m^3/hr (60 SCFH) case. The rapid movement of the temperature peak signals a higher feed rate for the 1.7 m^3/hr (60 SCFH) case, that can be inferred from figure 4.111. The higher feed rate along with a higher air flow rate seems to some how make the air fuel ratios for both the case to be similar (refer figure 4.112). In the case of 1.7 m^3/hr (60 SCFH), the conditions in the bed are more like combustion conditions rather than gasification. This is because the ash at the bottom of the bed could not be removed from the bed, resulting in an apparent decrease in the effective bed height available for gasification. One more reason for such rapid peak shifts in the bed a can be attributed to the properties of LB. It was observed that during gasification, the chicken-litter biomass particles tended to stick together, though not fuse due to ash melting. This caused them to burn as a single large porous particle rather than as separate particles. The clumping tendency prevented the movement of burnt particles towards the bottom of the bed, thus resulting in the more rapid movement of the oxidation zone further into the bed. In other words, in this case the downward movement of the fuel is almost negligible, thus amplifying the peak shift for these fuels. Upon checking the temperatures at 12.7 mm (0.5"), and 50.8 mm (2.0") above the grate, it can be seen that the temperatures at both the locations are almost similar at about 450 K (350.33 ºF). This is an indication that irrespective of the air flow rates, the fuel at the bottom of the bed has entirely burned out, resulting in ash accumulation in the bottom of the bed.

For LB particle size range between 4 and 6.4 mm (0.157" and 0.25"), figure 4.110, shows the comparative temperature profiles under air flow rates of 1.27 and 1.7 m^3/hr (45 and 60 SCFH). For smaller particles, the temperature dynamics in the bed seems to reflect the ones exhibited by the larger particles. There is a distinct peak for both the cases, with the peak reaching the free board after 60 minutes into the run for the case of 1.7 m^3/hr (60 SCFH). This behavior was also shown by the larger particles under air flow rates of 1.7 m^3/hr (60 SCFH).

After 15 minutes into the run, the peaks for the 1.7 m^3/hr (60 SCFH) case is located much further into the bed as compared to the 1.27 m^3/hr (45 SCFH) case. The location of the peak suggests the affect of higher air flow rate on the burning rate of the particles. Thus, the higher burning rate as in the case of the 1.7 m^3/hr (60 SCFH) case results in a more rapid peak movement into the bed after 15 minutes into the run. The peak temperature in the case of 1.7 m^3/hr (60 SCFH) case is also higher as compared to the 1.27 m^3/hr (45 SCFH) case by about 100 K (180 ºF). The higher peak temperature is attributed to the higher air flow rate resulting in higher burn rates. The temperatures at 12.7 mm (0.5"), and 50.8 mm (2.0") above the grate for the 1.7 m^3/hr (60 SCFH) case are higher than the 1.27 m^3/hr (45 SCFH) case by about 75 K (135 ºF). This suggests that, due to higher burning rates associated with higher flow rates, the ash content in this location is much higher as compared to the 1.27 m^3/hr (45 SCFH) case, resulting in lower combustible matter available for heat generation in this location. The higher temperatures recorded for the 1.7 m^3/hr (60 SCFH) case in the 101.6 and 171.5 mm (4.0" to 6.75") region indicate a higher rate of drying and pyrolysis in the bed, ultimately leading to a higher fuel feed rate (refer figure 4.111) at least in the initial stages of gasification. In this case, the temperature peak shift is more affected by the ash content in the bed, rather than convective heat transfers associated with higher air flow rates.

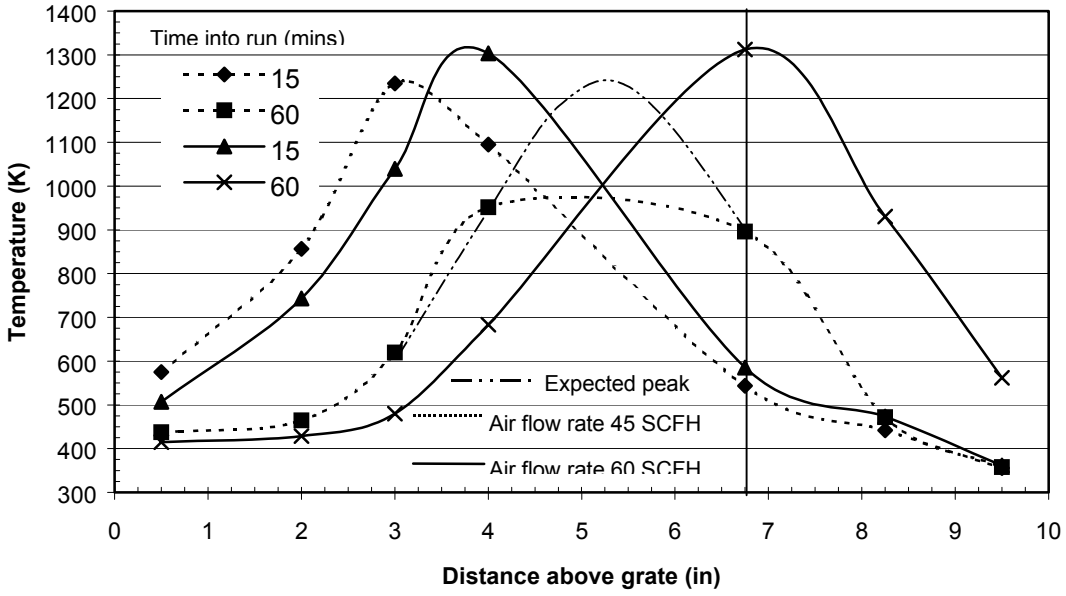

Figure 4.110: Comparative temperature profiles for LB (4-6.4 mm (0.157" – 0.25")) at air flow rates of 1.27 and 1.7 m_3/hr (45 and 60 SCFH)

After 60 minutes into the run, the temperature peak for the 1.7 m^3/hr (60 SCFH) case has moved to the top of the bed, whereas the peak for the 1.27 m^3/hr (45 SCFH) has moved to about 139.7 mm (5.5") above the grate. As in the previous case discussed for larger sized chicken-litter biomass particles, the smaller sized particles also tend to clump and fuse, without slagging in the bed. This causes the fuel in the bed to fuse to form one large porous particle, and prevents the downward movement of the burnt fuel particles. The result, rapid movement of the temperature peak towards the free surface. The rate of movement is positively affected by the higher air flow rates, resulting in higher burn rates and higher peak temperatures. The fusion also makes the air flow through the large porous particle more tortuous thus reducing the spatial spread of the temperature profile. Nevertheless, the temperatures for both the cases, recorded at 12.7 mm (0.5"), and 50.8 mm (2.0") above the grate are similar, showing same degree of reaction in the bed, irrespective of the air flow rates. The low temperatures reveal that the material in the base of the bed is almost ash. In the later stages of gasification, the rapid movement of the peak associated with fusion in the bed, tend to lower the fuel feed rate, and finally the overall feed rates for both the cases are relatively close (refer figure 4.111). A lower feed rate and higher air flow rate results in a higher air fuel ratio for the 1.7 m^3/hr (60 SCFH) case, and can be referred from figure 4.112. A continuous disposal of ash at the grate is required in order to achieve gasification conditions inside the gasifier.

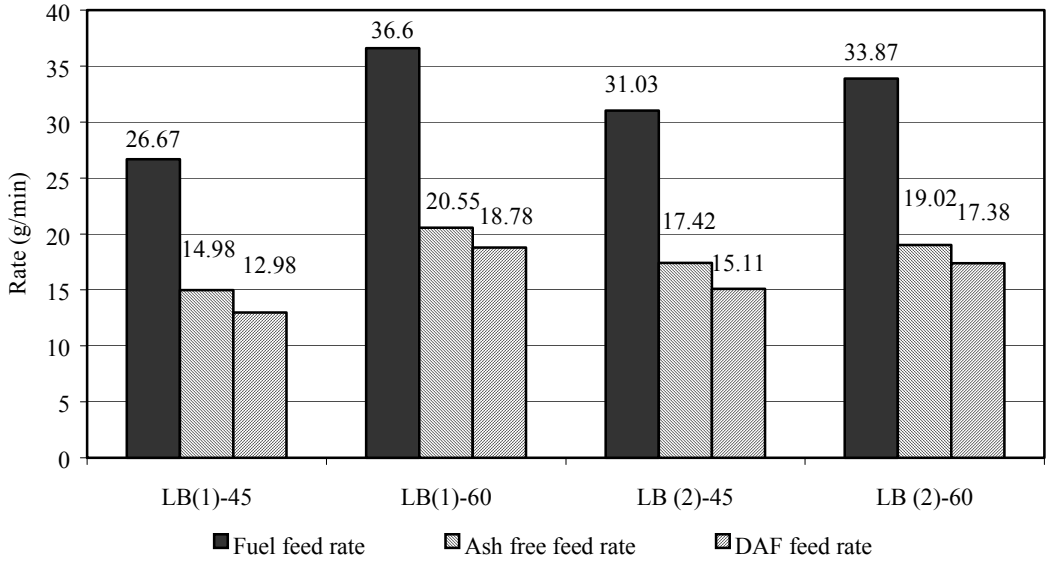

Figure 4.111: Comparative average chicken litter biomass (LB) feed rates for different experiments

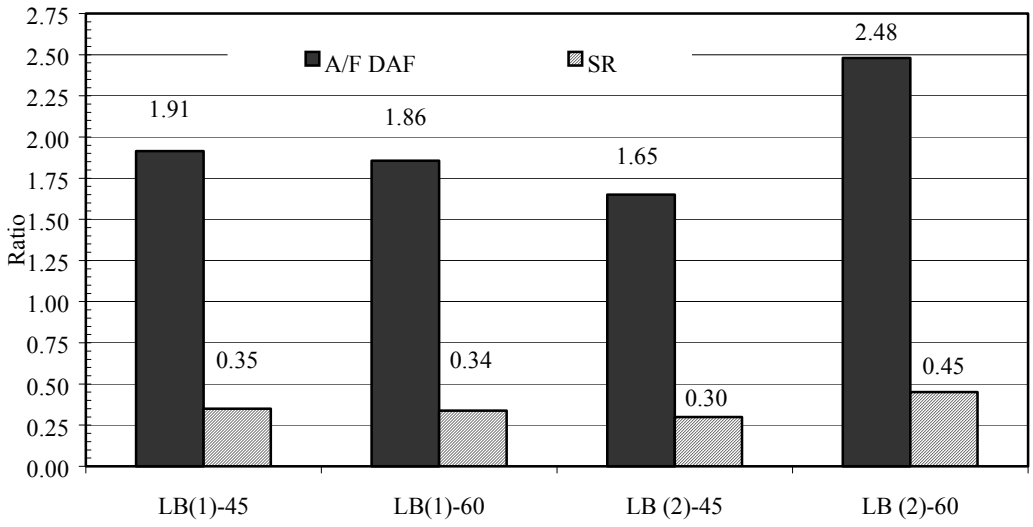

Figure 4.112: Comparative average A/F(DAF) and SR ratios for LB under different operating conditions (LB (1), 6.4-12.7 mm (0.25" –0.5"), LB (2),4-6.4 mm (0.157" – 0.25"))

To study the effect of particle size on the temperature profiles in the bed refer figures 4.113, and 4.114. From figure 4.113, it is seen that irrespective of the particle size, under same air flow rates, the temperature profiles are similar. Even the peak temperatures in the bed are similar for both the cases. This is due to the fuel agglomeration in the bed that results in such similar profiles. Therefore, the burn rate is controlled more by the air flow rate rather than the particle size. The same result can b inferred for the 1.7 m^3/hr (60 SCFH) case by referring to figure 4.114. In this case,

irrespective of the particle size the peak temperature in the bed reaches the top of the bed by 60 minutes into the experiment run. In this case, also the air flow rate seems to dictate the burning rate, rather than the particle size having any effect on the temperature profile or the peak temperature in the bed. However, the peak temperature for the 1.7 m^3/hr (60 SCFH) case is higher by about 100 K (180 ºF) as compared to the 1.27 m^3/hr (45 SCFH) case. This is because of the higher air flow rate resulting in higher heat generation in the bed, leading to higher peak temperatures. The similarity in temperature profiles is due to the fuel agglomeration in the bed, resulting in similar burning rates irrespective of the size.

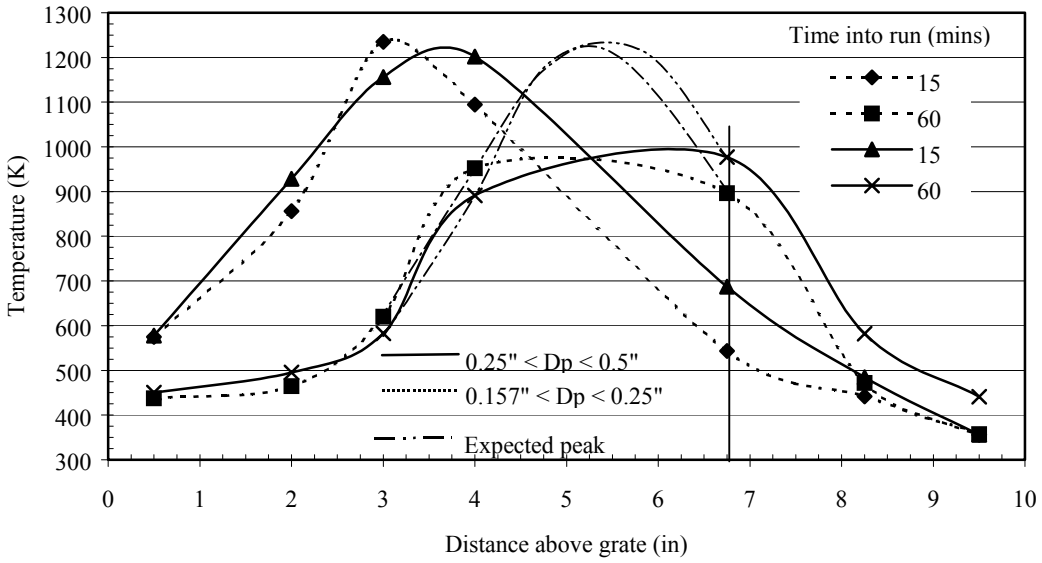

Figure 4.113: Particle size effect on the temperature profile in the bed under air flow rate of 1.27 m^3/hr (45 SCFH) (LB)

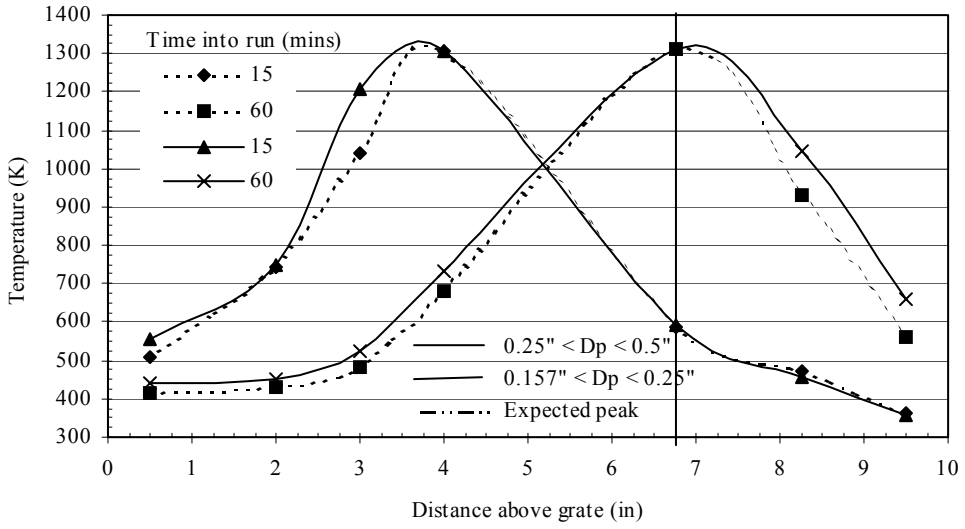

Figure 4.114: Particle size effect on the temperature profile in the bed under air flow rate of 1.7 m^3/hr (60 SCFH) (LB)

In conclusion the temperature dynamics exhibited by LB, seems to be greatly affected by the ash content of the fuel. This requires that in order to maintain the proper gasification conditions in the gasifier, there needs to be continuous ash removal from the grate. The ash fusion was exhibited for all the cases, and was more severe in the case of higher air flow rates. The particle size does not affect the ash fusion tendencies in the bed, but the air flow rates seem to aggravate the ash fusion in the bed. The particle size effect is subdued because the fuel agglomeration in the bed creates a large porous particle in the bed (irrespective of the particle size), and behaves as a whole unit instead of individual particles. The peak temperatures achieved for LB is lower than those achieved by AFB, and coal. This is directly related to the heating value of the fuel, since the LB has a heating value of only 3971 kJ/kg (1881 Btu/lb), as compared to 6442 kJ/kg (3052 Btu/lb) for fly ash surfaced AFB, and 9376 kJ/kg (4443 Btu/lb) for coal. The lower heating value results in heat generation due to fuel oxidation, resulting in lower peak temperatures in the bed.

4.3.2.5. Coal: Chicken litter biomass blend (CLB)

In the case of coal and AFB blends, the coal seemed to play an important role in determining the temperature characteristics in the bed. It not only reduced the rate of peak shift in the bed, but also inhibited the agglomeration in the bed. It shall be interesting to see, if it has such a beneficial effect on the temperature profiles for the coal and LB blends? The proximate and ultimate analysis of the coal and LB blend is given in table 4.37. From the table it is obvious that the ash content of the blend is reduced to about 24 % as compared to nearly 44 % in the of LB. The reduced ash content will positively affect the temperature dynamics in the bed. Although, there is not much change in the volatile matter content of the blend (as received basis), the fixed carbon content of the blend increases by almost three folds as compared to the LB. At the same time, the heating value of the blend increases by almost 60 % as compared to that of LB.

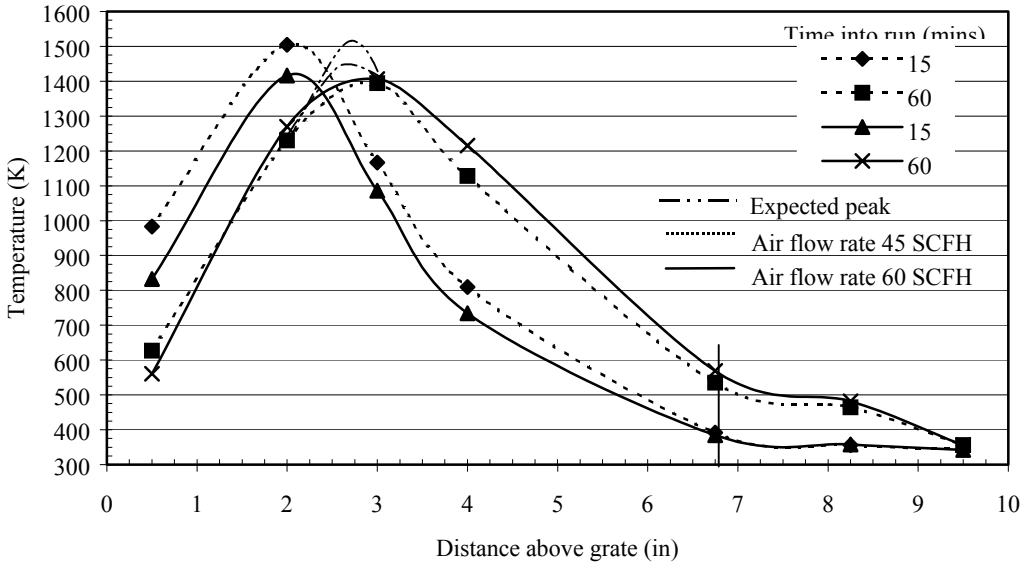

Figure 4.115: Comparative temperature profiles for CLB (CLB (1), 6.4-12.7 mm (0.25" – 0.5"), CLB (2), 4-6.4 mm (0.157" – 0.25")) at air flow rates of 1.27 and 1.7 m^3/hr (45 and 60 SCFH)

For coal and LB blends (CLB) particle size range between 6.4 and 12.7 mm (0.25" and 0.5"), figure 4.115 shows the comparative temperature profiles under air flow rates of 1.27 and 1.7 m^3/hr

(45 and 60 SCFH). The presence of peak is evident for both the cases. The shape of the temperature profile is almost similar to that exhibited by the coal and AFB blends under similar operating conditions. Thus at first glimpse, coal seems to have a prominent effect on the temperature profile in the bed.

After 15 minutes into the run, the location of peak temperatures for both the case is at about 50.8 mm (2.0") above the grate. Initially the air flow rate does not seem to affect the location of the peak temperature. However, the peak temperature for the 1.27 m^3/hr (45 SCFH) is higher than the 1.7 m3/hr (60 SCFH) case by about 100 K (180 ºF). This behavior is similar to that exhibited by large sized coal particles under similar operating conditions. In the case of coal particles, the peak temperature in the case of 1.27 m^3/hr (45 SCFH) was higher as compared to the 1.7 m^3/hr (60 SCFH) case. Thus, the peak temperature is affected by the presence of coal in the blend. The predominance of coal in dictating the peak temperature in the bed is due to the fact that the heating value of coal is about 2.5 times as that of LB. Thus for every kilogram of the blend burned, the contribution of coal towards the heating value is about 71 %, while the rest is contributed by LB. The lower peak temperature for a higher flow rate is due to two effects, one the faster burning rate of LB due higher air flow rates, and second due to the higher convective heat transfer rates in the bed associated with higher air flow rates. Comparing the temperatures in the bed at 12.7 mm (0.5") above the grate shows that the temperature in the 1.27 m^3/hr (45 SCFH) case is higher than the 1.7 m^3/hr (60 SCFH) case by about 160 K (288 ºF). This shows that the burnt fraction of the fuel at this location is higher in the 1.7 m^3/hr (60 SCFH) case. This results in higher ash concentration thus reducing the temperature at this location. A lower temperature at the base of the bed, associated with a higher convective transfer rate in the bed results in lower peak temperatures in the bed. Another factor to be taken into consideration is that the as the sensible heat energy available at the base of the gasifier is lower, the heat energy available for the successive higher levels is also lower. This can be explained by referring figure 4.116.

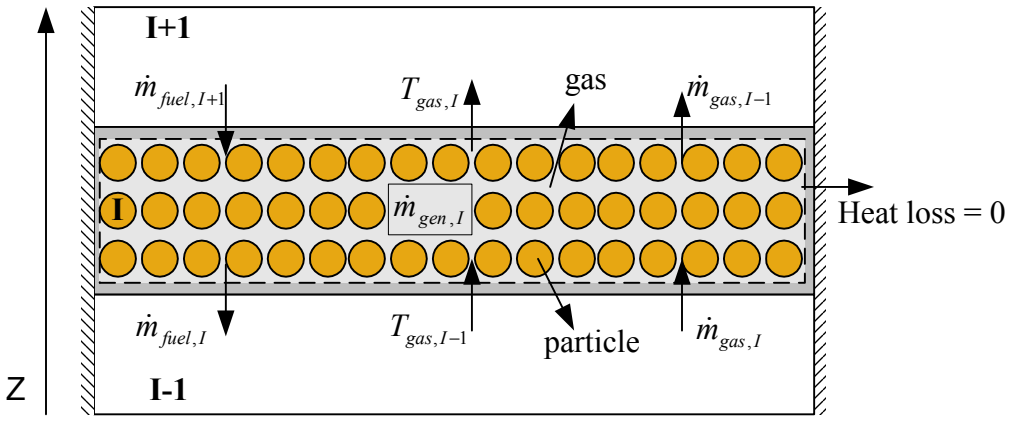

Figure 4.116: Control volume for understanding the energy exchange in the bed

In figure 4.116, the energy balance for the control volume gives some interesting insights into the behavior of the bed. (Consider, the bed to be divided in small control volumes, and the location of the control volume of interest is at the lower portion of the bed, i.e. around 12.7 mm (0.5") above the grate) In the following discussion three consecutive control volumes *I-1*, *I*, and *I+1* are taken into consideration, and the energy exchange across these control volumes shall be discussed. The assumptions in the following discussion are:

The gas phase average temperature and the solid phase average temperature are equal.

The specific heat of the solid phase is constant through out the bed.

The heat loss through the sidewalls is negligible.

The heat transfer due to conduction and radiation has been neglected.

Expressing the energy exchange in the control volume (*I*) in mathematical form gives the following results:

Energy of the gas and solid phase entering the control volume (*I*) is:

$$\dot{E}_{in} = \dot{m}_{f,I+1} c_{p,fuel} T_{f,I+1} + \dot{m}_{g,I} c_{p,g,I} T_{g,I} \qquad \textbf{(4.3.30)}$$

Energy of the gas and solid phase exiting the control volume (*I*) is:

$$\dot{E}_{out} = \dot{m}_{f,I} c_{p,fuel} T_{f,I} + \dot{m}_{g,I-1} c_{p,g,I-1} T_{g,I-1} \qquad \textbf{(4.3.31)}$$

Energy generation in the control volume (*I*) is:

$$\dot{E}_{gen} = \dot{m}_{het} HV_{het} + \dot{m}_{\hom} HV_{\hom} - \dot{m}_{pyro} HV_{pyro} - \dot{m}_{evap} h_{fg} \qquad \textbf{(4.3.32)}$$

Energy balance for the control volume (*I*) gives:

$$\dot{E}_{in} + \dot{E}_{gen} = \dot{E}_{out} + \dot{E}_{stored} \qquad \textbf{(4.3.33)}$$

In the lower portion of the bed (near the grate), $\dot{m}_{het} \approx 0$ (as burnt fraction is high), $\dot{m}_{\hom} \approx 0$, so $\dot{E}_{gen} \approx 0$.

Since the specific heat of ash is small compared to char, $\dot{E}_{stored} \approx 0$. Thus equation 4.3.33 simplifies to,

$$\dot{E}_{in} = \dot{E}_{out} \qquad \textbf{(4.3.34)}$$

Further since burnt fraction is high, then $\dot{m}_{f,I+1} \approx \dot{m}_{f,I}$, and $\dot{m}_{g,I} \approx \dot{m}_{g,I-1}$, thus

$$T_{g,I-1} \approx T_{g,I} \qquad \textbf{(4.3.35)}$$

The above result shows that in the lower portion of the bed when the ash content is high, resulting in low heterogeneous reactions, then the temperature rise between two successive control volumes is small. In the 1.7 m^3/hr (60 SCFH) case for the large sized coal and LB blends, the temperature at 12.7 mm (0.5") above the grate is low owing to the higher ash content in the bed, so as the incoming gas comes into the gasifier through the grate, the sensible heat addition to it is low due to the low heat capacity of the ash in the bed. When the sensible heat gained by the gas phase is low then at each successive control volumes the lower temperature of the incoming gas results in lower reaction rates in the bed, thus resulting in lower peak temperatures. The lower gas phase temperatures results in lower burning rates, hence lower peak temperatures.

The temperatures in the 76.2 to 171.5 mm (3.0" to 6.75") region is almost similar for both the cases, hinting at a similar air flow rate. This also proves that initially the higher air flow rate has not affected the initial drying and devolatilization rates in the bed.

After 60 minutes into the run, the peak shift for the 1.7 m^3/hr (60 SCFH) case is about 12.7 mm (0.5") greater than that of the 1.27 m^3/hr (45 SCFH) case. It is interesting to note that in the case of 45 SCFH, there is less spatial spread of the temperature curve, whereas for the 1.7 m^3/hr (60 SCFH) there is a higher spread. This spread causes the temperatures in the 101.6 to 171.5 mm (4.0" to 6.75") region to be higher, hence resulting in a drying and devolatilization rate. This causes an increase in the fuel feed rate. For the 1.7 m^3/hr (60 SCFH) case, the temperature spread causes more

portion of the bed to be at temperatures higher than the pyrolysis temperatures of both coal and LB. This further enhances the drying and devolatilization rate in the bed, and further boosts the fuel feed rate. The fuel feed rates can be observed in figure 4.118 and the air fuel ratio ca be observed in figure 4.119.

In spite of the higher peak achieved in the case of coal and chicken litter blends, there was no appreciable agglomeration in the bed. This may be due to the lower ash content of the blend, and the lower inter-particle contact between the chicken-litter biomass particles. This proves that the agglomeration in case of the LB is more influenced by the inter-particle contact between particles, rather than by the temperature in the bed. At this point it should be mentioned, that there was small clinker formation in the bed (though on a very small scale), which was caused due to contact between chicken-litter biomass particles at elevated temperatures. Nevertheless, the clinker formation also proves that at high temperatures in the bed of about 1500 K (2240.33 ºF) the ash melting takes place, resulting in the formation of clinkers. The clinkers are different from the agglomeration in the bed and shall be discussed at the end of this section.

For coal and LB blends (CLB) particle size range between 4 and 6.4 mm (0.157" and 0.25"), figure 4.117 shows the comparative temperature profiles for the different air flow rates. As expected, both the cases exhibit a distinct peak in the bed.

After 15 minutes into the run, the temperature peak for the 1.27 m^3/hr (45 SCFH) case is located at 38.1 mm (1.5") above the grate, while it located at about 50.8 mm (2.0") above the grate for the 1.7 m^3/hr (60 SCFH) case. Surprisingly the peak temperature for both the cases are almost equal to about 1475 K (2195.33 ºF). The temperature at 12.7 mm (0.5") above the grate for the 1.27 m^3/hr (45 SCFH) case is higher than the 1.7 m^3/hr (60 SCFH) case by about almost 300 K (540 ºF). Such a huge difference can only be explained due to the higher burning rate associated with the higher flow rate. The vast temperature difference shows a huge disparity in the burning rates for both the cases. As discussed in the earlier case for larger particles, a lower temperature at the bottom translates into a lower peak temperature. However, in this case this is not the reason for such a peak, the higher convective transfer rates in the bed are a more likely cause. This can be ascertained by checking the spatial temperature distribution in the bed. In the case of 1.7 m^3/hr (60 SCFH), it is clearly seen that the temperatures at 76.2 and 101.6 mm (3.0" and 4.0") above the grate are way higher than those for the 1.27 m^3/hr (45 SCFH) case. This proves that the higher convective rates in the bed cause the lower of peak due to higher rates of heat loss in the bed. The higher convective transfer rates cause unequal burning of the blends. The chicken-litter biomass in the blend burns at a lower temperature due to its lower ignition temperature. This increases the void fraction in the bed, and further boosts the convective heat transfer rates, and causes more spatial distribution of the temperature in the bed. The higher temperatures in the 76.2 mm (3.0") to the 171.5 mm (6.75") region of the bed in case of the 1.7 m^3/hr (60 SCFH) result in higher drying and devolatilization rates, ultimately translating into a higher feed rate for the 1.7 m^3/hr (60 SCFH) case.

After 60 minutes into the run, it can be seen that the peak temperature for the 1.27 m^3/hr (45 SCFH) case lies at about 63.5 mm (2.5") above the grate, whereas for the 1.7 m^3/hr (60 SCFH) case it lies at about 95.25 mm (3.75") above the grate. The rate of peak shift is higher for the 1.7 m^3/hr (60 SCFH) case due to higher convective heat transfer rates resulting in faster burning in the bed. The temperature at the 101.6 to 171.5 mm (4.0" to 6.75") is consistently higher for the 1.7 m^3/hr (60 SCFH) case. This proves that the higher air flow rate influences the temperature profile in the bed for smaller sized particles.

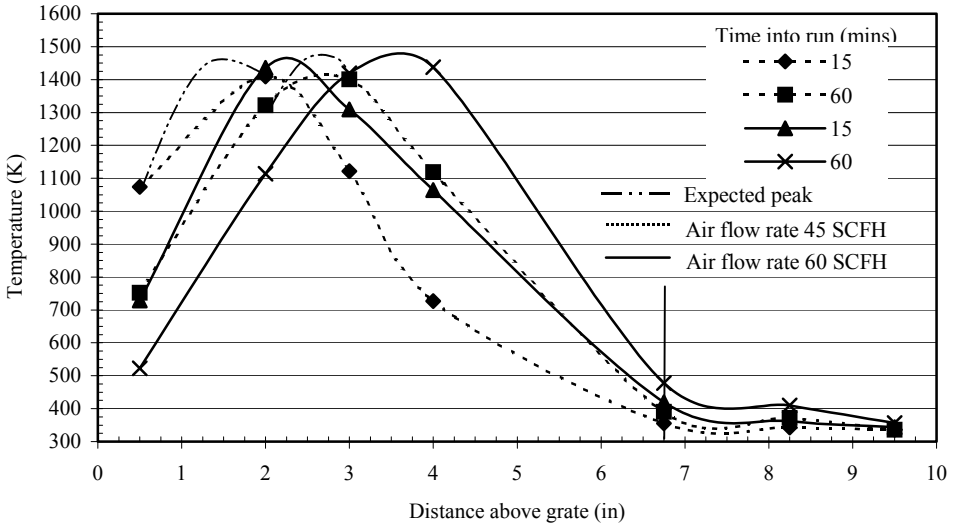

Figure 4.117: Comparative Temperature profiles for CLB (4-6.4 mm (0.157" – 0.25")) under air flow rates of 1.27 and 1.7 m^3/hr (45 and 60 SCFH)

In the 1.7 m^3/hr (60 SCFH) air flow rate case there was ash fusion in the bed. Although not as severe as observed in the LB case, but it was more pronounced than that observed for the larger blend particles under an air flow rate 1.7 m^3/hr (60 SCFH). This again goes on to prove that the particle size does play an important role in the ash fusion in the bed. In this case, the clinkers formed were larger in dimension, but not large enough to affect the temperature distribution in the bed. The ash fusion was localized and mostly present at about 101.6 mm (4.0") above the grate. Since in the initial stages of the experiment, tar condensation was invariably observed at about this location, this gives a hint that the condensed tar coupled with the clumping tendency of LB is the starting point of the agglomeration. In the case of blends, due to higher temperatures, the ash fusion takes place resulting in clinker formation.

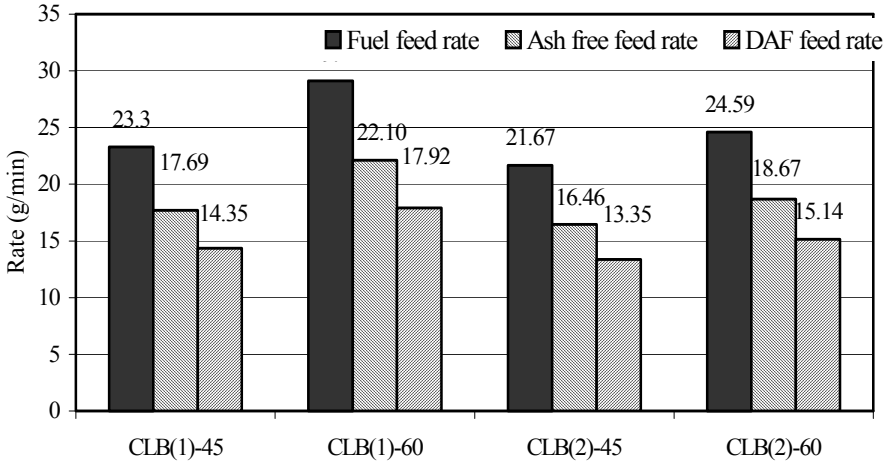

Figure 4.118: Comparative average coal and LB blend (CLB) feed rates for different experiments

In conclusion, it is seen that the peak temperature in the case of coal and LB blends is more affected by the coal in the blend, due to the higher heating value of coal. The reduction in the overall ash content of the blend reduces the agglomeration in the bed. However, it is observed that smaller sized particle show a higher tendency to agglomerate. Nevertheless, in the case of only LB, the particle size had no effect on the ash fusion in the bed. Thus, from the above discussion it can be concluded that if the ash content is high, then particle size does not affect the agglomeration in the bed, whereas in case of lower ash content, the smaller particles tend to exhibit higher tendencies for agglomeration. The higher temperature in the bed caused ash fusion at some locations resulting in clicker formation in the bed. The rate of peak transfer in the bed is reduced due to the lower ash content in the blend. The slower rate of peak transfer shall enable a lower frequency of ash disposal at the grate in order to maintain proper gasification conditions in the bed. In case of larger particles, the air flow rate does not affect the peak transfer rate, but a higher air flow rate results in lower peak temperatures in the bed. For smaller particles, the air flow rate shows no effect on the peak temperature in the bed, but increases the rate of peak shift in the bed in case of higher air flow rates.

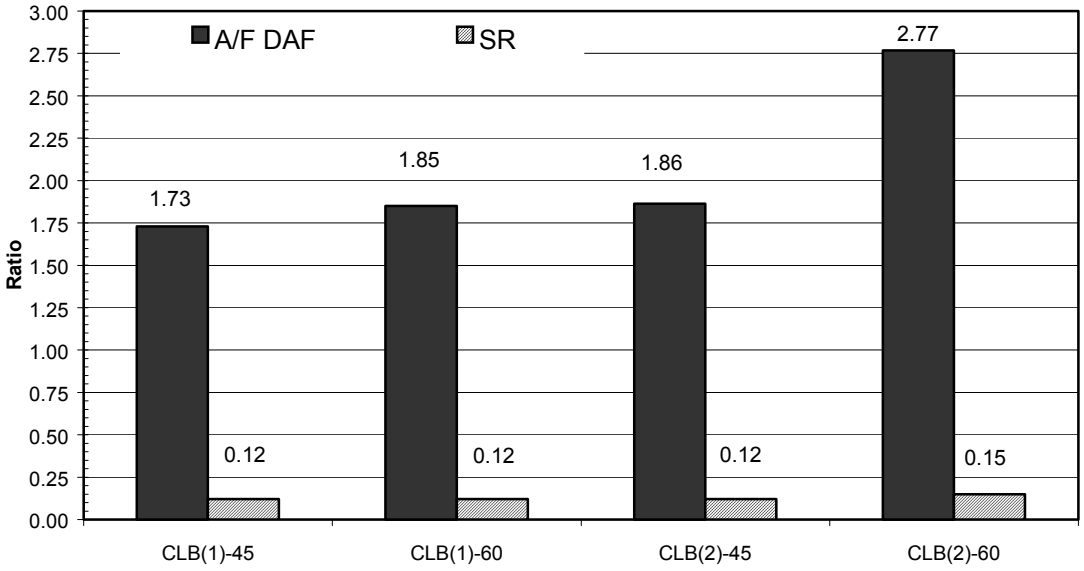

Figure 4.119: Comparative average A/F (DAF) and SR ratios for coal and LB blends under different operating conditions

4.3.3. Gas species profile

The temperature dynamics helped understand the various regions in the gasifier for different types of fuels. The ultimate output of a gasifier is the production of combustible species. Then knowledge of the gas species concentrations at different locations in the bed is necessary. Since the case in discussion involves transient studies, it is essential to have snap short images (data) about the conditions in the bed. Ideally, the transient study requires the simultaneous measurement of gas

species at various locations in the bed. This data collection has to be done over an extended period in order to understand the process dynamics.

In order to collect the gas species data simultaneously an online system is required, which could be used to draw samples almost simultaneously from different locations in the bed and analyze them. This requires a dedicated online gas chromatograph system in order to detect the gas species of interest. Unfortunately, in this case, no online gas analysis system was available. Therefore, samples had to be manually stored and analyzed later. In addition there was also a limit to the number samples that could be analyzed, so in the end only 5 gas samples were collected for each experiment. The five gas samples were collected from the 5 different ports provided for such a purpose. Collection of gas samples started from location 1, after about 5 minutes into the run (this is the time after the required bed height was reached), and the remaining were collected in intervals of 5 minutes, i.e. sample from port 2 was collected after approximately 10 minutes into the run and similarly sample from port 5 was collected after approximately 30 minutes into the run. This limited data on the gas species makes it all the more difficult to analyze the data to get information about the process dynamics. This is because the conditions in the bed change from port to port and in some cases, the changes are so rapid, that reliable conclusion could not be made from the gas species data. Thus, the limited data is not able to capture the species dynamics along with the temperature dynamics of the process. Keeping this limitation in mind, the gas species profiles for all the cases shall be discussed. For details about the gas sampling and conditioning, and the gas chromatography, refer DOE, Quarterly Progress Report #7, and #8 (12/15/01-6/14/2002).

During gasification, pyrolysis is the most important process in terms of gas generation as majority of the gases are produced during this process. While the gas production is mainly due to pyrolysis, the major volumes of CO_2, and CO are produced due to heterogeneous reactions in the oxidation and gasification zones of the gasifier. This implies that CO and CO_2 are predominantly produced in the lower region of the bed, whereas the other gases are produced in the upper region of the bed. As discussed earlier in this chapter, the production of CH_4 is mainly due to pyrolysis, and CH_4 is never completely converted in the reduction zone, the extent of pyrolysis of the fuel can be predicted by means of the concentration of CH_4 in the gasifier.

a) The conditions in the bed affect the ultimate yield from pyrolysis. The main product distribution from pyrolysis is the formation of tar, char, and gas species. The distribution ratio depends on various conditions in the bed. Further more, the tar formed under goes secondary reactions in the gas phase or with the particle surface to yield gases, char, and tar. The conditions in the gasifier bed affect not only the yield of gases during the devolatilization, but also the composition of the product gas released during devolatilization.

During pyrolysis, generally H_2O, CO_2, and tar evolve at lower temperatures and hydrocarbons (HC), CO, and H_2 evolve at higher temperatures. During pyrolysis there are two types of reactions taking place, 1) the primary reactions are generally responsible for the release of volatile matter including the gases and tar, 2) the secondary reactions are responsible for the reaction of tar. According to Saxena *et al*. (1990) the tar molecules are very reactive, unstable, and heavy. The tar formed during the primary reactions can either crack due to high temperatures in the bed, or react with the solid particle and form char.

The particle size is one of the most influential parameters affecting the product gas yield and composition, the char yield, and the temperature time history of the particles. Though the devolatilization process is complex, it is sufficient to mention that at least a basic treatment of the gas species collected for all the different fuels shall give some incite into the gasification characteristics of the fuels.

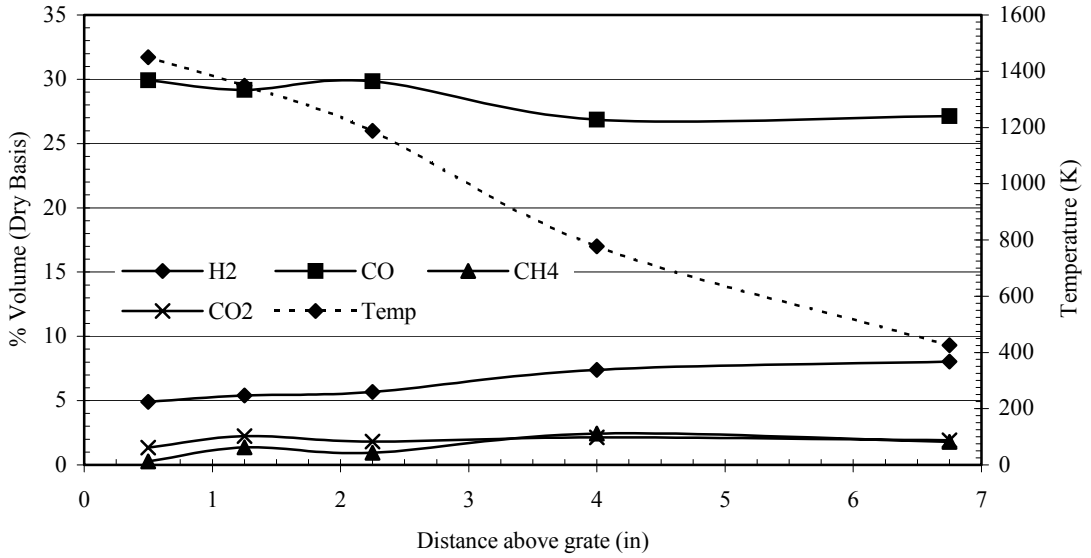

Figure 4.120: Gas species profiles for Coal (6.4-12.7 mm (0.25" – 0.5")) under an air flow rate of 1.27 m^3/hr (45 SCFH)

4.3.3.1. Coal

In the following discussion, the gas species profiles for coal shall be discussed. In all the graphs showing the gas species profile in the bed, the temperature at the location of gas collection is also shown. This shall help in better interpretation of the results. Figure 4.120 and 4.121 show the gas species profiles for large sized coal particles gasified under air flow rates of 1.27 m^3/hr (45 SCFH) and 1.7 m^3/hr (60 SCFH) respectively.

From figure 4.120, it observed that the CO is the maximum at 12.7 mm (0.5") above the grate (indicating char oxidation), and stay at that range until about 57.15 mm (2.25") and then decreases towards the upper portion of the bed. For H_2 the opposite is true, it seems to be a minimum at the base and slowly increases towards the upper region of the bed where pyrolysis is dominant. There is not much spatial variation for CO_2, but for CH_4 there is a light increase in the concentration along the bed. At the bottom of the bed, the lower temperature of about 1450 K (2150.33 ºF) signifies that gasification reactions are taking place, producing CO, and at the same time consuming the CO_2 form the bed. This is logical as the gasification is endothermic in nature, thus decreasing the temperature in the bed. The presence of H_2 and CH_4 at this location is due to pyrolysis of the coal particles. It suggests that for the larger particles, devolatilization is not completed within the time interval during which the samples were collected. Until about 57.15 mm (2.25") above the grate, this condition of gasification and pyrolysis seems to be taking place simultaneously, leading to increase in the CH_4 and H_2 species. Until, 57.15 mm (2.25") above the grate the temperature is relatively high as compared to the upper region of the bed, suggesting that gasification reactions are in effect. However, beyond 57.15 mm (2.25") further into the bed the temperature in the bed has dropped significantly and the CO concentration fall to about 27 %, and the H_2 content increase to about 9 % by volume. This shows that in this region, the gasification reactions have stopped and the major contribution to the gas phase is due to pyrolysis of the fresh fuel. The decrease in CO concentration may be due to the dilution caused by the formation of H_2 and CH_4. So, for the coal the oxidation and gasification zone

seems to be until 57.15 mm (2.25") above the grate, whereas the region above that seems to be the drying and devolatilization region.

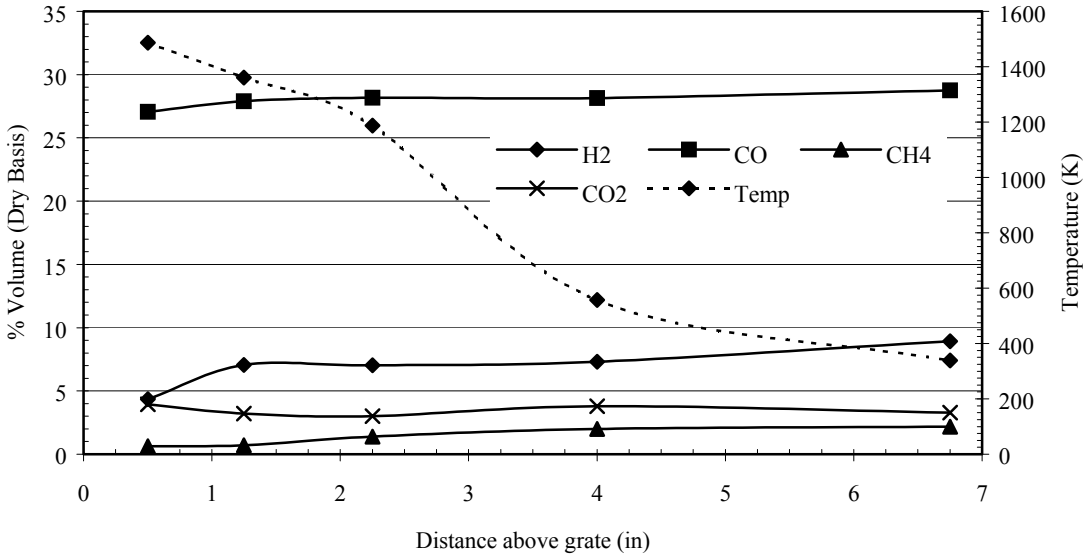

Figure 4.121: Gas species profiles for $Coal_1$ under an air flow rate of 1.7 m^3/hr (60 SCFH)

From figure 4.121, it can be observed that the temperature at 12.7 mm (0.5") above the grate is about 1490 K (2222.33 ºF), which is about 40 K (72 ºF) higher than that seen for the 1.27 m^3/hr (45 SCFH) case. This higher temperature is due to higher air flow rates, causing higher burn rates and resulting in higher production of CO_2 in that location. This can be observed by comparing figures 4.120 and 4.121, the concentration of CO is lower, and the concentration of CO_2 is higher for the 1.7 m^3/hr (60 SCFH) case. This higher temperature shows that reaction II to be more dominant than the reaction I or reaction III, as it is more exothermic compared to them. However, the concentrations of H_2 and CH_4 are similar for both the cases. Suggesting that the particles are at the same pyrolysis stage, and even for the higher air flow rate, the pyrolysis rate is not significantly different from the 1.27 m^3/hr (45 SCFH) case. Thus, the higher temperature in the bed is due to higher production of CO_2 in the char zone. Further, into the bed, it is observed that the species profiles are relatively flat, with the concentration of H_2 and CH_4 increasing soon after the 31.75 mm (1.25") location. This shows that the drying and pyrolysis is significant even at 31.75 mm (1.25") above the grate. Although one may be inclined to argue that, the H_2 gas concentration could increase due to reaction IV. Looking at the profile for CH_4 leads to the conclusion that the increase in H_2 is mainly due to pyrolysis, as under low pressures CH_4 in the bed is only due to devolatilization and not due to reaction V. However, after 57.15 mm (2.25") above the grate the temperature in the bed fall rapidly, showing an increase in the production of CH_4, and H_2. Therefore, the region above 57.15 mm (2.25") above the grate seems to be the drying and devolatilization region in the bed. The lesser spatial variation in the upper region of the bed could be due to the higher convective transfer rates in the bed, causing enhanced mixing, and thus diluting the fluctuation in the gas phase composition.

In order to conclude that the H_2 and CH_4 formation in the bed is mainly due to pyrolysis, another experiment was conducted for the larger coal particles under an air flow of 1.27 m^3/hr (45 SCFH). The experiment was conducted over a period of 7 hours, and the results of this experiment are shown in figure 4.122. The data in figure 4.122 shows the gas species profiles at 31.75 mm

(1.25") above the grate collected over a period of 7 hours. From figure 4.122, it can be seen that as time progresses the concentration of H_2 and CH_4 decreases from highs of 7 % and 1 % respectively, while that of CO increases. It can be observed that as the temperature starts decreasing, the CO concentration starts increasing, this can only be due the gasification reaction setting in i.e. reaction III becomes the dominant reaction and hence reduces the temperature in the bed. After 2 hours into the run the concentration of CH_4 becomes nil, this is because the higher production of CO implies the carbon atom in coal is utilized for the formation of CO (reactions I, and III), and the hydrogen atom is utilized for the formation of H_2 gas. The formation of hydrocarbon requires higher energies and hence higher temperatures in the bed, so as the temperature in the bed drops the concentration of CH_4 goes to zero while there is still production of H_2 in the bed. Since the feed air was relatively dry, the only source of hydrogen in the bed is from the fuel, so the H_2 gas is produced only through the pyrolysis process in the bed. Thus, it can be concluded that the presence of H_2 and CH_4 indicates incomplete devolatilization in the bed.

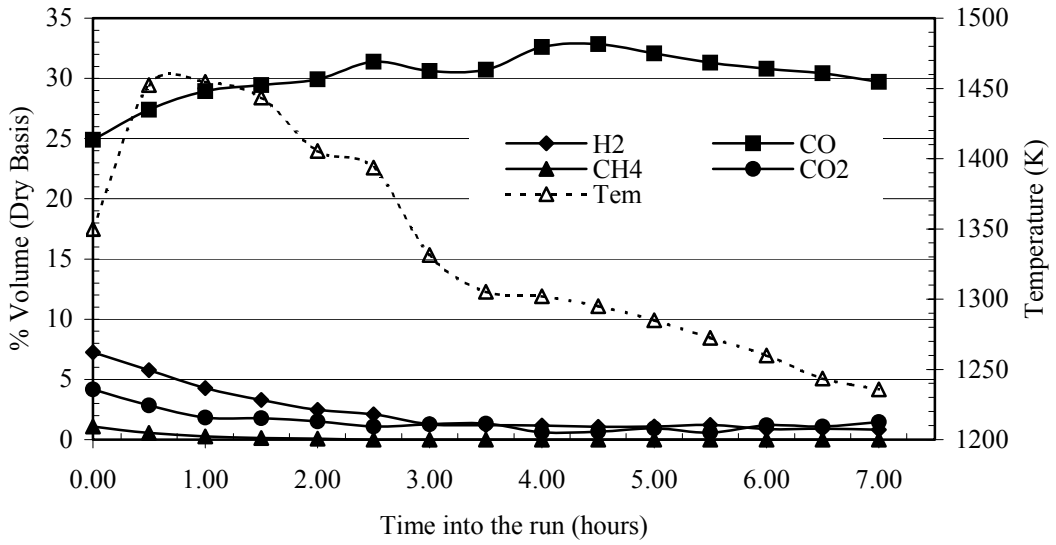

Figure 4.122: Gas species profile for Coal (6.4-12.7 mm (0.25" – 0.5")) at 31.75 mm (1.25") above the grate for an air flow rate of 1.27 m^3/hr (45 SCFH) (experiment run for 7.00 hours)

For smaller particles, figures 4.123 and 4.124 show the gas species profiles for the 1.27 m^3/hr (45 SCFH), and 1.7 m^3/hr (60 SCFH) cases respectively.

For smaller particles with an air flow rate of 1.27 m^3/hr (45 SCFH), the figure 4.123 shows that the gas species profiles are relatively flat. The temperature at 12.7 mm (0.5") above the grate is about 1550 K (2330.33 ºF), which shows that the reaction 4.3.II is the dominant reaction in this region. Since the water shift reaction is expected to be in equilibrium under such high temperatures, the presence of higher concentration of H_2 seems to lower the concentration of CO_2 in the gas phase. The over all effect of higher H_2 and lower CO_2 concentrations is to decrease the concentration of CO in the bed. At 31.75 mm (1.25") above the grate, there is a sudden increase in the concentrations of H_2, and CH_4 indicating the presence of devolatilization taking place. Further, into the bed the concentrations of H_2 and CH_4 increase monotonically, while the concentration of CO does not fluctuate much. The region above 31.75 mm (1.25") in the bed can be treated as the drying and devolatilization region.

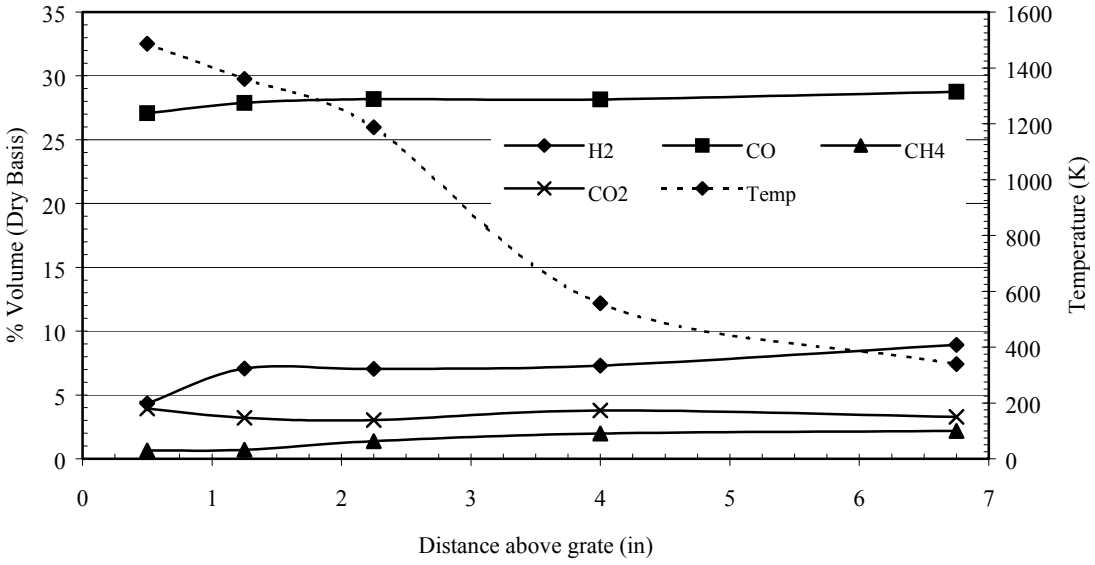

Figure 4.123: Gas species profiles for Coal (4-6.4 mm (0.157" – 0.25")) under an air flow rate of 1.27 m^3/hr (45 SCFH)

Comparing figures 4.123, and 4.124 it can be observed that there is no appreciable difference between the two graphs. In effect, this shows that the air flow variation is not large enough to cause appreciable difference in the gas species profiles. In this case due to higher air flow rates, the production of CO_2 form reaction 4.3.II, is slightly higher causing higher CO_2 concentration, when compared with the 1.27 m^3/hr (45 SCFH) case. This higher CO_2 results in a slightly lower concentration of CO. However, the concentrations of H_2, and CH_4 are similar to the 1.27 m^3/hr (45 SCFH) case, showing that the devolatilization rates are not affected much due to the variation in air flow rates. In this case, also, the concentrations of H_2 and CH_4 rapidly increase beyond the 57.15 mm (2.25") mark, thus showing the beginning of the drying and devolatilization region in the bed, or rather the end of the oxidation and gasification region in the bed.

Figures 4.125 shows the heating value of the gas at the top of the bed and is based on the gas sampling results obtained at the top of the bed. It can be seen that as the air flow rate increases, the heating value of the product gas leaving the gasifier increases. Thus, the higher flow rate seems to provide more heat in the bed causing a large number of particles to participate in pyrolysis and hence in the production of combustible gases.

Figure 4.126, shows the percentage contribution of the various gases towards the higher heating values of the product gas. It can be seen that the percentage contribution is similar for all the cases.

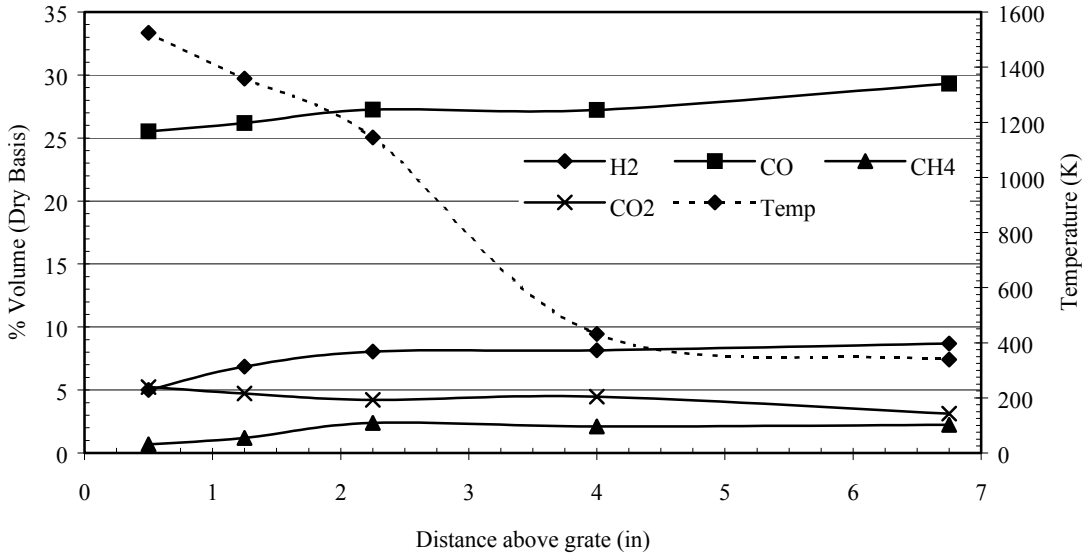

Figure 4.124: Gas species profiles for $Coal_2$ under an air flow rate of 1.7 m^3/hr (60 SCFH)

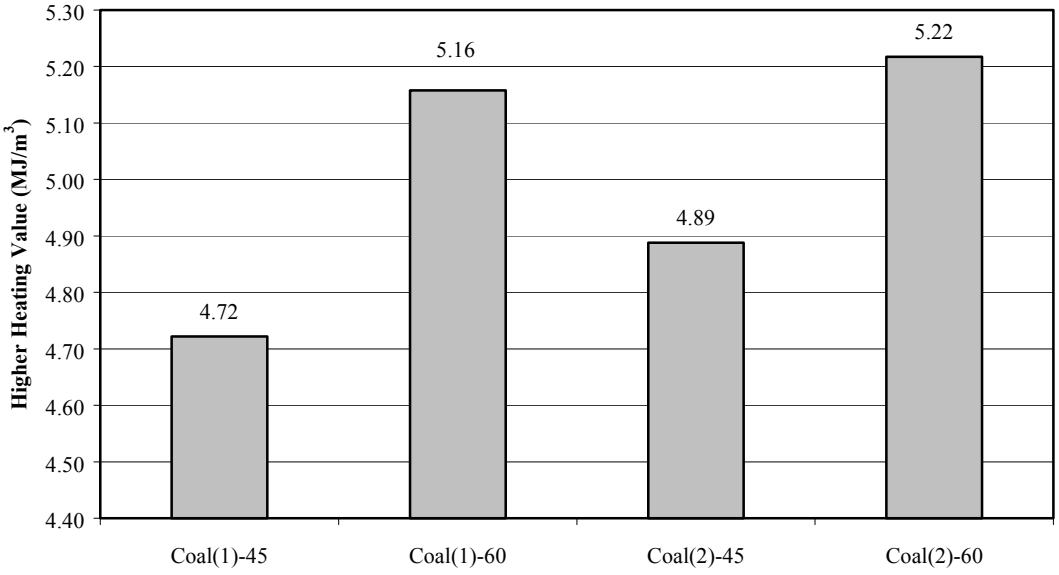

Figure 4.125: Comparative higher Heating Values of the product gas leaving the gasifier, for coal gasification under different operating conditions (Coal (1), 4.5-6.4 mm (0.175" – 0.25"), Coal (2), 6.4-12.7 mm (0.25" – 0.5"))

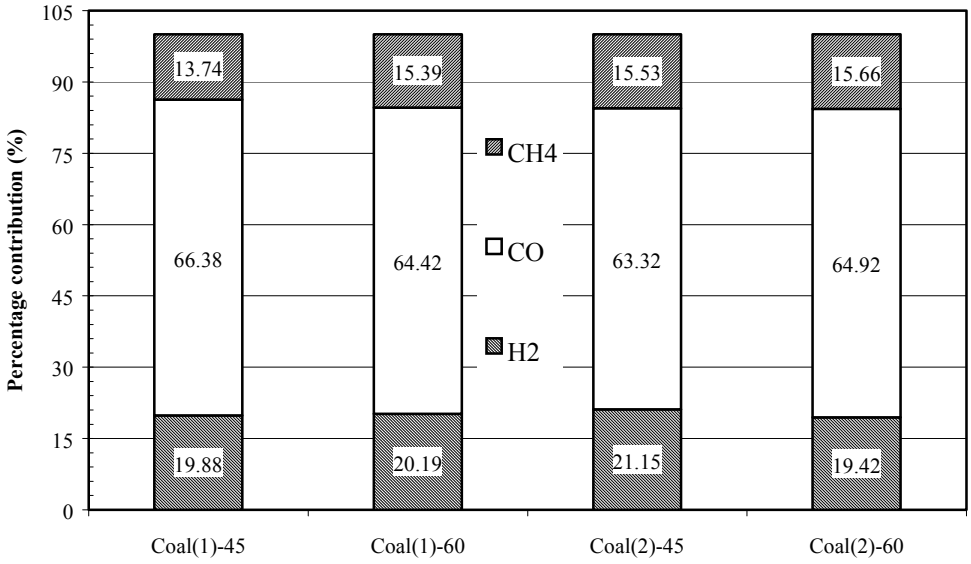

Figure 4.126: Contribution of various product gases towards the product gas leaving the gasifier, for coal gasification under different operating conditions (Coal (1), 4.5-6.4 mm (0.175" – 0.25"), Coal (2), 6.4-12.7 mm (0.25" – 0.5"))

4.3.3.2. Advanced FB (AFB)

Figure 4.127 shows the gas species profiles for large particle AFB with an air flow rate of 1.27 m^3/hr (45 SCFH). Comparing the temperature profiles at the sampling locations for AFB and coal in figures 4.127, and 4.120 it is clearly observed that the temperatures at the sampling locations are very different for both the cases. This is because the temperature front for AFB travels faster as compared to coal. Such rapid dynamic changes in the bed, limit the interpretation of the gas species data to accurately predict the conditions in the bed. Keeping this fact in mind the gas species profiles for AFB shall be discussed.

In figure 4.127, it can be seen that at 12.7 mm (0.5") above the grate the concentration of CO is a maximum. This indicates that gasification reactions are occurring and due to the endothermic nature of the reactions, the temperature has dropped. The temperature drop could also be due to the higher accumulation of ash, due to higher ash content of the fuel. But the high porosity of the AFB results in more effective mass transport within the particle and hence allows more surface are for reaction, so the reactions 4.3.I, and 4.3.III can lead to higher production of CO in the bed. At the same time, the presence of H_2, and CH_4 indicates that the particles at this location are still undergoing pyrolysis. Moving further into the bed the temperature increases, indicating the rapid movement of the temperature front in the bed. It can be seen that the temperatures at 31.75 mm (1.25"), 57.15 mm (2.25"), and 50.8 mm (4.0") are almost equal to 1200 K (1700.33 ºF), which is nearly the combustion condition in the bed. Therefore, at these locations simultaneous oxidation and gasification reactions are taking place leading to the formation of both CO and CO_2 through reactions 4.3.I, 4.3.II, and 4.3.III. At the same time since the particles have not yet been completely devolatilized, the higher temperatures in the bed enhances the higher production of H_2, and CH_4 in the bed. However, beyond the 50.8 mm (4.0") mark, the temperature falls, and the fuels particles are relatively fresh (virgin) and have higher volatile content. This combined with the high temperature (about 700 K (800.33 ºF)) in

the upper region of the bed causes a higher release of CH_4, and H_2 in the bed. Moreover, since the pyrolysis temperature of AFB is about 550 K (530.33 ºF), the pyrolysis in the upper part of the bed begins at a relatively higher height in the bed as compared to that of coal. These factors result in a high calorific gas being produced at the top of the bed and can be referred from figure 4.131. Figure 4.132 shows the contribution by the product gases towards the calorific value of gas leaving the gasifier.

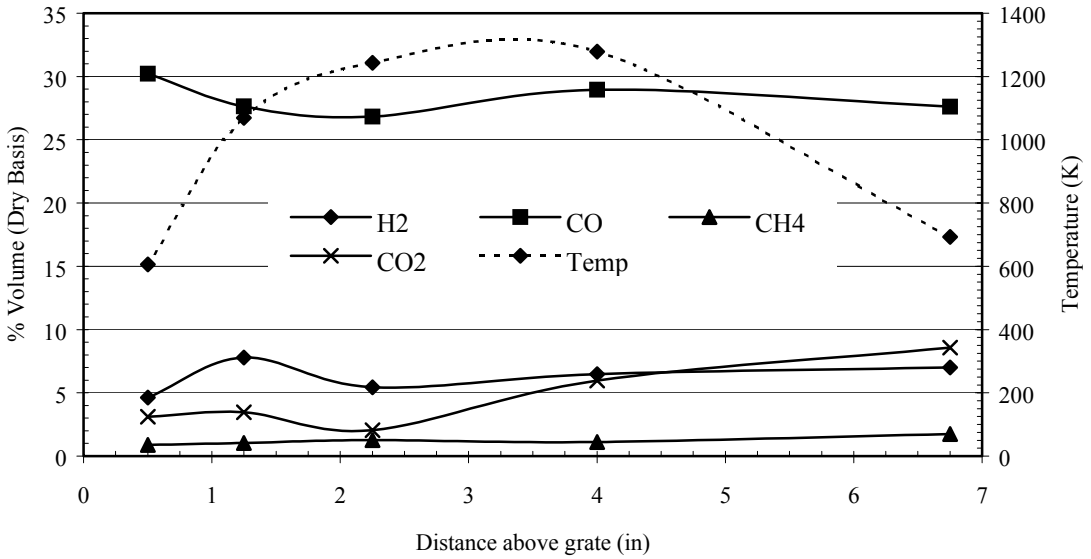

Figure 4.127: Gas species profiles for AFB (6.4-12.7 mm (0.25" – 0.5")) under an air flow rate of 1.27 m^3/hr (45 SCFH)

Figure 4.128, shows the gas profiles for large AFB particles with an air flow of 1.7 m^3/hr (60 SCFH). In this case, until 50.8 mm (4.0") above the grate, the temperatures in the bed indicates that there is oxidation and gasification going on in the bed. The concentrations of H_2, and CH_4 are increasing along the bed height. However, beyond 101.6 mm (4"), the temperature in the bed drops sharply indicating the drying and devolatilization region in the bed. The higher temperatures in the bed, along with relatively fresh fuel increase the product yield of H_2, and CH_4 in the bed. Thus, the calorific value of the product gas leaving the gasifier is increased. To conclude, the rapid rate of temperature shift in the bed is due to the oxidation and gasification front moving faster into the bed. This causes the length of the oxidation and gasification zones to increase, and the drying and devolatilization regions to decrease. Thus the data collected at 12.7 mm (0.5"), 31.75 mm (1.25"), 57.15 mm (2.25"), and 101.6 mm (4") above the bed correspond to the gasification zone, and the data at the top of the bed corresponds to the drying and devolatilization zone.

Figures 4.129, and 4.130 show the gas species profiles for smaller sized particles under air flow rates of 1.27 and 1.7 m^3/hr (45 and 60 SCFH). In figures 4.129, and 4.130 the CO profile exhibits a minima at 31.75 mm (1.25") above the grate, but beyond that, it stabilizes to about 27%. For the 1.7 m^3/hr (60 SCFH) case, the CO concentration at 12.7 mm (0.5") is lower due dilution caused by N_2 present in the incoming air. For both the cases the H_2 and CH_4 concentration rise continuously, indicating the presence of pyrolysis through out the bed. The higher pyrolysis yield, due to higher bulk density of the fuel in the bed, seems to out weigh the dilution caused by N_2 due to higher flow rates. For both the cases, beyond 57.15 mm (2.25") above the grate, there is a rapid

increase in the production of H_2, and CH_4, marking the drying and devolatilization zone in the bed. It should be noted that, though there seems to devolatilization taking place over the entire bed, but near the base of the bed, the oxidation and gasification reaction contribute the maximum to the product gas species. Therefore, the reactions 4.3.I to 4.3.III are predominating in the lower portion of the bed, until about 57.15 mm (2.25") into the bed.

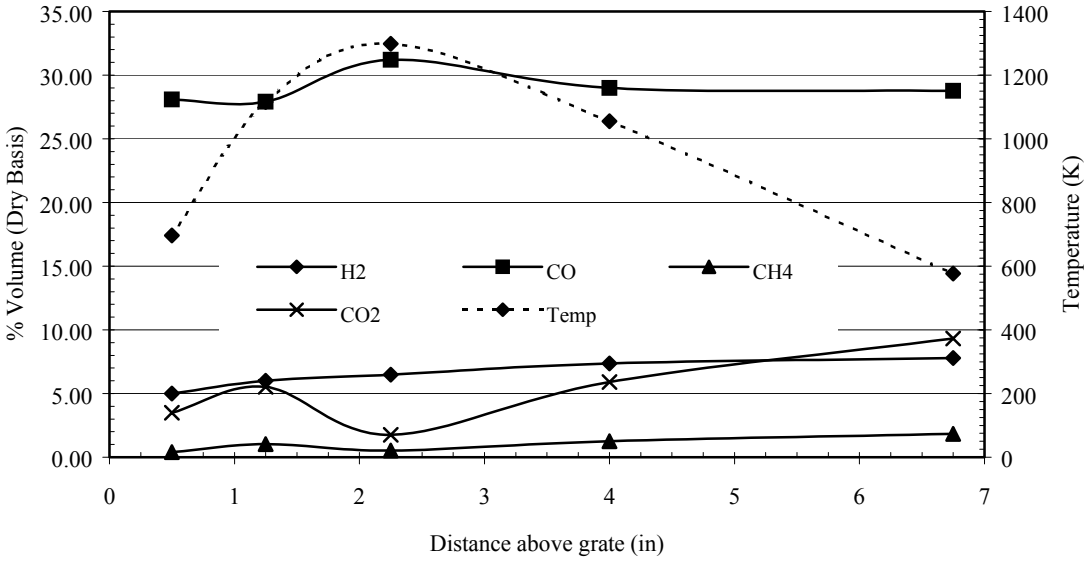

Figure 4.128: Gas species profiles for AFB (6.4-12.7 mm (0.25" – 0.5")) under an air flow rate of 1.7 m^3/hr (60 SCFH)

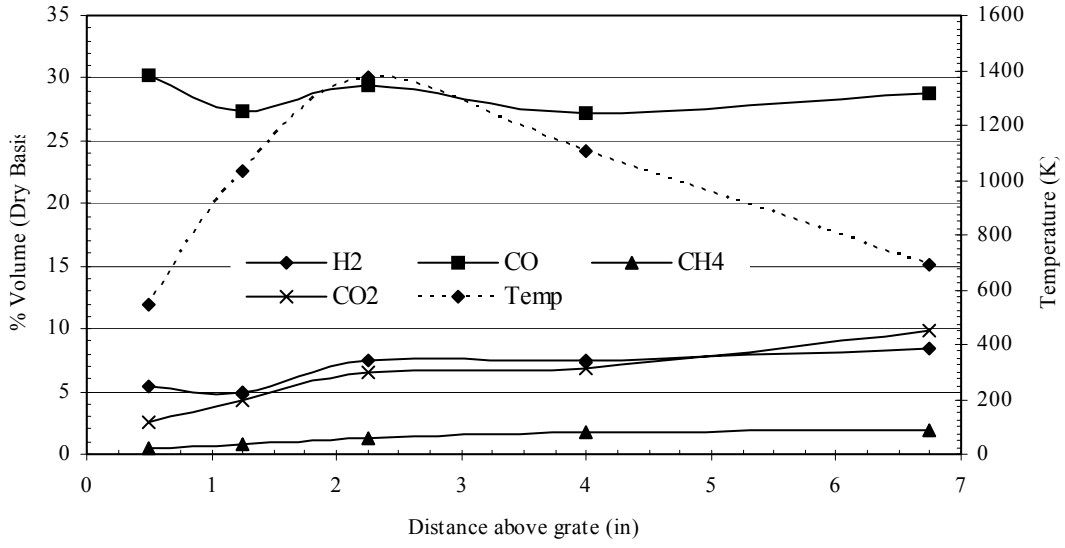

Figure 4.129: Gas species profiles for AFB (4-6.4 mm (0.157" – 0.25")) under an air flow rate of 1.27 m^3/hr (45 SCFH)

One common behavior for AFB is that at the top of the bed, the concentration of CO_2 increases for all cases. This is expected, as from table 1.4, it can be observed that one of the main gas species produced during pyrolysis of AFB is CO_2. So the increase in the CO_2 concentration proves the major product during pyrolysis of AFB is indeed CO_2.

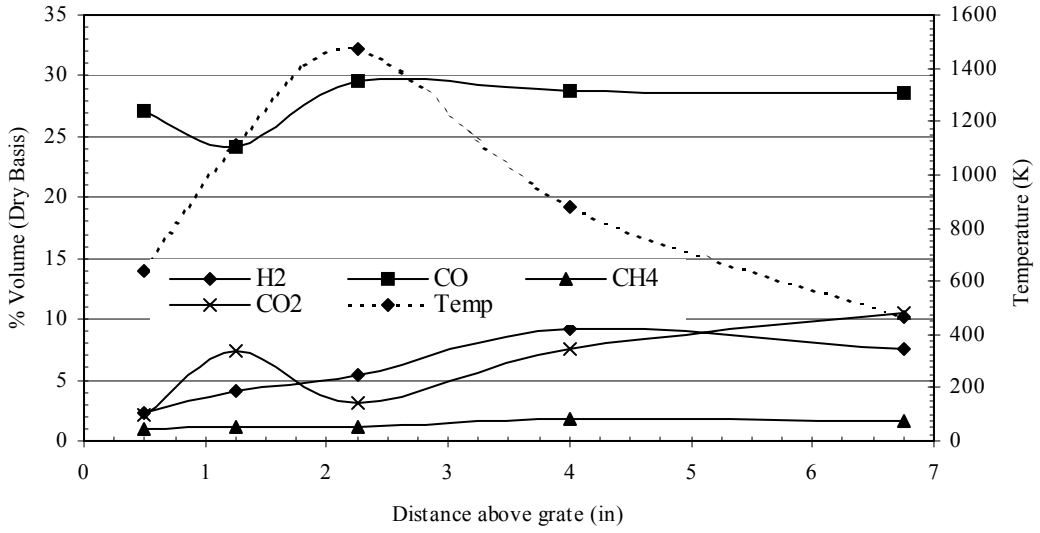

Figure 4.130: Gas species profiles for AFB (4-6.4 mm (0.157" – 0.25")) under an air flow rate of 1.7 m^3/hr (60 SCFH)

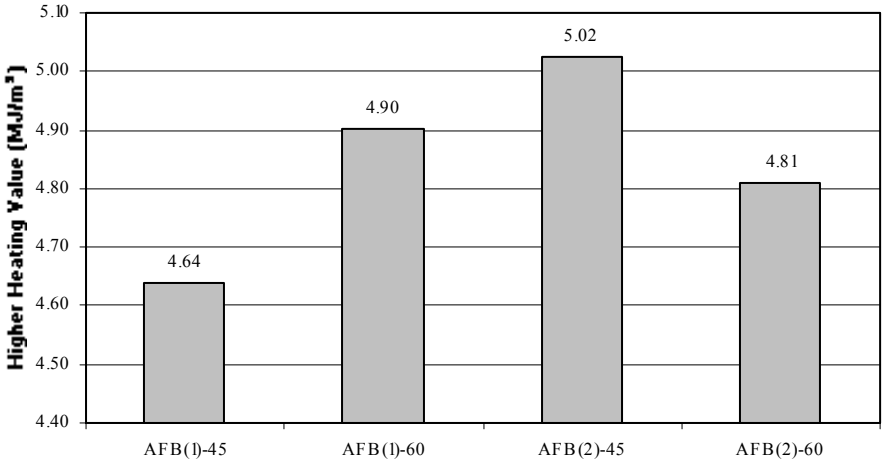

Figure 4.131 Comparative Higher Heating Values of the product gas leaving the gasifier, for AFB gasification under different operating conditions (AFB (1), 4.5-6.4 mm (0.175" – 0.25"), AFB (2), 6.4-12.7 mm (0.25" – 0.5"))

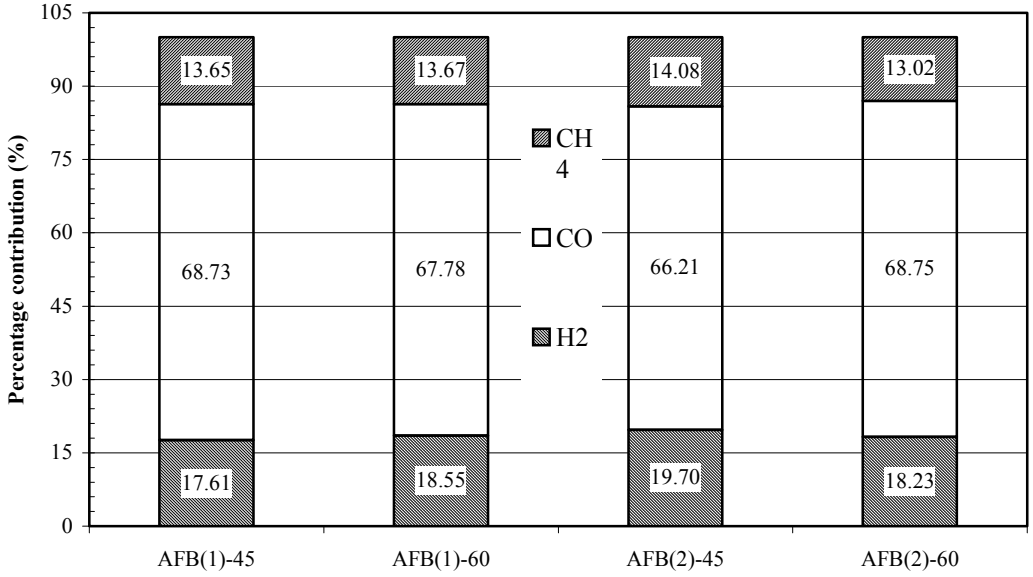

Figure 4.132: Percentage contribution of various product gases towards the product gas heating value leaving the gasifier, for AFB gasification under different operating conditions (AFB (1), 4.5-6.4 mm (0.175" – 0.25"), AFB (2), 6.4-12.7 mm (0.25" – 0.5"))

4.3.3.3. Coal and Fly ash surfaced FB blend (CAFB)

Figures 4.133, and 4.134, show the gas species profiles for larger particles sized blends under air flow rates of 1.27 and 1.7 m^3/hr (45 and 60 SCFH). The average temperature in the 12.7 mm (0.5") to 57.15 mm (2.25") zone in the bed is higher than that for coal. This higher temperature at this location indicates that the oxidation and gasification zone is up to 57.15 mm (2.25") into the bed. The higher temperature in the bed increases the devolatilization rate and the volatile matter yield of the fuels. In both the figures 4.133, and 4.134, it is seen that there is a sudden increase in the concentrations of H_2, and CH_4 at 57.15 mm (2.25") above the bed. This is because the higher temperature in the bed at that location causes a higher devolatilization rate. Moving further into the bed, the gas profiles are flat, showing that the main processes taking place in the post 57.15 mm (2.25") region are the drying and devolatilization. The high degree of CH_4 formation shows that the higher temperature in the bed causes greater release of CH_4 in the bed. This seems to be due to coal, as table 1.4 shows that the main pyrolysis gas from coal is CH_4. However, for the 1.7 m^3/hr (60 SCFH) case, the H_2, and CH_4 yield is higher than the 1.27 m^3/hr (45 SCFH) case in between the 57.15 mm (2.25") to 101.6 mm (4") region. This might be because of the higher mass transport in the bed as result of the higher air flow rates. The higher devolatilization rate results in higher gas species yield, and this increases the calorific value of the gas leaving the gasifier.

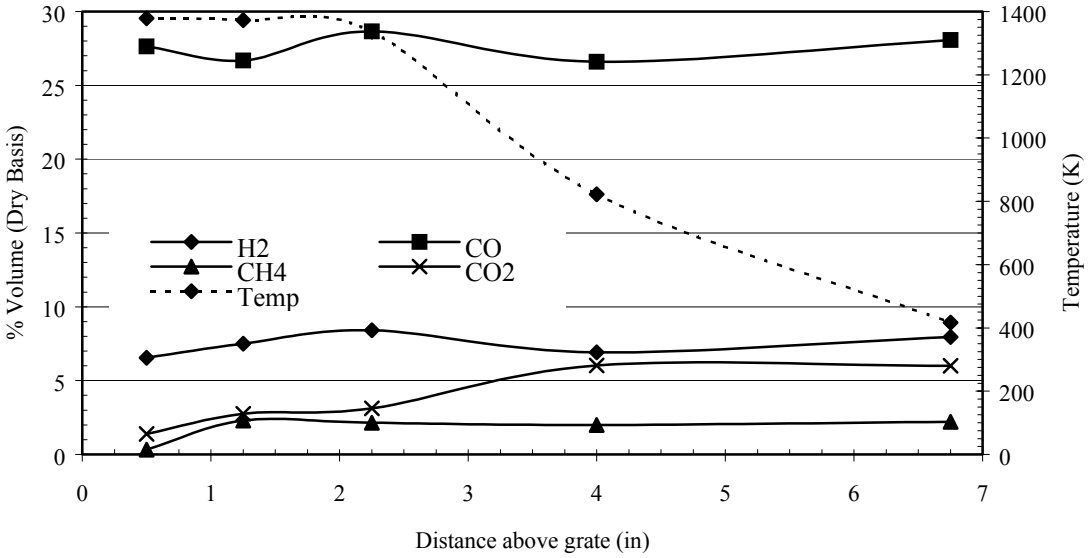

Figure 4.133: Gas species profiles for CAFB (6.4-12.7 mm (0.25" – 0.5")) under an air flow rate of 1.27 m^3/hr (45 SCFH)

Figure 4.137 shows the comparative heating values of the product gases leaving the gasifier. It can be observed that for the 1.27 m^3/hr (45 SCFH) case involving the larger particles, the heating value of the product gas is highest for CAFB fuel, as compared to coal and AFB. However the highest heating values are obtained for coal of 5 mm (0.2") size at 1.7 m^3/hr (60 SCFH). Since the heating value of the gas produced is expected to be in between that of coal and AFB, the higher heating value suggests a synergistic effect of the individual fuels on the behavior of the blend.

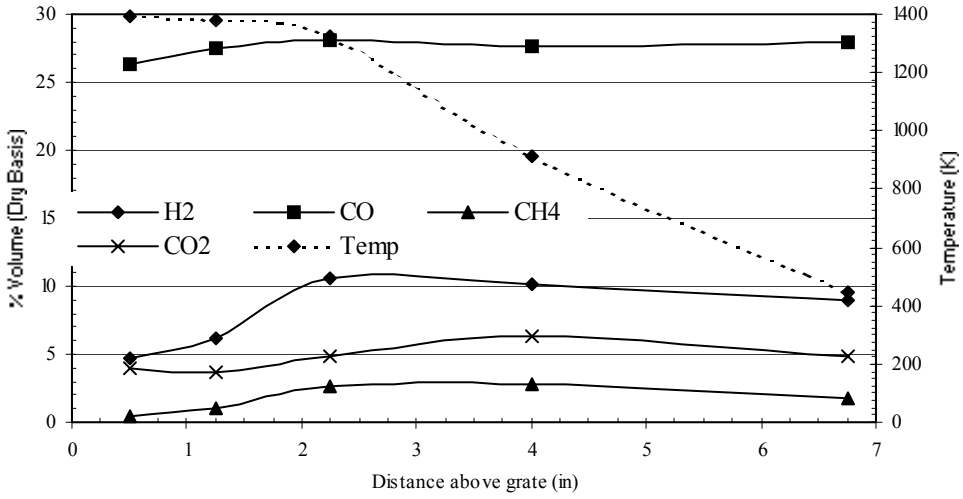

Figure 4.134: Gas species profiles for CAFB (6.4-12.7 mm (0.25" – 0.5")) under an air flow rate of 1.7 m^3/hr (60 SCFH)

Figures 4.135, and 4.136 show the gas species profiles for the smaller sized particles under air flow rates of 1.27 and 1.7 m^3/hr (45 and 60 SCFH) respectively. From figure 4.135, it can be observed that the gas species profiles are very similar to the larger particle case. In this case, the H_2, CH_4 species concentration increases rapidly beyond the 57.15 mm (2.25") mark indicating the dry and devolatilization region in the bed. For the 1.7 m^3/hr (60 SCFH) case, figure 4.136 shows a slightly different story. The CO concentration is unusually high at the bottom of the bed until about 57.15 mm (2.25") above the grate. This can be explained by looking at the temperatures at those locations, which reveal that reaction 4.3.III is the reason for such a decrease in the temperature and an increase in the CO concentration in the bed. In addition, the concentrations of H_2, and CH_4 are low in this region, suggesting that the high air flow rate has resulted in faster char formation. However, beyond the 57.15 mm (2.25") mark, the sudden rise in the concentrations of H_2, and CH_4 indicate the dominance of the drying and pyrolysis beyond the upper region of the bed.

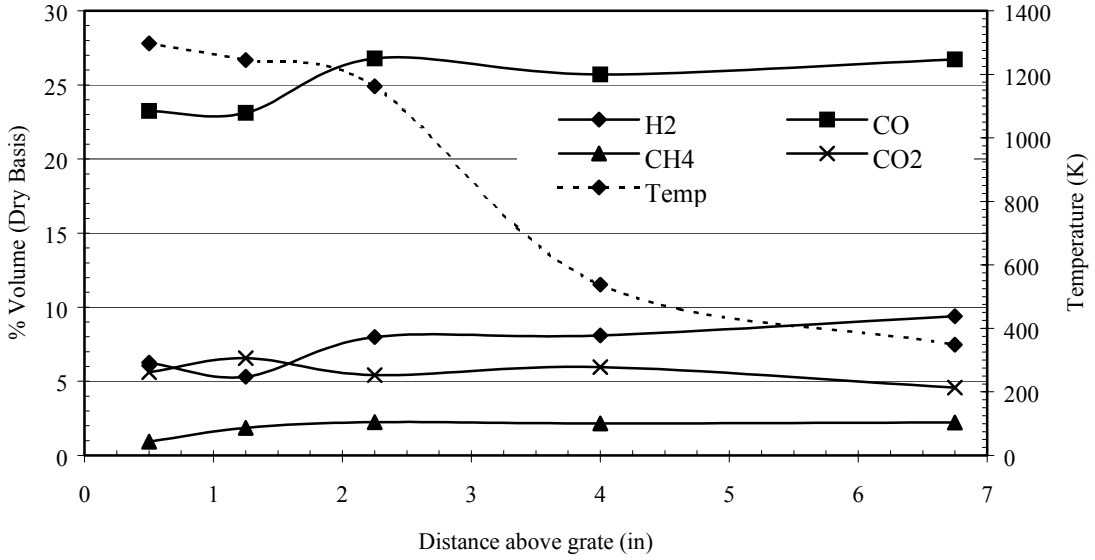

Figure 4.135: Gas species profiles for CAFB (4-6.4 mm (0.157" – 0.25")) under an air flow rate of 1.27 m^3/hr (45 SCFH)

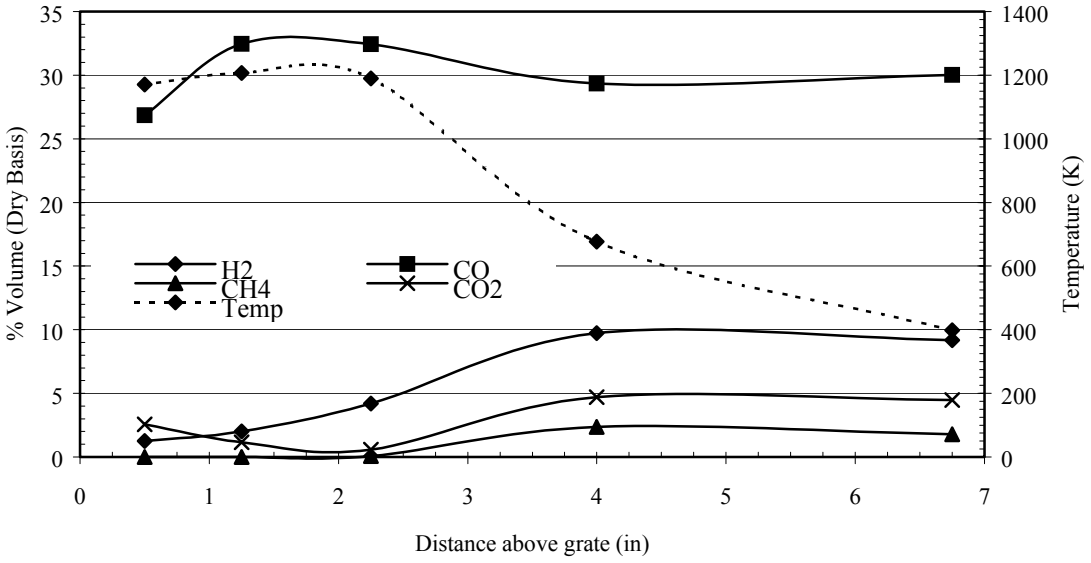

Figure 4.136: Gas species profiles for CAFB (4-6.4 mm (0.157" – 0.25")) under an air flow rate of 1.7 m^3/hr (60 SCFH)

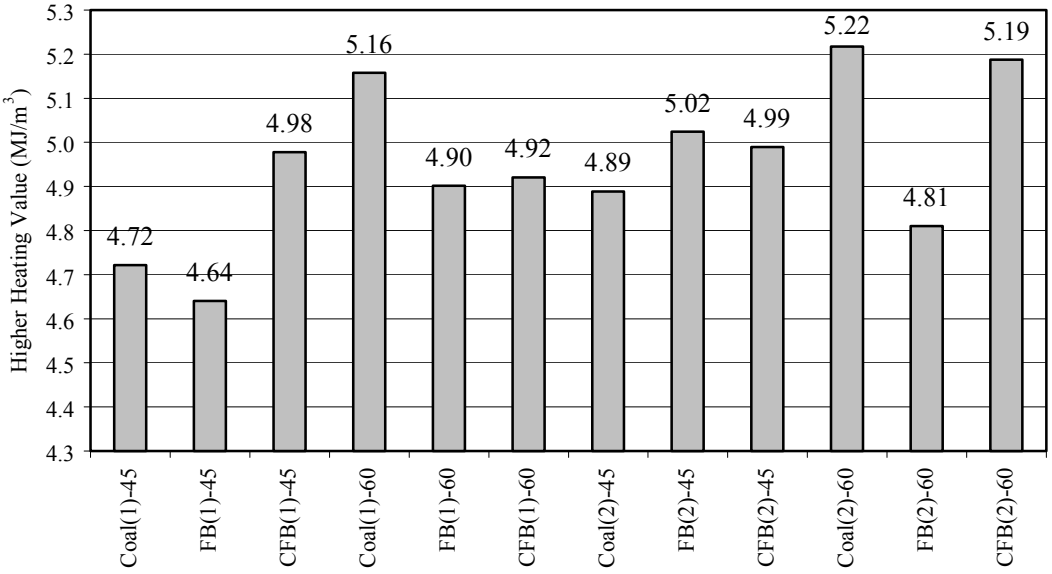

Figure 4.137: Comparative Higher Heating Values of the product gas leaving the gasifier, for coal, AFB, and CAFB gasification under different operating conditions ((1), 4.5-6.4 mm (0.175" – 0.25"), (2), 6.4-12.7 mm (0.25" – 0.5"))

4.3.3.4. Chicken litter biomass (LB)

For LB the pyrolysis data is not openly available. So, the important gas species released during the pyrolysis process cannot be anticipated for this fuel. However, since the LB is expected to behave more like AFB, it would be safe to conclude that the main gas released during LB pyrolysis is CO_2. This conclusion can only be validated after studying the gas profiles for LB. Figures 4.138, and 4.139 show the gas species profiles for large sized LB particles under air flow rates of 1.27 and 1.7 m^3/hr (45 and 60 SCFH).

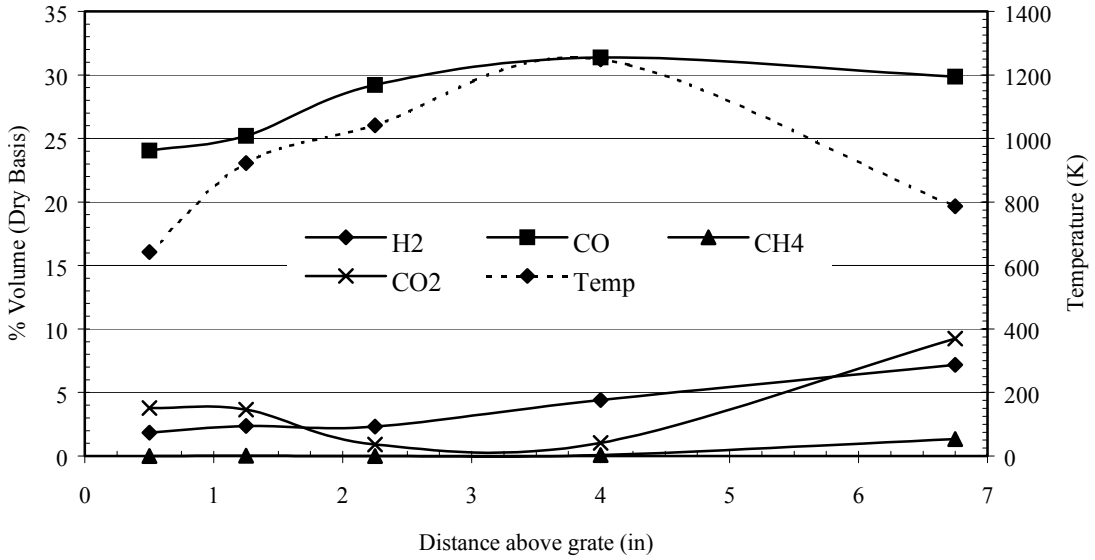

Figure 4.138: Gas species profiles for LB (6.4-12.7 mm (0.25" – 0.5")) under an air flow rate of 1.27 m^3/hr (45 SCFH)

In figure 4.138, it is observed that the concentration of CO increases until 101.6 mm (4") above the grate. At the same time, the concentration of CO_2 decreases until 101.6 mm (4") above the grate. Looking at the temperature in the bed until this location, suggests that the burn fraction is slowly decreasing along the bed. Due to lower solid fuel concentration at the base, the production of CO and CO_2 is low, as smaller amount of fuel surface area is available for reaction. However, moving from 12.7 mm (0.5") towards the 101.6 mm (4") mark, the increased solid fuel concentration enable more surface area available for reactions, thus increasing the concentration of CO. The presence of H_2 at the lower portion of the bed, also indicates that devolatilization is not yet complete in the bed. This may not be due to reaction 4.3.IV since the temperature is low. Owing to the low temperature in the bed, CH_4 production is totally inhibited in the bed. Beyond the 101.6 mm (4") mark, the temperature in the bed drops, indicating the dominance of drying and devolatilization in this region. The concentrations of H_2, CO_2, and CH_4 increase rapidly in this region, which is mainly due to accelerated pyrolysis taking place because of the higher temperature in this region.

From figure 4.139, which shows that the CO concentration in the bed increases and the CO_2 concentration decreases until 101.6 mm (4") above the grate. This is due to the similar reasons as discussed for the 1.27 m^3/hr (45 SCFH) case. Looking at the temperature profile in the until 101.6 mm (4") shows that the low concentration of CO is due to high burn fraction of the fuel in this region. Beyond 101.6 mm (4"), the concentrations of H_2, CO_2, and CH_4 increase rapidly increase, indicating the drying and devolatilization in the bed. The air flow rate does not seem to have that significant an

effect on the calorific value of the gas leaving the gasifier and can be easily inferred from figure 4.149. The small difference is because of the temperature in the drying and devolatilization region. The higher temperature in the 1.27 m^3/hr (45 SCFH) case results in higher devolatilization rate, thus resulting in increased gas yield from the fuel.

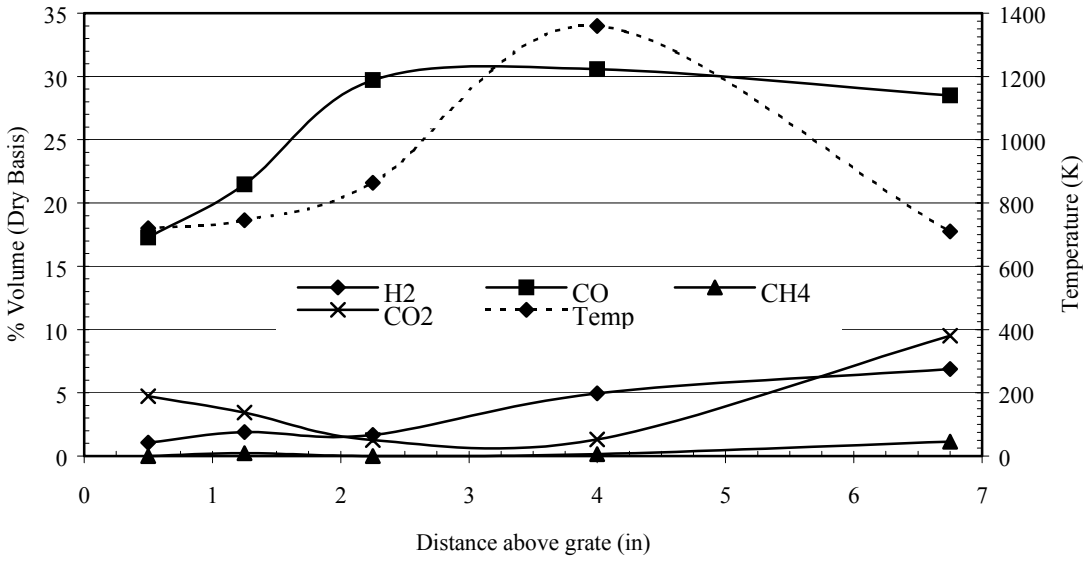

Figure 4.139: Gas species profiles for LB_1 under an air flow rate of 1.7 m^3/hr (60 SCFH)

Figure 4.140, shows the gas species profiles for the smaller sized LB particles under an air flow rate of 1.27 m^3/hr (45 SCFH). The trend in the profiles is same as that shown by the larger LB particles under similar operating conditions. The CO and H_2 concentrations increase almost monotonically in the bed. The temperature profile provides the reason for such a behavior. The decrease in burn fraction of the fuel with increased distance from the grate results in such a behavior. Until 101.6 mm (4") into the bed, both oxidation and gasification dominant, but the presence of H_2 in the lower portion of the bed shows that the devolatilization process is not yet complete for the fuels even at 12.7 mm (0.5") above the grate. Beyond the 101.6 mm (4") mark, the temperature drops significantly, making the drying and devolatilization the main processes in this region.

Figure 4.141 shows the gas species profiles for the smaller sized LB particles under an air flow rate of 1.7 m^3/hr (60 SCFH). The striking feature of this profile is the presence of O_2 at 12.7 mm (0.5") above the bed. This indicates that the air fuel ratio is very high locally at the bottom of the bed and is caused due to low solid fuel concentration at this location. The higher burn fraction is due to higher burning rates associated with higher air flow rates. This decreases the concentration of CO, and H_2, and increases the concentration of CO_2 at this location. Moving further into the bed the concentration of O_2 goes to zero, resulting in an increase in the concentrations of CO, and H_2. Until 101.6 mm (4") above the grate, the concentration of CO increases, showing the dominance of reactions 4.3.I and 4.3.VIII in the bed. However, beyond 101.6 mm (4") above the grate, the temperature drop is significant, and once again, the pyrolysis process become dominant in this region and causes the rapid release of CH_4, H_2, and CO_2.

An interesting observation is that the CO_2 release in the pyrolysis region is high for all the cases of LB. This result is similar to that observed for AFB, and it can be concluded that the main gas of pyrolysis for LB is CO_2. Thus, the pyrolysis products for both the AFB and LB seem to be similar.

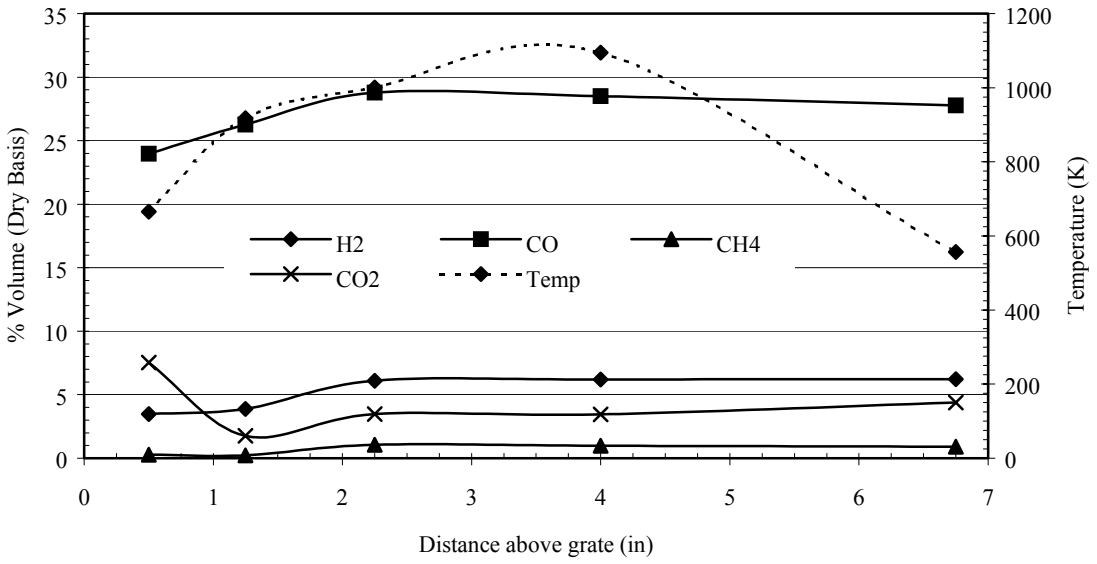

Figure 4.140: Gas species profiles for LB (4-6.4 mm (0.157" – 0.25")) under an air flow rate of 1.27 m^3/hr (45 SCFH)

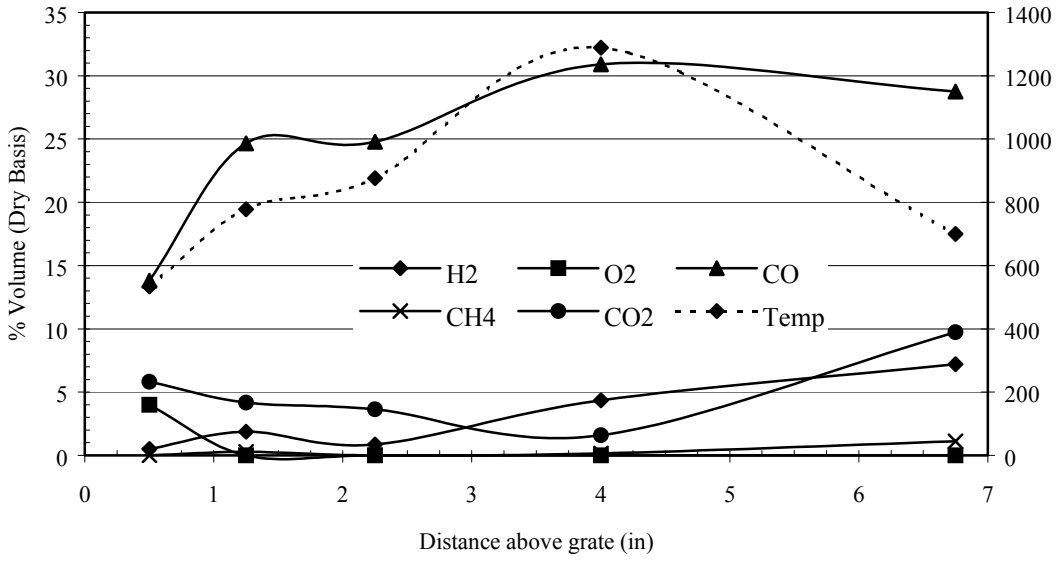

Figure 4.141: Gas species profiles for LB (4-6.4 mm (0.157" – 0.25")) under an air flow rate of 1.7 m^3/hr (60 SCFH)

4.3.3.5. Coal and LB blend (CLB)

As in the case for CAFB fuels, it shall be interesting to observe whether the coal and LB exhibit any favorable synergistic behavior. The figures 4.142, and 4.143 show the gas profiles for the large sized CLB particles under air flow rates of 1.27 and 1.7 m^3/hr (45 and 60 SCFH) respectively.

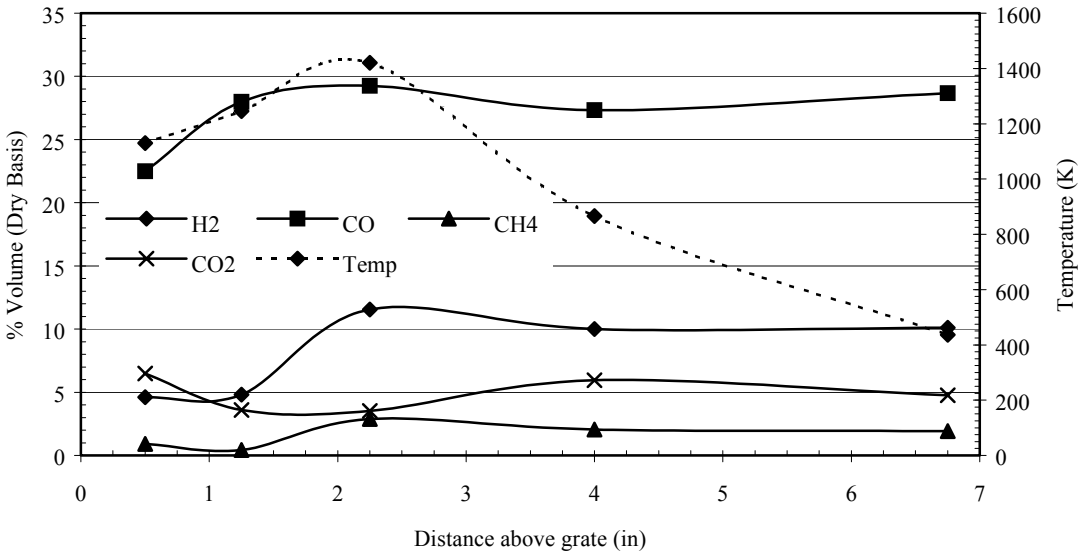

Figure 4.142: Gas species profiles for CLB (6.4-12.7 mm (0.25" – 0.5")) under an air flow rate of 1.27 m^3/hr (45 SCFH)

In figure 4.142 for CLB blends, it can be observed that the temperature in the bed increases until 57.15 mm (2.25") above the grate. Initially the lower temperature at the base of the bed is low indicating a high as fraction in the bed, and a higher local air fuel ratio in this region causes the gas phase oxidation of CO to CO_2. This causes the CO concentration in the 12.7 mm (0.5") location of the bed to be lower. Further into the bed the ash fraction in the bed decreases, increasing the surface area available for heterogeneous reactions, and hence causing higher temperatures in the bed. The out come of this is the dominance of reaction 4.3.III that causes the reduction of CO_2 back to CO thereby increasing its concentration in this region. The H_2 and the CH_4 concentrations also show an impressive rise at the 57.15 mm (2.25") location, indicating that the devolatilization of the CLB fuels in not complete at this location. Moreover, the high temperature at this location enhances the formation of hydrocarbons, which is CH_4 in this case. Beyond 57.15 mm (2.25") into the bed, the temperature decreases, signaling the end of the gasification reactions, and the dominance of the drying and devolatilization processes in the upper region of the bed. Thus, there is not much variation in the gas profiles in between 57.15 mm (2.25") and 171.5 mm (6.75") of the bed.

In case of higher air flow rate of 1.7 m^3/hr (60 SCFH) for the larger CLB particles, the gas species profiles are similar to the 1.27 m^3/hr (45 SCFH) case of the same fuel. The CO concentration increases from the bottom of the bed towards the 57.15 mm (2.25") mark. This is due to the same reasons as discussed in the previous case of air flow rate of 1.27 m^3/hr (45 SCFH). In addition, the increased air flow rate has not only increased the burn rate at the bottom of the bed, but also increased

the dilution of the product gas due to higher N_2 flow rate through the bed. Moving further into the bed, the concentrations of H_2, and CH_4 monotonically increase, this is also due to the same reason as discussed in the 1.27 m^3/hr (45 SCFH) case for the same fuel. The region beyond the 57.15 mm (2.25") location is the drying and devolatilization zone in the bed. Thus, it can be concluded that the higher air flow rate for the CLB fuel does not affect the gas species profiles in the bed to a great extent. Although the higher generation of CO, due to increased reactions 4.3.I and 4.3.VIII, slightly increase the heating value of the gas leaving the gasifier, the dilution due to high N_2 flow rate tend to slightly decrease the calorific value of the gas leaving the gasifier. This result can be inferred from figure 4.146, which shows that the heating value of the gas for the 1.7 m^3/hr (60 SCFH) case is slightly lower when compared to the 1.27 m^3/hr (45 SCFH) case of the same fuel.

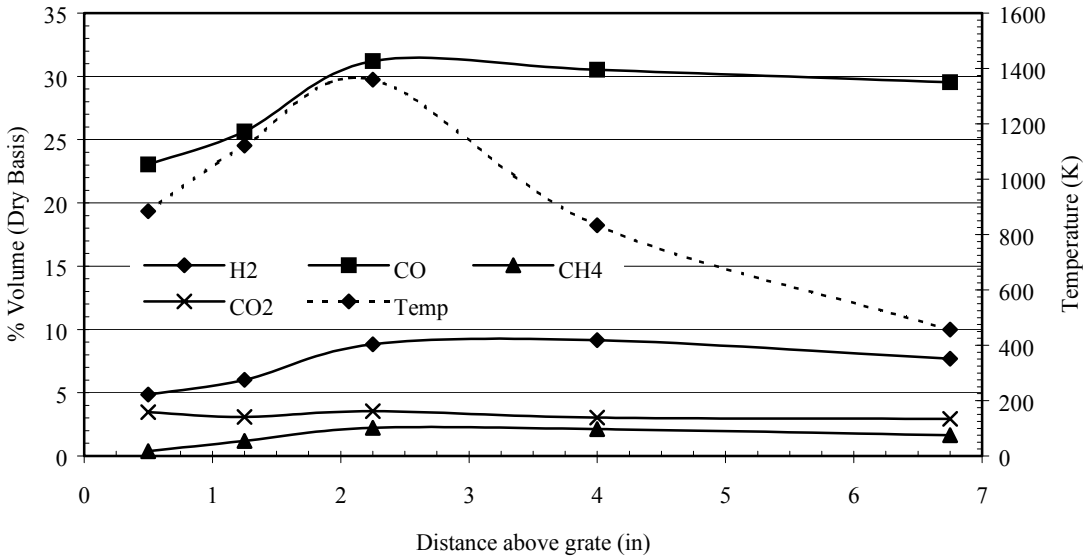

Figure 4.143: Gas species profiles for CLB (6.4-12.7 mm (0.25" – 0.5")) under an air flow rate of 1.7 m^3/hr (60 SCFH)

Figures 4.144, and 4.145 show the gas profiles for the smaller sized CLB particles under air flow rates of 1.27 and 1.7 m^3/hr (45 and 60 SCFH) respectively. For both the air flow rates, the gas profiles are not only similar, but also similar to the large particle sized CLB fuel case. This shows that neither the air flow rate nor the particle size seems to affect the gasification characteristics for the CLB fuel to such an extent.

In figure 4.144, it can be observed that the CO concentration increase as the distance above the grate increases, and tends to stabilize at about 57.15 mm (2.25") above the bed. Beyond this point the temperature in the bed decreases, and is too low to support gasification reactions. Therefore, the formation of CO is almost negligible beyond the 57.15 mm (2.25") mark. Though the high temperature at the 12.7 mm (0.5") location in the bed is high, he concentration of CO is low because of the gas phase oxidation of the CO to CO_2. For H_2, and CH_4 there is also an increased concentration at 57.15 mm (2.25") above the grate, this signals that the fuel at this location is actively undergoing pyrolysis. Thus, the region beyond the 57.15 mm (2.25") mark in the bed is mostly drying and pyrolysis region.

From figure 4.145, it can be observed that the gas species profiles are every similar to the lower air flow rate case of the same fuel. As in the previous case, in this case also the CO concentration in the bed increases as the distance above the grate increases. The higher burn fraction of the fuel at the 12.7 mm (0.5") location, along with a high air low rate causes a decrease in the concentrations of all the gases, excepting N_2. The CH_4 and H_2 release rate seems to increase beyond the 57.15 mm (2.25") mark, indicating the dominance of the pyrolysis region beyond this location in the bed. Thus beyond the 57.15 mm (2.25") mark, the gas species concentration profile are relatively variance free.

It is interesting to observe that in all the cases of CLB fuel, there was no marked increase in the CO_2 concentration towards the top of the bed. However, in the case of LB fuel, there was always an increase in the CO_2 concentration towards the top of the bed. Therefore, the presence of coal seems to decrease the CO_2 release and slightly increase the CH_4 release at the top of the bed. In some cases, like the 1.27 m^3/hr (45 SCFH) case for both the small and large sized particles, it boosts the calorific value of the fuel. The results can be observed in figure 4.146. However, for all the other cases, the heating value of the product gas produced by the CLB fuels seems to be in between the heating values of the product gas produced by the coal and litter biomass fuels.

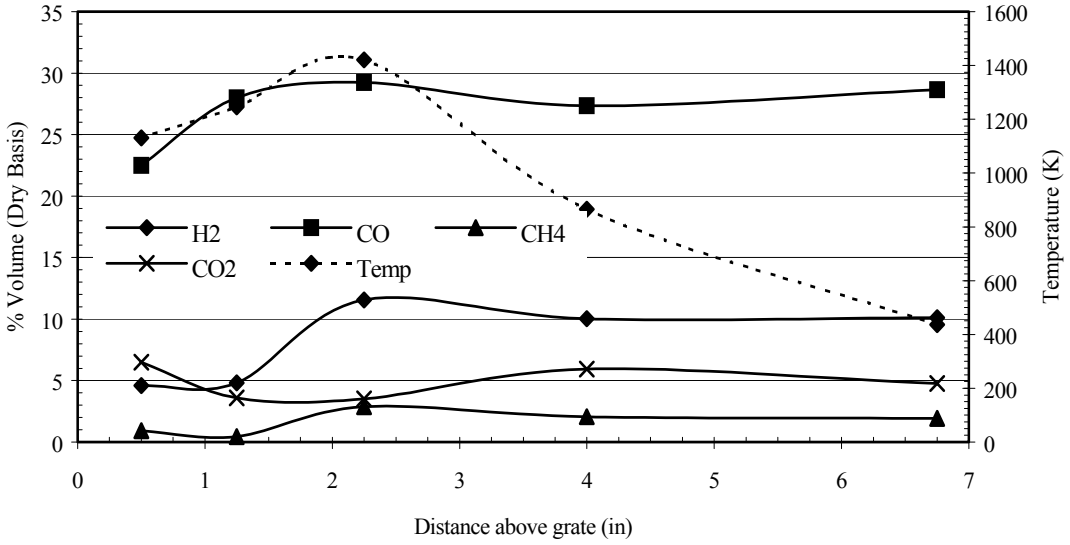

Figure 4.144: Gas species profiles for CLB (4-6.4 mm (0.157" – 0.25")) under an air flow rate of 1.27 m^3/hr (45 SCFH)

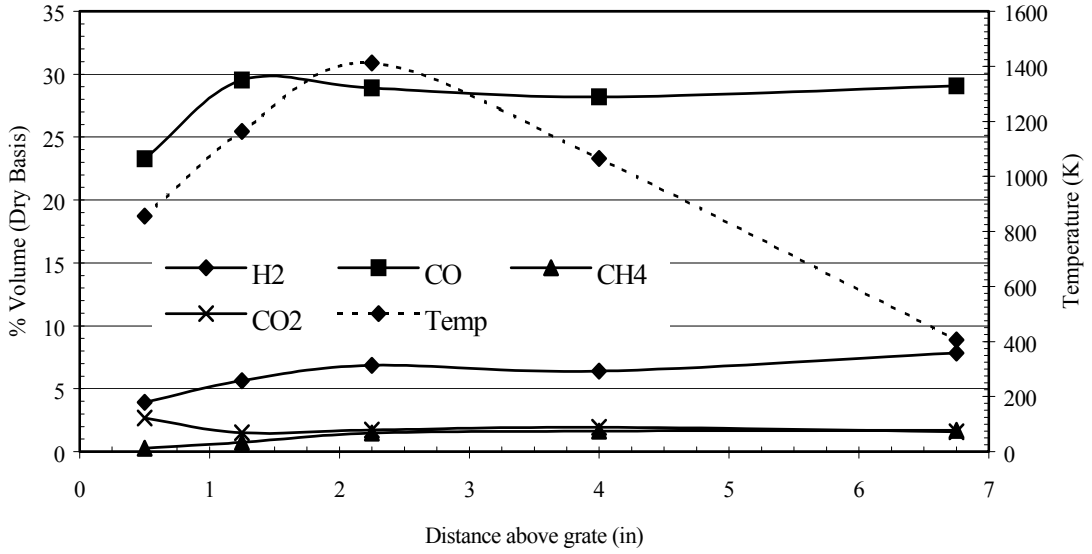

Figure 4.145: Gas species profiles for CLB (4-6.4 mm (0.157" – 0.25")) under an air flow rate of 1.7 m^3/hr (60 SCFH)

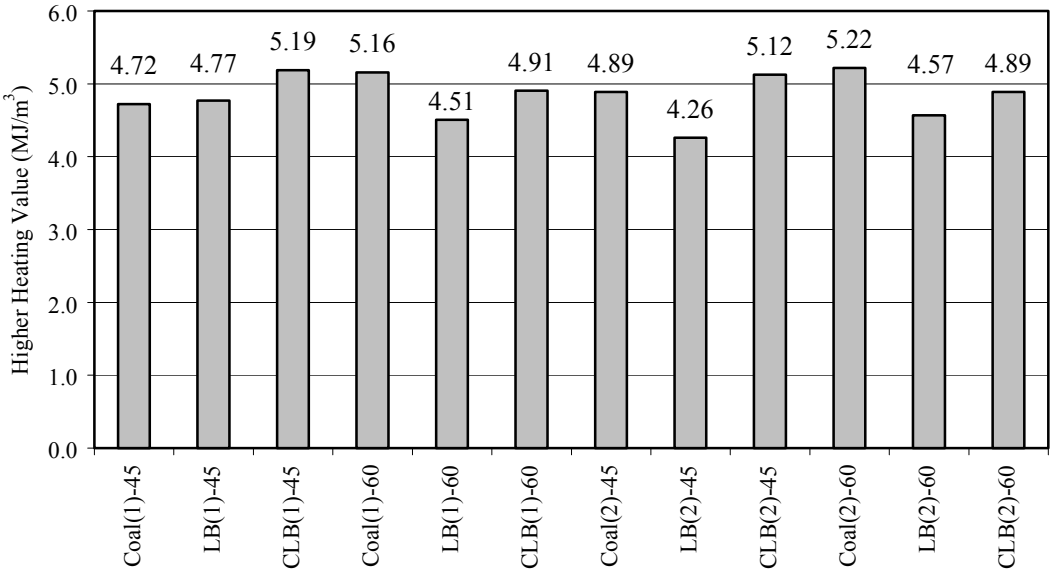

Figure 4.146: Comparative Higher Heating Values of the product gas leaving the gasifier, for coal, LB, and CLB gasification under different operating conditions

4.3.4. Ash fusion temperature study

As reported in the earlier section there was agglomeration and even clinker formation in the fuel bed for some fuels. For coal, there was no agglomeration or ash fusion in the bed, while for the fly ash surfaced AFB there was agglomeration in the bed to a certain extent (for the smaller particles at an air flow rate of 1.7 m^3/hr (60 SCFH)). However, litter biomass showed the most severe form of agglomeration in the bed. Moving on to gasification of coal blends (CAFB and CLB), the peak temperature for the blends was higher as compared to the biomass fuels, which resulted in ash fusion (clinker formation) in the bed. Before moving further, it would be of interest to learn the difference between ash fusion and agglomeration in the bed.

Bed agglomeration is when relatively small particles stick together forming larger masses of material. Local hot spots can create local bed agglomeration and result in poor flow distribution in the bed. Agglomeration is due to the melting of mineral matter in the ash that causes the particles to stick to each other. On the contrary, the ash fusion in the bed is also due to melting of ash, but in this case, the high temperature causes the ash to slag and upon cooling, the slag solidifies and forms clinkers in the bed. It is worthwhile to note that the clinker formation is also an agglomeration process.

The fuel samples were sent to the Huffman laboratories, CO. for determination of ash fusion temperatures for all the fuels. The ash fusion temperatures were determined by the procedure outlined in the ASTM D-1857 standard (1992). This ash fusibility test was originally designed to indicate the likely clinker forming characteristics of ash from lump coal in stoker-fired furnaces (Fieldener *et al*., 1918). The method uses both reducing and oxidizing atmospheres for determining the ash fusion temperatures. The ash fusion temperatures recorded as the characteristic of various stages of ash melting are:

a) The initial deformation temperature (IDT) when the ash just begins to fuse as shown by the first sign of deformation or rounding of the apex of the cone. The IDT has been accepted as the temperature where the ash first softens and becomes sticky.

b) The softening temperature (ST) is when the cone has fused down to a spherical lump in which the height is equal to the width at the base.

c) The hemispherical temperature (HT) is when the cone has fused down to a hemispherical lump, and the height is equal to half the width of the base.

d) The fluid temperature (FT) is when the height becomes a sixteenth of the width.

During gasification, and especially combustion of large particles, the gas phase burning is associated with reducing conditions at the particle surface. Therefore, for gasification process the AFT results obtained under reducing conditions are more relevant. Table 4.39 shows the ash fusion temperature for all the fuels under reducing as well as oxidizing conditions.

Table 4.39: Comparative ash fusion temperatures for all the fuels

Ash fusion Temperature (K)	Coal		AFB		LB		SFB	
	Red*	Oxi**	Red*	Oxi**	Red*	Oxi**	Red*	Oxi**
Initial Deformation Temperature	1419	1459	1456	1484	1419	1413	1457	1483
Softening Temperature	1422	1461	1475	1508	1475	1449	1520	1524
Hemispherical Temperature	1428	1462	1499	1528	1505	1502	1558	1575
Fluid Temperature	1435	1463	1580	1587	1579	1561	1622	1636

* Reducing conditions

** Oxidizing conditions

Table 4.39 shows that the IDT for coal and LB under reducing conditions are similar, and in fact, it is less than those of AFB, and SFB. Interestingly during the gasification experiments, coal did not exhibit any tendency to fuse, but the other biomass fuels did exhibit such tendencies. This means, that under actual gasification conditions, the biomass fuel has a lower IDT as compared to coal. This observation is not consistent with the AFT results obtained in the laboratory conditions.

Wall *et al*. (1999) have reported that the ash fusion tests are highly inaccurate, as it is subjective, and empirical test, which is made on observation instead of actual measurements. Due to these reasons, the ash fusion tests give no direct indication of the propensity of the heated ash to become sticky and cause agglomeration.

Wall *et al*. (1998) have attributed the difference between ash fusion temperatures for laboratory and combustion ash to the loss of potassium and reactions between the mineral residues at the higher temperatures experienced during actual combustion conditions. In case of co-firing straw and coal in a laboratory fluidized bed combustor, Lin *et al*. (1999) have shown that the presence of high K_2O in the straw ash led to rapid agglomeration in the bed. Freeman *et al*. (1997) have reported that despite the low ash, and low mineral matter content of coal, the presence of high percentages of alkaline oxides caused severe fouling, which was caused by the condensation of volatile alkali species on the much cooler parts of the boiler. Kyi *et al*. (1999) have reported that during combustion the sodium in Loy-Yang coals was released primarily in the form of NaCl, which caused severe slagging. They concluded that the Na in coals was present in a form readily released into the gas phase during combustion, and Vuthaluru *et al*. (1998) suggested the addition of mineral additives for binding the Na during combustion. Thus, the presence of alkali metals seems to affect the actual ash fusion temperatures of the ash. Table4.40 shows the ash composition of the various fuels.

Table 4.40: Ash analysis of various coal and biomass fuels

Compound	Coal	AFB	LB	SFB
Aluminum, % as AL_2O_3	15.66	9.12	5.26	9.98
Calcium, % as CaO	21.7	9.5	11.85	8.1
Iron, % as Fe_2O_3	4.68	2.91	3.06	3.06
Magnesium, % as MgO	5.35	2.88	3.86	2.4
Manganese, % as MnO	0.01	0.06	0.12	0.06
Phosphorous, % P_2O_5	2.11	3.1	13.93	2.18
Potassium, % as K_2O	0.1	5.05	11.56	4.37
Silicone, % as SiO_2	29.86	60.22	33.02	57.9
Sodium, % as Na_2O	1.53	1.63	5.08	1.4
Sulfur, %SO_3	10.34	1.86	4.03	1.33
Titanium, % as TiO_2	1.23	0.62	0.52	0.62

Table 4.41: Ash slagging propensity indicator for various fuels.

Parameter	Coal	AFB	LB	SFB
Basic Oxides (%)	40.57	23.12	40.17	21.48
B/A ratio	0.71	0.31	0.91	0.28
$Na_2O + K_2O$ (%)	1.98	7.03	18.88	6.41
Rs	0.25	0.23	0.66	0.12

The ash analysis can be used to predict the slagging and fusing propensities of the fuels. Table 4.41 lists a few indicators of slagging tendency in the bed. Duzy *et al*. (1965) have indicated that as the percentage of base increases the ash fusion temperature decreases, and reaches a minimum at about 55 % base and increases again. The base to acid (B/A) ratio is another way of calculating the basic oxides percentage. A higher base acid ratio favors evaporation of mineral species enriching the ash vapor with vaporized alkalis, increasing the ash-fusing propensity. Table 4.41, shows the similarity of the base acid ratios for coal and LB, proving that in this case, the basic oxides percentage, or the base acid ratio clearly have no effect on the actual ash fusion temperatures observed during gasification experiments. Since Na and K seems to play important roles in ash fusion temperature, comparing the values of these alkalis for the various fuels, tends to reveal the actual cause of agglomeration in the bed. From table 4.41, it can be observed that the alkaline oxides in the form of Na and K are very high for LB (18.88 %) and AFB (7.03 %) as compared to the other fuels. In fact, the alkaline oxides percentage for LB is almost ten times as that of coal and about three times as that of AFB, and SFB. This indicates that Na, and K oxides tend to decrease the actual AFT for the fuels. The slagging index (Rs) for LB is about 2.5 times as that for coal, and AFB, indicating that the sulfur in the fuel also plays an important role in agglomeration in the bed. Refer appendix 1 for calculation of the base acid ratio, the basic oxides percentage, and the slagging index. Therefore, the ash agglomeration in biomass is due to the presence of alkalis like Na, and K.

There were two different types of ash fusion observed during the gasification experiments. Skrifvars *et al*. (1994) have identified three agglomeration mechanisms: partial melting, viscous flow,

and gas/solid reactions. These mechanisms can help explain the nature of ash fusion observed in the bed for the biomass fuels.

In case of partial melting, the liquid phase on the ash causes agglomeration. The liquid phase in the biomass fuels is caused due to the condensation of the Na, and K alkalis on the ash surface. Figure 4.147 shows the photographic view of the ash agglomeration caused in the LB fuel. The large dark spots in the figure are due to small stones present in the litter biomass.

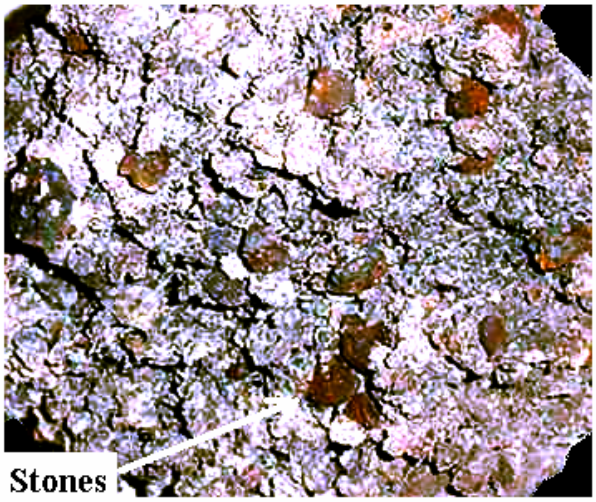

Figure 4.147: Photographic view of the ash agglomeration caused in the LB fuel

The viscous flow mechanism is due to the presence of silica in the ash. At the high temperatures the silica in the ash can melt and form a silicate system in the liquid phase which is so viscous that it forms a supercooled liquid, a glass, below the solidus temperature. In the case of coal and biomass blend fuels, the high temperatures in the bed (1500 K (2240.33ºF)), and the presence of glassy material in the ash of these fuels seems to support that silica in the biomass fuels cause the ash fusion in the coal blends. Figure 4.148 shows the photographic view of the ash fusion in case of CLB fuel. The white areas in the figure indicate the glassy material formed due to solidification of liquefied silicate compounds.

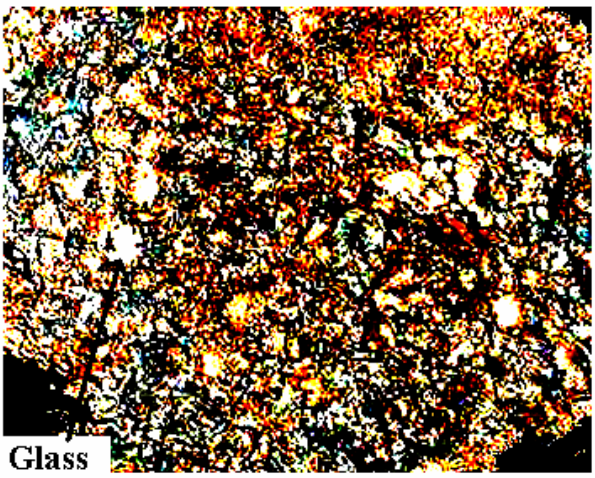

Figure 4.148: Photographic view of the ash agglomeration caused in the CLB fuel

4.3.5. Gasification efficiency

An important factor determining the actual technical operation, as well as the economic feasibility of using a gasifier system, is the gasification efficiency. Updraft gasifiers are generally used to produce gas used in direct burning. The product gas from the gasifier is directly burned generating heat. The derivation of the equation for determining the gasification efficiency is given in appendix 2.

During the current study, the mass flow rate of the product could not be measured due to high tar content in the product gas leaving the gasifier. In addition, there was no ash disposal at the grate, and the system was not under a steady state operation. The product gas composition at the top of the bed was measured midway into the run. It was assumed that the gas sample represented the average product gas composition for the entire experiment. Theoretical thermal efficiency of the gasifier was determined under the above assumptions.

Figures 4.149, and 4.150 show the comparative (theoretical) thermal gasification efficiencies for different under different operating conditions.

From figure 4.149, it can be observed that the gasification efficiency is the lowest for coal (for an air flow rate of 1.27 m^3/hr (45 SCFH)), as compared to AFB, and CAFB fuels. However, as the air flow rate increase to 1.7 m^3/hr (60 SCFH), the efficiency increases by about 68 %. This is because an increase in the air flow rate increases the stoichiometric ratio, thereby higher burning rates, and higher temperatures in the bed, which lead to higher pyrolysis of the fuel in the devolatilization region. The higher pyrolysis gas yield increases the calorific value of the product gas, and thus the thermal efficiency. This is also observed for AFB, LB, CAFB (figure 4.150), and CLB fuels, implying that an increased air flow rate increases the thermal efficiency of the gasifier.

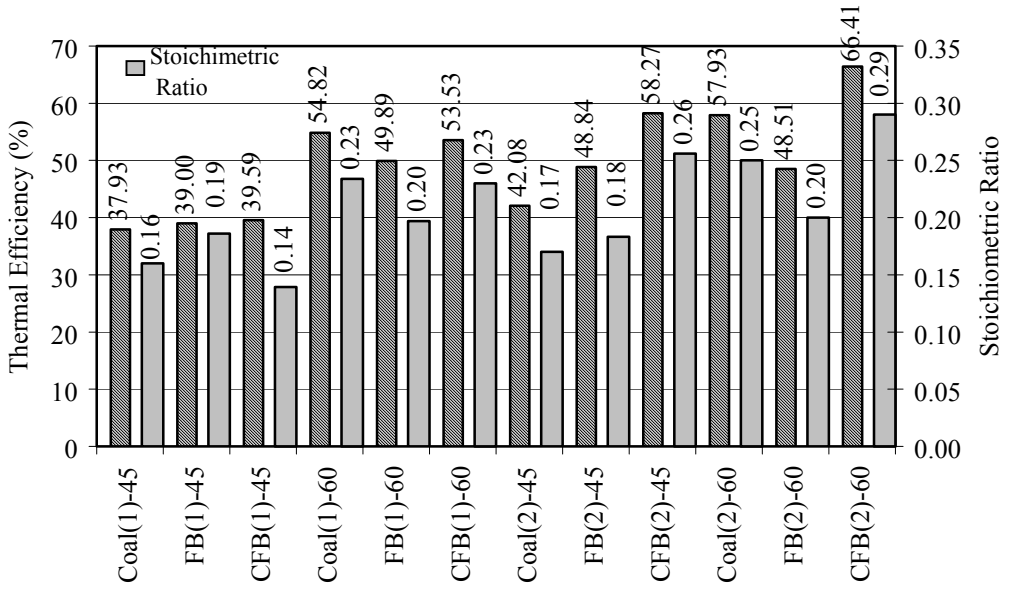

Figure 4.149: Comparative thermal gasification efficiencies and corresponding stoichiometric ratios, for coal, AFB, and CAFB fuels under different operating conditions

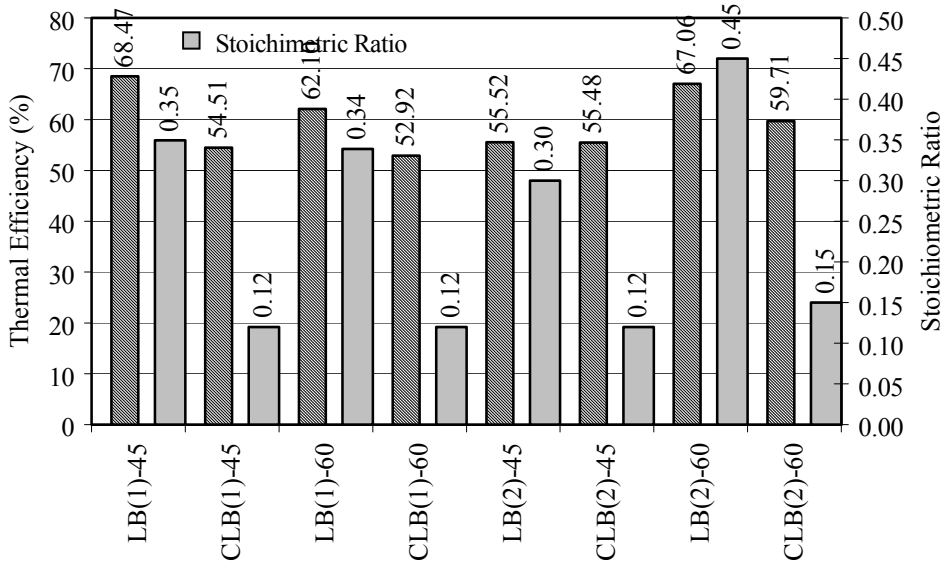

Figure 4.150: Comparative thermal gasification efficiencies and corresponding stoichiometric ratios, for LB, CLB, HFB, and LHFB fuels under different operating conditions

4.4. Numerical Modeling

4.4.1. Cofiring Modeling Coal: LB

4.4.1.1. Code Modification

This numerical study modified and employed the PCGC2 code (Pulverized Combustion and Gasification of Coal: 2-Dimensional) originally developed by Brigham Young University (PCGC2, 1989). The modules of PCGC2 are summarized as follows.

Gas Phase: Steady state Favre-averaged Navier-Stokes (FANS) method; convective and radiative heat transfer; k-ε turbulence model; PDF method for chemical properties; fuel NO_x model.

Solid phase: Sphere shape for particles; two-step pyrolysis model; particle size swelling during pyrolysis; kinetics-diffusion controlled heterogeneous char reactions; Lagrangian approach for particle tracking with consideration of gravity and drag forces; heat transfer due to convection, radiation, pyrolysis and char reactions; transport equation for particle number density with consideration of particle dispersion.

Gas-solid coupling: PSI-Cell (Particle Source In Cell) method.

The PCGC2 model and code were later modified by Texas A&M University (Sami, 2000, Wei, 2002) with three mixture fractions,

$$\eta_1 = \frac{m_1}{m_0 + m_1} \qquad \textbf{(4.4.1)}$$

$$\eta_2 = \frac{m_2}{m_0 + m_1 + m_2} \qquad \textbf{(4.4.2)}$$

$$\eta_3 = \frac{m_3}{m_0 + m_1 + m_2 + m_3} \qquad \textbf{(4.4.3)}$$

where m_0, m_1, m_2, and m_3 denote local masses that originate from different streams or sources, and they are assumed with invariant respective chemical compositions. The PCGC code was previously modified with 3 mixture fraction for using with coal: FB blends when the blend is fired in a boiler burner. Results were repeated elsewhere (Dhanapalan, *et al*, Sami, *et al*). Under the project research program, the PCGC2 model and code are further modified for coal: LB blends. The modifications include a) vaporization model, b) phosphorus compounds emission, c) additional char reactions, and d) inclusion of adiabatic boundary conditions.

4.4.1.1a. Vaporization

The original PCGC2 model does not have a vaporization sub-model for pulverized fuel combustion. Moisture was assumed to be completely released as vapor before the fuel particles entered the boiler burner. The particles were thus assumed dry and the vapor was treated as a part of primary air stream. This treatment completely ignored the vaporization effects on combustion and thus introduced errors to time scales for combustion. Since moisture content can be as high as 30 % for coal and even higher for biomass, it is necessary to consider vaporization process when modeling

pulverized coal and biomass blend combustion. The PCGC2 is modified in this study such that wet pulverized fuel particles are allowed to enter the furnace and vaporization occurs at combustion conditions. The mixture fraction PDF analysis is modified using three mixture fractions which track primary air stream, fuel blend offgas and released vapor respectively. The composition of the fuel offgas is assumed to be constant, which are equal to composition of the fuel blend on DAF basis. The vaporization sub-model is incorporated into the PSI-Cell method in PCGC2 to calculate the vaporization rate, the moisture content of particles, and the source terms for H_2O in gas phase equations for continuity, momentum, enthalpy and mixture fraction. Calculation for chemical equilibrium properties using Gibbs free energy minimization method is modified correspondingly.

For the incorporated moisture vaporization sub-model, two layers are assumed to exist inside a particle during vaporization: a dry outer layer and a wet inner layer, or wet core. The dry layer is the outer part of particle with porous structure and thus it has zero moisture content. The wet core is the inner part of particle with uniform moisture distribution and fixed initial moisture content. Vaporization is thus controlled both by diffusion through the dry outer layer of particle (internal diffusion) and by diffusion in the vapor boundary outside the particle (external diffusion), and the diffusion rate is calculated by

$$r_{wp} = \frac{Y_{wps} - Y_w}{R_{\text{int}} + R_{ext}} \qquad \textbf{(4.4.4)}$$

where r_{wp} is water vaporization rate, Y_{wps} is water vapor mass fraction at surface of the wet core, estimated from phase equilibrium assumption, Y_w is the local water vapor mass fraction in gas phase, R_{int} is the internal resistances due to internal diffusion, and R_{ext} is the external resistance due to external diffusion. If the vapor diffusivities for diffusion through internal and external layers are assumed to be the same,

$$r_{wp} = Sh\,\rho D_w \pi\, d_{wp} \left(Y_{wps} - Y_w\right) F_{B,e} \qquad \textbf{(4.4.5)}$$

where ρ is gas phase density, D_w is water vapor diffusivity, d_{wp} is the wet core diameter, Sh is Sherwood number. Following Bird et al. (1960),

$$Sh = 2 + 0.654\,\mathrm{Re}^{0.5}\, Sc^{1/3} \qquad \textbf{(4.4.6)}$$

where Sc is the Schmidt number, Re is the Reynolds number based on particle diameter, $F_{B,e}$ is blowing correction factor for evaporation process,

$$F_{B,e} = \frac{1}{B_e} \ln\left(1 + B_e\right) \qquad \textbf{(4.4.7)}$$

and

$$B_e = \frac{Y_{wps} - Y_w}{1 - Y_{wps}} \qquad \textbf{(4.4.8)}$$

Y_{wps} is calculated by assuming thermodynamic phase (i.e., from saturation pressure at given T_p) equilibrium. It is noted that the wet core zone shrinks and the dry layer front moves deeper inside particle during vaporization. The wet core diameter must be calculated repeatedly with the remaining mass of moisture in particle. Since the vaporization time scale is much larger than turbulent fluctuation time scales, gas density and mass/mole fraction of vapor can be substituted by their turbulence mean values respectively.

4.4.1.1b. Perform PO_2 and P_4O_{10} emission calculations

LB contains significant amounts of phosphorous as compared to coal and FB. During LB combustion, gaseous phosphorous oxides are released as pollutants. Thus combustion will result in more phosphorus compounds in gas phase. The PCGC2 equilibrium routines were modified to include P compounds.

4.4.1.1c. Four major char reactions

In the present study, all char reactions from 4.3.I to 4.3.IV are now included for heterogeneous reaction routines of PCGC2. Reaction (4.3.I) is the dominant reaction under typical combustion temperature. Reaction (4.3.II) is significant under low temperature (e.g. ignition conditions). At high temperatures, Reaction (4.3.II) is usually 100 to 1000 times slower than (4.3.I). Reactions (4.3.III) and (4.3.IV) can be significant under some conditions at high temperature. For example, in pulverized combustion, the near burner region has high temperature and low oxygen content due to VM oxidation while H_2O may be high due to evaporation of moisture from wet fuel. In these regions, steam-char reaction (4.3.IV) cannot be neglected.

4.4.1.1d. Adding adiabatic boundary condition into PCGC2

The previous PCGC2 code only allows constant temperature boundary conditions. This causes difficulties for parametric study due to unknown wall temperature. Since adiabatic furnace wall is ideal for achieving the maximum fuel burnout and the higher combustion efficiency due to its zero heat loss to ambient, adiabatic boundary condition are implemented into PCGC2 code in the present study.

4.4.1.2. Computational Results

After the PCGC2 code was modified and tested, numerical simulations were performed for several cases of co-firing of pulverized coal and LB and the results are compared with experimental data to validate the modifications. Effects of moisture evaporation on flame structure and pollutant emissions were investigated. Parametric study was then performed for effects of moisture, air-fuel ratio and swirl number on combustion behavior and pollutant emissions. Turbulent mean mass fractions were calculated for 15 gaseous species: H_2, N_2, O_2, CH_4, H_2O, H_2S, CO, CO_2, NH_3, HCN, NO, P_4O_{10}, PO_2, SO_2, and SO_3. Except for NO, NH_3 and HCN which were calculated by solving the turbulence transport equations, all the species were assumed to exist at chemical equilibrium and their turbulence mean concentrations are determined using the mixture fraction PDF method.

The dimension of the reactor (furnace) is sketched in Figure 4.151. Most of the air for combustion, referred as to the secondary air, is preheated and imparted swirling motion through a swirler and enters burner through the primary inlet. The secondary inlet is connected to a diffuser, or quarl, to provide recirculation zone and a radiant heat source. A cylindrical coordinate system (x, r, θ) is used with its origin fixed at the center of the primary inlet and the x coordinate being along the reactor longitudinal axis. Because the turbulence mean flow in the reactor is axis symmetric, the three-dimensional flow problem is reduced to a two-dimensional problem in (x, r) coordinate system. Computational grid is generated with 49×67 points in (x, r) plane. Figure 4.152 shows the grid in the near burner region. Due to the higher gradients of flow and chemical properties near burner, the mesh is made finer near the burner as compared to downstream. The combustion length is 1.67 m (5.48').

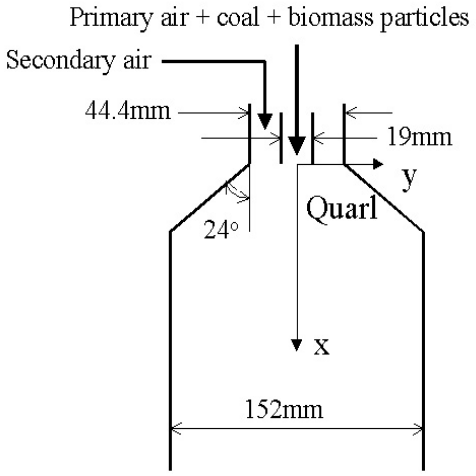

Figure 4.151: Sketch of burner dimension and flow streams.

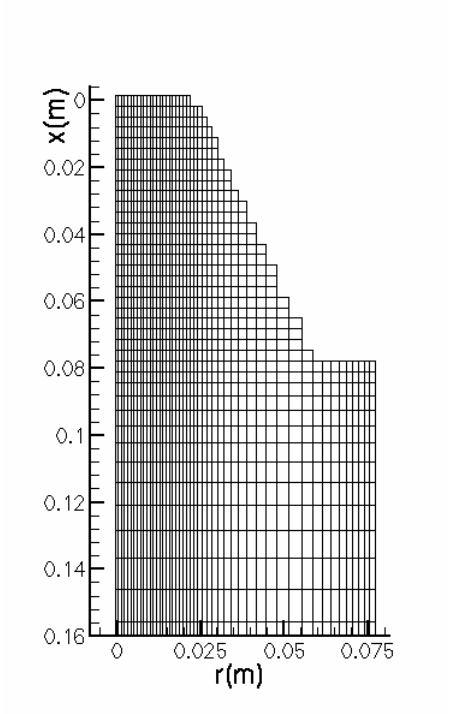

Figure 4.152: Computational grid in near-burner region.

The ultimate and proximate analyses, heating values and other fuel properties are presented in Table 4.42. The molecular formulae for DAF coal and DAF LB are $CH_{0.715}O_{0.181}N_{0.0137}S_{0.00143}$ and $CH_{1.55}O_{0.603}N_{0.0918}S_{0.00871}Cl_{0.0111}P_{0.0268}$ respectively. The higher heating value of coal as compared to LB is attributed to a significantly higher carbon content and lower oxygen and nitrogen content. Particle size distributions for both coal and LB are assumed to follow Rosin-Rammler distributions:

$$F_m(d) = 1 - \exp\left[-\left(\frac{d}{\delta}\right)^n\right] \quad \textbf{(4.4.9)}$$

where d is particle diameter, $F_m(d)$ is mass fraction of particles with diameters less than d, δ and n are empirical constants obtained from experimental data of Thien (2002) and are given in Table 4.43.

Table 4.42: Fuel ultimate and proximate analyses and other properties

	Coal	LB
Ultimate analysis on DAF bases (%)		
C	75.74	46.18
H	4.55	6.02
O	18.21	37.07
N	1.21	4.94
S	0.29	0.66
Cl	<0.1	1.07
P	—	3.20
Proximate analysis (%)		
Moisture	15.12	11.6
FC	42.38	10.92
VM	37.17	50.7
Ash	5.33	26.8
Other properties		
HHV (DAF) (kJ/kg)	29804.9	19581.3
Adiabatic Temperature (K)	2178	1869
A:F $_{stoich}$ (DAF)	9.4461	5.941
Heat of Formation (kJ/kg)(DAF)	-1500.45	-4881.87

Table 4.43: Empirical constants in Rosin-Rammler distribution (Thien, 2002)

Fuel	n	δ (μm)
Coal	4.1559	74.73
LB	1.0751	187.0

In all numerical computations, it is assumed that particles enter burner from ten uniformly distributed locations at the primary inlet. At each location, particles are divided into ten size groups: five groups for coal and five groups for LB. Thus totally 10×10 = 100 particle trajectories are used. It is assumed that 90 % mass of the dry part of fuel blend is coal and the left 10 % is LB. Mass distributions of coal and LB size groups in dry fuel blend are presented in Figures 4.153 (a) and (b) respectively. The pyrolysis models for coal and LB are a two-step model and a one-step model respectively. The pyrolysis kinetics is given in Table 4.44. For NO calculations only fuel NO is considered in NO_x calculation. Fuel N is assumed released in the form of HCN and NH_3 that undergo the following reactions

$$HCN + O_2 \rightarrow NO + \ldots \quad \textbf{(4.4.NO.I)}$$

$$HCN + NO \rightarrow N_2 + \ldots \quad \textbf{(4.4.NO.II)}$$

$$NH_3 + O_2 \rightarrow NO + \ldots \quad \textbf{(4.4.NO.III)}$$

$$NH_3 + NO \rightarrow N_2 + \ldots \qquad \textbf{(4.4.NO.IV)}$$

The related parameters are previously given in Table 4.45.

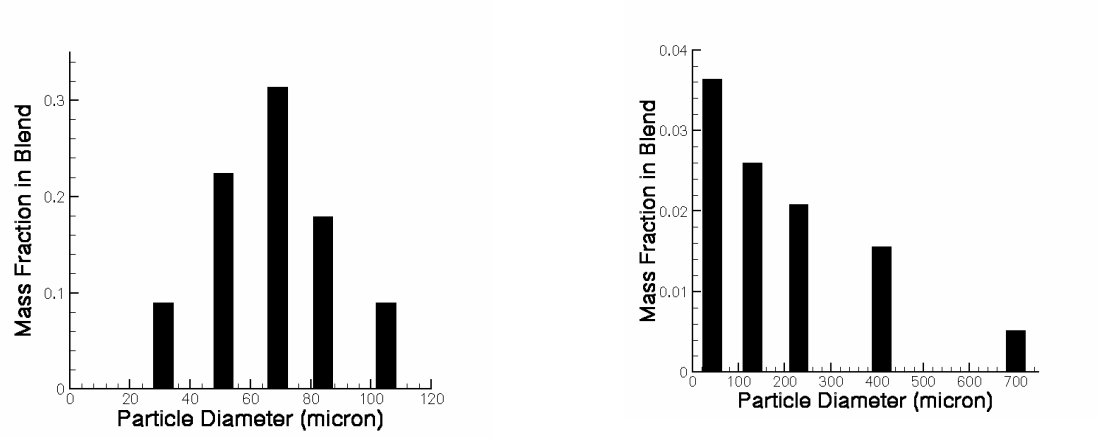

(a) (b)

Figure 4.153: Coal and LB size distribution. (a) Coal, (b) LB.

Table 4.44: Parameters for pyrolysis models for coal and LB (Arrhenius type kinetic rate coefficient for reactions *i* is $k_i = A_i \exp(-E_i / R_u T)$)

	A (s^{-1})	E (J/kmole K)
Bituminous Coal Reaction 1 Bituminous Coal Reaction 2 (Ubhayakar, 1977)	3.7×10^5, 1.5×10^{13}	7.36×10^7, 2.51×10^8
LB Reaction	6×10^4	8×10^7

Table 4.45: Reaction Rate Parameters for Fuel NO Mechanism

i	A_i (s^{-1})	E_i (J $kmol^{-1}$)
1	1×10^{10}	2.803×10^8
2	3.0×10^{12}	2.510×10^8
3	4.0×10^6	1.339×10^8
4	1.8×10^8	1.130×10^8
5	4.1×10^{-4} kmol $Number^{-1}s^{-1}$	1.5×10^8

Moisture contents of coal and LB are 15.12 % and 14.4 % (as received basis) respectively. Mass ratio of wet coal to wet LB is 90:10 in fuel blend (due to similarity in moisture calculations, approximately 90 % mass of the dry part of fuel blend is coal and the left 10 % is LB). The calculated H_2O mole distribution is presented in Figure 4.154. The high H_2O region inside the quarl is due to the strong moisture vaporization. The H_2O concentration drops to a very low level (mole fraction < 0.06) just beyond the quarl because H_2O reacts with CO through the equilibrium reaction

$$H_2O + CO \rightleftharpoons CO_2 + H_2 \qquad \textbf{(4.4.I)}$$

The equilibrium in gas phase favors the oxidation of CO with H_2O. Further downstream the secondary air mixes and reacts with the combustible gases, resulting in a small increase of H_2O level.

The effects of moisture vaporization on CO, CO_2 and H_2 levels in the near burner region are significant. This can been observed from Figure 4.155 which gives distributions of mixture fractions 2 and 3, H_2O, CO, CO_2 and H_2 near the burner. (Mixture fraction 2 (denoted as η_2) represents mass fraction of fuel offgas in its mixture with air). The high η_2 region suggests strong pyrolysis. (Mixture fraction 3 (denoted as η_3) represents mass fraction of original moisture in gas phase). The high η_3 region is located farther away from the inlets than the high η_3 region since the moisture vaporization process precedes the fuel pyrolysis process. The high CO region just outside the quarl is due to oxidation of volatiles by oxygen from the primary air. The corresponding CO_2 level is low (0.02 ~ 0.06 in mole fraction) because fuel is rich in gas phase. Farther away from the quarl, CO concentration drops while CO_2 concentration increases due to oxidation of CO by the oxygen from the secondary air. It is noticed that near the burner a high H_2 region (mole fraction > 0.21) exists corresponding to moderate levels of CO (mole fraction = 0.15 ~ 0.21) and CO_2 (mole fraction = 0.06 ~ 0.1) and a low level of H_2O. This is due to reaction (1), which consumes CO and H_2O to produce H_2 and CO_2. Downstream of this region, H_2 concentration drops quickly because H_2 is oxidized into H_2O with addition of the secondary air. All these species and the mixture fraction have V-shaped contours near burner due to the flow recirculation.

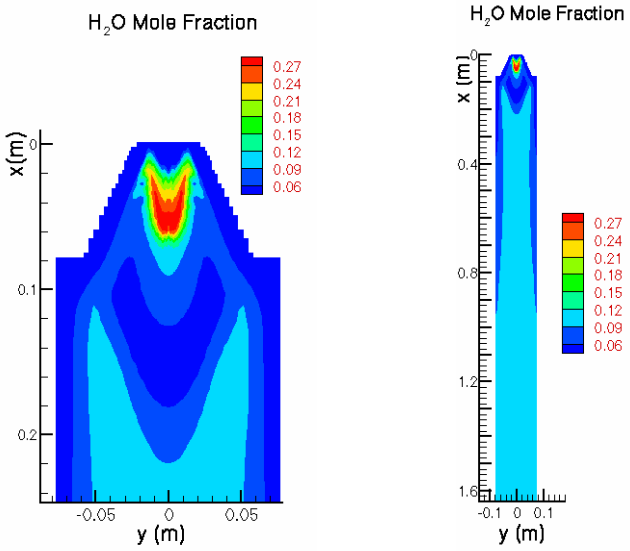

Figure 4.154: H_2O distributions in center plane for wet coal-LB blend combustion by current modified code. Left: near burner region. Right: whole furnace.

The LB contains phosphorous as high as 3.2 % (on DAF basis) while phosphorous level in coal and FB are negligible compared to LB. Thus, coal-LB blend combustion produces significant amount of gaseous P_4O_{10} and PO_2. Figure 4.156 (a) shows the calculated distributions of P_4O_{10}, PO_2, temperature, and mixture fraction 2 (η_2) near the burner for coal-LB blend combustion with 10 % excess air, 0.7 swirl number, and adiabatic boundary conditions. Figure 156 (b) gives the distributions in the entire furnace. It is seen that near the burner there exists a high P_4O_{10} region (160 ~ 200 ppm). However, in other regions of the furnace, P_4O_{10} level is very low (less than 8 ppm). Corresponding to the high P_4O_{10} regions are a low PO_2 region (less than 50 ppm), a high η_2 region

(higher than 0.4), and a moderate temperature region (1200 ~ 1400 K (1700 ~ 2060 ºF)). This suggests that fuel pyrolysis initially produces gaseous P_4O_{10} rather than PO_2. Around the flame, as temperature increases sharply from about 1400 K (2060 ºF) to over 2000 K (3140 ºF), P_4O_{10} decreases very steeply from about 180 ppm to less than 60 ppm while PO_2 increases sharply from about 50 ppm to 400 ~ 450 ppm. This indicates that at high temperature, P_4O_{10} is quickly reduced into PO_2 since equilibrium calculation at high temperature favors PO_2. In the post-flame region, PO_2 around the centerline decreases slowly in the axial direction while it distributes more uniformly in the radial direction. At the furnace end, the cross-sectional averaged P_4O_{10} and PO_2 concentrations are 7.4 ppm and 267.3 ppm respectively. Dependence of PO_2 and P_4O_{10} on temperature is clearly seen from above distributions, which agrees well with the results of Frandsen et al. (1994). According to Frandsen et al. (1994), for the equilibrium reaction

$$P_4O_{10}(g) \leftrightarrow 2PO_2(g) + 0.5O_2(g) \qquad \textbf{(4.4.II)}$$

P_4O_{10} is dominant between 430 K (314 ºF) and 1400 K (2060 ºF). Formation of PO_2 begins at about 1350 K (1970 ºF). Above 1800 K (2780 ºF), PO_2 is the main phosphorous species while P_4O_{10} is negligible.

4.4.1.2a. Swirl number effects

Numerical predictions are conducted for coal-LB blend combustion for two cases with the swirl number as 0.7 and 1.0 respectively. Moisture contents for coal and LB are 15.12 % and 14.8 % (as received basis) respectively. Mass ratio of coal to LB (as received) is 9:1. Fuel flow rate is set at 0.00133 kg/s with 10 % excess air. Temperatures of the primary and the secondary air at inlets are 298 K (77 ºF) and 373.15 K (212 ºF) respectively. Because the wall of boiler is not well insulated in experiments, the wall temperature is assumed as 1100 K (1520 ºF). Figure 4.157 shows velocity vector plots in the furnace center plane near the burner. For swirl number equal to 0.7, reverse flow is obvious in the region between the primary and the secondary jets but nearly unseen around the centerline. For swirl number equal to 1.0, the reverse flow is stronger and clearly observed around the centerline from y = 0.13 ~ 0.21 m (5.1 ~ 8.3 “), namely, the length of reverse flow along the centerline is 0.08 m (3.1 “) which is approximately the size of Z. The primary jet is a little shorter for the higher swirl number due to effect of the stronger reverse flow. Figure 4.158 shows the temperature distribution near the burner. The high temperature zone moves closer to burner as the swirl number increases from 0.7 to 1.0, i.e., the higher swirl number results in a shorter flame length. This is because the stronger reverse flow associated with the higher swirling motion conveys the hot production gases closer to the burner resulting in earlier ignition of the incoming fuel-air mixture.

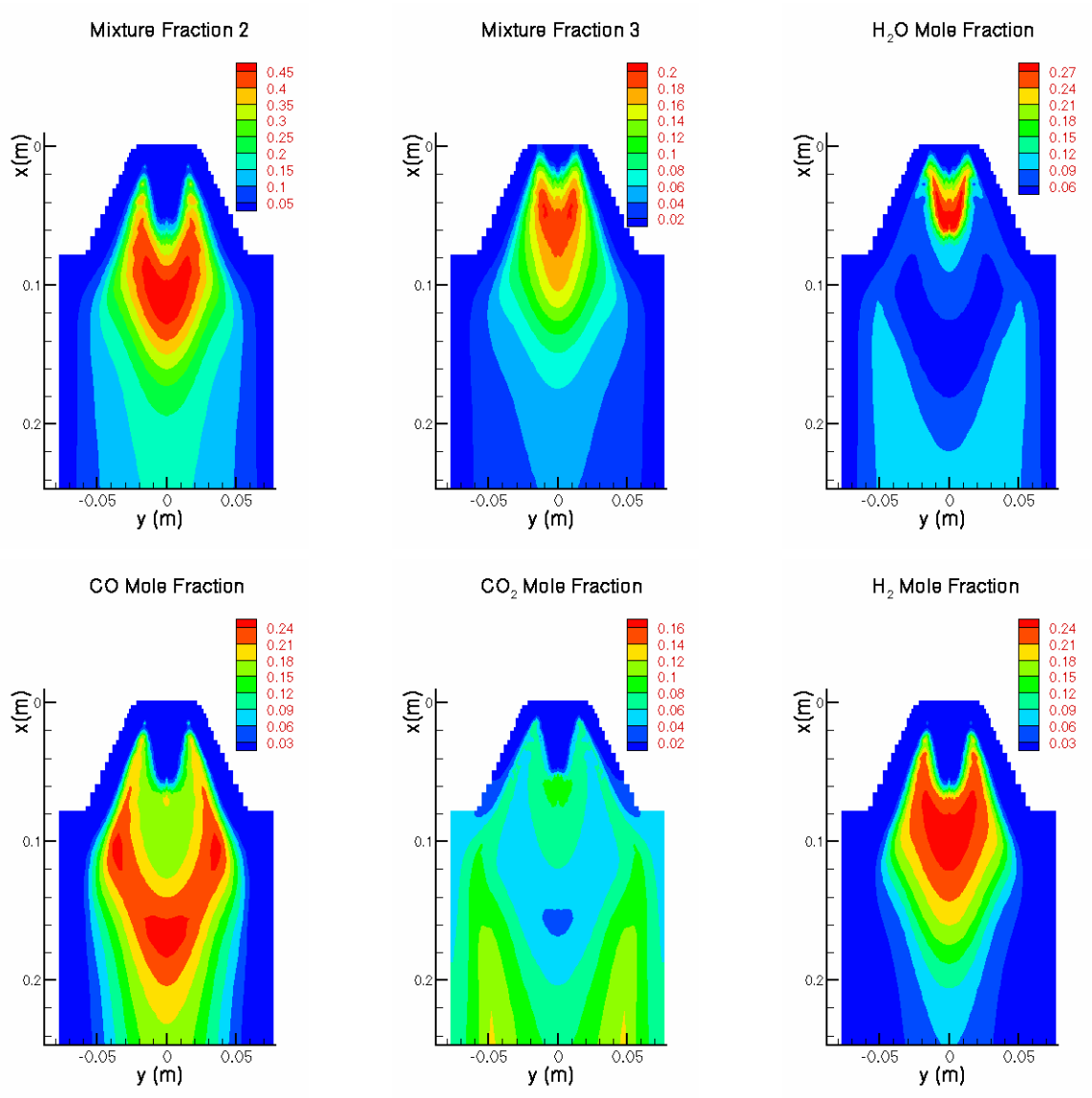

Figure 4.155: Distributions of mixture fractions 2 and 3, H_2O, CO, CO_2, and H_2 in center plane near burner for wet coal-LB blend combustion.

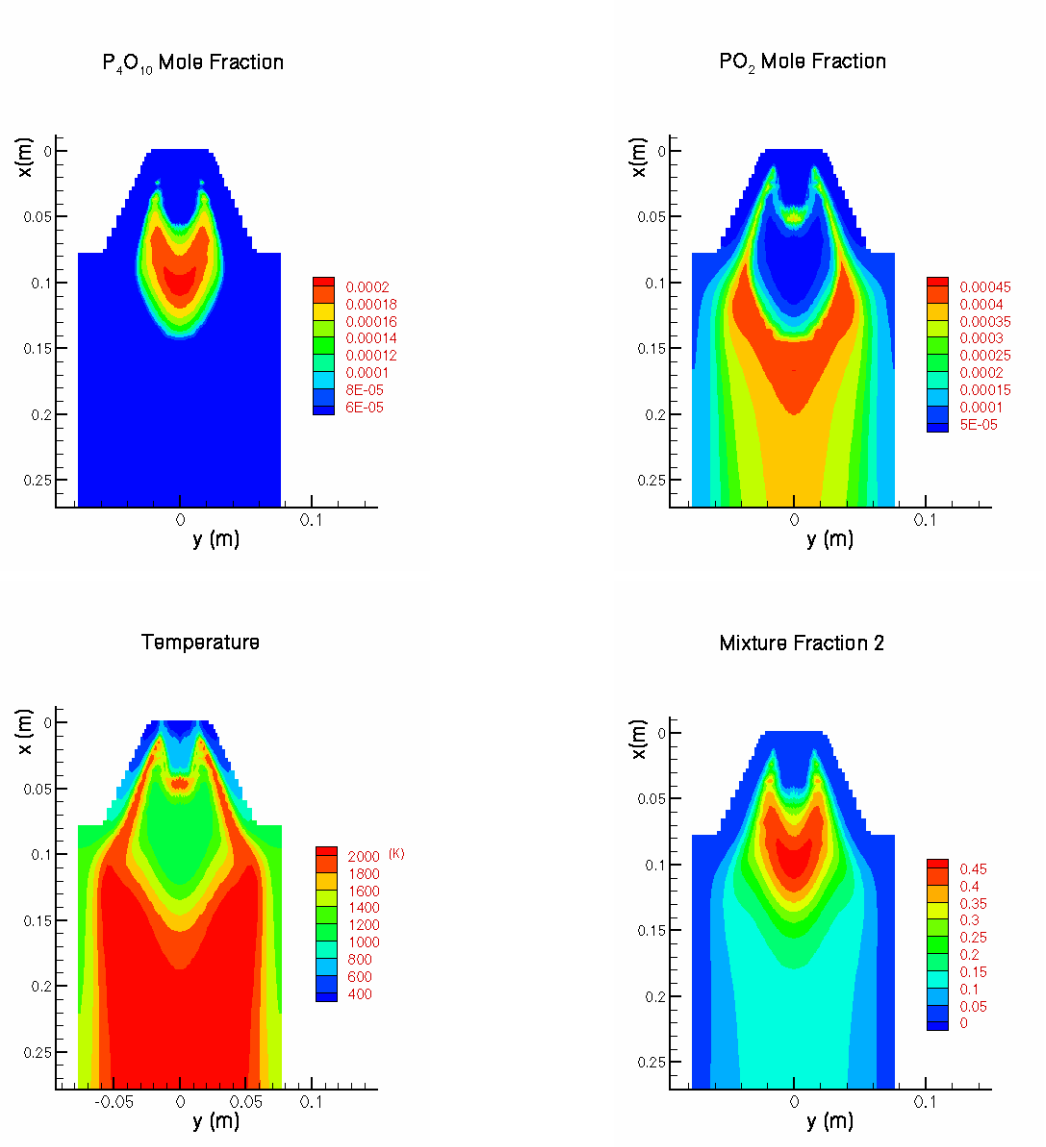

Figure 4.156(a): Distributions of P_4O_{10} and PO_2 mole fractions, temperature, and mixture fraction 2 in center plane around burner for coal-LB blend combustion.

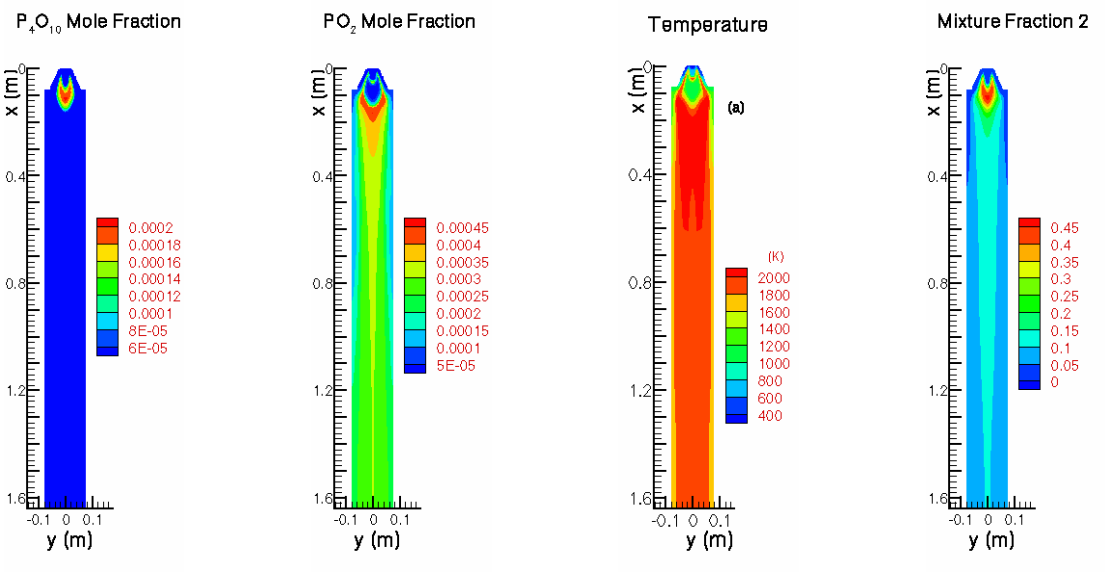

Figure 4.156(b): Distributions of P_4O_{10}, PO_2, temperature, and mixture fraction 2 in center plane of the whole furnace for coal-LB blend combustion.

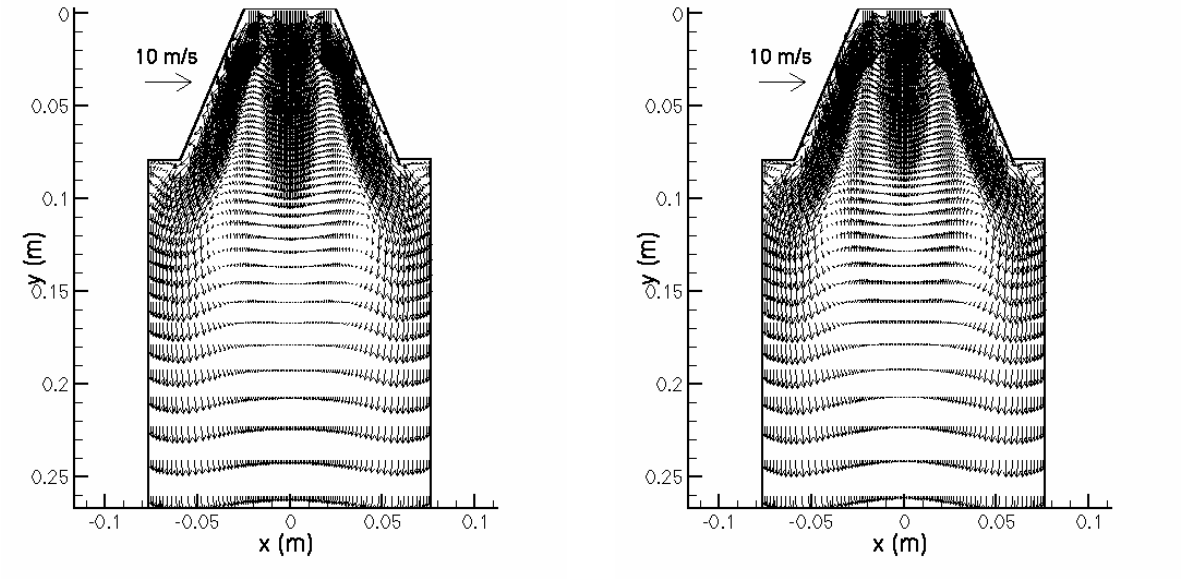

(a) (b)

Figure 4.157: Velocity vectors in center plane near burner for coal-LB blend combustion. (a) Swirl number = 0.7. (b) Swirl number = 1.0.

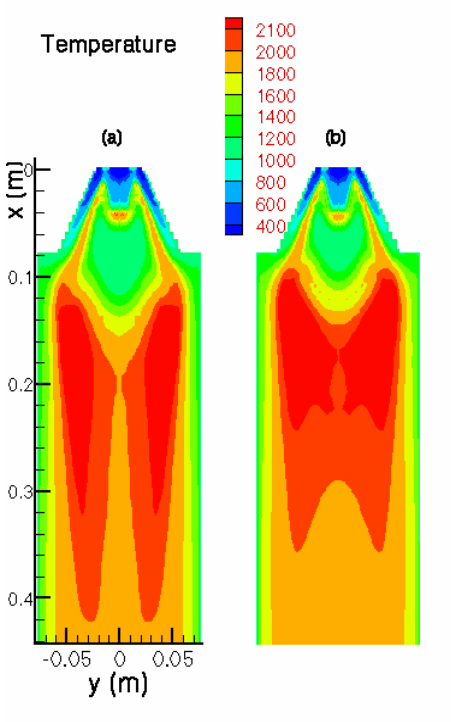

Figure 4.158: Distributions of temperature (in Kelvin) in center plane near burner for coal-LB blend combustion. (a) Swirl number = 0.7. (b) Swirl number = 1.0.

Figure 4.159 shows the computational and experimental CO profiles along the furnace axis. It is seen the swirl number has significant effects on the CO distribution near burner. As the swirl number increases from 0.7 to 1.0, the high CO zone near burner shrinks in axial scale and shifts closer to burner due to the increasing suction effect of the swirling motion. In the downstream region, it is shown that CO level is slightly lower for swirl number equal to 1.0. The predicted CO mole fraction reasonably agrees with experimental data.

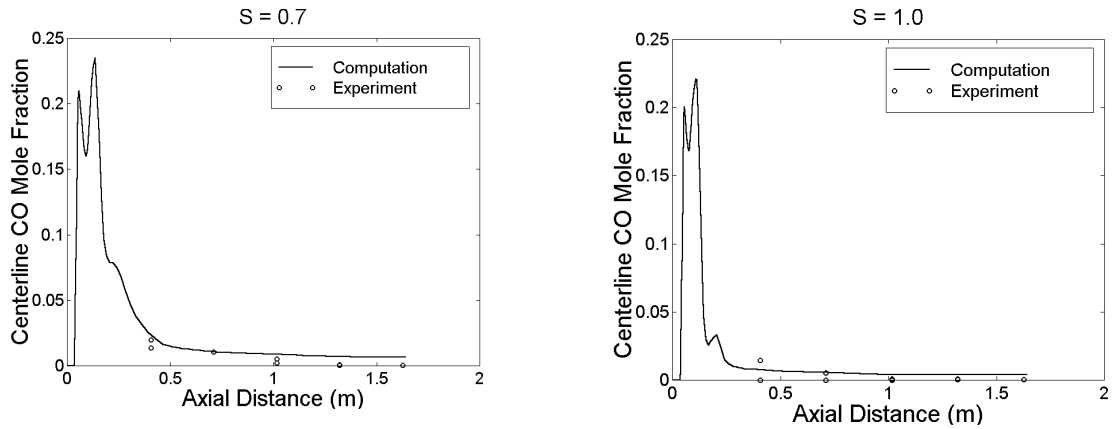

Figure 4.159: Profiles of centerline CO for coal-LB blend combustion. Symbols represent experimental data. (a) Swirl number = 0.7. (b) Swirl number = 1.0.

Figure 4.160 presents distributions of NO concentration in the center plane of the burner. Figure 4.161 gives the computational and experimental data of NO profiles along the furnace axis. It is observed that the two high peaks of NO near burner moves closer to burner with increasing the swirl number because higher swirl number causes stronger suction effect and shorter flame length. NO distribution in furnace is controlled two factors: 1) NO production due to fuel nitrogen oxidation, and 2) NO reduction due to reactions of NO with HCN, NH_3 and char. The first and second high peaks near burner are due to oxidation of volatile nitrogen species (HCN and NH_3) by the primary air and the secondary air respectively. The lower peak of NO between them is due to NO reduction as the result of oxygen depletion in the primary air and continuous release of fuel nitrogen. As swirl number of the secondary air increases, two opposite trends exist near burner: 1) mixing gets stronger between the primary air and volatiles causing more NO; 2) less secondary air is entrained due to the shorter flame length causing less NO. With increasing the swirl number, the first high peak of NO raises significantly because the first effect is dominant, whereas the second high peak drops slightly because the second effect dominates locally. The figure shows that the first effect is much stronger than the second effect near the burner. After the second high peak, NO level drops rapidly to another low point due to the low local oxygen level again. Further away from the burner, mixing of the secondary air causes gradual O_2 increase around the axis, increasing the NO concentration again. In the downstream region of the furnace, since most oxygen is consumed, NO concentration decreases slowly due to reduction by HCN, NH_3 and char. It is found that due to stronger mixing between air and fuel offgas for the higher swirl number yields a slightly higher NO level than the lower swirl number in the downstream region of the burner. For swirl number equal 1.0, the predicted and measured NO concentrations have a good agreement. For swirl number equal to 0.7, numerical predictions are 10 % ~ 60 % higher than experimental results. The over prediction could be due to the assumption that nitrogen content in volatiles and char offgas are the same. However, the trend of NO variation with swirl number is predicted correctly.

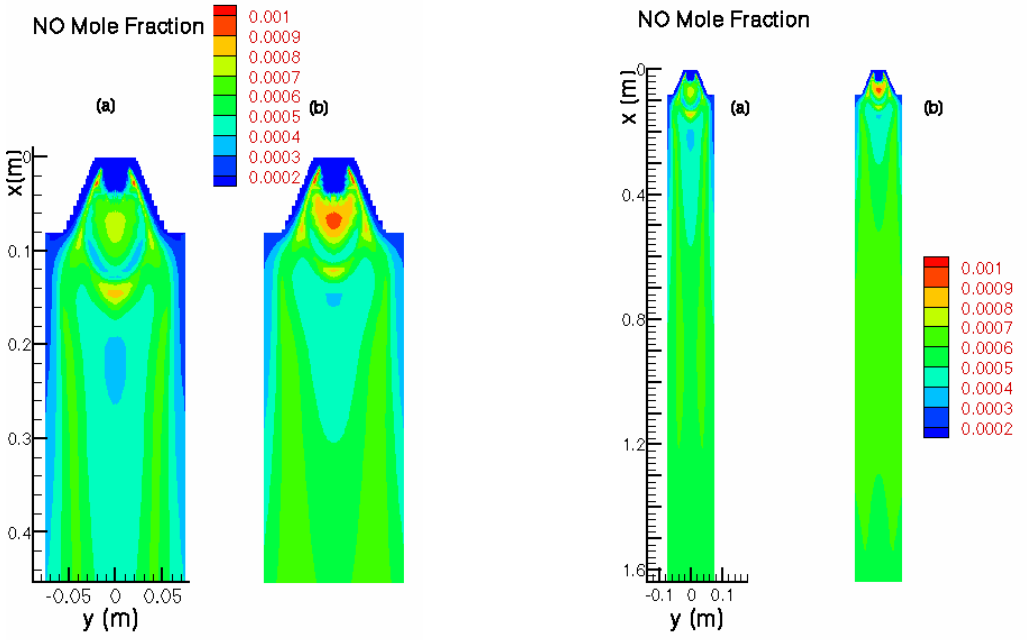

Figure 4.160: NO distributions in center plane for coal-LB blend combustion. (a) Swirl number = 0.7. (b) Swirl number = 1.0. Left two figures: near burner region. Right two figures: whole furnace.

Figure 4.162 gives P_4O_{10} profiles along the furnace axis. No experimental data is available for P_4O_{10} distribution. P_4O_{10} is high in the flame core below 1350 K (1970 ºF), but low in the high temperature post-flame region. The high P_4O_{10} region is found smaller and closer to burner as the swirl number increases because the flame length decreases with increasing the swirl number. In the post flame region, the P_4O_{10} level is higher for higher swirl number due to the higher O_2 concentration (Wei, 2002). Recall that increasing O_2 concentration causes more P_4O_{10} and less PO_2 levels from reaction equation (2). The effect of swirl number on P_4O_{10} concentration is not significant in the downstream region and at furnace exit. The cross-sectional averaged P_4O_{10} level decreases slightly and PO_2 level increases slightly.

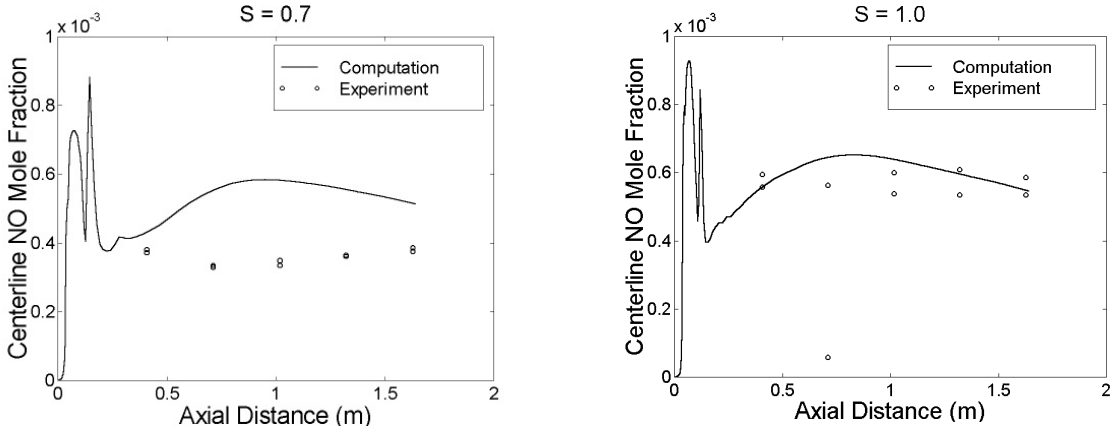

(a) (b0

Figure 4.161: Profiles of centerline NO for coal-LB blend combustion. Symbols represent experimental data. (a) Swirl number = 0.7. (b) Swirl number = 1.0.

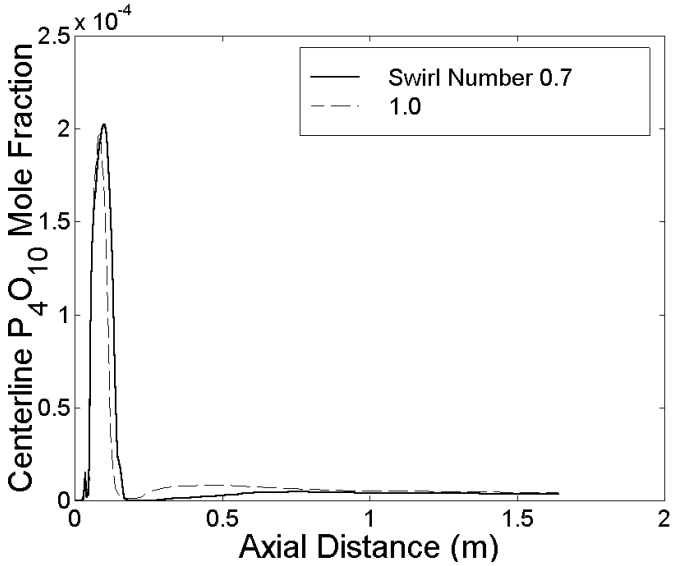

Figure 4.162: Profiles of centerline P_4O_{10} for coal-LB blend combustion with swirl number 0.7 and 1.0.

Figure 4.163 presents PO_2 profiles along the furnace centerline. Again no experimental data is available for PO_2 distribution. Contrary to P_4O_{10} distribution, PO_2 is low in the flame core but high in the high temperature post-flame region. It is observed that the post-flame high PO_2 region shifts closer to burner as the swirl number increases because higher swirl number causes shorter flame. In the post flame region, the PO_2 level is lower for the higher swirl number due to the higher O_2 levels (Wei, 2002). The effect of swirl number on PO_2 concentration is not significant in the downstream region and at furnace exit where PO_2 decreases slightly as the swirl number increases.

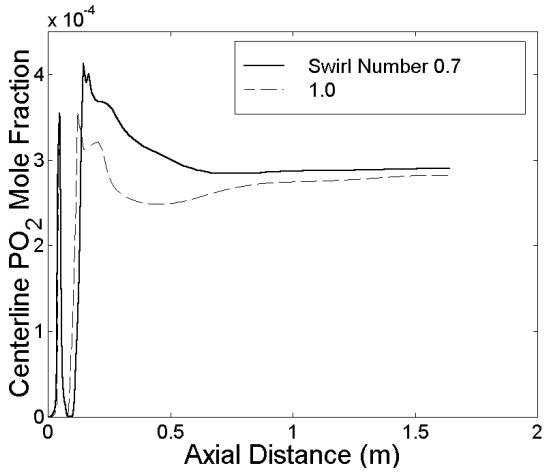

Figure 4.163: Profiles of centerline PO_2 for coal-LB blend combustion with swirl number 0.7 and 1.0.

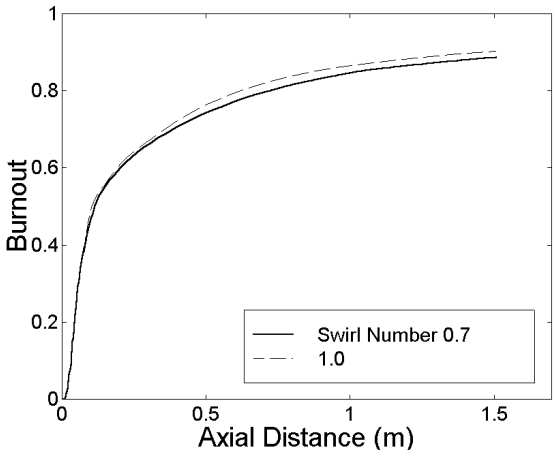

Figure 4.164: Burnout versus axial distance for coal-LB blend combustion with swirl number 0.7 and 1.0.

Distribution of the burnout fraction of the fuel is shown in Figure 4.164. The sharp increase of burnout near burner is due to pyrolysis, and the mild increase after that is due to char burning. It is found the swirl number has very weak influence on the burnout during pyrolysis. However, during

char burning, burnout increases with the swirl number due to stronger mixing of the secondary air with fuel and higher oxygen availability to char oxidation.

4.4.1.2b. Excess air effects

In the present study, different levels of excess air are achieved by adjusting flow rate of the secondary air only. Since the secondary air is swirled, increasing the excess air increases both the axial and angular momentum of the secondary air. Increasing the angular momentum causes 1) stronger recirculation flow near burner, namely, stronger reverse flow and stronger suction effect, 2) stronger air-fuel mixing, and 3) shorter flame length. Thus, effects of excess air on combustion could be similar to the effects of swirl number on the combustion.

Numerical predictions are conducted for combustion of coal-LB blend with 5 %, 10 %, 15 % and 20 % excess air. The mass ration of wet coal to LB is 9:1 in fuel blend. The fuel flow rate is 0.00133 kg/s (79.8 g/min) to obtain a maximum of 30 kW thermal power throughput rate. Figure 4.165 presents velocity vector distributions in the center plane near the burner. It is found that increasing the excess air, the velocity of the reverse flow increases, i.e., the recirculation flow gets stronger. The primary jet can penetrate the reverse flow for excess air less than 10 %. For 15 % and 20 % excess air, the lengths of reverse flow along furnace axis are 0.06 m (2.4 “) and 0.09 m (3.5 “) respectively. It is also observed that the secondary jet along the wall gets stronger as the excess air level increases because the axial momentum of the secondary air is stronger for higher excess air. Since the increasing reverse flow weakens the primary jet the primary jet becomes shorter (length between fuel exit and forward stagnation point) as excess air increases. Figure 4.166 shows temperature distributions in the furnace center plane. It is observed that the flame moves closer to burner as excess air percentage increases. In the quarl, a thin layer of high temperature surrounds the flame core because the local air-volatile ratio is around stoichiometric conditions.

Figure 4.167 gives profiles of NO along the furnace axis. It is found that excess air has significant effects on NO distribution. Similar to swirl number effect, there exist two opposite trends near the burner as excess air increases: 1) more oxygen is available and air-fuel mixing is stronger causing higher NO production, 2) less air is entrained due to shorter flame length causing less NO production. Due to local dominance of the first trend it is found that NO level inside the quarl significantly increases with increasing the excess air percentage. The high peak of NO outside the quarl moves closer to the burner as the excess air increases due to the increasing suction effect, whereas its value changes little because the two opposite trends have similar strengths in that region. In the downstream part of the furnace, NO level is higher for higher excess air because more O_2 is available. Comparing with experimental data, NO mole fraction is over-predicted moderately.

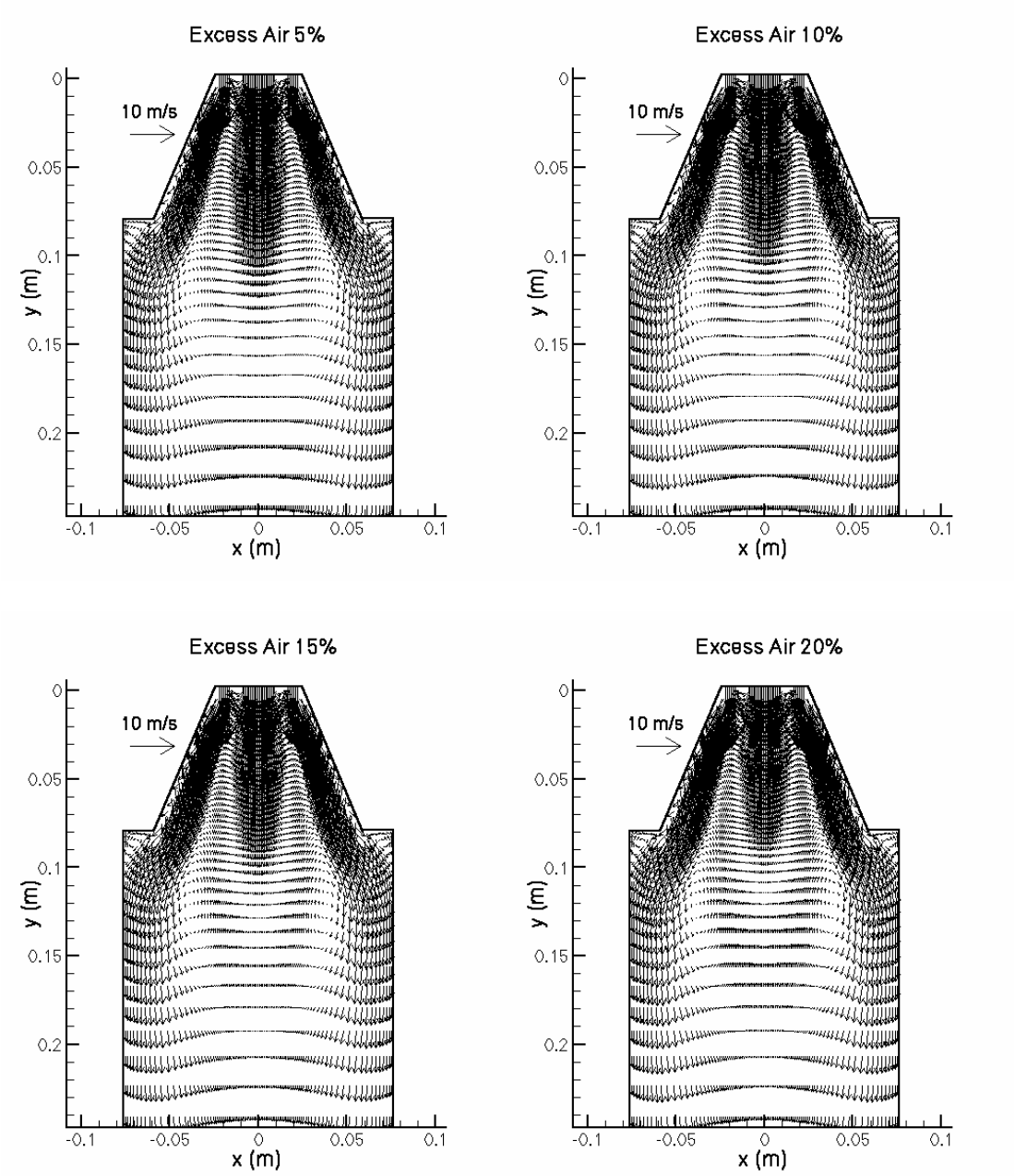

Figure 4.165: Velocity vectors near burner in center plane for coal-LB blend combustion at different excess air levels.

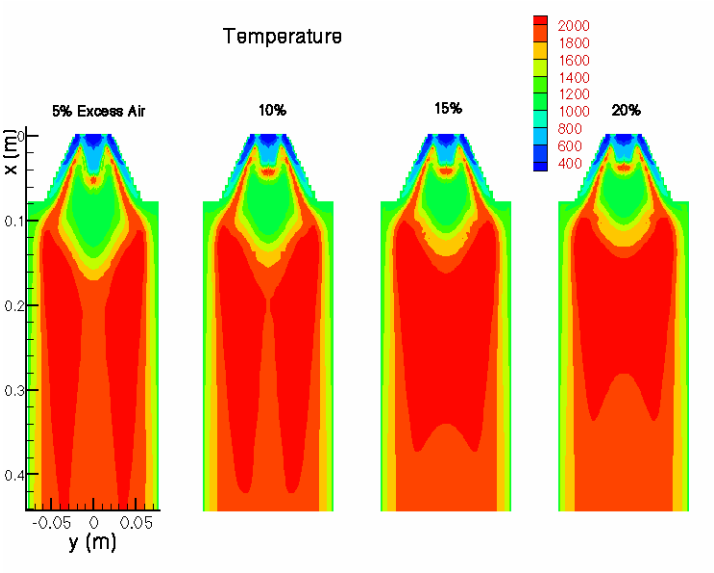

(a)

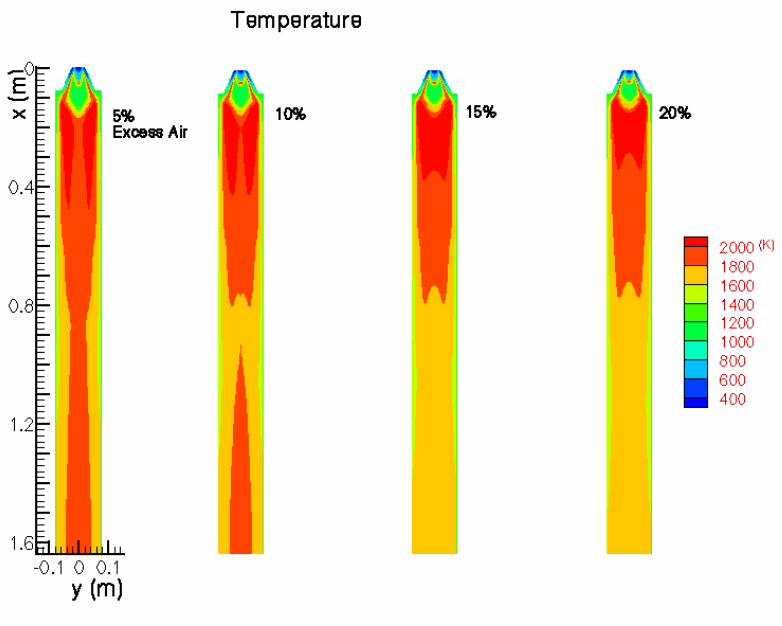

(b)

Figure 4.166: Temperature distributions in center plane for coal-LB blend combustion at different excess air levels. (a) Near burner region. (b) Whole furnace

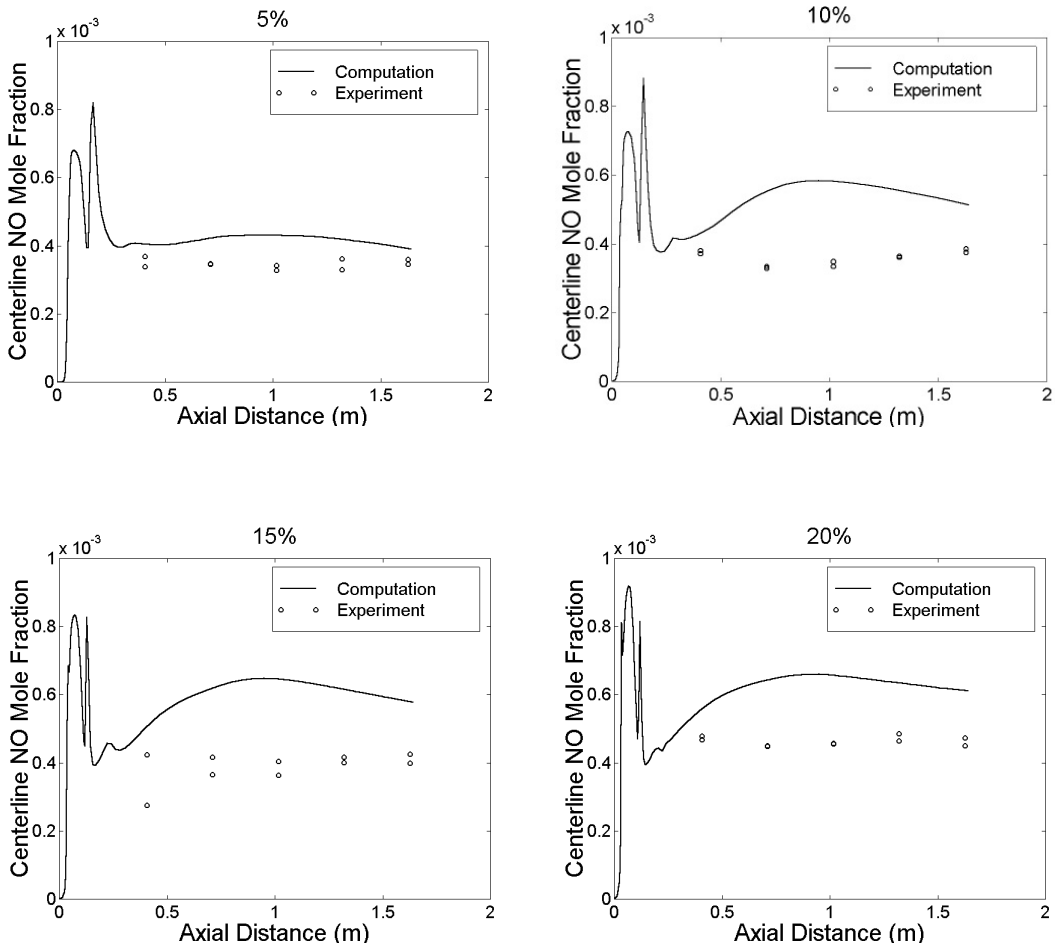

Figure 4.167: Profiles of centerline NO for coal-LB blend combustion at different excess air levels. Symbols represent experimental data.

Figure 4.168 shows distributions of P_4O_{10} along the furnace central axis. Unfortunately, no experimental data is available to compare the computational results. As the excess air increases, the high P_4O_{10} region inside flame core shifts closer to burner due to the decreasing flame length, while the low P_4O_{10} level in the post-flame region increases slightly due to increase in O_2 concentration. The excess air does not affect the peak value of P_4O_{10} near the burner because O_2 in the flame core is mainly from the primary air. Figure 4.169 gives PO_2 profiles along the furnace axis. Unfortunately, no experimental data is available. It is observed that the post-flame high PO_2 region shifts closer to burner as excess air level increases because higher excess air causes shorter flame. In the post-flame region, the PO_2 level is lower for higher excess air due to higher O_2 levels. At furnace end, the cross-sectional averaged PO_2 mole fraction decreases from 271 ppm to 243 ppm by 10.3% as excess air increases from 5 % to 20 %, resulting in slightly lower PO_2 emissions.

Computations for combustion of only coal (without blending with biomass) are also conducted for 5 %, 10 %, 15 % and 20 % excess air percentages and the results compared with those of coal-LB blend combustion. The feed rate of coal is 0.00127 kg/s (75.9 g/min) for the maximum of 30 kW_t (100,000 Btu/h) power throughput rate. Figure 4.170 gives cross-sectional averaged NO levels versus axial distance. Due to the higher fuel nitrogen of LB than coal, coal-LB combustion yields higher NO level than coal combustion. Figure 4.171 presents NO emissions at furnace exit. It

is clear NO emission increases with increasing excess air. For both coal and coal-blend combustion, NO emission is slightly lower than 0.26 kg/GJ (0.274 kg/mmBtu) for 5 % and 10 % excess air but higher than that for 15 % and 20 % excess air.

4.4.1.2c. Moisture effects

a) Fuel blend moisture

Moisture in fuel is regarded as liquid water, and its latent heat is significant (2444 kJ/kg (2578 Btu/kg)). Under combustion condition, since more heat is taken from fuel particles with higher moisture content during vaporization, increasing moisture level could decrease particle temperature thus delay occurrences of pyrolysis and char burning causing increased flame standoff distance, lower burnout, and variations in pollutant emissions. Combustion behavior could also be affected by moisture content due to the reaction (1), especially in the near the burner region where H_2O level is high.

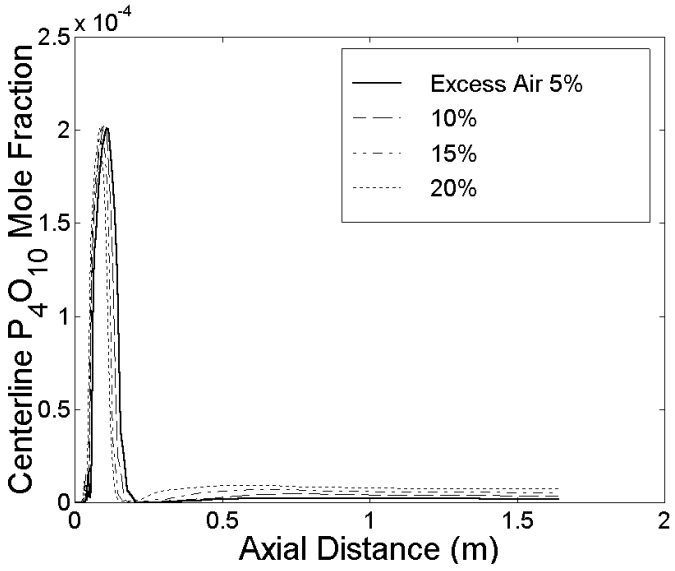

Figure 4.168: Profiles of centerline P_4O_{10} for coal-LB blend combustion at different excess air levels.

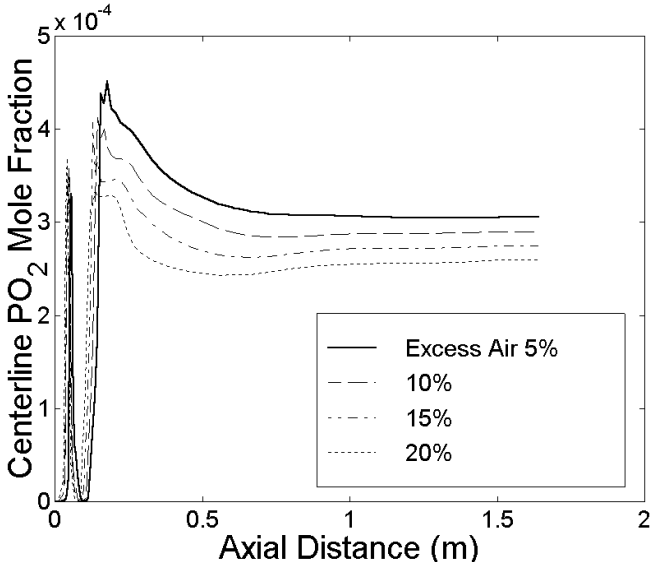

Figure 4.169: Profiles of centerline PO_2 for coal-LB blend combustion at different excess air levels.

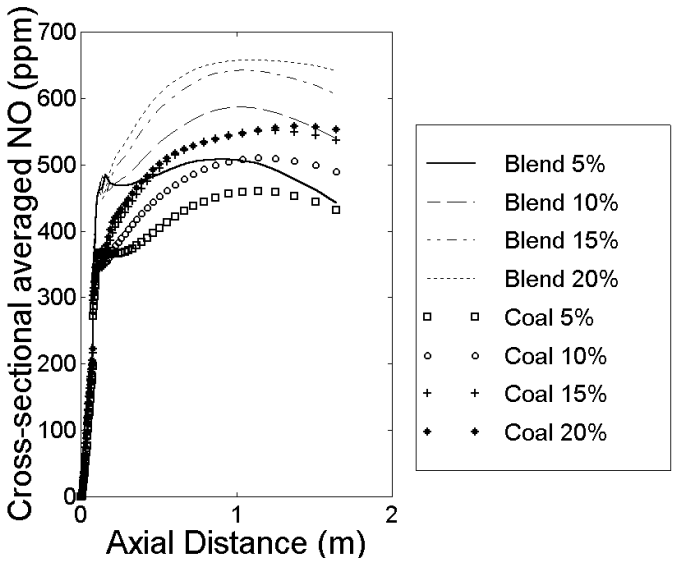

Figure 4.170: Cross-sectional averaged NO versus axial distance for coal and coal-LB combustion's at different excess air levels.

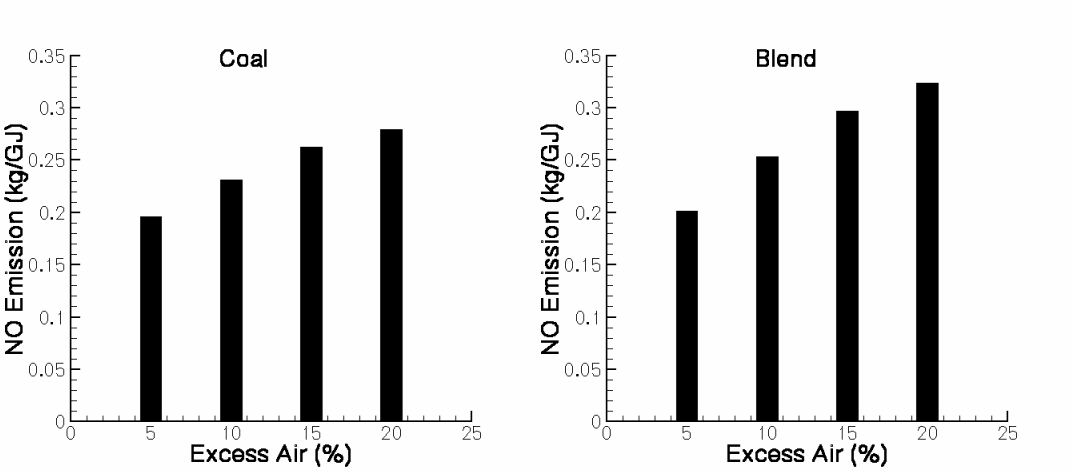

Figure 4.171: NO emission at furnace exit for coal and coal-LB combustion at different excess air levels.

Assuming coal and LB have the same moisture percentage, numerical predictions for coal-LB blend combustion are conducted for 10 %, 20 % and 30 % moisture contents in fuel blend. Mass ratio of coal (dry) to LB (dry) in fuel blend is kept as 9:1. The flow rate of wet fuel blend varies with moisture content, but the effective flow rate for the dry part of fuel blend is fixed at 1.133 kg/s to maintain 30 kW (100,000 Btu/h) thermal power throughput rate with excess air at 10 % and swirl number of 0.7. Adiabatic thermal boundary conditions are used to avoid additional complexities introduced by heat loss through wall. Unfortunately no experimental data is available to compare with the computational results.

Figure 4.172 show the cross-sectional averaged burnout versus axial distance. It is obvious that burnout decreases with increasing moisture content. At the furnace exit, burnout is 0.909, 0.892 and 0.874 for 10 %, 20 % and 30 % moisture respectively. It is also found that, apart from excess air and swirl number which influence burnout during char burning stage, moisture affects burnout in both the pyrolysis and char burning stages.

Figure 4.173 shows temperature distributions in the furnace center plane. It is observed that the flame length increases with increasing the moisture level. In the flame core, temperature decreases as moisture level increases because more heat is removed from gas phase during vaporization at higher moisture level. Figure 4.174 presents temperature profiles along the furnace axis. The sharp peak near the burner corresponds to the small high temperature area very close to the primary inlet. The second high peak corresponds to the flame location. However, in the post flame region, temperature around the centerline is slightly higher for higher moisture since fuel is lean in the gas phase, and more fuel offgas exists around the axis as moisture content increases (Wei, 2002).

Figure 4.175 presents H_2O profiles along the furnace axis. As described previously, there is high H_2O region in quarl due to strong vaporization followed by a comparatively low H_2O region due to reaction (4.4.I). In the post-flame region, H_2O is reproduced due to oxidation of the combustible gases by the secondary air. It is seen that H_2O increases significantly almost everywhere in furnace as moisture content increases from 10 % to 30 %.

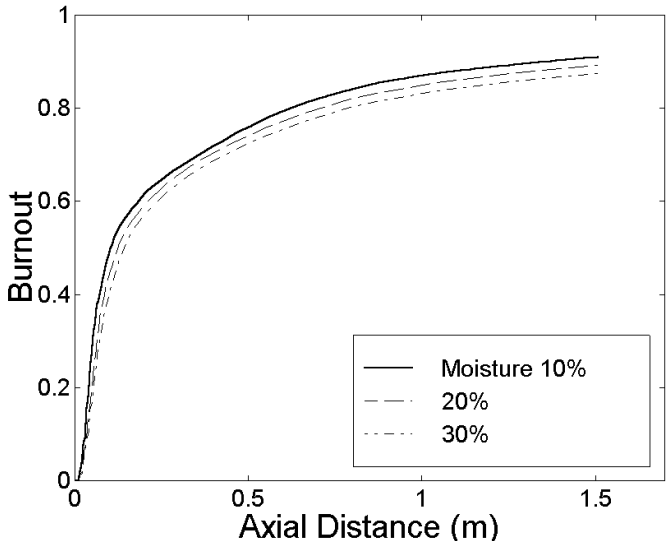

Figure 4.172: Burnout versus axial distance for coal-LB blend combustion at different blend moisture levels.

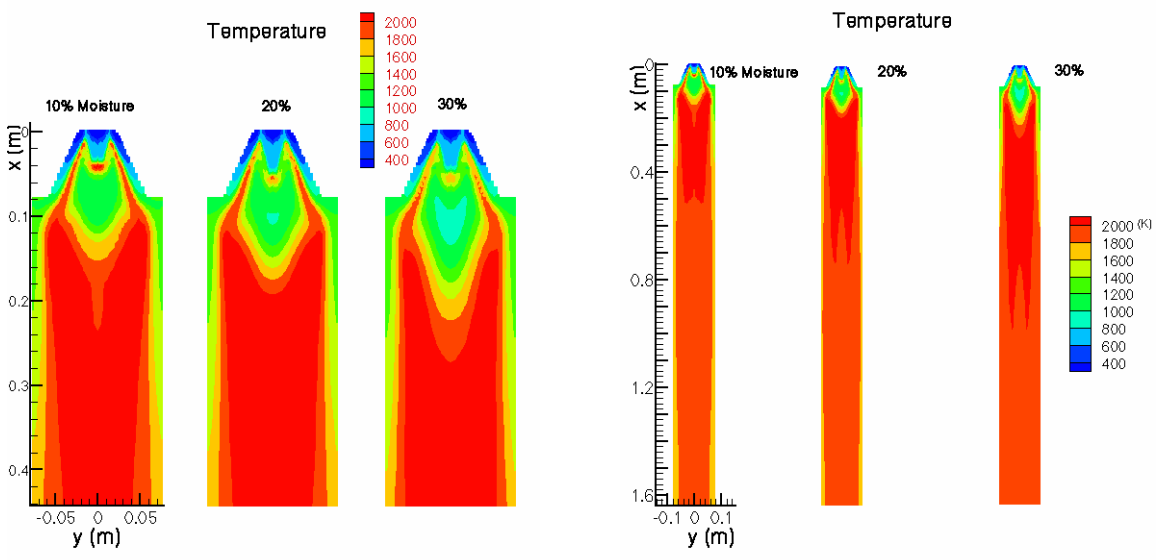

(a) (b)

Figure 4.173: Temperature distributions in center plane for coal-LB blend combustion at different blend moisture levels. (a) Near burner. (b) Whole furnace.

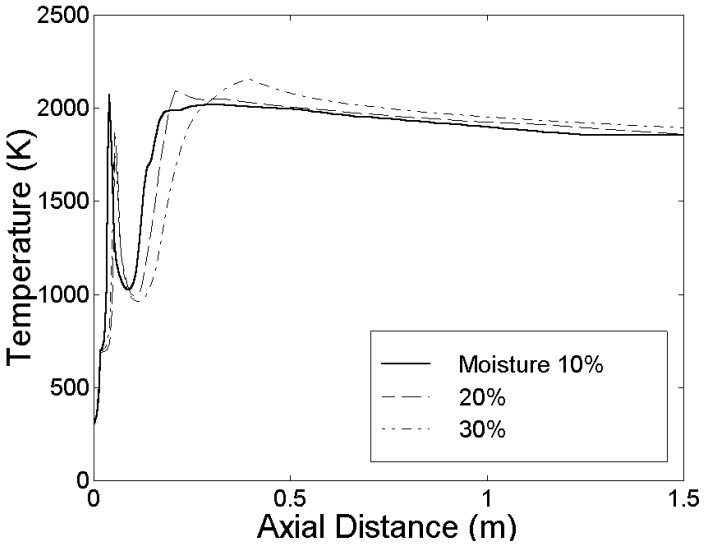

Figure 4.174: Profiles of centerline temperature for coal-LB blend combustion at different blend moisture levels.

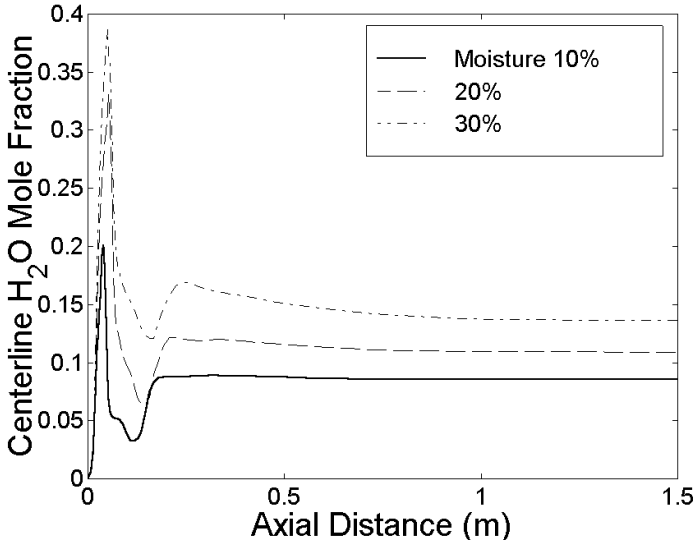

Figure 4.175: Profiles of centerline H_2O for coal-LB blend combustion at different blend moisture levels.

The CO mole fraction distributions are presented in Figure 4.176. Due to the moisture evaporation delay, the high CO region near burner becomes larger in size and moves farther away from burner as the moisture content increases. It is also seen that the peak value of CO level decreases with increasing the moisture content due to release of more water vapor near the burner as moisture content increases, causing higher transformation of CO into CO_2 through reaction (4.4.I). Figure 4.177 shows CO profiles along the furnace axis. It is found that in the post-flame region (i.e.

after the second peak of CO), CO increases with increasing moisture content. This is possibly due to the vaporization delay effect on combustion.

Figure 4.178 shows NO distributions in the center plane. Figure 4.179 gives the cross-sectional average NO mole fraction versus the axial distance. With increasing moisture level, the high NO region around the quarl moves away from burner due to the vaporization delay. In the downstream region, NO level decreases as the moisture content increases. This is due to lower burnout, or less nitrogen release at higher moisture levels. Since the gas phase is fuel lean, less nitrogen release causes less NO production. Figure 4.180 shows NO emission at furnace exit for different moisture levels. For moisture content 10 %, 20 % and 30 %, NO emission at furnace exit is below the 0.26 kg/GJ (0.274 kg/mmBtu).

Figure 4.181 shows the P_4O_{10} profiles along the furnace axis. The high P_4O_{10} region inside flame core shifts away from the burner as moisture increases due to vaporization delay on pyrolysis. It is also found that the peak value of P_4O_{10} concentration decreases as fuel moisture content increases, which is attributed to the decrease of O_2 concentration (see Wei, 2002). As mentioned previously, less O_2 causes less P_4O_{10} but more PO_2 due to reaction (2). At the furnace exit, the cross-sectional averaged P_4O_{10} level increases slightly.

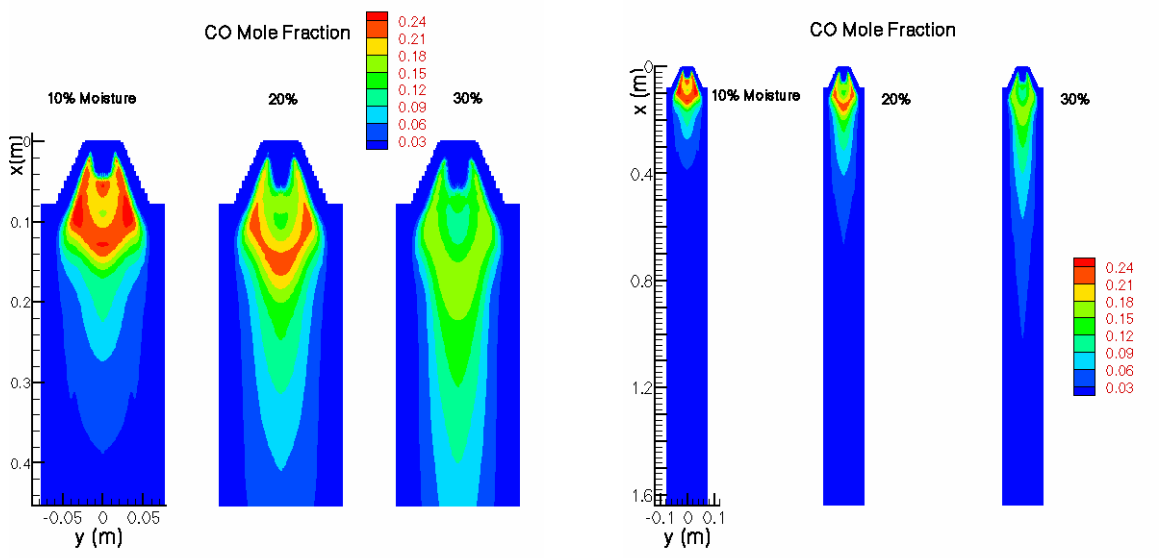

(a) (b)

Figure 4.176: CO distributions in center plane for coal-LB blend combustion at different blend moisture levels. (a) Near burner. (b) Whole furnace.

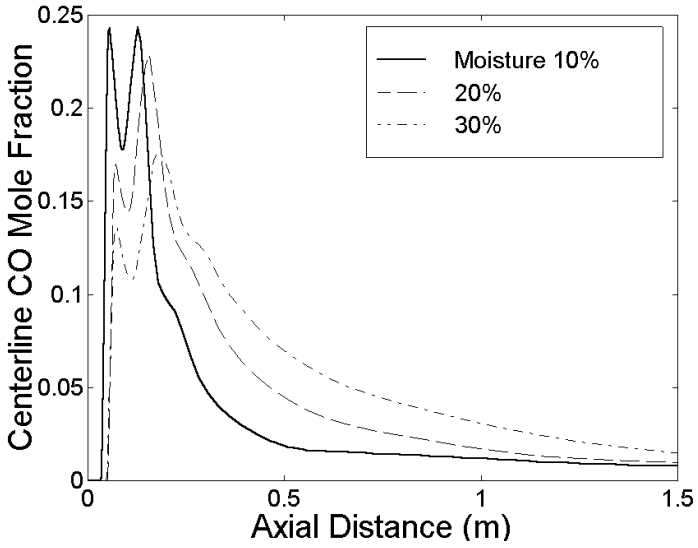

Figure 4.177: Profiles of centerline CO for coal-LB blend combustion at different blend moisture levels.

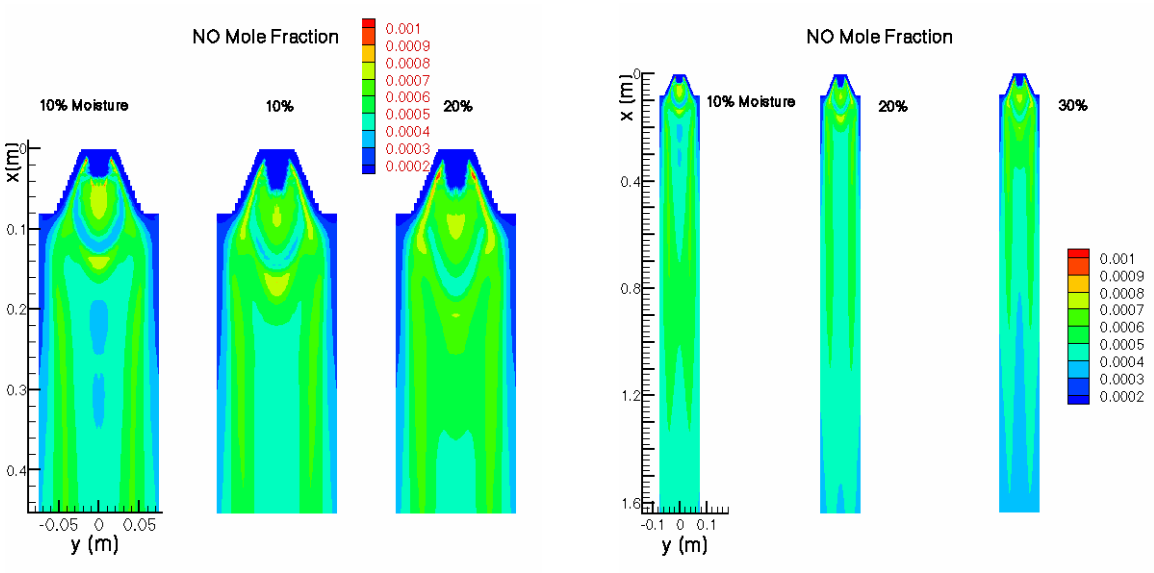

(a) (b)

Figure 4.178: NO distributions in center plane for coal-LB blend combustion at different blend moisture levels. (a) Near burner. (b) Whole furnace.

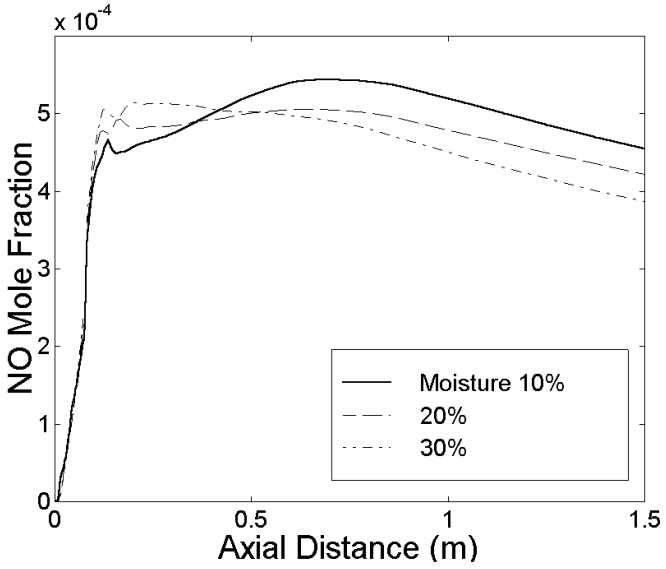

Figure 4.179: Cross-sectional averaged NO versus axial distance for coal-LB blend combustion at different blend moisture levels.

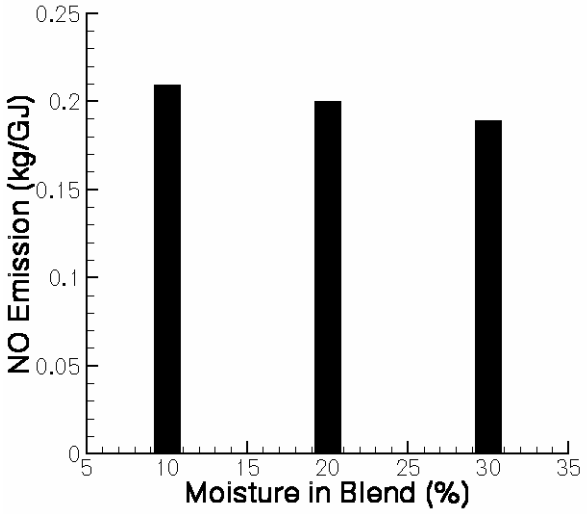

Figure 4.180: NO emissions at furnace exit for coal-LB blend combustion at different blend moisture levels.

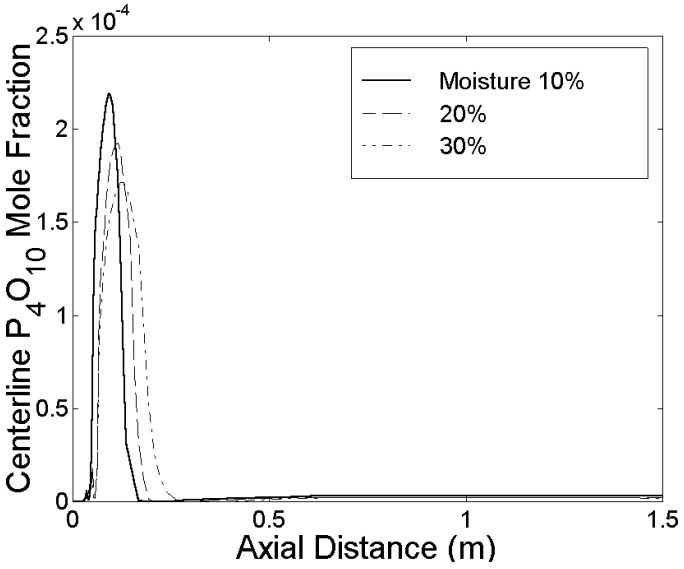

Figure 4.181: Profiles of centerline P_4O_{10} for coal-LB blend combustion at different blend moisture levels.

Figure 4.182 shows the PO_2 profiles along the furnace axis. As moisture increases, the post-flame high PO_2 region outside the quarl shifts away from the burner due to the increasing flame length, and its peak value decreases because more O_2 is available to oxidize PO_2 into P_4O_{10}. At the furnace exit, as moisture content in fuel mixture increases from 10 % to 30 % the cross-sectional averaged PO_2 level decreases from 274 to 244 ppm.

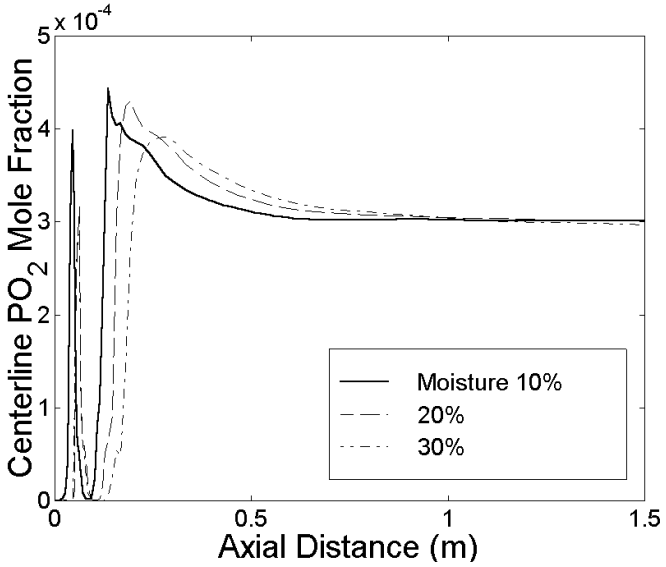

Figure 4.182: Profiles of centerline PO_2 for coal-LB blend combustion at different blend moisture levels.

b) Biomass moisture

Assuming coal to be dry while LB has 10 %, 20 % and 30 % moisture content, numerical computations are carried out for combustion of coal-LB blend to investigate the effects of biomass moisture. Mass ratio of coal to LB (dry part) is 9:1 in fuel blend. Other parameters are the same as in section 3.1. Figure 4.183 shows the variation of the cross-sectional averaged burnout with axial locations. Burnout distributions are found similar for different biomass moisture contents. Increasing biomass moisture from 10 % to 30 % means moisture content in fuel blend increases from 1 % to 3 % only. Such a small moisture increase could not influence the combustion. Figure 4.184 shows temperature profiles along the furnace centerline. Temperature distribution does not change significantly with moisture, and no obvious increase of flame length is found, which indicate biomass moisture does not affect flame structure when the fuel blend contains small fraction of biomass (weight basis). Figure 4.185 shows the NO profiles along the furnace centerline. Different biomass moisture levels give similar NO distributions. In the post-flame region, NO increases very slightly with increase in moisture content of biomass. The computational results show that when biomass fraction in fuel blend is low (10 %), increasing moisture content in biomass does not cause significant changes in flame length, flame structure, temperature distribution, and species distributions.

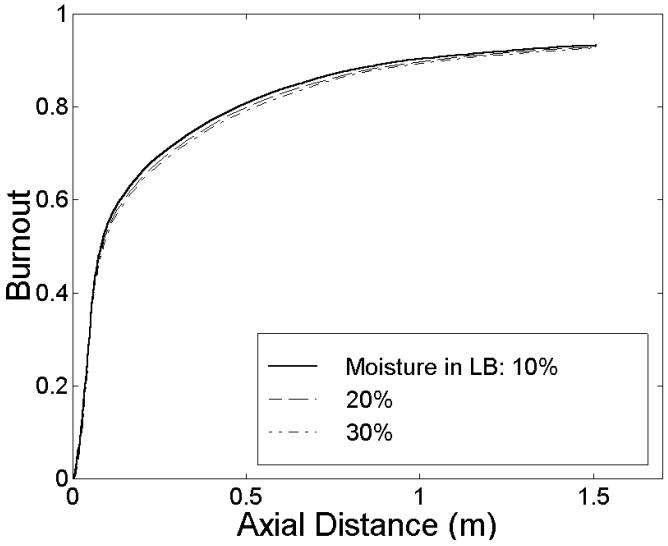

Figure 4.183: Burnout versus axial distance for coal-LB blend combustion at different biomass moisture levels.

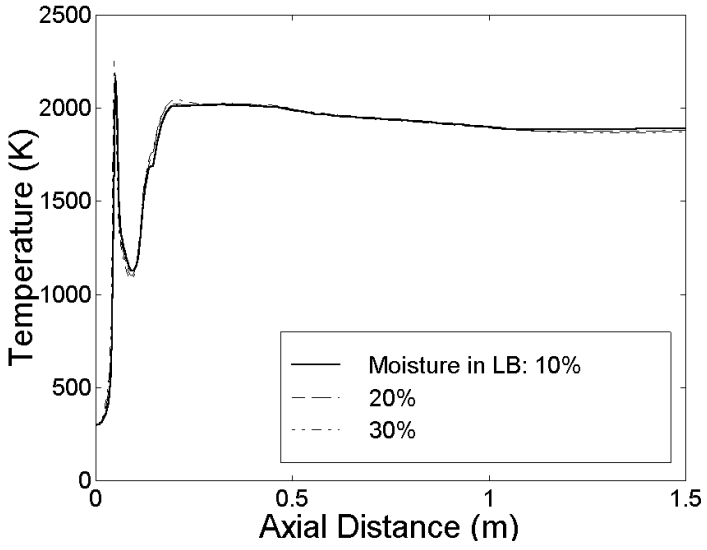

Figure 4.184: Profiles of centerline temperature for coal-LB blend combustion at different biomass moisture levels.

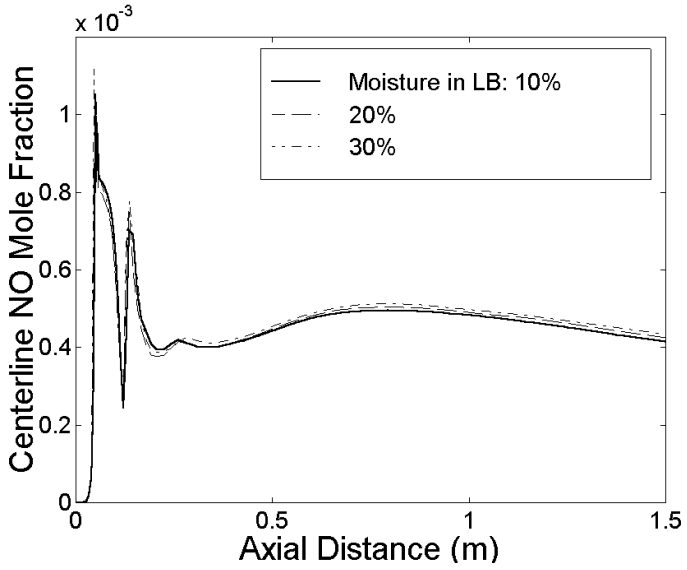

Figure 4.185: Profiles of centerline NO for coal-LB blend combustion at different biomass moisture levels.

4.4.2. Reburn Modeling

Reburn technology is a process where the NO_x produced by coal fired main burners is reduced with additional burners called reburners fired with natural gas or coal as reburn fuel under slightly fuel rich conditions. When animal waste was used as a reburn fuel, the reduction of NO was found to be of the order of 80% and almost independent of stoichiometry upto 10% deficient air. In order to understand the mechanisms governing NO reduction, a reburn model is presented here to predict the capture of NO_x by reburn fuel. The main fuel flow typically supplies 80-90 % of required thermal output while the remainder is supplied by reburn fuel. Thus, given the rating of the burner and heating values, the flow rates of main fuel and reburn fuel can be calculated. The main fuel $CH_X O_Y N_X$ is fired along with air and "x" moles of NH_3 to simulate the desired amount of NO_x. The "x" value is calculated assuming complete oxidation of NH_3 into NO and H_2O. Flame temperature and species mass fractions are calculated assuming complete combustion and given percentage of heat loss. The hot NO containing main gases are assumed to mix with cold reburn fuel stream. An exponential mixing model is used to simulate the mixing of main burner product gas jet along with the reburn jet in the reburn zone. As the reburn jet mixes with hot main gases, temperature of gas increases which in turn heats up the particles in the reburn jet. The solid particle in the reburn stream is assumed to undergo pyrolysis producing char, volatiles, fuel bound nitrogen (FBN) compounds and ash; further the char along with char N reacts heterogeneously to produce CO, CO_2, CH_4, NO etc. The pyrolysis and evolution of FBN are assumed to be first order and volumetric while the heterogeneous reactions occur with constant density. The volatile matter is assumed to consist of CO_2, CH_2, and H_2 while the gaseous N compounds released by particles include HCN, NH_3, and N_2. The mass fraction of each species evolving from fuel nitrogen can be given as input into the code, or the empirical curve fit data for coal and biomass can be used to calculate the product distribution of N into the gas phase. The global reaction schemes are used to depict the NO formation and destruction process in the reburn zone. Upto 5 homogeneous reactions involving FBN, 4 homogenous reactions involving oxidation of volatiles (CO, H_2, CH_2, CH_4) and 6 heterogeneous reactions (C+1/2 O_2 producing CO and CO_2, C+CO_2, C+H_2O, C+H_2, C+NO) are used in the model. Blowing corrections are used in determining the species concentration at particle surface. Homogenous and heterogeneous reactions along with the mixing cause increased gas temperature and change in NO concentration. The input to the code are: a) Main burner: total heat throughput of the boiler burner, % heat input in main burner, heat loss from main burner, ultimate and proximate analysis, LHV of the fuel, percentage of excess air (main burner equivalence ratio), temperature, NO concentration required to be simulated; b) Reburner: Fuel property, ultimate and proximate analysis, initial particle size, LHV of the fuel, FBN pyrolysis distribution (optional), specific heat and density of the fuel, heat of pyrolysis of the volatile matter, distribution of O_2, CO_2, and N_2 in the reburn gas being supplied along with the reburn fuel, c) Reburn Zone: reburn equivalence ratio. The output results are particle dia d_p, density ρ_p, particle burn rate $\dot{m}_p$, gas phase temperature T_g, particle temperature T_p, and mass fraction of species Y_k including NO distribution in the reburn zone as a function of time. Note that the current model accounts for combustion of main fuel and reactions between reburn fuel and main-burner gases. Due to the small-scale test facility, the experimental data have been generated without 'overfire' air, so an 'overfire' air model has not been incorporated into the code.

4.4.2.1. Main Burner Modeling

The main burner is modeled to burn any fuel having an empirical formulae $CH_X O_Y N_X$ along with NH_3 to simulate the desired amount of NO_x entering the reburn zone. The NH_3 injection is dependent on the amount of NO_x required down stream of the main burner. The assumptions in the main burner modeling are:

a) The main burner fuel $CH_XO_YN_X$ is assumed to oxidize completely in the main burner zone.

b) The production of NO_x is solely attributed to the complete oxidation of NH_3 introduced with the main fuel. The model ignores Thermal and Fuel NO_x formation. The equation represents the overall reaction in the main burner zone.

c) In case NO_x is produced by certain % of conversion of N in fuel to NO (can be specified as an input to the code), then one may set NH_3 moles to be zero (w = 0).

$$CH_xO_yN_z + wNH_3 + \left(1+\frac{a}{100}\right)\left(1+\frac{x}{4}-\frac{y}{2}\right)(O_2+3.76N_2) \rightarrow CO_2 + \left(\frac{x}{2}+\frac{3w}{2}\right)H_2O$$
$$+\left(\frac{a}{100}\left(1+\frac{x}{4}-\frac{y}{2}\right)-\frac{5w}{4}\right)O_2 + (w+zf_N)NO + \left[\frac{(1-f_N)z}{2}+3.76\left(1+\frac{a}{100}\right)\left(1+\frac{x}{4}-\frac{y}{2}\right)\right]N_2 \quad \text{(4.4.III)}$$

For a given thermal throughput (boiler rating), and fraction of total heat throughput through the main burner, the mass flow rate of fuel in the main burner is calculated as

$$\dot{m}_{fuel} = \frac{HTP_{f,MB} \times R_{Boiler}}{LHV_{MB}} \quad (4.4.10)$$

The temperature of the burnt gases leaving the main burner is calculated taking into account the heat loss in the main burner zone. The heat loss from the main burner zone is defined as a fraction of the Lower Heating Value (LHV) of the main burner fuel.

The temperature is calculated from the energy balance between the inlet and outlet of the main burner. Assuming that the main burner fuel, the primary air, and NH_3 enter the main burner at room temperature (298 K (77 ºF)), the energy balance equation is given as

$$H_{in,mainburner} = H_{out,mainburner} + Q_{loss} \quad (4.4.11)$$

where Q_{loss} assumes positive values for losses.

$$H_{in,mainburner} = h_{f,fuel} + h_{t,fuel} + \frac{\dot{m}_{NH_3}}{\dot{m}_{fuel}}\left(h_{f,NH_3} + h_{t,NH_3}\right) + \frac{\dot{m}_{air}}{\dot{m}_{fuel}}\left(h_{t,air}\right)$$ (kJ/kg of main burner fuel supplied) **(4.4.12)**

$$\dot{m}_{fuel} = \dot{m}_{MB} \qquad \text{‘}_{MB}\text{’ main burner} \quad (4.4.12a)$$

$$h_{t,fuel} = \int_{T_{ref}}^{T_{MB,in}} c_{p_k} dT\,,\ h_{t,fuel} = h_{NH_3,fuel} = h_{air,fuel} = 0 \text{ if } T_{MB,\,in} = 298 \text{ K (77 ºF)}$$

The $h_{f,\,fuel}$ is calculated from the LHV of the main burner fuel.

$$h_{f,fuel} = \frac{\left(\overline{h}_{f,CO_2} + \frac{X}{2}\overline{h}_{f,H_2O}\right)}{MW_{fuel}} + LHV_{MB}$$ (kJ/kg of main burner fuel supplied) (4.4.13)

where $\bar{h}$, is in kJ/kmole

The heat loss in the main burner expressed as a fraction of the LHV of the main burner fuel, is calculated as

$$Q_{loss} = d \times LHV_{MB} \quad \text{(kJ/kg of main burner fuel supplied)} \tag{4.4.14}$$

Therefore from equation 3,

$$h_{f,fuel} + h_{t,fuel} + \frac{\dot{m}_{NH_3}}{\dot{m}_{fuel}}\left(h_{f,NH_3} + h_{t,NH_3}\right) + \frac{\dot{m}_{air}}{\dot{m}_{fuel}}\left(h_{t,air}\right) = \frac{\dot{m}_{prod,MB}}{\dot{m}_{fuel}}\left(\sum_k Y_k h_{T,k,MB}\right) + d \times LHV_{MB} \tag{4.4.15}$$

where

$$\dot{m}_{prod,MB} = \dot{m}_{NH_3} + \dot{m}_{MB} + \dot{m}_{air} \tag{4.4.16}$$

*The mass fraction of the individual species '*k*' is calculated as,*

$$Y_{k,MB} = \frac{X_{k,MB} MW_{k,MB}}{\sum_k X_{k,MB} MW_{k,MB}} \tag{4.4.17}$$

$$h_{T,k,MB} = h_{f,k,MB} + \int_{T_{ref}}^{T} c_{p_{k,MB}} dT \tag{4.4.18}$$

Therefore, the equation (7) can be written as

$$\sum_k Y_{k,MB}\left(h_{f,k,MB} + \int_{Tref}^{T} c_{p_{k,MB}} dT\right) = \frac{\dot{m}_{MB}}{\dot{m}_{prod,MB}}\left[\begin{array}{l}(1-d)LHV_{MB} + \dfrac{h_{f,CO_2} + \frac{X}{2}h_{f,H_2O}}{MW_{fuel}} + h_{t,fuel} + \\ \dfrac{\dot{m}_{NH_3}}{\dot{m}_{MB}}\left(h_{f,NH_3} + h_{t,NH_3}\right) + \dfrac{\dot{m}_{air}}{\dot{m}_{MB}}\left(h_{t,air}\right)\end{array}\right] \tag{4.4.19}$$

The temperature of the product leaving the main burner zone can be calculated from equation (4.4.19). A simple iterative scheme like the Newton Raphson method may be used for this purpose.

Therefore using equations (4.4.17) and (4.4.19) the mass fraction of the species in the product gas leaving the main burner zone and the temperature of the same can be calculated. The mass flow rate of a species '*k*' leaving the main burner can be calculated as

$$\dot{m}_{k,MB} = \dot{m}_{prod,MB} \times Y_{k,MB} \tag{4.4.20}$$

4.4.2.2 Reburn Fuel Model

Thien *et al*., 2001b, and Freeman *et al.*, 2003, have reported that Feedlot biomass can be used as an effective reburn fuel, to reduce the NO_x emissions from boiler burners. The chemical formula of the reburn fuel is given as $CH_{X1}O_{Y1}N_{Z1}$. The composition of the reburn fuel is assumed to be

$$CH_{X1}O_{Y1}N_{Z1} \xrightarrow{composition} FC + VM + FBN + Ash \quad \textbf{(4.4.IV)}$$

The different components of the solid fuel react differently.

FC is assumed to consist of pure carbon and gets oxidized via heterogeneous reactions (X – XV).

$$FC \xrightarrow{oxidized} CO_2, CO, CH_4 \quad \textbf{(4.4.V)}$$

Solid fuel pyrolysis is through finite kinetics, which depends on the type of reburn fuel. The volatile matter composition is assumed constant throughout the pyrolysis period of the fuel. The composition of the volatile matter is determined from the ultimate analysis of the reburn fuel by using atom balance and heating value of the reburn fuel along with heat of pyrolysis of the volatile matter. A single reaction model has been assumed for determining the volatile matter release rate from the solid fuel into the gas phase. The details of the reaction model shall be covered later in the report. The volatile matter composition is assumed to be,

$$CH_XO_Y \xrightarrow{Pyrolysis\,(Coal)} CO, CO_2, CH_4, H_2 \quad \textbf{(4.4.VI)}$$

$$CH_XO_Y \xrightarrow{Pyrolysis\ (Feedlot\ Biomass)} CO, CO_2, CH_4, H_2O \quad \textbf{(4.4.VII)}$$

$$FBN \xrightarrow{pyrolysis} HCN, NH_3, N_2 \quad \textbf{(4.4.VIII)}$$

$$FBN \xrightarrow{oxidized} NO \ \textit{(at the char surface)} \quad \textbf{(4.4.IX)}$$

Where FBN is fuel bound nitrogen. The FBN undergoes both pyrolysis (equation 4.4.VIII) and heterogeneous oxidation (equation 4.4.IX) at the char surface. A single reaction model is used for the pyrolysis of fuel nitrogen. The details of the reaction rate shall be discussed later in the report.

FBN is oxidized and pyrolyzed from the particle surface. The pyrolysis products of FBN are (equation 4.4.VIII) assumed to be N_2, NH_3, and HCN. The mass fraction of each species evolving from fuel nitrogen can be given as input into the code, or the empirical curve fit data for coal and biomass can be used to calculate the product distribution of N into the gas phase. For coal, the curve fit has been done from the experimental data given by William *et al.*, 1945, and for biomass, it has been done from the experimental data given by Zhou *et al.*, 2000.

The ash is assumed to be inert and undergoes no chemical and physical change during combustion of the reburn fuel in the reburn zone and is assumed to be retained in the fuel.

The mass flow rate of the reburn fuel supplied to the burner is calculated from the fraction of the heat throughput through the reburn fuel in the boiler burner.

$$\dot{m}_{RB,daf} = \frac{\left(1 - HTP_{f,MB}\right) \times R_{Boiler}}{LHV_{RB,daf}} \quad \textbf{(4.4.21)}$$

$$\dot{m}_{RB,as\cdot received} = \frac{\dot{m}_{RB,daf}}{\left(1 - Y_{RB,ash}\right)} \quad \textbf{(4.4.22)}$$

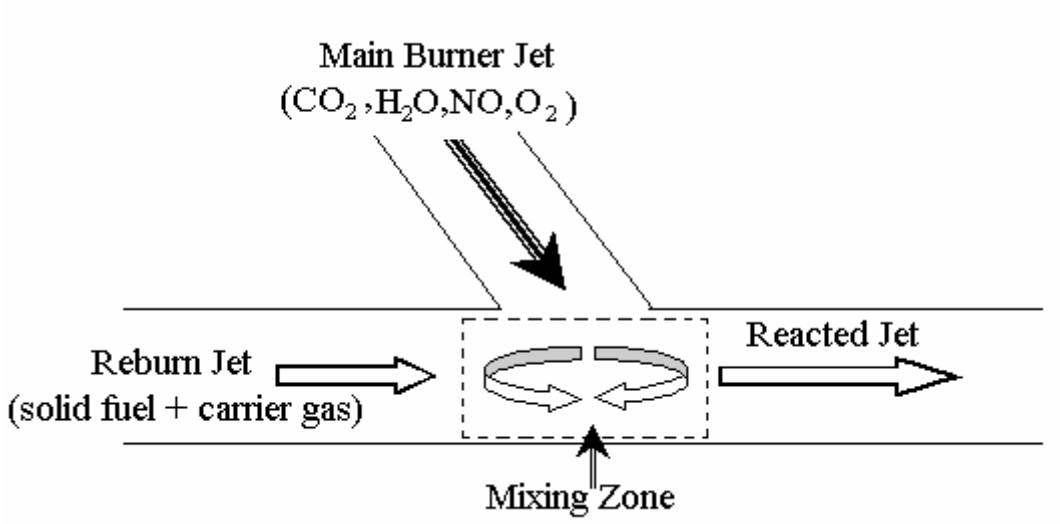

Figure 4.186: Schematic of the mixing model

4.4.2.3 Mixing Model Development

An exponential mixing model (Stickler *et al.,* (1983), Alzueta *et al.*, 1998) is used to simulate the mixing of main burner product gas jet along with the reburn jet in the reburn zone. Figure 4.186 shows a schematic of the mixing model used. In this model, the main-burner product gas jet is entrained into the reburn jet gradually, thus increasing the mass flow rate of the reburn jet. This particular model was used because of its simplicity to implement and more importantly in this model the reburn jet undergoes greater change in the stoichiometry during the mixing process and appears to lead to favorable results.

$$\dot{m}_{RB,t} = \dot{m}_{RB,t=0} + \dot{m}_{prod,MB}\left(1-\exp\left(-\frac{t}{\tau_{mix}}\right)\right) \qquad \textbf{(4.4.23)}$$

Therefore, the mass added to the reburn jet from the main burner jet in time period dt is

$$d\left(\dot{m}_{RB,t} - \dot{m}_{RB,t=0}\right) = d\dot{m}_{added} = \left[\frac{\dot{m}_{prod,MB}}{\tau_{mix}}\exp\left(-\frac{t}{\tau_{mix}}\right)\right]dt \qquad \textbf{(4.4.24)}$$

Since the global ϕ_{RZ} is given an input to the code, the O_2 supplied along with the reburn fuel is calculated from the following equation.

$$\phi_{RZ} = \frac{\dot{m}_{O_2,stoic}}{\dot{m}_{O_2,RZ}} = \frac{\dot{m}_{RB,fuel}\nu_{O_2}}{\dot{m}_{O_2} + \dot{m}_{O_2,RS}} = \frac{\dot{m}_{RB.fuel}\nu_N}{\dot{m}_{u.m} + \dfrac{\dot{m}_{RB,fuel}\nu_u}{Q_{RS}}} = \frac{\left(\dfrac{\dot{m}_{O_2}}{\dot{m}_{RB,fuel}}\right)_{Stoic,RZ}}{\left(\dfrac{\dot{m}_{O_2}}{\dot{m}_{RB,fuel}}\right)_{Act,RZ}} \qquad \textbf{(4.4.25)}$$

$\dot{m}_{O_2,stoic}$ stoichiometric O_2 required for unit mass of reburn fuel

$\dot{m}_{O_2,RZ}$ O_2 supplied from main burner and O_2 supplied through reburn injector

$$\nu_{O_2} = \left(1 + \frac{X1}{4} - \frac{Y1}{2}\right)\frac{MW_{O_2}}{MW_{fuel}} \quad \textbf{(4.4.26)}$$

$$\dot{m}_{O_2,MB} = \dot{m} Y_{O_2,MB} \quad \textbf{(4.4.27)}$$

Solving for ϕ_{RS}

$$\phi_{RS} = \frac{\dot{m}_{RB,daf}\left(\frac{MW_{O2}}{MW_{RB,daf}}\right)\left(1+\frac{X1}{4}-\frac{Y1}{2}\right)\phi_{RZ}}{\dot{m}_{RB,daf}\left(\frac{MW_{O2}}{MW_{RB,daf}}\right)\left(1+\frac{X1}{4}-\frac{Y1}{2}\right) - \phi_{RZ} Y_{O2,MB}\dot{m}_{prod,MB}} \quad \textbf{(4.4.28)}$$

Therefore, the mass flow rate of O_2 supplied along with the solid reburn fuel is calculated as,

$$\dot{m}_{O2,RS} = \frac{\dot{m}_{RB,daf}\left(\frac{MW_{O2}}{MW_{RB,daf}}\right)\left(1+\frac{X1}{4}-\frac{Y1}{2}\right)}{\phi_{RS}} \quad \textbf{(4.4.29)}$$

Since other gases like CO_2, and N_2 are also supplied along with the reburn O_2, the mass fraction or the composition of the gases supplied along with the reburn fuel are given as input in the code. The total mass flow rate of the gas phase supplied along with the solid reburn fuel is,

$$\dot{m}_{gas,RS} = \frac{\dot{m}_{O2,RS}}{Y_{O2,RS}} \quad \textbf{(4.4.30)}$$

Therefore, the mass flow rate of the gases supplied along with the solid reburn fuel are calculated as,

$$\dot{m}_{k,RS} = Y_{k,RS}\dot{m}_{gas,RS} \quad \textbf{(4.4.31)}$$

4.4.2.4 Chemical Reactions

4.4.2.4a. Homogeneous Reburn Reactions

The reburn reactions take place in the gas phase where the NO is primarily reduced and formed due to interaction with other species. The global reaction scheme is used to depict the NO formation and destruction process in the reburn zone. The reactions considered are,

1) Hydrocarbon (HC) reduction: Chen *et al.*, 1996

$$CH_x + NO \rightarrow HCN + products \quad \textbf{(4.4.X)}$$

where

CH_X is the summation of all the HC radical species present in the flame.

$$w_{NO,I} = -2.26\times10^9\, X_{NO} X_{CH_x} \exp\left(\frac{-76233}{RT_g}\right) \ \textit{(kmol/m}^3\textit{-s)} \quad \textbf{(4.4.32)}$$

2) Ammonia oxidation: De Soete, 1975

$$NH_3 + O_2 \rightarrow NO + H_2O + \tfrac{1}{2}H_2 \quad \textbf{(4.4.XI)}$$

$$w_{NH_3,II} = -4\times10^6 X_{NH_3} X_{O_2}^{b_{II}} \exp\left(\frac{-133900}{RT_g}\right) \text{ (1/s)} \quad \textbf{(4.4.33)}$$

where b_{II} the order of reaction with O_2 depends on X_{O2} in the gas phase, and is calculated by a curve fit from the data provided by De Soete, 1975. It is calculated as

$$\begin{aligned} &\ln(X_{O_2}) > -3, \quad b_{II} = 0 \\ &-5.671 \le \ln(X_{O_2}) \le -3, \quad b_{II} = curvefit \\ &\ln(X_{O_2}) < -5.671, \quad b_{II} = 1 \end{aligned} \quad \textbf{(4.4.34)}$$

3) Ammonia reduction: De Soete, 1975

$$NH_3 + NO \rightarrow N_2 + H_2O + \tfrac{1}{2} H_2 \quad \textbf{(4.4.XII)}$$

$$w_{NH_3,III} = -1.8\times10^8 X_{NH_3} X_{NO} \exp\left(\frac{-113000}{RT_g}\right) \text{ (1/s)} \quad \textbf{(4.4.35)}$$

4) HCN oxidation: De Soete, 1975

$$HCN + O_2 \rightarrow NO + CO + \tfrac{1}{2} H_2 \quad \textbf{(4.4.XIII)}$$

$$w_{HCN,IV} = -10^{10} X_{HCN} X_{O_2}^{b_{IV}} \exp\left(\frac{-280328}{RT_g}\right) \text{ (1/s)} \quad \textbf{(4.4.36)}$$

where b_{IV} the order of reaction with O_2 depends on X_{O2} in the gas phase, and is calculated by a curve fit from the data provided by De Soete, 1975. It is calculated as

$$\begin{aligned} &\ln(X_{O_2}) > -3, \quad b_{IV} = 0 \\ &-5.671 \le \ln(X_{O_2}) \le -3, \quad b_{IV} = curvefit \\ &\ln(X_{O_2}) < -5.671, \quad b_{IV} = 1 \end{aligned} \quad \textbf{(4.4.37)}$$

5) HCN reduction**:** De Soete, 1975

$$HCN + NO \rightarrow N_2 + CO + \tfrac{1}{2} H_2 \quad \textbf{(4.4.XIV)}$$

$$w_{NH_3,V} = -3\times10^{12} X_{HCN} X_{NO} \exp\left(\frac{-251000}{RT_g}\right) \text{ (1/s)} \quad \textbf{(4.4.38)}$$

4.4.2.4b. Other Homogeneous reactions

Apart from the NO_x reaction, there are other homogeneous reactions, which tend to consume the O_2 present in the reburn zone.

6) CO oxidation: Williams, 2000

$$CO + \tfrac{1}{2} O_2 \rightarrow CO_2 \quad \textbf{(4.4.XV)}$$

$$w_{CO,VI} = -4\times10^{14} [CO][O_2]^{0.25} [H_2O]^{0.5} \exp\left(\frac{-20202}{RT_g}\right) \text{ (kmol/m}^3\text{-s)} \quad \textbf{(4.4.39)}$$

7) H2 oxidation**:** Jones *et al.*, 1988

$$H_2 + \tfrac{1}{2} O_2 \rightarrow H_2O \qquad \textbf{(4.4.XVI)}$$

$$1.36\times10^{19}\, T_g^{-1}\left(\frac{Y_{H_2}}{2}\right)^{0.25}\left(\frac{Y_{O_2}}{32}\right)^{1.5}\rho_g^{1.75}\exp\left(\frac{-20130}{T_g}\right) \textit{(kglm}^3 - s) \qquad \textbf{(4.4.40)}$$

8) CH_4 oxidation**:** Bartok, 1991

$$CH_4 + 2O_2 \rightarrow CO_2 + 2H_2O \qquad \textbf{(4.4.XVII)}$$

$$w_{CH_4,VIII} = -2.8\times10^{9}\left[O_2\right]^{1.3}\left[CH_4\right]^{-0.3}\exp\left(\frac{-202600}{RT_g}\right) \textit{(kmol/m}^3\ s) \qquad \textbf{(4.4.41}\textit{)}$$

4.4.2.4b. Heterogeneous reactions:

The following heterogeneous reactions occur at the particle surface. The kinetic rate constants for the heterogeneous reactions are given as,

10) Carbon oxidation: Annamalai *et al.*, 1993

$$C + O_2 \rightarrow CO_2 \qquad \textbf{(4.4.XVIII)}$$

$$k_{C,X} = 1.6\times10^{5}\exp\left(\frac{-20000}{T_p}\right) \quad \textit{(1/s)} \qquad \textbf{(4.4.42}\textit{)}$$

11) Carbon Oxidation: Annamalai *et al.*, 1993

$$C + \tfrac{1}{2} O_2 \rightarrow CO \qquad \textbf{(4.4.XIX)}$$

$$k_{C,XI} = 2.3\times10^{7}\exp\left(\frac{-26200}{T_p}\right) \quad \textit{(1/s)} \qquad \textbf{(4.4.43)}$$

12) Carbon oxidation: Annamalai *et al.*, 1993

$$C + CO_2 \rightarrow 2CO \qquad \textbf{(4.4.XX)}$$

$$k_{C,XII} = 3.42T_p\exp\left(\frac{-15600}{T_p}\right) \quad \textit{(1/s)} \qquad \textbf{(4.4.44)}$$

13) Steam carbon reaction: Bryden *et al.*, 1996

$$C + H_2O \rightarrow H_2 + CO \qquad \textbf{(4.4.XXI)}$$

$$k_{C,XIII} = 1.67\times k_{C,XII} \quad \textit{(1/s)} \qquad \textbf{(4.4.45)}$$

14) Methane formation: Schoeters, 1985

$$C + 2H_2 \rightarrow CH_4 \qquad \textbf{(4.4.XXII)}$$

$$k_{C,XIV} = 3\times10^{-3}\times k_{C,XII} \quad \textit{(1/s)} \qquad \textbf{(4.4.46)}$$

15) C and NO reaction: Mitchel *et al.*, 1982

$$C + NO \rightarrow CO + \tfrac{1}{2} N_2 \qquad \textbf{(4.4.XXIII)}$$

$$k_{C,XV} = 1.57 \times 10^5 \exp\left(\frac{-34000}{RT_p}\right) \quad (1/s) \qquad \textbf{(4.4.47)}$$

The mass loss rate for each of the reactions X – XVI, is calculated as

$$\dot{m}_{C,i} = \rho_w k_{c,i} Y_{kr,w}^{n_i} \pi d_P^2 \qquad \textbf{(4.4.48)}$$

$$k_{C,i} = A_{C,i} \exp\left(\frac{-E_{C,i}}{RT_p}\right) \qquad \textbf{(4.4.49)}$$

The total carbon consumption rate for a particle of size d_p *is given as*

$$\dot{m}_C = \sum_{i=X}^{XV} \dot{m}_{C,i} \qquad \textbf{(4.4.50)}$$

In order to calculate heterogeneous reactions on the particle surface, the species concentration must be determined first. The species mass fraction at the particle surface ($Y_{kr,w}$) is calculated as follows.

With the assumption of a first order reaction ($n_i = 1$) at the particle surface, the analysis of the mass transfer across the frozen film yields the following expression for the species mass fraction at the particle surface (Annamalai and Puri, 2004).

$$Y_{k,w} = \frac{Y_{k,\infty}}{\exp(X)} + \frac{(\exp(X)-1)\left[Y_{k,pyro}\dot{m}_{pyro} + Y_{k,N-pyro}\dot{m}_{N-pyro} + Y_{k,N-oxi}\dot{m}_{N-oxi} + \left(\sum_l Sn_l \upsilon_{k,l} \rho k_{c,l} d_p \right) \right]}{\pi Sh \rho d_p DX \exp(X)} \qquad \textbf{(4.4.51)}$$

Where

$$X = \frac{\dot{m}_p}{\left(Sh \rho D \pi d_p\right)} \qquad \textbf{(4.4.50)}$$

$$\dot{m}_p = \dot{m}_{pyro} + \dot{m}_{N-pyro} + \dot{m}_c + \dot{m}_{N-oxi} \qquad \textbf{(4.4.50a)}$$

$$Sh = 2 + 0.6 \,\mathrm{Re}^{\frac{1}{2}} Sc^{\frac{1}{3}} \qquad \textbf{(4.4.51)}$$

Sn_l =-1 if a species 'k' is consumed at the particle surface, or +1 only if species is produced at the particle surface and if reaction order depends upon the species produced.

From the above equation (48), it can bee seen that the oxygen mass fraction at the particle surface ($Y_{k,w}$) is calculated in terms of the bulk gas mass fraction (Y_k) next to the particles by a mass balance that accounts for the blowing effects (Stefan flow) from the particle and chemical reactions at the surface.

4.4.2.4d Volatile Matter release from the solid reburn fuel:

A single reaction model has been assumed for determining the volatile matter release rate from the solid fuel into the gas phase.

$$\frac{dm_{pyro}}{dt} = \left(\frac{V_{\text{int}} - V}{V}\right) A_{pyro,fl} \exp\left(\frac{-E_{pyro,fl}}{RT_p}\right) m_{particle} \quad \textbf{(4.4.52)}$$

The activation energy for Wyoming coal (low sulfur coal) and feedlot biomass were given by Sami, 2000, and are tabulated in Table 4.49.

4.4.2.4e. FBN pyrolysis rate:

A single reaction model has been assumed to determine the N release rate from the solid into the gas phase Mitchel *et al.*, 1982.

$$\frac{dm_{N-pyro}}{dt} = k_{N-pyro} Y_N \left(\frac{V_{\text{int}} - V}{V_{\text{int}}}\right)^{0.364} m_{particle} \quad \textbf{(4.4.53)}$$

Where Y_N is the mass fraction of FBN in the fuel particle.

$$k_{N-pyro} = 2.63 \times 10^5 \exp\left(\frac{-142675}{RT_p}\right) \quad \textbf{(4.4.54)}$$

4.4.2.4f. FBN oxidation:

The FBN oxidation at the char surface is related to the char burning rate and is given as,

16) FBN oxidation at the fuel surface: Mitchel *et al.*, 1982

$$N_{(S)} + \tfrac{1}{2} O_2 \rightarrow NO \quad \textbf{(4.4.XXIV)}$$

$$\frac{dm_{N-oxid}}{dt} = \left(\frac{m_N}{m_{part}}\right) \frac{dm_{C,XV}}{dt} \quad \textbf{(4.4.55)}$$

4.4.2.5 Governing Transient equations

1) Species balance equation:

The gas phase species added to the gas phase from the solid particles is given as,

$$\frac{dm_k}{dt} = S_{pyro,k} + S_{Htr,k} + S_{Hmr,k} + S_{N-pyro,k} + S_{N-oxid,k} \quad \textbf{(4.4.56)}$$

The source terms are calculated from the reaction kinetics mentioned earlier in the previous section.

The overall mass conservation equation for the gas phase is,

$$\frac{dm_{gas}}{dt} = \frac{dm_{pyro}}{dt} + \frac{d|m_C|}{dt} + \frac{dm_{N-pyro}}{dt} + \frac{dm_{N-oxid}}{dt} \quad \textbf{(4.4.57)}$$

2) Particle diameter:

Assuming, that the decrease in particle size is due to oxidation of FC on the char surface the particle diameter is calculated as,

$$\frac{d\left(d_p\right)}{dt} = -\frac{2\dot{m}_C}{\pi\rho_p d_p^2} \quad \textbf{(4.4.58)}$$

In the current model, only one uniform particle size is used as the initial diameter of the reburn fuel particle. The user gives the initial particle size of the reburn fuel as input.

3) Energy equation for solid phase

The energy equation is used to calculate the particle temperature at the surface. Since the particle size is small (order of 100 μm), it is assumed to have uniform temperature. Thus, the surface temperature of the particle is also the bulk temperature of the particle.

$$m_{part} c_{part} \frac{dT_P}{dt} = -\left(\dot{q}_{conv} + \dot{q}_{rad}\right) + \dot{q}_{ch,p} \quad \textbf{(4.4.59)}$$

The source terms for the energy equations are calculated as follows:

a) Convection term

Assuming quasi-steady state behavior around the particle, the overall convective heat transfer rate between the particle and the gas is given as,

$$\dot{q}_{conv} = h\left(T_p - T_g\right)\pi d_p^2 F_B \quad \textbf{(4.4.60)}$$

$$F_B = \left(\frac{z}{e^z - 1}\right), \textit{ (Borman, 1998)} \quad \textbf{(4.4.60a)}$$

$$z = \frac{\dot{m}_C + \dot{m}_{pyro} + \dot{m}_{N-pyro} + \dot{m}_{N-oxi}}{Sh\pi\rho_g D d_p} \quad \textbf{(4.4.60b)}$$

b) Radiation term

$$\dot{q}_{rad} = F_R \sigma_{SB} \varepsilon\left(T_p^4 - T_{rad}^4\right)\pi d_p^2 \quad \textbf{(4.4.61)}$$

c) Chemical reaction term

The heat liberation rate due to chemical reactions at the particles is given as,

$$\dot{q}_{ch,p} = \sum_{i=1}^{N} \dot{m}_{C,i} HV_i + \dot{m}_{pyro}\left(H_p + HV_p\right) \quad \textbf{(4.4.62)}$$

4) Energy equation for gas phase

Gas phase energy equation is used to calculate the temperature of the gas phase.

$$\frac{d\left(m_{gas}h_{T,gas}\right)}{dt} = \dot{q}_{conv} + \dot{q}_{rad} + \dot{q}_{ch} + \dot{q}_{m} \quad \textbf{(4.4.63)}$$

$$\dot{q}_{m} = \left(\dot{m}_{c} + \dot{m}_{pyro} + \dot{m}_{N-pyro} + \dot{m}_{N-oxid}\right)c_{p}\left(T_{p} - T_{ref}\right) \quad \textbf{(4.4.64)}$$

$$\dot{q}_{ch} = \sum_{i=I}^{IX} w_{hm,i} HV_{i} \quad \textbf{(4.4.65)}$$

4.4.2.6 Procedure

The current model formulation uses solid feedlot biomass as the reburn fuel. Reburn fuel pyrolysis, FBN evolution and oxidation, and global char reactions along with global homogeneous reactions have been incorporated into the model. The governing differential equations outlined in the previous section, are solved explicitly and integrated over time to determine the NO reduction in the reburn zone using feedlot biomass as the reburn fuel.

4.8.6a. Input data

The following information is given as an input by the user (Tables 4.46, 4.47, and 4.48).

Main Burner

Table 4.46: Input data for main burner

S. No.	Input data for main burner	
	Parameter	
1	Main burner fuel	C_3H_8*
2	Total Throughput through the burner (main + reburn)	30 kW_t (100,000 Btu/hr)*
3	Heat through put through main burner	21 kW_t (71655 Btu/hr)*
4	LHV of the main burner fuel	46357 kJ/kg (21968 Btu/lb)
5	% excess air	5% *
6	Simulated NO (dry basis) leaving the main burner zone	600 ppm *
7	Temperature of the main burner gases entering the reburn zone	1800 K (2780.33 ºF)

* taken form experimental data (section 4.2)

Reburn Burner

Table 4.47: Input data for reburn burner

S. No.	Input data for Reburn burner	
	Parameter	
1	Reburn fuel	Coal, FB
2	Heat through put through main burner	7 kW_t (23885 Btu/hr)*
3	Equivalence ration in the reburn zone (global)	1.0, 1.05, 1.1 *
4	Temperature of the reburn fuel + reburn supply gases entering the reburn zone	300 K (80.33 ºF)*
5	Characteristic mixing time scale	35 ms
6	Reburn supply gas supplied with the reburn fuel	Air*
7	Residence time	Hot ~ 1 s, cold ~ 4 s *

* taken form experimental data (section 4.2)

Reburn Supply

Table 4.48: Reburn fuel properties and pyrolysis data

Property		Coal	FB
Proximate analysis	DL	15.1	7.7
	Ash	5.56	44.8
	FC	42.4	6.5
	VM	37.2	41.5
Ultimate analysis (DAF)	C	75.9	49.8
	H	4.6	6.1
	O	18.3	40.3
	N	1.2	3.8
LHV (kJ/kg) as received basis		22638	8661
Density (kg/m^3)		1300	1000
Pyrolysis kinetics	A (1/s) **	$1.5*10^{13}$	$1.67*10^{13}$
	B (kJ/kmole) **	$2.51*10^{5}$	$1.75*10^{5}$
Heat of pyrolysis of VM (kJ/kg)		-400	-400
Composition of the VM		CO, CO_2, CH_4, H_2 or H_2O	
Initial particle size (μm)		60^{+}	80^{+}
FBN distribution N_2: NH_3: HCN (mass basis)		2: 2:6**	2: 6:2**

$^{+}$ from Rosin-rammler distribution, for 70% < d_p

** Sami, 2000

4.4.2.7 Results

The simulations were carried out for both coal and FB for ϕ_{RZ} equal to 1,1.05, and 1.1. The mixing time scale was estimated theoretically using the entrainment rates formulation given by Forney *et al.*, 1996. Incorporating the experimental data into the calculations yielded a mixing time scale of 35 ms for ϕ_{RZ} = 1.1. This time scale was used for all the computations. The main aim of the modeling was to study the effect of HCN and NH_3 on NOx reduction. So an basic computation was carried out for ϕ_{RZ} = 1.0 with FB as the reburn fuel, and then the NOx reduction by NH_3 and HCN kinetics were adjusted to match the experimental results reported by Thien 2002. After matching the computational results with the experimental results the following reaction rates were used instead of the ones given in reaction III, and V.

Ammonia reduction:

$$NH_3 + NO \rightarrow N_2 + H_2O + \tfrac{1}{2} H_2 \qquad \textbf{(4.4.XII)}$$

$$w_{NH_3,III} = -1.8\times10^{9.14} X_{NH_3} X_{NO} \exp\left(\frac{-113000}{RT_g}\right) (1/s) \qquad \textbf{(4.4.32)}$$

HCN reduction:

$$HCN + NO \rightarrow N_2 + CO + \tfrac{1}{2} H_2 \qquad \textbf{(4.4.XIII)}$$

$$w_{HCN,V} = -3\times10^{12.53} X_{HCN} X_{NO} \exp\left(\frac{-251000}{RT_g}\right) (1/s) \qquad \textbf{(4.4.38)}$$

Now keeping all the parameters constant and varying ϕ_{RZ} and fuel properties (in case of reburn fuel change, coal or FB) rest of the computation was carried out. Since the hot residence time in the reactor was approximately 1 s, all the computations were carried out for a time period of 1 s. Figure 4.187 shows the comparative experimental and computational results of the NOx reduction achieved by both coal and FB. The % reduction was calculated as,

$$\%\,\mathrm{Re}\,duction = \left(\frac{X_{NO,inlet} - X_{NO,outlet}}{X_{NO,inlet}} \right) \times 100 \qquad \textbf{(4.4.66)}$$

Where $X_{NO,inlet}$ is the NOx mole fraction at the inlet of the reburn zone (dry basis), and $X_{NO,outlet}$ is the NOx mole fraction at the outlet of the reburn zone after 1s residence time (dry basis).

From figure 4.187 it can be seen that the results both FB and coal are reasonably comparable for ϕ_{RZ} = 1.0 and 1.05. Where as the difference was the maximum for ϕ_{RZ} = 1.1.

The possible reasons are,

a) Error in mixing time estimations.
b) The mixing time has been assume d to be constant (35 ms) for all the equivalence ratios, but in the actual case it varies as the mass flow rate of the reburn fuel supply gas varies according to the reburn equivalence ratio.
c) Use of monosized particle stream
d) FBN distribution (N_2: NH_3: HCN) and single step FBN pyrolysis

Thus a model which includes a competing pyrolysis model of FBN, an efficient characteristic mixing time scale which is correlated to the reburn equivalence ratio, and a improved model for FBN distribution to N_2: NH_3: HCN is needed to better correlate the experimental and reburn results.

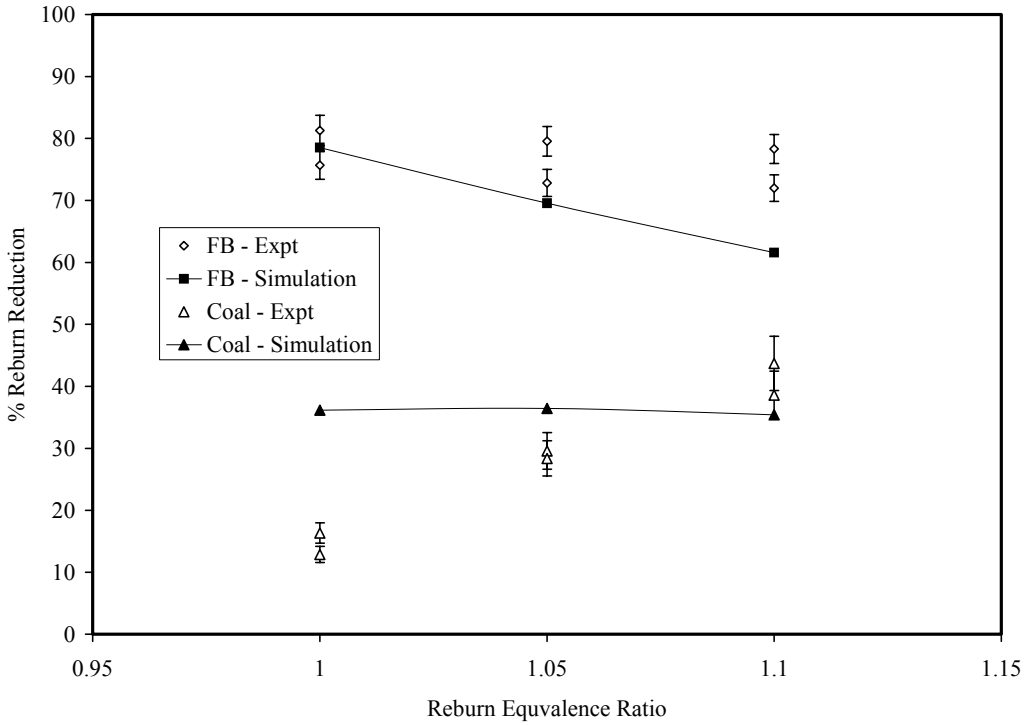

Figure 4.187: Comparison of reburn reduction for coal, FB, and blends between experiment and simulation.

4.5 Fuel Collection, Transportation, and Economic Analysis

4.5.1 Feedlot Biomass Fuels

To keep biomass fuel costs competitive with coal and natural gas fuels, the collection and transportation costs must be kept to a minimum. The various collection methods result in varying ash and moisture contents. Thus, transportation costs with ash and moisture must be investigated. A spreadsheet-based software has been developed on economic analysis of CFB fuels with the help of a senior undergraduate student (Senior thesis project) and assistance of Mr. Lanny McDonald (2000). Figure 4.187 shows a schematic of the various steps involved in cofiring feedlot or litter biomass with coal in coal fired boiler.

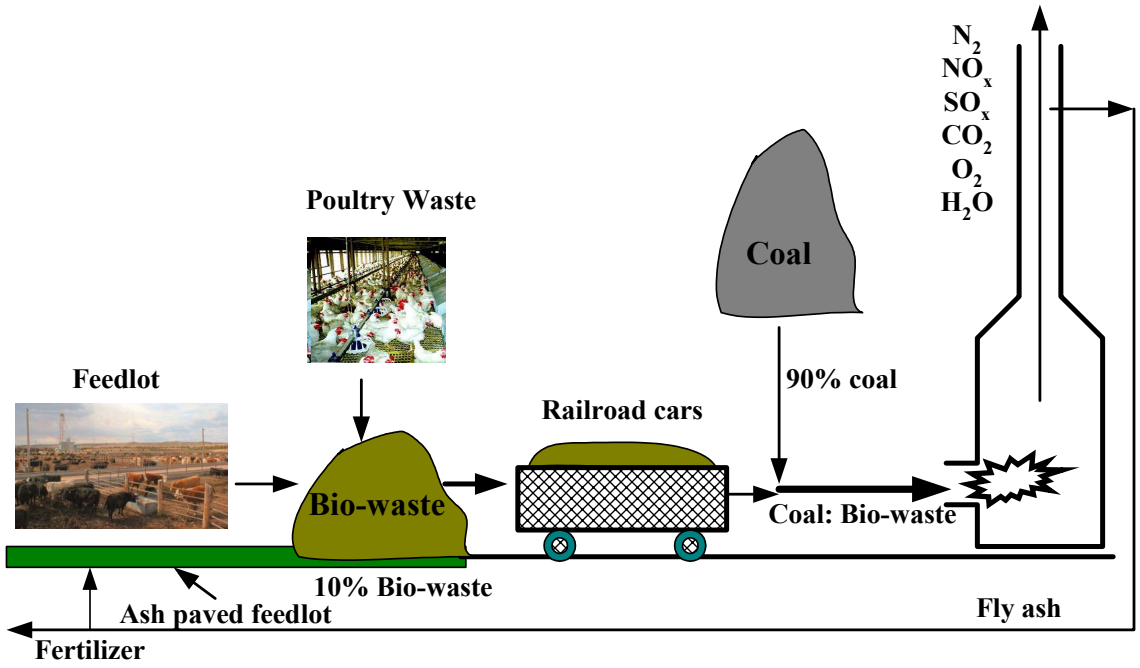

Fig.4.187: Coal:Feedlot Biomass Blend Energy Conversion Technology; biomass is collected from ash paved feedlots, transported via trucks to power plants, mixed with coal, fired in existing burners, flyash collected and recycled back to feedlot/poultry house and excess use for land reclamation and /or as fertilizer

Amosson *et al*. (1999) conducted an economic survey of cattle feedlots in the Texas Panhandle to determine the current cost of manure handling and delivery to farmers. Totally 47 feedlots were represented in the survey. Manure pricing for feedlots larger than 15,000 head averaged $ 0.05 paid by the feedlots to the contract manure collectors/haulers, and in turn the manure contractors charged the farmers an average of $2.28 per ton plus $0.11/ton-mile (one-way haul distance basis) for hauling and spreading. The handling practices at the feedlots showed that 40 % of the manure came straight from the feedpens loaded onto the trucks; 40 % of the manure came from stacks of mounds inside the pens; 16 % came from stockpiles more than 2 months old; 1 % came from compost windrows; and 3 % came from sediment cleaned out of runoff holding ponds. Haul distances to farmland for manure use as fertilizers reportedly averaged 14.5 km (9 miles), with a range of 0.4 to 80.5 km (0.25 to 50 miles). Typical haul distances of 11-24 km (7-15 miles) have increased about one-third within the last year as the cost of anhydrous ammonia fertilizer that

competes economically with manure has increased (Livestock Weekly, 2001). About 77% of the feedlots reported, that most of the manure is applied to irrigated farmland, and the remaining 23% is applied to predominantly non-irrigated cropland (Amosson, *et al*., 1995). However, the region suffers from a declining water table, which indicates a reduction of irrigated acreage in the future, which will probably lessen the farmer demand for manure. It has been reported that most feedyards use a combination of several pieces of mechanical equipment to harvest/collect, handle, and transport manure (Amosson et al 1995). The survey indicated that for collection, 46 % of the feedlots use a box scraper, 92 % use a wheel loader, 8 % use a bucket loader, and 23 % use an elevating (paddle) scraper. For manure transportation to the farmland, 92 % of the feedlots or their contractors utilize a spreader truck, 35 % use a semi-truck, and 42 % use a dump truck.

Quality control problems with feedlot biomass reported by farmers include (a) presence of rocks, concrete and debris and (b) salts (Livestock Weekly, 2001). On the positive side, the end users value the organic matter in manure in addition to the nutrient content.

Amarillo Power Plants

In order to use FB as fuel in nearby power plants Harahap (2000) conducted an economic analysis of feedlot biomass management at both conventional unpaved and paved feedlots. Calculated CO_2 and SO_2 emissions for a 90 % coal: 10 % manure blend fuel for a 2,146 MW electric power plant operating at 40% efficiency were provided as well. The economic analysis included cost of feedlot biomass collection and transportation, cost saving for the plant, and ash produced for disposal or utilization. Collected manure from unpaved and from flyash-paved feedlots was assumed to have 10 % moisture in both cases and ash contents of 47.4 % and 25 %, respectively. Results showed that using the unpaved feedlot biomass as 10 % of the fuel resulted in a fuel cost reduction of 1.7 % as compared to coal firing only, whereas paved-feedlot biomass reduced annual fuel cost by 4.7 %. A concern is the increased ash requiring or marketing for disposal utilization. CO_2 emissions were projected to be 5.7 % less for the unpaved feedlot biomass mixture than for coal as the only fuel, while SO_2 emissions could be 30 % greater. Economical hauling distance was estimated to be about double for the paved feedlot biomass (~ 193 km (120 miles)) than for the unpaved feedlot biomass (~ 100 km (62 miles)). Overall, the report estimated that use of a 10 % blend of feedlot biomass with coal was economically advantageous as compared to coal only, and the paved feedlot biomass option would be more advantageous than unpaved feedlot biomass. The cost per GJ for FB is shown in figure 4.188 assuming the distance of power plant to be 25 miles.

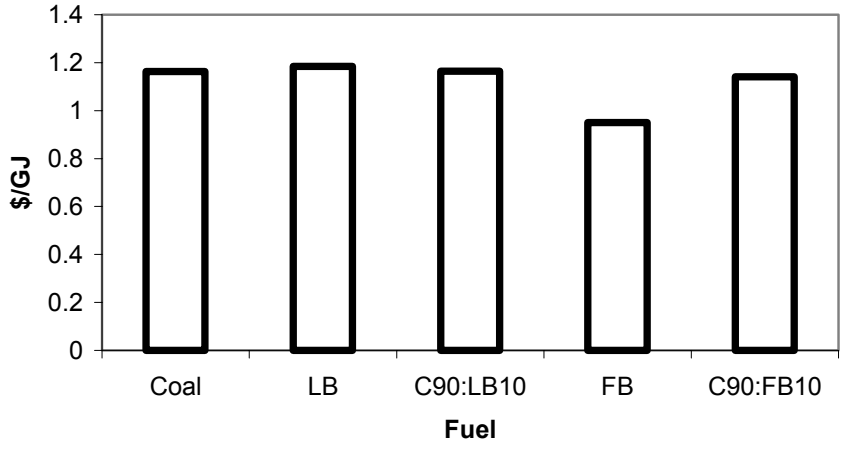

Figure 4.188: Fuel costs

Reburn Systems

Comparison of cost for initial NOx levels of 300 and 600 ppm show that SNR cost between $ 0.57 and $ 0.41 per pound of NO_x removed whereas catalytic removal costs between $2.54 and $1.54 per pound in addition to the SNR process having a lower capital cost. A major disadvantage to the SNR method is the possible production of N_2O. N_2O is considered a greenhouse gas since it absorbs infrared radiation. Relatively high levels of N_2O have been measured in the exhaust stream of stationary sources using nitrogen additives in a post combustion SNR method. The SNR process needs to operate where N_2O formation is limited while reducing NO_x (Bowman,1992).

The coal fired Xcel Energy around Amarillo releases about 29,000 tons of NO_x per year and hence the SNR cost could be up to 15 million dollars per year for 50 % removal. For catalytic processes, the cost is almost 3 to 5 times higher. However these SNR materials have little fuel/heating value whereas FB is a fuel and thus there is fuel savings for the power plant!

Benefits and Impacts to the Feedlots

A 50,000 head feedlot uses 50,000 mcf ($1.4x10^6 m^3$) of natural gas and 3.9 million kWh of electricity at a total cost of $470,000 each year (Sweeten *et al*., 1986). About 1500 wet tons of excreta are produced by 50,000 heads feedlot with 89 % moisture content. Due to moisture loss and ash addition from feed yard of the partially composted FB (30 % moisture, 30 % ash, 40 % combustibles) and hence collected in the feed yard is only about 500 tons per day. If this manure is sold as a fuel at $6.80/ton delivered, the cost of collection and transportation is estimated as $ 5.03 per ton to power plant within 25 mile. Hence, net revenue for feedlot operation is $1.77 per ton. If they sell at same price as coal, the additional revenue for 50,000 head feedlot is $ 323,000 per year. The total feedlot capacity around Amarillo (including nearby counties in New Mexico and Oklahoma) is 3.6 million heads of cattle, which can generate net revenues of about 23 million dollars per year assuming negligible combustible loss. On the other hand if power plants purchase at $ 5.03 per ton, the fuel cost savings for the plant could be 23 million dollars. These estimations are based on the presumption that all the FB generated could be used as fuel.

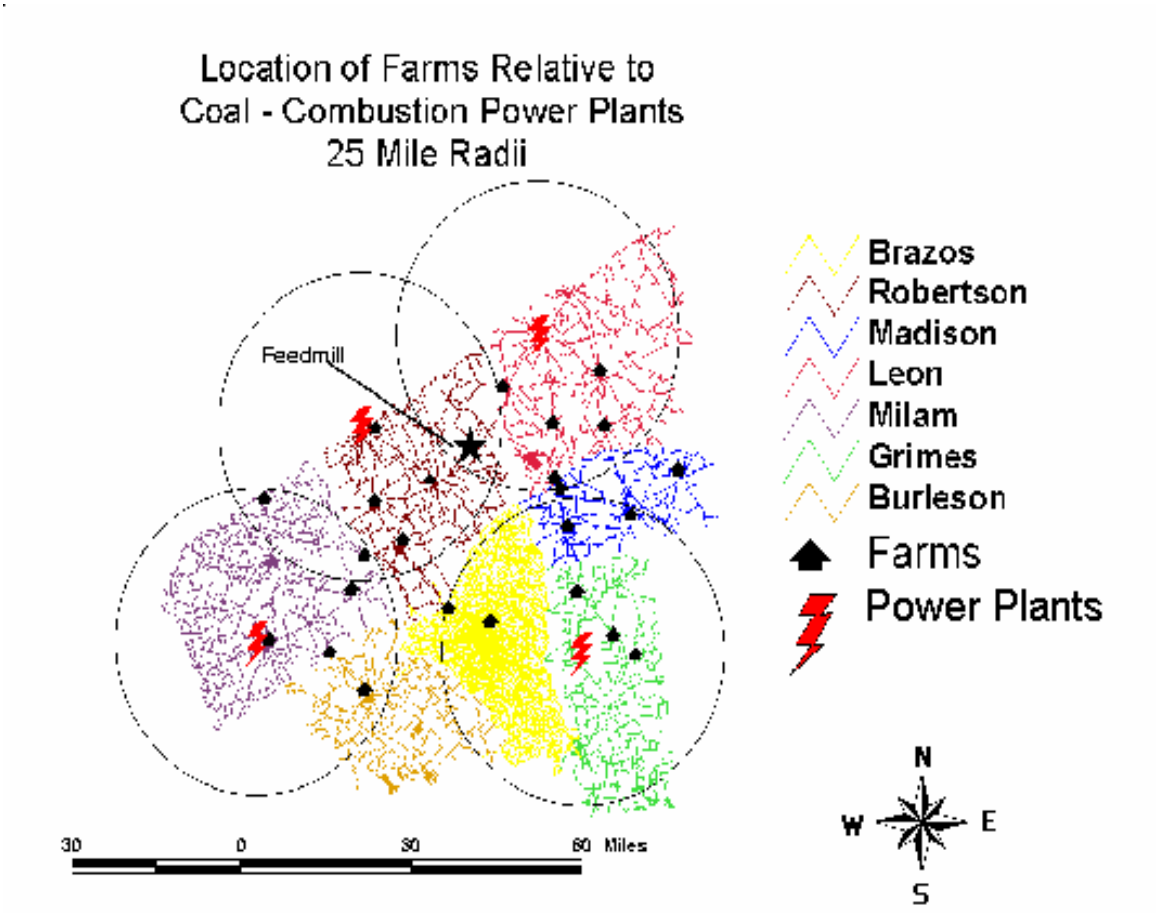

Figure 4.189: Location of Power Plants in Texas and Proximity to Broiler Operations

4.5.2 Litter Biomass Fuels:

Figure 4.189 shows contract growers' farms for the firm, feed mill location, location of power plants in the area, and location of farms within the 25-mile radius of a power plant. Due to company policy, exact addresses of the farms were not disclosed. Therefore, distance of the nearest city from a farm to the power plant was approximated as distance of that farm to the power plant. As shown in Figure 4.189, all 58 farms are located within 50 miles of the feed mill and one of the four power plants. Table 4.49 provides information on farms within 25 miles of each power plant including farms per city, distance from a power plant to the city near those farms, total tons of biomass generated per city, total cost of removal per farm and city, and transportation cost of one ton of litter biomass to the nearest power plant. Based upon the information provided by the firm on litter production and removal from the broiler houses, it was assumed that each farm had an average of 6.6 broiler houses, producing 200 tons of litter per house per year at a litter removal cost of $10 per ton. In addition, the cost of transportation to the plants was assumed as $2.5/mile for trucks with a litter biomass carrying capacity of 20 tons (i.e., $ 0.125/ton-mile). Table 4.49 shows that cost of removing and transporting one ton of litter biomass to the nearest power plant ranged from $10.45 to $15.63 and the average cost per ton was $13.0. The cost per GJ of heat was investigated for LB, Coal, and the C90:LB10 blends as shown in Figure 4.188. For the analysis, it was assumed that coal costs $25/ton (Jones, 2000). In Figure 4.188 it was assumed that the price of LB is $13 per ton, as ten

dollars of the cost is for cleaning of the litter houses by the chicken house operators, which would be incurred regardless of the use for the litter. The results of the fuel analysis show that the use of the C90:LB10 blend is similar in cost as compared to coal and hence the broiler house operator just recover the collection and transportation cost.

Power Plants

The Texas A&M The university power plant supplies 70 % of the required electrical power, along with chilled and hot water, and domestic cold and hot water. The hot water for building is supplied at 333.15-355.37 K (140-180 °F) by condensing steam at 137.9 kPa (20 psig) (382 K (228 ºF)), to provide a heating capacity of capacity of 348 GJ/hr (330 mmBtu/hr) or steam flow rate of 170 tons per hr. For domestic hot water at 335.93 K (145^{o} F), the capacity is 40 GJ/hr (38 mmBtu/hr) or 20 tons of steam per hr.

Nominal electrical capacity is 38 MW (129 mm Btu/hr) (nominal) with a peak of 62 MW (211 mmBtu/hr) supplying 70 % of demand and 50 % of peak demand. The boiler is natural gas fired. Steam is produced at 4.1 MPa (600 psig) and 672.04 K (750 ^{o}F). There are 3 steam turbines with a total nominal capacity of 21.5 MW (73 mmBtu/hr) (steam produced by gas fired boiler at 215,4564 kg/hr (75,000 lb/hr)), and a gas turbine with 16 MW (54 mmBtu/hr) capacity. The exhaust from the gas turbine at 774.82 K (935 °F) is used to produce 79,378 kg/hr (175,000 lb/hr) of steam. Another boiler is in stand-by mode with a capacity of 45,359 kg/hr (100,000 lb/hr). The maximum capacity is 340194 kg/hr (750,000 lb/hr) or 375 tons per hour. The steam is bled at 1.03 MPa and 137.91 kPa (150 and 20 psig) for other uses. About 11.3 million m^3 (400 million ft^3) of natural gas is used per month (1999 gas price: $ 9.6 million per year with $ 2.00 per 28 m^3 (1000 ft^3) or $ 2 per million BTU; HHV of natural gas ≈ 51726 kJ/kg (1000 BTU/ft^3 or 22,200 Btu/lb)). The cost of electricity is 5 ¢ per kWh.

If litter biomass is bought at $ 13 per ton with a heat value of 4000 BTU per lb., the cost of fuel is reduced to $ 0.625 per million BTU, which is 1/3 of the cost of the natural gas. For 20 % biomass based on mass (or 5 % based on BTU), the cost of the blend is $1.93 per million BTU. To supply 5 % of the BTU, we need only 30,000 tons of litter biomass. The Sanderson poultry farms with 300 chicken houses located within a radius of 113 km (70 miles) from A&M can supply 60,000 tons per year. Hence, fuel savings with cofiring are 0.68 million dollars per year if 60,000 tons of litter biomass are used. If the proposed program is successful, the standby boiler may be used for co-firing. However, this plant is located in the central part of campus and thus the use of LB for cofiring is doubtful.

Table 4.49: Transportation and cleanout cost estimates for litter biomass.

Power Plant	Farms / City	Distance to Plant (miles)	Transportation and Cleanout Cost per House ($)*	Ave. Cost per Farm ($)	Cost per City ($)	Total CL per city (ton)	Cost per Ton ($)
Plant A	2	2	2050	13,530	27,060	2640	10.25
	1	27	2675	17,655	17,655	1320	13.38
	1	19	2475	16,335	16,335	1320	12.38
	1	31	2775	18,315	18,315	1320	13.88
	1	34	2850	18,810	18,810	1320	14.25
	2	27	2675	17,655	35,310	2640	13.38
Plant B	2	2	2050	13,530	27,060	2640	10.25
	2	13	2325	15,345	30,690	2640	11.63
	1	22	2550	16,830	16,830	1320	12.75
	13	23	2575	16,995	220,935	17160	12.88
Plant C	1	20	2500	16,500	16,500	1320	12.50
	2	38	2950	19,470	38,940	2640	14.75
	1	10	2250	14,850	14,850	1320	11.25
	2	13	2325	15,345	30,690	2640	11.63
	1	12	2300	15,180	15,180	1320	11.50
	4	36	2900	19,140	76,560	5280	14.50
	1	29	2725	17,985	17,985	1320	13.63
	2	38	2950	19,470	38,940	2640	14.75
	1	45	3125	20,625	20,625	1320	15.63
Plant D	6	13	2325	15,345	92,070	7920	11.63
	1	20	2500	16,500	16,500	1320	12.50
	5	24	2600	17,160	85,800	6600	13.00
	1	33	2825	18,645	18,645	1320	14.13
	3	33	2825	18,645	55,935	3960	14.13
	1	28	2700	17,820	17,820	1320	13.50
							Ave. **$12.96**

*Figures are based on 6.6 houses per farm, 200 tons of litter removed per house per year at $10.0 per ton; transportation cost is $2.5 per 1.6 km (1 mile) per 20-ton load.

5. Summary and Conclusions

The following is the task-wise summary of results and conclusions obtained from the current studies.

Task 1: Fundamental experiments on fuel characterization and combustion studies

Task 1a: Coal and Feedlot Biomass

1. The FB can be classified as raw manure (RM, 1 day old), partially composted (PC, 30 days old) and finished composted (FiC, 120 days old). The main value of composting for combustion fuel is to promote uniformity and improve physical and chemical properties. Typically there is 30 % combustible loss over one year period. The drop in heat value is not significant for PC compared to FiC.
2. The DAF HHV was almost constant at 19500 kJ/kg (8400 Btu/lb) for ration, FB-raw, PC, and FC but lower compared to Wyoming coal DAF heating value of kJ/kg (12,960 Btu/lb).
3. The N and S contents per mmBtu increased with composting.
4. Cl content could be as high as 1.2 % while coal has less than 0.01 %.
5. The fuel N and S contents of 2.3 and 0.8 kg /GJ (2.6 and 0.13 lb per mmBtu) in FB-PC, were considerably higher compared to coal of 0.4 kg/GJ (0.9 lb per mmBtu) and 0.2 kg/GJ (0.4 lb per mmBtu).
6. The volatile oxide percentage decreased with composting.
7. Based on heating values and alkaline oxides, FB-PC seems preferable compared to RM and FiC.
8. Even though the percentage of volatile oxides in ash decreased, the total amount of volatile oxides increased due to an increase in the percentage of the ash.
9. The adiabatic flame temperature for most of the biomass fuels can be empirically correlated with ash and moisture percentage. T (K) =2285 - 1.8864*H_20 + 5.0571*Ash - 0.3089*H_2O*Ash - 0.1802 * H_2O^2 -0.1076*ASH^2; T (F)=3653 - 3.3952*H_20 + 9.1028*Ash - 0.5560*H_2O*Ash - 0.3244 * H_2O^2 -0.1937*ASH^2.

Task 1b: Litter Biomass

1. Analyses were performed on as excreted broiler manure (EM), cleanout litter (CL), and dry litter (DL), to determine fuel quality and characteristics. The heating value of dried litter is 19600 kJ/kg (5187 Btu/lb) while dry ash free (DAF) heating values remained at about from 19350 kJ/kg (8300 Btu/lb) for EM, CL and DL. The Litter Biomass (LB) is a lower quality fuel than coal due to its high nitrogen, high sulfur, high moisture, high ash, and low heating value.
2. All LB fuels have similar properties on a dry ash free basis except for nitrogen, which is higher in EM than in CL. The N and S contents in DL are 2.5 kg/GJ (5.8 lb/mmBtu).
3. Litter based fuels are higher in volatile oxides and phosphorus (3.2 %) leads to higher rates of fouling and corrosion.
4. Use of litter with coal in a 90:10 blend results in similar fuel costs as compared to coal, and reduction in the fouling potential as compared to pure litter.
5. Based on these findings, further testing of BL fuels in a small-scale boiler burner is necessary to assess fouling and corrosion potential along with combustion efficiencies of these fuels. The effects of PO_2 and P_4O_{10} on fouling has not been investigated.

Task 1c: Pyrolysis and comparison of FB, LB and Coal

1. Feedlot biomass (cattle manure) starts pyrolysis at about 273 ºC (523 ºF) while coal pyrolyses at a higher temperature of 377 °C (711 °F).
2. LB and FB have greater volatile matter (80 %) on a dry ash free basis as compared to coal (45 %). LB biomass lose volatiles more rapidly and at lower temperatures 227 ºC (440 ºF) for biomass, 347 ºC (645 ºF) than coal.
3. FB and LB biomass, coal, and 90:10 blends were fit to the parallel reaction model with E_m and σ of 232,000 kJ/kmol and 48,000 kJ/kmol for full size coal, 202,000 kJ/kmol and 57,000 kJ/kmol for full size FB, and 187,700 kJ/kmol and 39,300 kJ/kmol for full size LB.
4. FB and LB biomass have a larger standard deviation in activation energy than coal, because they are less homogeneous substances.
5. Coal has a recognizable group ignition temperature (540 K (512.33 ºF)), while biomass does not, because the of the high volatile matter content in biomass and low temperature release.
7. Even based on DAF heating values, the FB and LB have values 60 % of heating value of coal. Further the ash in FB is around 40 % and in LB it is around 25 % while for coal the ash is only about 5 %. The higher ash percentage can cause problems in boiler burners by causing fouling and boiler tube corrosion, and reducing the adiabatic flame temperature.
8. The heating values of FB and LB are much lower than coal, so the mass flow of fuel has to be increased in order to maintain the same heat throughput when firing blends. Even more troubling is the increased Sulfur and Nitrogen in FB. When the fuel burns N and S in the fuel will combine with O_2 from the air to form NO and SO_2, which are recognized air pollutants.
9. The results show that FB has greater ash content, lower carbon content higher volatile matter on DAF (dry ash free) basis and a lower heating value than coal. On a heat basis, FB contains 4 times more Nitrogen than coal. The results show that the ash and moisture content in a fuel can have a large effect on the flame temperature, and therefore should be carefully controlled. On a dry ash free basis, the FB will consist of almost all volatile matter, with very little fixed carbon, while the combustible portion of the coal is made up of equal parts fixed carbon and volatiles. A comparison of the FB fuel to the LB fuels shows that the both the biomass fuels have similar properties, with the FB having more ash.

Task 2: Boiler burner experiments for cofiring of CFB and CLB fuels and reburn tests

Cofiring

1. The 90:10 blend has a HHV of 19100 kJ/kg (8200 BTU/lb) compared to coal 20400 kJ/kg (8800 BTU/lb) showing a reduction of 7 % in HHV.
2. Biomass blends and coal have a similar burnt mass fraction (0.95).
3. Co-firing with 10 % FB and 90 % coal results in improved combustion compared to 100 % coal.
4. At 10 % excess air, co-firing with 10 % FB and 90 % coal results in reducing the NO_x emissions from 290-ppm, 0.162-kg/GJ (0.3768-lb/mmBtu) to 260-ppm, 0.1475-kg/GJ (0.343-lb/mmBtu). For the blend, the reduction is possibly due to a combination of a higher volatile matter, which depletes the oxygen rapidly and the release of fuel nitrogen in the form of ammonia from biomass.
5. The CO emission for the blend is higher compared to coal due to limited residence time.

Reburning

1. Feedlot biomass with 80 % reduction in NO_x is a more effective reburn fuel than coal with 40 % reduction, potentially due to its high volatile matter content, and fuel nitrogen in the form of NH_3.
2. The reburning behavior of coal: biomass fuel blends falls between that of coal and pure feedlot biomass.

Task 3: Fixed bed studies on CFL and CLB fuels

1. Ash was not removed during gasification; Coal containing less ash (5 %) can yield values close to steady state after a longer period while FB and LB having high ash exhibited transient nature of gasification. Hence temperature profiles with a peak changed with time. At 1.3 SCMH (45 SCFH) for coal, AFB and LB of 5 mm (0.2") dia the temperature peaks were observed to be 1120 °C (2050 °F), 930 °C (1700 °F) and 980 °C (1790 °F).
2. The heating values of low Btu gases produced from coal, AFB and LB are about 5.0 MJ/m^3 (135 Btu/SCF) for coal, 4.8 MJ/m^3 (130 Btu/SCF) for FB, and 4.5 MJ/m^3 (120 Btu/SCF) for LB.
3. In gasification at atmospheric pressure, CH_4 % is the lowest while CO is the highest
4. Parametric tests of the air flow rate and the particle size on gasification have been conducted for all the fuels and the results are summarized below:

Air flow rate effect

5. For coal, the increase in air flow shifted the peak towards the free board and increased the heating value of the product gas leaving the gasifier by 10 %.
6. For larger FB particles, the heat value of product gases increased. For the smaller particles, the higher air flow rate resulted in tendency for bed agglomeration in the bed, resulting in oxidation of the pyrolysis gases, thereby decreasing the heating vale of the product gas.
7. For CFB, the rate of peak temperature shift was in between coal and FB. An increase in air flow rate decreased the calorific value of the product gas leaving the gasifier for the large particles, whereas the opposite was observed for the smaller particles.
8. Although, the presence of coal in the blend increased the peak temperature in the bed (when compared to FB under similar conditions), the reduced ash content of the blend (as compared to the FB ash content) decreased the agglomeration in the bed.
9. For larger LB particles, the increased air flow rate slightly decreased the calorific value of the product gas leaving the gasifier, but increased in the case of smaller LB particles.
10. The temperature peak shift towards the free board was the highest amongst all the three primary fuels, and increased with an increase in the air flow rate. There was ash agglomeration in the bed for all the cases during LB gasification.
11. For CLB, the increased air flow rate decreased the calorific value of the product gas leaving the gasifier. The presence of coal, slowed down the rate of peak temperature shift in the bed, and almost consistently eliminated the agglomeration in the bed. Despite the reduced agglomeration, ash fusion due to slagging of the ash resulted in formations small clinkers in the bed. This may be due to the slagging of the silica in the blend at high temperatures.

Particle size effect

1. For coal, the larger particles yielded a lower product gas calorific value as compared to the smaller particles. For the smaller particles, a higher amount of combustibles per unit volume of

the bed as compared to the larger particles yielded a higher peak temperature in the bed. The oxidation zone was narrower for the smaller particles (without bed agglomeration) due to increased surface area per unit volume, which increased the oxidation rate in the bed.

2. For smaller FB particles, the temperature peak shift in the bed was slower as compared to the larger particles. Due to higher bulk density of the smaller particles, the product gas yield was higher, resulting in an increased heating value of the product gas as compared to the larger particles. The smaller particles at higher air flow rates agglomerated in the bed.
3. For CFB, the heating value of the product gas higher for the smaller particles as compared to the larger ones. The smaller particle also exhibited a smaller temperature peak shift in the bed, due to the narrower oxidation zone in the bed.
4. For LB, the particle size did not affect the heating value of the product gas largely. This was due to agglomeration in the bed, resulting in almost equal temperature shift rates for both the particle sizes. In addition, the agglomeration resulted in almost equal peak temperatures (920 ºC (1690 ºF)) for both the particle sizes.
5. For CLB, the larger particles resulted in slightly higher temperatures in the upper portion of the bed, thereby increasing the calorific value of the product gas leaving the gasifier. The peak temperatures for both the cases were largely affected by the presence of coal, and were almost equal to 1200 °C (2150 °F).

Ash fusion

1. The LB fuel exhibited agglomeration in the bed possibly due to the condensation of vaporized Na_2O, and K_2O on the particle surface.
2. The ash also played a role in the temperature dynamics of the bed. As the ash content of the fuels increased, the rate of temperature peak shift increased. The shift was the minimum for coal (ash content of 5 %), and the maximum for HFB with an ash content of 44 %.
3. The ash fusion in case of the CFB and CLB fuels may be due to the slagging of the silica in the ash forming a glassy material which is too viscous to flow, and caused formation of clinker in the bed.
4. Another interesting fact is that though the peak temperature achieved for large particles under an air flow rate of 1.27 m^3/hr (45 SCFH), and for smaller particles under an air flow rate of 1.7 m^3/hr (60 SCFH) is about 1500 K (2240.33 ºF), agglomeration occurs only in the later case.

Task 4: Numerical modeling of pulverized fuel (pf) fired burners and reburn systems

1. Moisture and P oxidation models were added to 2 dimensional PCGC2 code. P_4O_{10} concentration is high (e.g., around 200 ppm for 90:10 coal-LB blend) mainly in the flame core but very low in the post-flame region. PO_2 is unimportant in pre-flame region but has high concentration in post flame region. At the furnace exit, PO_2 level is high (e.g., around 300 ppm for 90:10 coal-LB blend) while P_4O_{10} is negligible (less than 10 ppm for 90:10 coal-LB blend). The exit PO_2 level is high (e.g., around 300 ppm for 90:10 coal-LB blend) while P_4O_{10} is negligible (less than 10 ppm for 90:10 coal-LB blend).
2. The increasing in moisture content delays pyrolysis and char combustion causing longer flame length and lower burnout.
3. The increase of swirl number from 0.7 to 1 leads to stronger flow recirculation and air-fuel mixing, a shorter flame length, decreased CO emission and increased NO due to better air-fuel mixing.
4. As excess air increases, burnout increases in post-flame region, NO increases, CO decreases P_4O_{10} increases and PO_2 decreases.

5. When biomass fraction in fuel blend is low (e.g., 10 %), effects of biomass moisture on combustion behavior and species emissions are negligible.
6. Tables 4.49 and 4.50 summarize the results on numerical modeling.

Table 4.50: Summary of pollutant levels at furnace end for coal-LB blend combustion with 0.7 swirl numbers, 10 % excess air, and different moisture levels in fuel blend (* denotes cross-sectional averaged concentration)

Moisture in Blend (%)	10	20	30
NO (kg/GJ)	0.209	0.200	0.189
CO (ppm)*	6033	6690	7719
P_4O_{10} (ppm)*	7.05	7.89	8.61
PO_2 (ppm)*	274.3	257.5	244.4
Burnout	0.909	0.891	0.873

Table 4.51 Effects of swirl number, excess air percentage, and moisture level in fuel blend on locations of flame pollutant peaks near burner

	Increasing swirl number	Increasing excess air percentage	Increasing moisture in fuel blend
Flame location	←	←	→
Peak CO	←	←	→
Peak CO_2	←	←	→
Peak NO	←	←	→
Peak PO_2	←	←	→
Peak P_4O_{10}	←	←	→

←: Closer to burner. →: Farther away from burner

Table 4.52: Summary of pollutant levels at furnace end for coal-LB blend combustion with different swirl numbers and 10 % excess air (* denotes cross-sectional averaged concentration)

Swirl Number	0.7	1.0
NO (kg/GJ)	0.255	0.279
CO (ppm)*	4776	4031
P_4O_{10} (ppm)*	7.95	6.11
PO_2 (ppm)*	262.7	277
Burnout	0.887	0.903

Table 4.53: Summary of pollutant levels at furnace end for coal-LB blend combustion with 0.7 swirl numbers and different excess air percentages (* denotes cross-sectional averaged concentration)

Excess air (%)	5	10	15	20
NO (kg/GJ)	0.201	0.255	0.297	0.324
CO (ppm)*	5333	4776	3981	3524
P_4O_{10} (ppm)*	6.87	7.95	9.06	10.37
PO_2 (ppm)*	271.4	262.7	253.5	242.8
Burnout	0.861	0.887	0.909	0.928

Task 5: Fuel collection, transportation, and economic analyses of FB and LB fuels

1. Results showed that the use the UPFB resulted in a fuel cost reduction of 1.7 % as compared to coal firing only, whereas PFB reduced annual fuel cost by 4.7 %.
2. The CO2 emissions were projected to be 5.7 % less for the UFB blend than for coal as the only fuel.
3. Economical hauling distance was estimated to be about double for the PFB (~ 193 km (120 miles)) than for the UPFB (~ 100 km (62 miles)).
4. The results of the LB analysis show that the use of the 90:10 coal: LB blend is similar in cost as compared to coal due to cleaning cost of the litter house and truck transportation cost.

6. References

Abbas, T., Costen, P., Kandamby, N., Lockwood, F., and Ou, J., 1994, "The Influence of Injection Mode on Pulverized Coal and Biomass Co-Fired Flames," Combustion and Flame, **99**, pp. 617-625.

Abramowitz, M., and Stegun, I., 1965, Handbook of Mathematical Functions, Dover, New York.

Adams, B., and Harding, N., 1998, "Reburning Using Biomass for NO_x Control," Fuel Processing Technology, **54**, pp. 249-263.

Aerts, D, 1997, "Co-firing Switchgrass in a 50 MW Pulverized Coal Boiler," Proc. 59th Annual American Power Conference, Chicago, IL, **59**, pp. 617-625.

Alzueta, M. U., Bilbao, R., and Millera, A., 1998, "Modeling Low – Temperature Gas Reburning. NOx Reduction Potential and Effects of Mixing," Energy & Fuel, **12**, pp. 329-338.

Amosson, S. H., Sweeten, J. M., Weinheimer, B., and Camarata, S., 1999, "Feedlot Manure Survey," Texas Agricultural Extension Service and Texas Cattle Feeders Association, Amarillo, TX, Report No. 99-35, Texas A&M University Agricultural Research and Extension Center at Amarillo, pp. 12.

Amosson, S. H., Smith, J., and Rauh, W., 1995, "Texas crop and livestock enterprise budgets TexasHigh Plains," Texas Agricultural Extension Service, College Station. pp. 112.

Annamalai, K., and Ryan, W., 1993, "Interactive Processes in Gasification and Combustion – II. Isolated Carbon, Coal and Porous Char Particles," Prog. Energy Combust. Sci., **19**, pp. 383-446.

Annamalai, K., Frazzitta, S., and Sweeten, J. M., 1997, "Combustion of Feedlot Manure for Energy Recovery," Proc. Livestock Waste Streams: Energy and Environment, Texas A&M University System, Amarillo, TX, pp. 34-43.

Annamalai, K., Thien, B., and Sweeten, J. M., 2000a, "Co-firing of Coal and Feedlot Biomass (FB) in a Laboratory Scale Boiler Burner", 17th Annual Pittsburgh International Coal Conference, Sept 11-14.

Annamalai, K., Sweeten, J. M., Mukhtar, S., Thien, B., Wei, G., Priyadarsan, S., and Sami, M. 2001, "Co-Firing Coal, Feedlot, and Litter Biomass (CFB and LFB) Fuels in Pulversized Fuel and Fixed Bed Burners," DOE Contract, DE-FG26-00NT40410, Pittsburgh, PA, Jul.

Annamalai, K., and Puri, I., 2001, Advanced Thermodynamics Engineering, CRC Press, Bocaraton, Florida, Software free at http://www.CRCpress.com/Electronic Download/Advanced Thermodynamics engineering.

Annamalai, K., Thien, B., and Sweeten, J. M., 2003a, "Co-Firing of Coal and Cattle Feedlot Biomass (FB) Fuels Part II: Performance Results from 100,000 Btu/hr Laboratory Scale Boiler Burner," Fuel, **82**(10), pp. 1183-1193.

Annamalai, K., Sweeten, J. M., Freeman, M., Mathur, M., O'Dowd, W., Walbert, G., and Jones, S., 2003b, "Co-firing of coal and cattle feedlot biomass (FB) Fuels, Part III: fouling results from a 500,000 BTU/h pilot plant scale boiler burner," Fuel, **82**(10), pp. 1195-1200.

Annamalai, K., and Puri, I., 2004, Combustion Engineering, CRC press, Bocaraton, Florida, In progress.

Anthony, D., Howard, J., Hottel, H., and Meissner, H., 1974, "Rapid Devolatilization of Pulverized Coal," Fifteenth (International) Symposium on Combustion, **15**, pp. 1303-1317.

APHA, 1995, "Standard Methods for Examination of Water and Wastewater," 19th ed., American Public Health Association, New York, U.S. Environmental Protection.

Arthur, J. R., 1951, "Reactions between Carbon and Oxygen," Trans. Faraday Soc., **47**, pp. 164-178.

America society for Testing and Materials, 1992, "Test Method for Fusibility of Coal and Coke Ash, Method D 1857," Annual Book of ASTM Standards, Philadelphia, PA, **5.05.**

Bartok, W., and Sarofim, A., 1991, Fossil Fuel Combustion, John Wiley & Sons, New York.

Beauchemin, S., Simard, R. R., and Cluis, D., 1996, "Phosphorus sorption-desorption kinetics of soil under contrasting land uses," J. Environ. Qual., **25,** pp. 1317-1325.

Bilbao, R., Millera, A., and Alzueta, M., 1994, "Influence of the Temperature and Oxygen Concentrations on NO_x Reduction in the Natural Gas Reburning Process", Industrial and Engineering Chemistry Research, **33**, pp. 2846-2852.

Bilbao, R., Alzueta, M., and Angela, M., 1995, "Experimental Study of the Influence of the Operating Variables on Natural Gas Reburning Efficiency," Industrial and Engineering Chemistry Research, **34**, pp. 4531-4539.

Bilboa, R., Alzueta, M., Millera, A., and Prada, L., 1997, "Dilution and Stoichiometric Effects on Gas Reburning: An Experimental Study", Industrial and Engineering Chemistry Research, **36**, pp. 2440-2444.

Bird, R. B., Stewart, W. E., & Lightfoot, E. N., 1960, "Transport Phenomena", John Wiley & Sons, New York.

Blasi, D. C., Signorelli, G., and Portoricco, G., 1999, "Countercurrent Fixed-Bed Gasification of Biomass at Laboratory Scale," Ind. Eng. Chem. Res. **38**, pp. 2571-2581.

Borman, G. L., and Ragland, K. W., 1998, "Combustion Engineering," McGraw – Hill, Boston, MA.

Bowman, C. T., 1992, "Control of combustion-generated nitrogen oxide emissions: Technology driven by regulation," 24th Symposium (International) on Combustion, The Combustion Institute, Pittsburgh, pp. 859-878.

Bryden, K. M., and Ragland, K. W., 1996, "Numerical modeling of Deep Fixed Bed Combustor," Energy Fuel, **10(2)**, pp. 269-275.

Chen, C. J., 2001, "The Effect of Moisture and Particle Size of Feedlot Biomass on Co-Firing Burner Performance," M.S. Thesis, Department of Mechanical Engineering, Texas A&M University, College Station, Texas, Dec.

Chen, W., and Ma, L., 1996, "Effect of Heterogeneous Mechanisms During Reburning of Nitrogen Oxide," AIChE Journal, **24**, pp. 1968-1976.

Collot, A.G., Zhuo, Y., Dugwell, D.R., and Kandiyoti, R., 1999, "Co-pyrolysis and Co-gasification of Coal and Biomass in Bench-Scale Fixed Bed and Fluidized Bed Reactors," Fuel, **78**, pp. 667-679.

Cooper, B. C., and Ellington, W. A., 1984, "The Science and Technology of Coal and Coal Utilization," Plenum Press, New York, NY.

De Soete G.G., 1975, "Overall Reaction Rates of NO and N2 Formation from Fuel Nitrogen," 15th Symposium (International) on Combustion, The Combustion Institute, pp. 1093 – 1102.

Dishman, B., 1998, Personal Communication, North Plains Compost, Hereford, Texas. Dec. 5.

DOE, 1999, "Reburning Technologies for the Control of Nitrogen Oxides Emissions from Coal-Fired Boilers," Topical Report Number 14, U.S. Department of Energy.

Du, X., 1995, "Ignition and Combustion of a Dense Stream of Coal Particles," Ph.D., Thesis, Department of Mechanical Engineering, Texas A&M University, College Station, Texas, Aug.

Duzy, A. F., and Walker, J. B., Jr., 1965, "Utilizations of Solid Fuel having Lignite Type Ash," Proc. US bureau of Mines Lignite Symposium, US Bureau of Mines Information circular, Apr. 29-30.

Eghball, B., and Power, J., 1994, "Beef Cattle Feedlot manure Management", Journal of Environmental Quality, **49**, pp.113-22.

Evans, D. D., and Emmons, H. W., 1977, "Combustion of Wood Charcoal," Fire Res., **1(1)**, pp. 57-66.

Fang, M., Yu, C., Luo, Z., Cheng, G., and Cen, K., 1998, "Study of Biomass Gasification and Combustion," Proc. International Conference on Energy and Environment, China Machine Press, Shanghai, China, pp. 476-484.

Fieldender, A. C., Wall, A. E., and Field, A. L., 1918, Bulletin, Department of the Interior, US Bur. Mines, pp. 129-146.

Forney, L. J., and Nafia,N. (1996) Optimum Jet Mixing in a Tubular Reactor, *AIChE Journal*, 42(11), 3113-3122.

Frandsen, F., Kim, D., and Rasmussen, P., 1994, "Trace element from combustion and gasification of coal – an equilibrium approach," Progress in Energy and Combustion Science, **20**, pp. 115-138.

Frazzitta, S., Annamalai, K., Sweeten, J. M., 1999, "Performance of a burner with coal and coal-bio-solid fuel blends," Journal of Propulsion and Power, **15,** pp. 181-186.

Freeman, M. C., Smouse, S. M., Sastrawinata, T., Walbert, G. F., and Rastam, M., 1997, "Believe it or not! Even 1% Ash Coal can cause Slagging Problems," Effects of Coal quality on Power Plants, Kansas, MO, May 20-22.

Freeman, M, Annamalai, K and Sweeten, J. M., 2003, "NOx Reduction with Feedlot Biomass as a Reburn Fuel in a 150 kW Pilot Scale Boiler Burner Facility," Presented at Alternative Power – Agricultural Biomass Fuels and Renewables, Electric Power Conference, ASME, Houston, TX, Mar. 4-6.

Gold, B., and Tillman, D., 1996, "Wood Cofiring Evaluation at TVA Power Plants", Biomass and Bioenergy, **10**, pp. 71-78.

Hansen, P., Anderson, K., Wieck-Hansen, K., Overgaard, P., Rasmussen, I., Frandsen, F., Hansen, L., and Dam-Johansen, K., 1998, "Co-firing Straw and Coal in a 150-MW Utility Boiler: in situ Measurements", Fuel Processing Technology, **54**, pp. 207-225.

Harahap, I., 2000, "Economic Analysis of Coal: Biomass Fuel Blends as Fuel for Power Plants," Personal communication, Mechanical Engineering Department, Texas A&M University, College Station, TX. Apr., pp. 14.

Herdan, G., 1960, Small Particle Statistics, Butterworths, London

Hertzberg, M., Cashdollar, K.L. and Lazzara, C.P., 1981, "The Limits of flammability of Pulverized Coals and other Dusts," 18th Symposium on Combustion, pp. 717-729.

Hobbs, M. L., 1990, "Modeling Countercurrent Fixed-Bed Coal Gasification," Ph.D. thesis, Department of Chemical Engineering, Brigham Young University, Provo, Utah, Dec.

Hobbs, M. L., Radulovic, P. T., and Smoot, L. D., 1992, "Modeling Fixed-Bed Coal Gasifiers," AIChE J. **38(5)**, pp. 681-702.

Hunt, B. E., Mori, S., and Katz, S., 1951, "Reactions of Carbon with Steam at Elevated Temperatures," Symposium theoretical aspects of Combustion and Gasification of solid Fuels. 120th Meeting, ACS, NY, NY.

Hutchinson, D., Rauh, W., and Amosson, S., 1995, "The Effects of Pen Surface Management on Cattle Performance," Total Quality Manure Management Manual, Texas Cattle Feeders Association, Chapter 3.

Jain, K. A., and Goss, R. J., 2000, "Determination of Scaling Factors for Throatless Rice Husk Gasifier." Biomass and Bioenergy, **18**, pp. 249-256.

Jones, J. A., and Sheth, A. C, 1999, "From Waste to Energy – Catalytic Steam Gasification of Broiler Litter," Proc. of the Renewable and Advanced Energy Systems for the 21st Century, Lahaina, Maui, Hawaii.

Jones, S., 2000, Personal Communications, Xcel Energy, Amarillo, Texas.

Jones, W. P., and Lindstedt, R. P. (1988) Global Reaction Schemes for Hydrocarbon Combustion, *Combust. Flame*, 73, 233-249.

Katyal, S. K., and Iyer, P. V. R., 2000, "Thermochemical Characterization of Pigeon Pea Stalk for its Efficient Utilization as an Energy Source," Energy Sources, **22**, pp. 363-375.

Kayal, T. M., and Chakravarty, M., 1994, "Mathematical Modeling of Continuous Updraft Gasification of Bundled Jute Stick- A Low Ash Content Woody Biomass," Biores. Technol., **49**, pp. 61-73.

Kicherer, A., Spliethoff, H., Maier, H., and Hein, K., 1994, "The Effect of Different Reburning Fuels on NO_x Reduction," Fuel, **73** pp. 1443-1446.

Kosky, P. G., and Floess, J. K., 1980, "Global Model of Countercurrent Coal Gasifiers," Ind. Eng. Chem. Process Des. Dev., **19**, pp. 586-592.

Krishnamoorthy, P. R., Seetharamu, S., and Bhatt, M. S., 1989, "Comparative Study of Biomass Fuels in an Updraft Gasifier," Proc. of the 24th Intersociety Energy Conversion Engineering Conference, **4**, pp. 1959 –1964.

Kurkela, E., Stahlberg, P., Simell, P., and Leppalahti, J., 1989, "Updraft Gasification of Peat and Biomass," Biomass, **19(1-2)**, pp. 37-46.

Kyi, S., and Chadwick, W. L., 1999, "Screening of Potential Mineral Additives for use as Fouling Preventives in Victorian Brown Coal Combustion," Fuel, **78(7)**, pp. 845-855.

Laurendeau, N. M., 1978, "Heterogeneous Kinetics of Coal Char Combustion and Gasification," Prog. Energy. Combust., **4(4)**, pp. 221-270.

Lawn, C., 1987, "Principles of Combustion Engineering for Boilers," Academic Press.

Lin, W., and Dam-Johansen, K., 1999, "Agglomeration in Fluidized Bed Combustion of Biomass – Mechanisms and Co-firing with Coal," 15th International Conference on Fluidized Bed Combustion, Savannah, GA, May 16-19.

Livestock Weekly, 2001, "Economist Touts Feedlot Manure in Place of Costly Fertilizer," Livestock Weekly, San Angelo, TX, Jun. 28, pp. 20.

Loison, R., 1966, "Heterogeneous Combustion – Combustion of Pulverized Coal", Generale De Thermique, **5**(58), pp. 961.

Malay, P., Zamansky, V., Ho, L., and Payne, R., 1999, "Alternative Fuel Reburning," Fuel, **78**, pp. 327-334.

McCaskey, T. A., 1995, "Feeding broiler poultry litter as an alternative waste management strategy," Animal Waste and the Land-Water Interface, Steele, K., ed., Boca Raton, Florida: Lewis Publishers, pp. 493-502.

McDonald, L. A., 2000, Personal communication, Texas Agricultural Extension Service, Texas A&M University System, Amarillo, TX, Apr. 26.

Miller, C., Lemieux, P., and Touati, A., 1996, "Evaluation of Tire-Derived Fuel for Use in Nitrogen Oxide Reduction by Reburning," Journal of the Air and Waste Management Association, **48**, pp. 729-735.

Mitchel, J. W. and Tarbell, J. M., 1982, "A Kinetic Model of Nitric Oxide Formation during Pulverized Coal Combustion," AIChE, **28**(2), pp. 302-311.

Natural Resource, Agriculture, and Engineering Service (NRAES), 1999, "Poultry waste management handbook," Publ. No. NRAES-132., Cooperative Extension, 152 Riley-Robb Hall, Ithaca, New York 14853.

Nowacki, P., 1980, "Lignite Technology," Noyes Data Corporation, Park Ridge, NJ.

Nuttall, H. E., Stoddart, W. G., and Chen, W. J., 1979, "Pyrolysis of Subbituminous New-Mexico Coal," J. Petrol. Technol., **31(4)**, pp. 418-420.

Patil, K. N., and Rao, C. S., 1993, "Updraft Gasification of Agricultural Residues for Thermal Applications," Proc. of the 4th National Meet on Biomass Gasification and Combustion, Interline Publishing, Bangalore, India, pp. 198-205.

PCGC-2, Revised User's Manual, 1989, Advanced Combustion Engineering Research Center, Brigham Young University and University of Utah, Provo, UT

Priyadarsan, S., Annamalai, K., Holtzapple M. T., and Sweeten, J. M., 2003a, "Transient Studies on Fixed Bed Gasification of Feedlot Biomass," Presented at ALTERNATIVE POWER – Agricultural Biomass Fuels and Renewables, Electric Power Conference, ASME, Houston, TX, Mar. 4-6.

Priyadarsan, S., Annamalai, K., Holtzapple M. T., and Mukhtar, S., 2003b, "Fixed Bed Gasification Studies on Chicken Litter Biomass under Batch Mode Operation," Presented at ALTERNATIVE POWER – Agricultural Biomass Fuels and Renewables, Electric Power Conference, ASME, Houston, TX, Mar. 4-6.

Raman, P., Walawender, W., Fan, T., and Howell, J., 1981b, "Thermogravimetric Analysis of Biomass: Devolatilization Studies on Feedlot Manure," Ind. Eng. Chem. Process Dev., **20**, pp. 630-636.

Raman, K. P., Walawender, W. P., Fan, L. T., and Chang, C. C., 1981a, "Mathematical Model for the Fluid-Bed Gasification of Biomass Materials. Applications to Feedlot Manure," Ind. Eng. Chem. Process Des. Dev., **20**(4), pp. 686-692.

Rodriguez, P., Annamalai, K., and Sweeten, J. M., 1998, "The Effect of Drying on the Heating value of Biomass Fuels," Transactions of the ASAE, **41**, pp. 1083-1087.

Sami, M., Annamalai, K., and Wooldridge, M., 2001, "Co-firing of Coal and Biomass Fuel Blends," Progress in Energy and Combustion Science, **27**, pp. 171-214.

Sami M., 2000, "Numerical Modeling Of Coal-Feedlot Biomass Blend Combustion And NO_x Emissions In Swirl Burner," PhD Thesis, Texas A&M University.

Saxena, S. C., 1990, "Devolatilization and Combustion Characteristics of coal Particles," Prog. Energy Combust. Sci., **16**, pp. 55-94.

Schoeters, J. G., 1985, "The Fundamentals of Wood Gasification," Proc. of the Symposium on Forest Products Research International – Achievements and the Future, Pretoria, South Africa, **5**, Apr. 22-26.

Skrifvars, B-J., Hupa, M., Backman, R., and Hiltunen, N., 1994, "Sintering Mechanisms in FBC Ashes," Fuel, **73**(2), pp. 171-176.

Smart, J., and Morgan, D., 1994, "The Effectiveness of Multi-fuel Reburning in an Internally Fuel-Staged Burner for NO_x Reduction," Fuel, **73**, pp. 1437-1441.

Smoot, L. D., and Smith, P. J., 1985, "Coal Combustion and Gasification," Plenum Press, New York, NY.

Spliethoff, H., and Hein, K. R. G., 1998, “Effect of co-combustion of biomass on emissions in pulverized fuel furnaces,” Fuel Processing Technology, **54**(1-3), pp. 189-205.

Spliethoff, H., Greul, U., Rudiger, H., and Hein, K., 1996, “Basic Effects on NO_x Emissions in air Staging and Reburning at a Bench Scale Test Facility,” Fuel, **75**, pp. 560-564.

Stassen, H. E., 1995, “Small-Scale Biomass Gasifier for Heat and Power: A Global Review,” World Bank Technical Paper Number 296, Energy Series, World Bank, Washington, D.C.

Stickler, D., Gannon, R., Young, L., and Annamalai, K., (1983), “Pulverized Fuel Combustion,” Proc. of International Symposium on Combustion Diagnostics, American Flame Research Committee, pp. 1-21.

Sweeten, J. M., 1979, “Manure Management for Cattle Feedlots”, Texas Agricultural Extension Service Publication L-1094, Texas Agricultural Extension Service, Texas A&M University, College Station, Texas, pp. 6.

Sweeten, J.M., 1985, “Agricultural Waste Utilization and Management,” Proc. Fifth International Symposium on Agricultural Wastes, Dec. 16-17.

Sweeten J. M., Korenberg, J., LePori, W., Annamalai, K., and Parnell, C.B., 1986, "Combustion of Cattle Manure for Energy Production," Energy in Agriculture, **5**, pp. 55-72.

Sweeten, J. M., Annamalai, K. Heflin, K., Freeman, M., 2002, “Cattle Feedlot Manure Quality for Combustion in Coal/Manure Blends,” Paper No. 024092, ASAE Annual International Meeting, Chicago, Illinois, Jul. 28-31.

Sweeten J., Korenberg, J., LePori, W., Annamalai, K., and Parnell, C.B., 1986, "Combustion of Cattle Manure for Energy Production," Energy in Agriculture, **5**, pp. 55 – 72.

Sweeten, J. M., Annamalai, K., Thien, B., and McDonald, L., 2003, “Co-Firing of Coal and Cattle Feedlot Biomass (FB) Fuels, Part I: Feedlot Biomass (Cattle Manure) Fuel Quality and Characteristics,” Fuel, **82**(10), pp. 1167-1182.

Tabatabaie-Rasi, A., and Trezek, G. J., 1987, “Parameters Governing biomass Gasification,” Ind. Eng. Chem. Res., **26**(2), pp. 221-228.

Tang, H., 1999, Personal Communication, Vortec Industries, (20943 Brant Avenue, Long Beach, CA 90810; phone 310/537-6624).

Thien, B., and Annamalai, K., 2001b, “Reduction of NO Through Reburning With Coal and Feedlot Biomass,” Proc. The Second Joint Meeting of the Combustion Institute, Oakland, CA, Mar. 25-28.

Thien, B, Annamalai, K., and Bukur, D., 2001a, “Thermo gravimetric Analysis of Coal, Feedlot Biomass and Blends in Inert and Oxidizing Atmospheres,” Proc. IJPGC, New Orleans, LA.

Thien, B., 2002, “Co-Firing With Coal – Feedlot Biomass Blends,” PhD Thesis, Texas A&M University.

Thien, B., Annamalai, K., and Bukur, D. B., 2003, "Pyrolysis and Group Ignition behavior of Coal, Feedlot Biomass and Blends under TGA Conditions," Presented at National Combustion Conference, Univ. of Illinois at Chicago, IL, Mar. 16-19.

Tognotti, L., Malotti, A., Petarca, L., and Zanelli, S., 1985, "Measurement of Ignition Temperature of Coal Particles Using a Thermo gravimetric Technique," Combustion Science and Technology, **44**, pp. 15-28.

Tsuji, T., Gupta, A. K., Hasegawa, T., Katsuki, M, Kishimoto, K, and Morita, M., 2002, "High Temperature Air Combustion: from Energy Conservation to Pollution Reduction," CRC Press, Washington, DC.

USDA, National Agricultural Statistics Service, 2002, U.S. Poultry Charts, http://www.usda.gov/nass/aggraphs/poultry.htm, Accessed on Jun. 14.

Vuthaluru, H.B., Vleeskens, J. M., and Wall, T. F., 1998, "Reducing Fouling form Brown Coals by Sodium-Binding Additives," Fuel Processing Technology, **55**(2), pp. 161-173.

Walker, P. L., Ruskino, F., and Austin, L. G., 1959, "Gas Reactions of Carbon," Adv. Catal., **11**, pp. 167.

Wall, T. F., Gupta, S. K., Gupta, R. P., Sanders, R. H., Creelman, R. A., and Bryant, G., W., 1999, "False Deformation Temperatures for Ash Fusibility Associated with the conditions for Ash Preparation," Fuel, **78**(9), pp. 1057-1063.

Wall, T. F., Creelman, R. A., Gupta, R. P., Gupta, S. K., Coin, C., and Lowe, A., 1998, "Coal Ash Fusion Temperatures – New Characterization Techniques, and Implications for Slagging and Fouling," Prog. Energy Combust. Sci., **24**, pp. 345-353.

Wei, G., 2002, "Numerical Study of Pulverized Coal-Litter Biomass Blend Combustion and Pollutant Emissions in a Swirl Burner," Ph.D. thesis, Texas A&M University, College Station.

William, H., and Hill, 1945, "Recovery of Ammonia, Cyanogen, Pyridine, and Other Nitrogenous Compounds from Industrial Gases," Chemistry of Coal Utilization - II, John Wiley & Sons Inc., New York, NY, pp. 1008 – 1135.

Williams, A., Pourkashanian, M., Jones, J. M., and Skorupska, N., 2000, Combustion and Gasification of Coal, Taylor & Francis, NY, NY.

Winegartner, E. C., and Rhodes, B. T., 1975, "An empirical study of the relation of chemical properties to ash fusion temperatures," J Eng Power-T, ASME'97, **3**, pp. 395-406.

www.chemfinder.com, www.abcr.de, 2003, Merck Index, Accessed on Jun. 27

Yang, B., Naja, T., Gibbs, B., and Hampartsoumian, E., 1997, "Optimization of Operating Parameters for NO Reduction by Coal Reburning in a .2 MW furnace," Journal of the Institute of Energy, **70,** pp 9-16.

Yoon, H., Wei, J., and Denn, M. M., 1978, "Model for Moving-Bed Coal-Gasification Reactors," AIChE J., **24**(5), pp. 885-903.

Zhou, J., Masutani, S., Ishimura, D., Turn, S., and Kinoshita, C., 2000, "Release of Fuel-Bound Nitrogen during Biomass Gasification," Ind. Eng. Chem. Res., **39**, pp. 626-634.

7. Acronyms

A/F: Air Fuel Ratio
AB: Agricultural Biomass
AFB: Advanced Feedlot Biomass
AFT: Ash Fusion Temperature
APF: Annular Primary Fuel
ASTM: American Society for Testing and Materials
ATP: Texas Advanced Technology Program
BL: Broiler Litter
CAB: Coal:Agricultural Biomass Blend
CAFO: Concentrated Animal Feeding Operations
CFBC: Circulating Fluidized Bed Combustion
CFB: Coal:Feedlot Biomass (Cattle Manure)
CFB: Coal:Feedlot Biomass
CHFB: Coal: High Ash Feedlot Biomass
CLB: Coal:Litter (Poultry Waste) Biomass
CPF: Central Primary Fuel
CTE: Commercial Testing and Engineering Co/
DAF: Dry Ash Free
EPA: Environmental Protection Agency
FB: Feedlot biomass (Cattle manure – conventional, i.e., high ash)
FC: Fixed Carbon
FiC: Finished Composted
FBC: Fluidized Bed Combustor
FIXB: Fixed Bed
FT: Fluid Temperature
GC: Gas Chromatograph
HFB: High ash Feedlot Biomass
HHV: Higher or Gross heating value
HT: Hemispherical Temperature
IDT: Initial Deformation Temperature
LB: Litter (Poultry Waste) Biomass
LHFB: Litter: High Ash Feedlot Biomass
LOI: Loss on ignition or % carbon in bottom and fly ash
MCFBC: Multi-Circulating Fluidized Bed Combustion
MSW: Municipal Sewage Waste
NETL: National Energy Technology Laboratory

NRAES: Natural Resource, Agriculture, and Engineering Service
PA: Primary Air
PC: Partially composted
PCGC2: Pulverized Coal Gasification and Combustion- 2 Dimensional
Pf: pulverized fuel fired
PM: Particulate Matter
RDF: Refuse Derived Fuel
RM: Raw manure
SA: Secondary Air
SB: Stoker Burner
SCFH: Standard Cubic Feet per Hour
SD: Standard Deviation
SFB: Simulated Feedlot Biomass artificially created with similar ash content
SNR: Selective Non-catalytic Reduction
SPS: Southwestern Public Service Co.
SR: Stoichiometric Ratio
SSFB: Soil Surfaced Feedlot Biomass
ST: Softening Temperature
TAES: Texas Agricultural Extension Service
TAMU: Texas A&M University
TBP: Boiling Point Temperature
TCD: Thermal Conductivity Detector
TCFA: Texas Cattle Feeders Association
TGA: Thermo-Gravimetric Analysis
TMP: Melting Point Temperature
TSP: Total Suspended Particles
USDA: US Dept of Agriculture
VM: Volatile matter

8. Nomenclature

a	Excess air percentage supplied to the main burner zone
$A_{C,i}$	Pre-exponential factor for reaction i
$A_{pyro,fl}$	Pre-exponential factor for pyrolysis of fuels, '$_{fl}$': coal, or biomass
b_{II}	Order of the reaction with O_2
c_{part}	Specific heat capacity of the solid fuel particle
$c_{pk,MB}$	Specific heat capacity of the main burner product gas species, 'k' (CO_2, NO, H_2O, N_2, O_2.)
coal 1	Size – 9.2 mm (0.375 ")
coal 2	Size – 5 mm (0.2 ")
d	Fraction of LHV of the main burner fuel lost from the main burner.
db	Dry basis
$E_{pyro,fl}$	Activation energy for pyrolysis of fuels, '$_{fl}$': coal, or biomass.
F_B	Blowing correction factor
F_R	Shape factor to account for shielding by other particles (assumed to be 1 in this case)
f_N	Fraction of fuel N converted into NO
h	Heat transfer coefficient for a particle of size dp, (h = Nu λ/dp)
h_{f,CH_2}	Heat of formation of CH_2
h_{f,CO_2}	Heat of formation of CO_2
$h_{f,fuel}$	Enthalpy of formation of the main burner fuel
h_{f,H_2O}	Heat of formation of $H_2O_{(gas)}$
$h_{f,NH3}$	Enthalpy of formation of NH_3
$H_{in,mainburner}$	Enthalpy of the reactants entering the main burner at 298 K (main burner fuel, NH_3, and air)
$H_{out,mainburner}$	Enthalpy of the products leaving the main burner at T K (CO_2, H_2O, N_2, NO, O_2)
h_m	Mass transfer coefficient
$h_{t,air}$	Thermal enthalpy of air
$h_{t,fuel}$	Thermal enthalpy of the main burner fuel
$h_{T,k,MB}$	Total enthalpy of the main burner product species
$h_{t,NH3}$	Thermal enthalpy of NH_3
$HTP_{f,MB}$	Fraction of total heat throughput supplied through the main burner
HV_{FC}	Heating value of FC
$HV_{C,i}$	Heating value of heterogeneous reactions
HV_i	Heating value of *i* th homogeneous reaction
HV_p	Heating value of the pyrolysis products, in the event volatiles oxidize in proportion to fixed carbon
H_p	Heat of pyrolysis of the volatile matter
i	Reaction number involving the species 'k'
$[k]$	Concentration of species 'k' (kmol/m^3)
'k'	Gas species O_2, CO, CO_2, CH_4, CH_2, H_2, H_2O, HCN, NH_3, NO, N_2
$k_{C,i}$	Specific reaction constant for reaction i, and
LHV_{MB}	Lower heating value of the main burner fuel
$LHV_{RB,fuel,daf}$	LHV of the reburn fuel on DAF basis

$LHV_{VM,daf}$	LHV of the VM on DAF basis
$\dot{m}_{air}$	Mass flow rate of air supplied into the main burner
$\dot{m}_{fuel}$	Mass flow rate of main burner fuel supplied into the main burner
$\dot{m}_{gas,RS}$	Total mass flow rate of the gas supplied along with the solid reburn fuel
$\dot{m}_{NH_3}$	Mass flow rate of NH_3 supplied into the main burner
$\dot{m}_{RB,daf}$	Mass flow rate of reburn fuel on DAF basis
$\dot{m}_{prod,MB}$	Total mass flow rate of the main burner jet
$\dot{m}_{RB,t=0}$	Mass flow rate of the reburn jet at t = 0
$\dot{m}_C$	Total carbon loss rate
$\dot{m}_{RB,t}$	Total mass flow rate of the reburn jet at time t
$\dot{m}_V$	Total volatile loss rate
m_C	Mass added to gas phase due to oxidation of FC (total carbon oxidation) in the solid fuel
m_k	Mass of species 'k'
$\dot{m}_N$	Mass of FBN remaining in the solid reburn fuel particle
$\dot{m}_{N,O}$	Initial mass of FBN in the reburn fuel particle
m_{N-oxid}	Mass added to gas phase due to oxidation of fuel nitrogen at particle surface
m_{N-pyro}	Mass released from the solid fuel into the gas phase due to devolatilization of N in the solid fuel
m_o	Initial mass of the particle
m_{part}	Mass of the solid fuel particle
m_{pyro}	Mass added to the gas phase due to devolatilization of volatile matter in the solid fuel
ms	milli second
$MW_{k,MB}$	Molecular weight of the main burner product gas species 'k' (CO_2, NO, H_2O, N_2, O_2)
$MW_{RB,daf}$	Molecular weight of the reburn fuel on DAF basis
MW_{VM}	Molecular weight of VM
$N_{(S)}$	Mass of FBN in the solid fuel particle
n	Number of samples
n_i	Order of reaction 'i' with respect to oxidizer
$\dot{q}_{ch}$	Enthalpy added as result of homogeneous chemical reactions in the gas phase.
$\dot{q}_m$	Enthalpy added to the gas phase due addition of mass from the particles
Q_{loss}	Heat loss from the main burner, Q_{loss} < 0 for heat loss from the main burner
R	Universal gas constant (8.314 kJ/kmol K)
R_{Boiler}	Rating of the boiler burner (kW)
S	Mass source terms
$S_{Htr,k}$	Heterogeneous reaction source term for species 'k'
$S_{Hmr,k}$	Homogeneous reaction source term for species 'k'
Sn_i	Equals to +1, if the species are produced for reaction i, and

Sn_i	Equals to –1, if the species are consumed for reaction i
$S_{N-oxid,k}$	Nitrogen oxidation source term for species 'k'
$S_{N-pyro,k}$	Nitrogen pyrolysis source term for species 'k'
$S_{pyro,k}$	Pyrolysis source term for species 'k'
S_v	Surface area per unit volume of fuel, (m^2/m^3)
t	Time
T_g	Temperature of the gas phase
$T_{MB,in}$	Temperature of the main burner fuel entering the main burner
T_{rad}	Radiative temperature surrounding the particle (assumed to be T_g in this case)
V	Volatile matter already released into gas phase
V_{int}	Initial volatile matter in the solid fuel
w	Moles of NO required down stream of the main burner zone
$w_{hm,i}$	Rate of i^{th} homogeneous reaction (kg/s)
$w_{k,i}$	Reaction rate of species 'k' in reaction number 'i'
X_k	Mole fraction of species 'k' in gas phase
X_k	Mole fraction of the main burner product gas species
Y_{ash}	Ash fraction of reburn fuel on as received basis
$Y_{k,MB}$	Mass fraction of product gases in the main burner, CO_2, NO, H_2O, N_2, O_2
$Y_{kr,w}$	Reactant 'kr' mass fraction at the surface of the particle, (ex. for reaction XII, reactant 'kr' is CO_2.)
$Y_{FC,daf}$	Mass fraction of FC in the reburn fuel on DAF basis
Y_N	Mass fraction of nitrogen remaining in the fuel
$Y_{N,O}$	Initial mass fraction of nitrogen in the fuel

Greek Symbols

α	swirl fin angle
β	Heating rate (K/min)
δ	Error (kg)
ΔC	Constant, depends on plate size
Δh	Height difference (m)
ε	Emissivity
η_g	Gasification efficiency
η_s	Fraction of sulfur captured
μ	Viscosity (kg/m-s)
ν	Stoichiometric mass of species 'k' per unit mass of the carbon in reaction 'i'
ρ	Density of fluid (kg/m^3)
ρ_{air}	Density of fluid air (kg/m^3)
ρ_{liq}	Density of manometer fluid (kg/m^3)
ρ_p	Particle density
σ	Standard deviation
σ_{SB}	Stefan-Boltzmann constant
τ_{mix}	Characteristic mixing time scale (sec)
ϕ	Equivalence ratio
ϕ_{RZ}	Equivalence ratio in the reburn zone
ϕ_{RS}	Equivalence ratio in the reburn supply zone